OXIDATION STUDIES OF A NOVEL BARRIER POLYMER SYSTEM

by

Martin Jonathan Ball

Doctor of Philosophy

THE UNIVERSITY OF ASTON IN BIRMINGHAM

January 1995

Oxidation Studies of a Novel Barrier Polymer System

by Martin Jonathan Ball

Ph.D. Thesis, 1995

Summary

The thermal oxidation of two model compounds representing the aromatic polyamide, MXD6 (poly m-xylylene adipamide) have been investigated. The model compounds (having different chemical structures, viz, one corresponding to the aromatic part of the chain and the other to the aliphatic part), based on the structure of MXD6 were prepared and reactions with different concentrations of cobalt ions examined with the aim of identifying the role of the different structural components of MXD6 on the mechanism of oxidation.

The study showed that cobalt, in the presence of sodium phosphite (which acts as an antioxidant for MXD6 and the model compounds), increases the oxidation of the model compounds. It is believed that the cobalt acts predominantly as a catalyst for the decomposition of hydroperoxides, formed during oxidation of the models in the melt phase, to free radical products and to a lesser extent as a catalyst for the initiation of the oxidation reaction by complex formation with the amide, which is more likely to take place in the solid phase.

An oxidation cycle has been proposed consisting of two parts both of which will occur, to some extent under all conditions of oxidation (in the melt and in the solid phase), but their individual predominance must be determined by the prevailing oxygen pressure at the reaction site. The different aspects of this proposed mechanism were examined from extensive model compound studies, and the evidence based on the nature of product formation and the kinetics of these reactions. Main techniques used to compare the rates of oxidation and the study of kinetics included, oxygen absorption, FT-IR, UV and TGA. HPLC was used for product separation and identification. A number of final products were identified, both volatile and non volatile in nature, which included a homologous series of monocarboxylic acids, dicarboxylic acids, aldehydes and alkyl amines. Furthermore, several aromatic acids, aldehydes and amines were also identified.

key words : cobalt, poly (m-xylyene adipamide), oxidation of hydrocarbons.

Acknowledgements

Contents.

Chapter 2. :- Experimental.

Chapter 3 :- Oxidation Studies of Benzene-1,3-Dimethyl Hexanamide (Model I).

Chapter 4. :- Oxidation Studies of Hexanedioate-bis-Benzylamide (ModelII).

Chapter 5. :- Possible Reactions of Cobalt Neodecanoate Sodium Phosphite and Their Influence on the Oxidation of Model I.

Chapter 6. :- Separation & Identification of the Degradation Products Produced From the Thermal Oxidation of the Model Compounds.

Chapter 7. :- Conclusion.

List of Figures.

Chapter 3.

Chapter 4.

List of Schemes.

Tables.

Chapter 6.

Chapter 7.

List of Abbreviations and Symbols.

D.S.C	Differential Scanning Calorimetry.
Ea	Activation Energy.
G.C.-M.S.	Gas Chromatography - Mass Spectroscopy.
H.P.L.C.	High Performance Liquid Chromatography.
FT-IR	Fourier Transform Infrared.
k	Rate Constant.
MXD	m-Xylylene diamine.
MXD6	Poly(m-xylylene adipamide).
Rt	Retention Time.
P.E.T	Poly(ethylene terephthalate).
ppm	Parts per Million.
R	Gas Constant.
T.G.A	Thermogravimetric Analysis.
U.V-Vis	Ultra Violet - Visible.
Δ	Thermal Energy.

Chapter 1. Introduction.

1.1. General Introduction.

Many market forces propel the growth of synthetic polymers in the market place. A major factor in this respect is the superior cost performance ratio of polymers versus traditional materials. Manufacturers are always on the lookout for ways to reduce the cost or increase the quality of their products, and synthetic polymers offer them the opportunity to do just that. Low cost and superior performance have led commodity, or general purpose plastics to drive the packaging industry to substitute thin polymer films for both paper and aluminium. This trend continues today, as polyester beverage bottles replace glass bottles to an ever increasing degree.

Packaging materials constitute one of the major areas of use of thermoplastic polymers and both scientific and practical interest centres round the ability of food packaging plastics to exclude oxygen. The ability to have and maintain an air tight seal is a critical parameter, since it determines the shelf life of the food. The property of acting as a barier to oxygen is a function of the compostion of the polymer. The design of plastic materials to maximise oxygen barrier properties is therefore of primary concern to the packaging industry.

Basic packaging materials such as polypropylene or poly(ethylene terephthalate) are inexpensive to produce but have a poor barrier towards oxygen and so are only used for products that have a low sensitivity or very quick turnover. Other polymers are available, such as polyamides, which have a much lower oxygen permeation rate but are either too expensive or not suitable for making the container. However an alternative technology has been developed in which compounds which scavenge oxygen are added in small amounts to normal packaging materials [1]. The inclusion of oxygen scavengers within the cavity of the package is one form of such packaging.

Typically, such oxygen scavengers are in the form of sachets which contain a composition which scavenges the oxygen through oxidation reactions. One such composition contains ferrous based compounds which oxidize to their ferric states. Another example is based on unsaturated fatty acid salts on a particulate absorbent [2]. However, one disadvantage of the use of sachets containing different chemical compositions is the need for additional packaging operations to add the sachet to each polymer system produced for packaging purposes.. A further disadvantage arising from the iron based sachets is that certain atmospheric conditions are sometimes required in order for oxygen scavenging to occur at an adequate rate.

Another means for regulating the exposure to oxygen involves incorporating an oxygen scavenger into the packaging itself. The incorporation of the sacvenging material, rather than the addition of a separate structure, as in the case of the sachet, to the package results in a more uniform scavenging effect throughout the polymer package. Such incorporation can provide a means of intercepting and scavenging oxygen as it is passing through the walls of the package, thereby maintaining the lowest possible oxygen level throughout the package. The incorporation of inorganic powder and/or salts, as the scavenger, in the polymer, causes degradation of the walls transparency and mechanical properties. In addition these compounds can lead to processing difficulties [3,4]. However based on a similar idea of incorporating the scavenger into the packaging itself Carnaud MetalBox began evaluating one such scheme, in which a metal catalyst-polyamide system acted as the oxygen scavenger, as opposed to the inorganic powder and/or salt [5]. Through the catalysed oxidation of the polyamide, the package wall regulates the amount of oxygen which reaches the cavity of the package. Such systems have the advantage of chemically binding the permeating oxygen to the polymer substrate, in contrast to more traditional physical barriers which merely impede the inevitable ingress of the oxygen into the pack. When the scavenging chemistry eventually ceases to function the basic physical barrier properties of the polymer blend remain unimpaired.

The discovery of this 'super-barrier' behaviour was accidental and hence it was important to understand how this can be achieved deliberately and controllably and this was the basis of the investigation discussed in this thesis. This is novel in that unlike most of the oxidative degradation processes in polymers studied in the past at Aston, the effect of oxidation in the present instance appears to produce a desirable rather than a deleterious effect. It is clearly important to understand the detailed chemistry of the changes occuring.

1.2. The Oxygen Scavenging System.

The general system (table 1.1) consists of a matrix polymer, an oxygen scavenging/absorbing component and a catalyst. The matrix polymer forms the bulk (>95%) of the packaging material, providing mechanical strength and much of the basic physical barrier to oxygen and other gases such as carbon dioxide and water vapour.

GENERAL SYSTEM	SPECIFIC SYSTEM	
* Structural Polymer	* PET (95-99%)	Processed as Polymer BLEND
* Oxidisable Component	* MXD6 Nylon (1-5%)	
* Metallic Catalyst	* Cobalt Salt (50-200ppm)	

Table 1.1 The OXBAR Oxygen Scavenging System (From "OXBAR" Carnaud MetalBox Packaging Technology plc).

The oxygen scavenging/absorbing component is melt blended with the matrix polymer and comprises approximately 5% of the total. MXD6 has been used as a general gas barrier (physical) but can also be induced to oxidise by the addition of a catalyst mopping up oxygen as it permeates into the package wall. The catalyst is a cobalt salt added at a low concentration (<200ppm Co). It triggers the oxidation of the MXD6 scavenger without itself becoming permanently bound to the oxidised polymer. Thus a small amount of cobalt participates in the capture of a large amount of oxygen [5].

1.3. Oxidation of Polymeric Materials.

1.3.1. The Basis of Polymer Oxidation.

The developement of polymeric materials was mainly accelerated because of the depletion of natural poducts (metals,wood,etc). The phenomena of corrosion in metals resemble those of degradation in polymers. The most important mechanism leading to polymer degradation is its reaction with oxygen, with or without heat, although degradation by heat alone is also important. Various oxygen containing groups are introduced along the polymer chain or at its ends by oxidation and some low molecular products are also formed.

The oxidation of polymers also causes deterioration in physical properties. As the oxidation proceeds, decrease in molecular weight and discolouration of the polymers are observed [6,7]. Thus the oxidative degradation of polymers is considered generally to be a deleterious process and therefore extensive efforts have been devoted to inhibit or supress it. The thermal oxidative degradation of organic materials has been widely studied and the accepted mechanism of oxidation of organic compounds [8] is shown in Scheme 1.1.

INITIATION $\qquad$ Production of $R \cdot$ or $RO_2 \cdot$ $\qquad$ (1.1)

PROPAGATION $\quad R \cdot + O_2 \ ----> \ RO_2 \cdot$ $\qquad$ (1.2)

$\qquad\qquad\quad RO_2 \cdot + RH \ ----> \ RO_2H + R \cdot$ $\quad$ (1.3)

TERMINATION $\quad R \cdot + R \cdot$ $\qquad\qquad\qquad\qquad$ (1.4)

$\qquad\qquad\quad R \cdot + RO_2 \cdot \qquad$ non-radical products $\quad$ (1.5)

$\qquad\qquad\quad RO_2 \cdot + RO_2 \cdot$ $\qquad\qquad\qquad\qquad$ (1.6)

$\qquad\qquad 2\ RO_2H \ ------> \ RO_2 \cdot + RO \cdot + H_2O$ $\qquad$ (1.7)
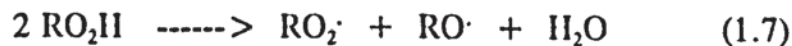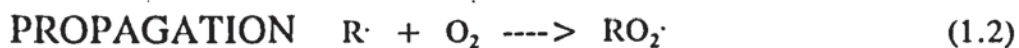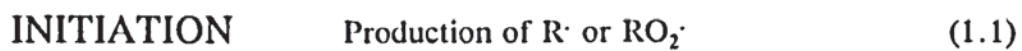
Scheme 1.1. General Mechanism of oxidation of organic compounds.

In the absence of an initiator, the initiation step, whereby free radicals are introduced into the system, is due to the thermal decomposition of hydroperoxides (reaction 1.7).

Each free radical formed during the initiation step is capable of forming many molecules of hydroperoxide via the propagation steps (1.2) and (1.3). These can then initiate further oxidation chains leading to the formation of yet more hydroperoxide. A chain reaction is therefore rapidly set up. If this continued unhindered, very rapid oxidation would occur, leading ultimately to an explosion. The reason that this does not occur is due to the removal of free radicals by the termination reactions (1.4), (1.5) and (1.6). Under conditions of plentiful oxygen supply, reaction (1.6) predominates because the reaction of alkyl radicals and oxygen, (1.2), is very fast. Reaction (1.4) is only important at low oxygen pressures.

Radicals that initiate autoxidation in polymers are formed by thermal energy, UV radiation, bombardment by high energy particles, mechanical stress, metal catalysis, and the addition of initiators. When polymer bonds are ruptured under any of these conditions and oxygen is present in the environment, autoxidation can occur. Many polymers, however, oxidize under relatively mild conditions in which the absorbed energy does not reach the level of the dissociation energies of carbon-carbon or carbon-hydrogen bonds as determined for simple parafins. Under these conditions, it seems unlikely that simple bond cleavage is the initiation step. It has been suggested [9,10] that traces of hydroperoxides introduced into the polymer during processing are the source of initiating radicals. Secondary degradation products such as carbonyl or carboxyl groups could also contribute to initiation by sensitizing adjacent bonds and thus lowering the dissociation energy. Hydroperoxide decomposition into radicals is accelerated by various catalysts, notably the transition metals and derivatives of these [11]. Polymers are normally in contact with metal surfaces during processing and traces of iron, manganese, copper, and so on, may be incorporated into the material, acting eventually as oxidation catalysts. Metallic impurities derived from polymerization catalysts are often catalysts for autoxidation, and removal of these residues is essential to obtain maximum stability of the polymer.

A typical rate curve for hydrocarbon oxidation is shown schematically in figure 1.1. Reaction starts slowly, accelerates through a period characterised as the autocatalytic stage, and then slowly subsides. The transition from acceleration through deceleration can result in a period of essentially constant reaction rate - the steady state rate.

Hydroperoxide concentration (figure 1.1) starts at a very low level, increases as autocatalysis begins, and reaches a maximum as reaction passes into the steady state rate. Competitive reactions of hydroperoxide formation and decomposition occur throughout the reaction, and the maximum concentration is reached when the rate of decomposition equals that of formation.
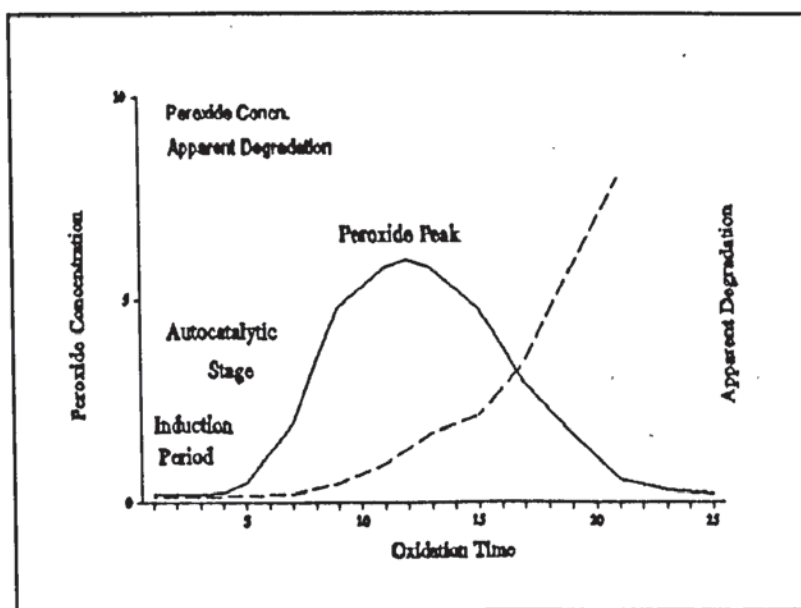
Figure 1.1.   Diagram showing how the Concentration of Peroxide and Apparent Degradation varies with Increased Oxidation.

1.3.2. Catalysis and Inhibition by Metal Ions.

Among the various impurities in polymers which affect the degradation of polymeric materials, metallic impurities often show the most pronounced effect on degradation. However, the effect of metallic compounds on the degradation of polymers is extremely complicated and is influenced by various factors including 1) the nature of the polymer substrate 2) the environmental conditions to which the polymers are exposed 3) the kind of metal 4) the valency of the metal 5) the anion or ligand of the metallic compounds. Osawa's study of the thermo-oxidative degradation of polypropylene [12,13,14] provides a good example of these various factors which influence the affect of the metallic compound.

To illustrate the effects of different metals and the environmental conditions, the effect of various metallic salts of fatty acids on the thermo oxidative degradation of powdered (ie, solid) polypropylene [12] was examined by oxygen uptake, and later compared with the oxygen uptake curves of isotactic polypropylene in the presence of various metal stearates in trichlorobenzene [13]. Firstly, in the solid polymer, the rate of oxygen absorption and the activation energy were greatly affected by the kinds of metal added to the solid polymer (see figure 1.2) [12]. The order of decreasing catalytic effect of the metallic salts of stearic acid was :Co > Mn > Cu > Fe > V > Ni > Ti=Ca=Ag > Al > Mg= Cd >control. The catalytic activity of the metallic salts with respect to the decomposition of t-butyl hydroperoxide was similar. Thus there appeared to be a correlation between the catalytic activity of metallic salts in the oxidation of the polymer and that in the decomposition of hydroperoxide. Furthermore, it was suggested that there is a correlation between the catalytic activity of metallic salts and the redox potential of the metal ions.

The oxygen uptake curves of isotactic polypropylene in the presence of various metal stearates in trichlorobenzene are shown in figure 1.3 [13]. The order of decreasing catalytic effect of the metal stearates at the early stage of oxidation of the polymer was as follows : Cu > Mn > Fe > Cr > Co > Ni > Ti > control > Al > Zn > V. The order of the catalytic effect of the metals is thus quite different from that in the solid polymer. Furthermore, in the oxidation of the polymer in a mixed solvent (trichlorobenzene and propionic acid) the oxygen uptake curves did not produce a leveling off period which was apparent in the single solvent system. In solution no correlation of the activity of the metal stearates in the polymer oxidation with that of the decomposition of t-butyl hydroperoxide in solution or with the oxidation potential of the metal was made. It seems likely then that the environment of the metal ion, particularly the polarity of the solvent, may affect its catalytic activity. The redox potential of the metal ion in organic solution may not necessarily correlate with that in aqueous solution.

fig 1.2 Oxygen uptake curves of polypropylene powder in the presence of various metal stearates. Temperature: 125°C; [Additive]: 0·5 wt%. [12]

fig 1.3 Oxygen uptake curves of polypropylene in trichlorobenzene solution in the presence of various metal stearates. Temperature: 125°C; [Polymer] = 2·38 M; [Metal] = 7·9 × 10⁻⁴ M. [13]

Having illustrated the importance of the kind of metal and environmental conditions on the effect of metalllic compounds on the oxidation of polypropylene the importance of metal valency [12] and ligand effects [14] was also investigated by Osawa, again in polypropylene. The catalytic activities of the metal compounds are greatly affected by the valency of the metal ion and, in general, the higher the valency of the metal the greater its catalytic activity. In particular Osawa used the cobalt(II,III) acetylacetonate catalysed thermal oxidative degradation of polypropylene to demonstrate this behaviour. Figures 1.4 and 1.5 [12] show that the oxygen uptake of IPP containing Co(III) takes place at a lower temperature than that of the polymer containing Co(II). The dependance of the thermal oxidation of the polymer on the concentration of cobalt acetylacetonates is quite different for Co(II) and Co(III). However, at the lower catalyst concentrations both Co(II) and Co(III) show similar catalytic activity.

The importance of the metal ligand, particularly focusing on the effect on catalytic activity of bonding character (covalent or ionic bonding) between a metal centre and anions (or ligands), was examined using a series of cobaltic compounds and studying their affect on the thermo-oxidative degradation of polypropylene by the oxygen absorption method. As shown in table 1.2 [14], the catalytic activity of the cobaltic compounds examined was remarkably dependent on the nature of the anion. It seems likely that the more ionic character there is in a metallic salt, the more effective it is for the catalysed degradation of the polymer. Conversely, the highly covalent character observed in a cobaltic compound such as Co(III)-Se-carbamate favours the inhibition of polymer oxidation.

Many other workers have examined some of the factors which influence the effect of metallic compounds on the degradation of polymers, particularly Chalk and Smith [15] (solvent effect), Betts and Uri [16] (valency) and particularly Kamiya [17,18,19], however the work of Osawa, on polypropylene, discussed in the section above provides a complete and clear example. It illustrates the difficulty in anticipating the effect of a specific metallic compound on the degradation of polymers. However, although there are various ways in which metallic compounds can influence the degradation of polymers, the metallic compounds may be classified into two groups, accelerators and retarders.

Aston University

Illustration removed for copyright restrictions

fig 1.4 Oxygen uptake curves of polypropylene powder containing various amounts of Co(acac)$_2$ at 120°C. Numbers on curves are wt% of Co(acac)$_2$ [12]

Aston University

Illustration removed for copyright restrictions

fig 1.5 Oxygen uptake curves of polypropylene powder containing various amounts of Co(acac)$_3$ at 90°C. Numbers on curves are wt% of Co(acac)$_3$. [12]

Table 1.2.
EFFECT OF VARIOUS COBALTIC COMPOUNDS ON THE THERMO-OXIDATIVE DEGRADATION OF POLYPROPYLENE [14]

Aston University

Illustration removed for copyright restrictions

Although it is very difficult to be certain about the mechanism of most metallic compounds in the degradation of polymers, the following functions have been identified.

1.3.2.1 Metallic Compounds as Radical Initiators.

1.3.2.1.1 Catalytic Decomposition of Hydroperoxides.

The pro-oxidant effect of transition metal ions in catalysing the decomposition of hydroperoxides to free radical products is well established [20]. The most effective ions are those which are capable of undergoing a one electron oxidation or reduction between two states of comparable stability e.g. $Co^{2+/3+}$ [15]. It is generally accepted that the catalysis occurs by a redox mechanism in which reactions (1.8) and (1.9) together bring about the breakdown of the hydroperoxide to free radical products [20].

$$M^{n+} + RO_2H \ ------> \ M^{n+1} + \cdot OH + RO\cdot \qquad (1.8)$$

$$M^{n+1} + RO_2H \ ------> \ M^{n+} + H^+ + RO_2\cdot \qquad (1.9)$$

$$\text{Overall,} \quad 2\,RO_2H \ \xrightarrow{\quad M^{n+}/M^{n+1} \quad} \ RO\cdot + RO_2\cdot + H_2O \qquad (1.10)$$
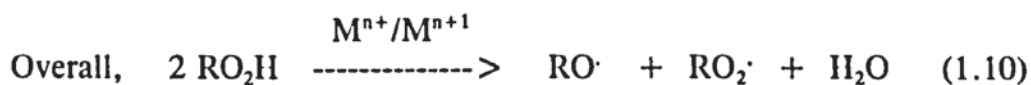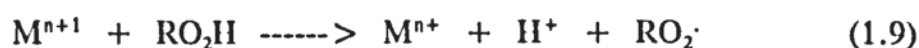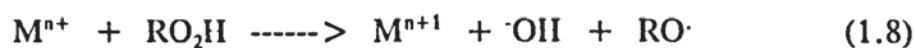
Although the end products of reaction (1.10) are identical to those of reaction (1.7), the activation energy of the former is much lower. The presence of small quantities of the metal ion is capable of such an effect due to the regeneration of the catalyst via reactions (1.8) and (1.9). Cobalt is an efficient trace metal ion catalyst for hydroperoxide decomposition, Dean & Skirrow [21] studied the effect of cobaltous acetate upon the decomposition of t-butyl hydroperoxide, the major products of the reaction were identified as oxygen and t-butyl alcohol with formaldehyde, acetone, di-t-butyl peroxide and water which they accounted for by the following chain reaction, (1.11-1.14).

$$Co^{3+} + ROOH \ -----> \ Co^{2+} + ROO\cdot + H^+ \qquad (1.11)$$

$$Co^{3+} + ROOH \ -----> \ Co^{3+} + RO\cdot + \cdot OH \qquad (1.12)$$

$$2ROO\cdot \ -----> \ 2RO\cdot + O_2 \qquad (1.13)$$

$$2ROO\cdot \ -----> \ ROOR + O_2 \qquad (1.14)$$
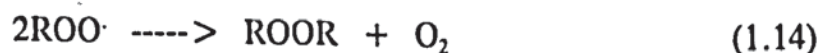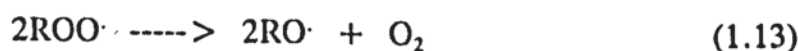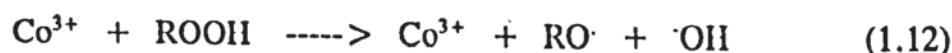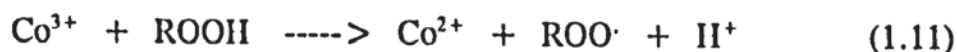
By measurement of the rate of oxygen evolution and hydroperoxide decay, the orders of reaction with respect to cobaltous acetate and t-butyl hydroperoxide have been shown to have values between 1.0 and 1.5. The combined order (>2.0) was explained by postulating the formation of a cobalt hydroperoxide complex as the first reaction step. However the idea that catalysis proceeds via the formation and unimolecular decomposition of a metal-hydroperoxide complex was first discussed by Banks and co-workers [22]. Complex formation easily explains the observation that the addition of hexadentate or octadentate ligands, which coordinate metal ions to their maximum extents, renders metal ions ineffective as catalysts [15],[23].

1.3.2.1.2 Direct Reaction with the Substrate.

Direct reaction of a metal ion with a substrate polymer in the early stage of the degradation may form a free radical (reactions 1.15 and 1.16) [24]

$$RH + MX_2 \longrightarrow R\cdot + MX + HX \qquad (1.15)$$
$$RH + MX \longrightarrow R\cdot + M + HX \qquad (1.16)$$

1.3.2.1.3 Activation of Oxygen.

Interaction of a transition metal ion with oxygen may lead to a charge transfer complex (reaction 1.17) or active oxygen, and these active species can then react with polymers (reactions 1.18 and 1.19) [24].

$$M^{n+} + O_2 \longrightarrow M^{n+}\text{---}O_2 \quad (or\ M^{(n+1)+} + O_2) \qquad (1.17)$$
$$M^{n+}\text{---}O_2 + RH \longrightarrow M^{n+} + R\cdot + \cdot O_2H \quad (or\ ROOH) \qquad (1.18)$$
$$(or\ O_2 + H^+ \longrightarrow HO_2) \qquad (1.19)$$
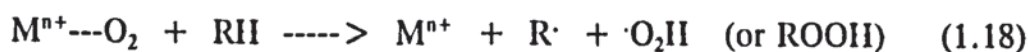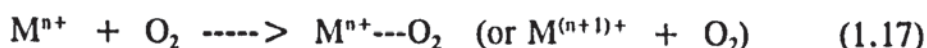
1.3.2.1.4 Decomposition of a Metallic Compound.

Direct decomposition of a metallic compound by an energy source such as light produces an active radical (reaction 1.20) which may subsequently attack the substrate (reaction 1.21) [24].

$$MX \longrightarrow M + X\cdot \qquad (1.20)$$
$$RH + X\cdot \longrightarrow R\cdot + HX \qquad (1.21)$$

1.3.2.1.5 Photosensitising Action.

Triplet sensitisers such as benzophenone accelerate photochemical reactions. Thus the similar energy transfer from excited metallic compounds to polymer substrates can be considered, see scheme 1.2 [25].

$$M \longrightarrow M^*$$
$$M^* + RII \longrightarrow M + RII^*$$
$$RII^* \longrightarrow R^{\cdot} + H^{\cdot}$$
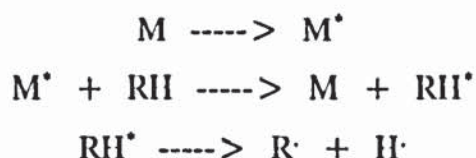
where M = ground state metal M^* = excited state metal
RII = ground state polymer RII^* = excited state polymer

Scheme 1.2 Photosensitisation by Metal Compounds.

1.3.2.2 Possible Modes of Action of Metallic Compounds in Retardation.

1.3.2.2.1 Radical Termination Reactions.

Inhibition of autoxidation has been observed when certain transition metal ions are present in solution at fairly high concentrations. The removal of chain propagating radicals takes place by reaction with either the higher or the lower valence state of a metal ion, probably by a one electron oxidation or reduction reaction.

$$RO_2^{\cdot} + M^{n+} \longrightarrow RO_2^{-} + M^{(n+1)+} \qquad (1.22)$$
$$R^{\cdot} + M^{(n+1)+} \longrightarrow R^{+} + M^{n+} \qquad (1.23)$$

For Co^{2+} [26-28] and for Mn^{2+} [15] termination probably occurs by reaction (1.22). It has already been mentioned that the metal ions that can easily undergo a one electron oxidation or reduction, catalyse the decomposition of the hydroperoxides by a redox mechanism. There is no appparent reason why such metal ions cannot promote chain termination by the similar coupling of reactions (1.22) and (1.23).

1.3.2.2.2 Scavenging of Hydroperoxides.

This group of metallic compounds, known as hydroperoxide decomposers, decomposes hydroperoxides effectively to harmless compounds. For example, metal dialkyldithiocarbamate decompose hydroperoxides according to scheme 1.3 [29,30].

$$\text{ROOH} + \text{R}_2'\text{N}-\text{C}\overset{S}{\underset{S}{\diagdown}}\text{M}\overset{S}{\underset{S}{\diagup}}\text{C}-\text{NR}_2' \longrightarrow$$

$$\text{RO}\cdot + \text{R}_2'\text{N}-\text{C}\overset{S}{\underset{S\cdot}{\diagup}} + \text{H}-\text{O}-\text{M}\overset{S}{\underset{S}{\diagup}}\text{C}-\text{NR}_2'$$

$$\text{R}_2'\text{H}-\text{C}\overset{S}{\underset{S}{\diagup}} + 3\text{ROOH} \longrightarrow (\text{R}_2'\text{N}-\text{C}-\text{S}-\text{OH}) + 2\text{ROH} + \text{RO}\cdot$$

$$\downarrow$$

$$\text{R}'-\text{N}=\text{C}=\text{S} + \text{SO}_2 + \text{R'OH}$$

$$\text{R}_2'\text{N}-\text{C}\overset{S}{\underset{S}{\diagdown}}\text{M}-\text{OH} \longrightarrow \text{R'N}-\text{C}\overset{S}{\underset{SH}{\diagup}} + \text{MO}$$

$$\text{R}_2'\text{N}-\text{C}\overset{S}{\underset{SH}{\diagup}} + 3\text{ROOM} \longrightarrow (\text{R}_2'\text{N}-\text{C}-\text{S}-\text{OH}) + 3\text{ROH}$$

$$\downarrow$$

$$\text{R}'-\text{N}=\text{C}=\text{S} + \text{SO}_2 + \text{R'OH}$$
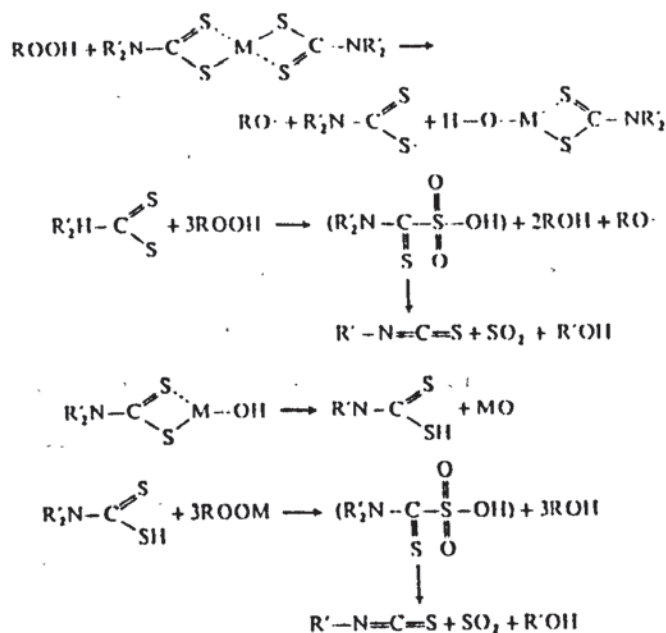
Scheme 1.3 Reaction of metal dithiocarbamate with hydroperoxides [30].

1.3.2.2.3 Screening or Absorption of Radiation.

In the screening process the penetration of UV radiation into polymers is prevented by additives. In the absorption process photostabilisers (UV absorbers) absorb UV light which is harmful towards polymers [12].

1.3.2.2.4 Quenching of Energy.

In this process the excited sate energy is transferred to a metallic compound, then converted into luminescence light and so on. Thus the metallic compound protects the polymer from degradation by reactions (1.24) and (1.25).

$$\text{RH} \relbar\joinrel\relbar\joinrel\rightarrow \text{RH}^\bullet \qquad\qquad (1.24)$$

$$\text{RH}^\bullet + \text{M} \relbar\joinrel\relbar\joinrel\rightarrow \text{RH} + \text{M}^\bullet \qquad (1.25)$$
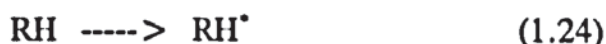
1.3.2.2.5 Quenching of Singlet Oxygen.

It has been suggested that singlet oxygen is involved in the photo-degradation of polymers [32]. In polyolefins singlet oxygen is believed to originate from carbonyl impurities [33]. Recently, deactivation of this singlet oxygen by metallic compounds has been recognised [34]. For example it has been shown that metal dialkyldithiocarbamates quench singlet oxygen as well as decomposing hydroperoxides.

1.3.2.3. Catalyst - Inhibitor Conversion.

Many groups of workers of workers have reported that if the concentration of certain metal ions (Co^{2+}, Cu^{2+}, Mn^{2+}) is increased beyond a certain value, catalysis of autoxidation abruptly ceases and catalysed oxidation does not resume until a lengthy induction period has ended [16,28]. This is shown in fig.1.6, which is taken from the work of Kamiya and Ingold [28] on the autoxidation of tetralin catalysed by Mn(II) and Co(II) decanoates. It can be seen that as the catalyst concentration is increased, a limiting rate of oxidation is reached and that a drastic decrease in the rate of oxygen uptake results when a certain concentration of metal ions is exceeded. The inhibition is thought to occur by the reaction of chain propagating radicals with the metal ions by reactions (1.22) and (1.23).

Aston University

Illustration removed for copyright restrictions

Figure 1.6 The Measured Rate of Oxidation of Tetralin in Chlorobenzene at 65°C as a Function of Manganese Decanoate Concentration [28].

Black [34] has shown that metal-hydroperoxide complex formation can explain the phenomenon of catalyst-inhibitor conversion.

$$M^{n+} + RO_2H \quad [M\text{-}RO_2H]^{n+} \longrightarrow M^{(n+1)+} + RO\cdot + HO^- \quad (1.26)$$

$$M^{(n+1)+} + RO_2H \quad [M\text{-}RO_2H]^{(n+1)+} \longrightarrow M^{n+} + RO_2\cdot + H^+ \quad (1.27)$$
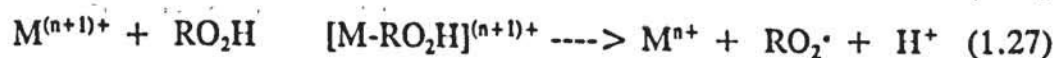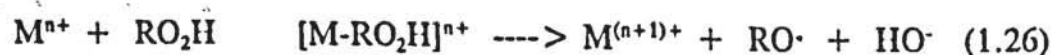
It was shown that when the concentration of Co^{2+} is less than the concentraion of hydroperoxide the metal ions are present in solution almost entirely as the complex, which causes chain termination by reaction (1.22) to be supressed. However, if the concentration of Co^{2+} exceeds that of the hydroperoxide, then free uncomplexed metal ions are present in solution and termination of alkylperoxy radicals takes place by reaction (1.22).

1.3.3. The Prevention of Oxidation.

The oxidation scheme (1.3) reveals several ways in which the oxidative chain reaction may be interupted, however these can be classified into two distinct mechanisms:-

a. Radical chain-breaking mechanism - removes the two important species normally involved in the chain propogating step, the alkylperoxy and alkyl radicals i.e radical scavenging.

b. Preventive mechanism - prevents the introduction of chain initiating radicals into the system.

a. Chain breaking anti-oxidant mechanism (CB) : the oxidation chain may be stopped by reaction of the free radicals produced in the propagation steps (1.2) and (1.3), as shown in scheme 1.1, to give products that are incapable of initiating further chains. Hindered phenols and aromatic amines are commonly used as chain breaking anti-oxidants. Their anti-oxidant activity is associated with their capacity to donate an electron to alkylperoxy and alkoxy radicals (CB-D),(reactions 1.28 & 1.29).

$$RO_2 + ArOH \longrightarrow ArO \cdot + RO_2H \qquad (1.28)$$
$$RO_2 + Ar_2NH \longrightarrow Ar_2N \cdot + RO_2H \qquad (1.29)$$

Phenols are effective antioxidants because the free radical products of these compounds are resonance-stabilised and thus nonreactive compared to most other free radicals.

Deactivation of alkyl radicals may occur via acceptance of an electron, as opposed to the donation, by an antioxidant such as nitroxyl radical. (CB-A mechanism, reaction 1.30). This mechanism is however only important under conditions where a significant concentration of alkyl radicals is present, i.e where there is a deficiency of oxygen or when the rate of initiation is very high [35].

$$\begin{array}{c} H \\ | \\ C\text{-}C\text{-} \end{array} + A\cdot \text{-------}> -C=C- + AH \qquad (1.30)$$
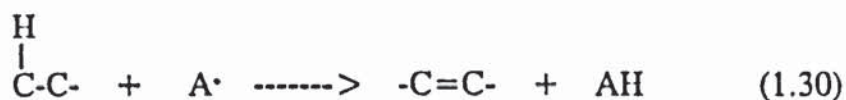
b. Preventive mechanisms : besides removal of oxygen from the system preventive mechanisms include the introduction of agents which prevent the initiation of free radical autoxidation chain mechanism by removing sources of free radical. Three main influences are important to the deterioration of materials in the presence of oxygen, heat, light and metal contamination and they act by either :-

    i) causing molecules to dissociate to give free radicals (C-C, O-O) or by

    ii) activating double bonds (C=C, C=O) to di-radicals.

These compounds are known as preventive antioxidants and can be metal ion deactivators, ultraviolet light deactivators or peroxide decomposers .

In the case of metal ion catalysed oxidation it is clear that removal of the metal ions will lead to a reduction in the extent of oxidation. The effectiveness of a metal ion as a redox catalyst probably depends on the ease of co-ordination and on the redox potential of the metal in the complex. Therefore inhibition of metal catalysed reactions maybe achieved either by stongly complexing to its maximum co-ordination number or by stabilising one valency state at the expense of others. The presence of hydroperoxides in the polymer is a prospective source of free radicals hence decomposition of the hydroperoxide to non-radical products will mean no further initiation due to radical formation from the hydroperoxide can occur, reaction (1.31).

$$\textbf{ROOH + Peroxide Decomposer (D) ----> Molecular products} \qquad (1.31)$$

Two types of hydroperoxide decomposers are known: i) Stoichiometric hydroperoxide decomposers (one hydroperoxide molecule is decomposed by each antioxidant molecule e.g trialkyl phosphites [36]) :-

$$(RO)_3P + R'O_2H \text{-----}> (RO)_3P=O + R'OH \qquad (1.32)$$

ii) Catalytic hydroperoxide decomposers (one molecule can lead to the decomposition of many molecules of hydroperoxide to inert products e.g $\{(RO)_2 PSS\}_2 Zn)$

Oxidative degradation processes
& antioxidant mechanisms

CB-A   chain breaking (electron acceptor)
CB-D   chain breaking (electron donor)
PD   preventive (peroxide decomposing)
UVA   uv absorbers
Q   quenchers
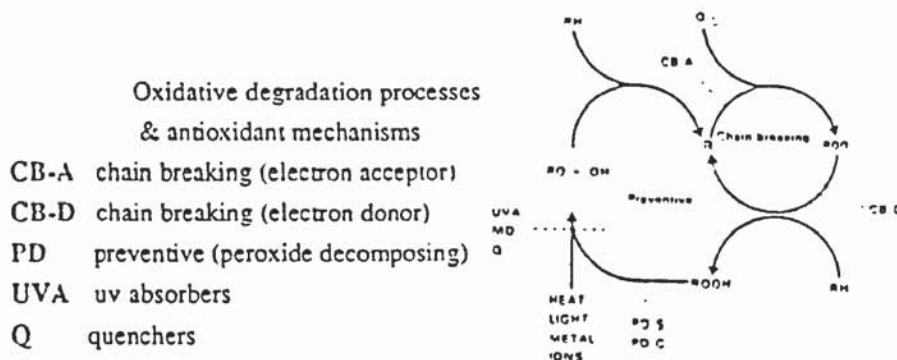
Scheme 1.4 Oxidative Degradation Processes and Antioxidant Mechanisms.

1.4. Thermal and Oxidative Degradation of Polyamides.

The elucidation of the chemistry of degradation of polyamides is still a very controversial subject and although a reasonable understanding of the subject may be obtained by investigating the bond energies associated with the polymer it is unsafe to base a mechanism of thermal degradation on bond energies alone due to the complexity of the process. Kamerbeek et al [37], then later Mortimer [38] asserted that the CH_2-NH bond was responsible for the initial polyamide cleavage. Their arguments were based on the assumption that the weakest bond would break more easily than the stronger bonds, see table 1.3.

Bond	Bond Energy (Kcal.mol^{-1})
CH_2-NH	62
CH_2-CO	71
CH_2-CH_2	80
OC-NH	83
N-H	84
C-H	98
C=O	173

Table 1.3 Bond Energies, of Bonds Related to the Amide Group, at 180°C [38].

However Kakar [39] found he could not assign all the products of nylon 6,6 thermal oxidation to the fission of the CH_2-NH bond alone and proposed that a second bond on nylon 6,6 was also being broken. For polyamides the next theoretically weak bond is the CH_2-CO bond. Although the bond strength is considerably higher than the CH_2-NH bond, hence suggesting the probability of fission to be low, other factors such as neighbouring groups may have a considerable effect on the actual possibility of fission. Goodman [40] believed decomposition involved fission of each bond in and adjacent to the amide group, see figure 1.7.

Points of scission
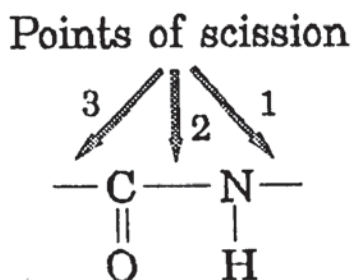
Figure 1.7 Amide Bond Fission According to Goodman [40].

The consequence of the fission of bonds (1) & (2) is the formation of their respective radicals. Dissociation of the CH_2-NH bond generates an amido and alkyl radical (1.33). The CH_2-CO bond dissociates to generate an alkyl and a hydroisocyanate radical (1.34). These radicals formed from either route will become stable entities via a number of different routes, which may or may not involve oxygen.

$$/\backslash/\backslash/CH_2\text{-CO-NH-CH}_2/\backslash/\backslash/ \text{-------} > /\backslash/\backslash/CH_2\text{-CO-NH}\cdot + \cdot CH_2/\backslash/\backslash/ \qquad (1.33)$$

$$/\backslash/\backslash/CH_2\text{-CO-NH-CH}_2/\backslash/\backslash/ \text{-------} > /\backslash/\backslash/CH_2\cdot + \cdot CO\text{-NH-CH}_2/\backslash/\backslash/ \qquad (1.34)$$

The mechanism of radical initiated autoxidation of hydrocarbons in the liquid phase has been studied extensively in recent years [41] and is now generally well understood. The reaction of amides with molecular oxygen, however, has not been so extensively investigated. Early investigations were centred around the oxidation of nylon.

Schwenker [42] first reported the influence of oxygen on the thermal degradation of nylon 6,6 using DTA. Russian Scientists investigating the oxidation of polycaproamide [43] showed that a direct relationship existed between the variation of the absorbance at a certain wavelength in the uv-spectra, and the amount of oxygen absorbed by polycaproamide. The absorption in this region served as a sensitive measure of the degree of oxidation. The oxidised polycaproamide contained a group or groups of atoms with characteristic absorptions in the particular region of interest (2200-3400 A). Furhter investigations showed that water, carbon dioxide, carbon monoxide, acetaldehyde, formaldehyde and methanol were formed in the oxidation of polycaproamide at 190°C, however there was still uncertainty concerning the group responsible for the particular absorbance they were monitoring as a measure of oxidation. The authors proposed a mechanism for the thermal oxidation of polyamides, which gave a good explanation for the formation of all these products. Initiation of the chain process of oxidation was believed to occur by stripping of the most labile hydrogen atom. According to studies of low molecular amines and polyamides the most labile hydrogen atom was situated at the carbon atom next to the N-H group.

Following these initial investigations a number of polyamide investigations were reported particularly by Valko [44], Valk [45] and Harding & MacNulty [46]. Later Sagar and Lock [47], investigating model systems, reported on peroxide and final products of oxidation and from these results progressed to a proposed mechanism for the autoxidation of N-alkyl amides [48,49]. Their, and other [50], kinetic studies also concluded that the oxidation of model systems for polyamides involves initial abstraction of hydrogen from the carbon adjacent to nitrogen.

Sharkey and Mochel also reached the same conclusion concerning the initial hydrogen abstraction [50]. They conducted their work using C_{14} labelled model compounds to determine the position of attack on the polymer chain. At elevated temperatures (>120°C) the following mechanism was thought to predominate (1.35):-

$$-CH_2-\underset{\underset{O}{\parallel}}{C}-\underset{\underset{H}{|}}{N}-\underset{\underset{H}{|}}{\overset{\overset{H}{|}}{C}}-CH_2-\ +\ O_2 \xrightarrow{\text{Heat}}\ -CH_2-\underset{\underset{O}{\parallel}}{C}-\underset{\underset{H}{|}}{\overset{\overset{H}{|}}{N}}-\underset{\underset{OOH}{|}}{\overset{\overset{H}{|}}{C}}-CH_2- \quad (1.35)$$
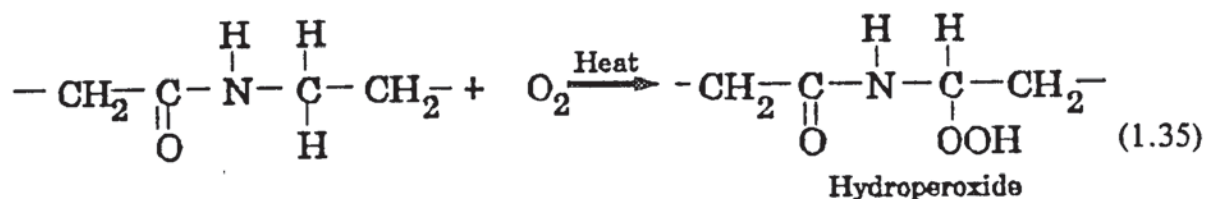
Hydroperoxide

Decomposition of the hydroperoxide leads to the scission of the polymer chain (1.36,1.37):-

$$-CH_2-\underset{\underset{O}{\parallel}}{C}-\underset{\underset{H}{|}}{\overset{\overset{H}{|}}{N}}-\underset{\underset{OOH}{|}}{\overset{\overset{H}{|}}{C}}-CH_2- \xrightarrow{\text{Heat}}\ -CH_2-\underset{\underset{O}{\parallel}}{C}-\underset{\underset{H}{|}}{\overset{\overset{H}{|}}{N}}-\underset{\underset{O\cdot}{|}}{\overset{\overset{H}{|}}{C}}-CH_2-\ +\ \dot{O}H \quad (1.36)$$

$$\cdot CH_2-\underset{\underset{O}{\parallel}}{C}-\underset{\underset{H}{|}}{\overset{\overset{H}{|}}{N}}-\underset{\underset{O\cdot}{|}}{\overset{\overset{H}{|}}{C}}-CH_2- \xrightarrow{\text{Heat}}\ -CH_2-\underset{\underset{O}{\parallel}}{C}-\underset{\underset{H}{|}}{N}-\underset{\underset{H}{|}}{C}=O\ +\ \dot{C}H_2- \quad (1.37)$$
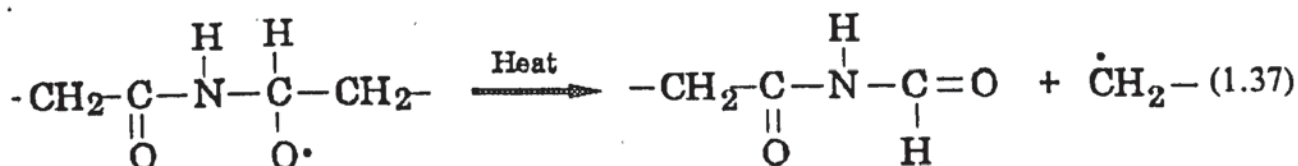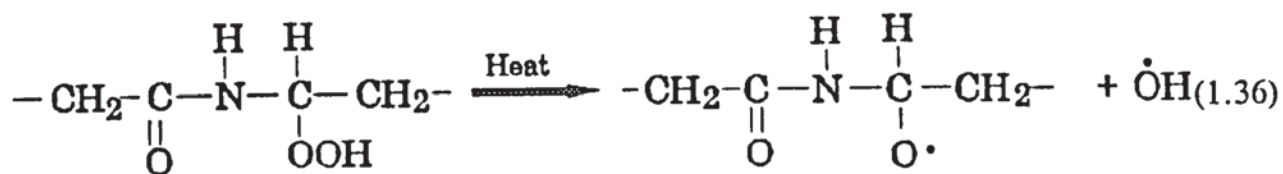
The role of peroxides in autoxidation has been well established for a number of years and peroxidic products of oxidation have been isolated from a large number of autoxidised substrates [51]. It was indicated by Lock and Sagar that some of the stable products of autoxidation of N-alkyl-amides arose as a result of the decomposition of unstable intermediates [47]. Further work by Sagar [48] dealt with the properties of a number of N-alkyl-amide peroxides that were isolated from oxidised amides. Formation of the hydroperoxide during autoxidation was dependent upon the ability of the $RO_2\cdot$ radical to abstract a H atom fom the substrate. The study [48] included the effect of transition metal ions, of variable valency, upon the decomposition of hydroperoxides. The effect was shown to be considerable, for example Sagar showed as little as 0.4ppm of Co^{2+} (as cobaltous acetate tetrahydrate) increased the initial apparent 1st-order rate constant of decomposition of 1-propionamidopropyl hydroperoxide at 77°C ten-fold as shown in figure 1.8 [48]. The catalytic effect disappeared after about 50% of the hydroperoxide had decomposed, and the final apparent 1st-order rate constant was close to that of the uncatalysed decomposition. Similar decreases with time have been observed for the cobalt catalysed decomposition of tetralin hydroperoxide [52].

Figure 1.8 Kinetics of Peroxide Decomposition under Nitrogen at 77°C [48].

Sagars [49] also studied the thermal oxidation of N-n-propylpropionamide in the temperature range 77-131°C. It was found [49] that the formation of hydroperoxide was initially autocatalytic and then approached a steady rate (fig.1.9). The presence of added hydroperoxide reduced the induction period (figure 1.10 & 1.11) [49] but was without effect on the steady rate of formation of hydroperoxide. Formation of the stable products (propionamide, N-propionylpropionamide, N-formylpropionamide) was also autocatalytic but lagged behind that of hydroperoxide. Their formation was not interupted when, after an appreciable build-up of hydroperoxide, the oxygen stream was replaced by nitrogen (fig.1.12 & 1.13) [49]. This showed clearly they were formed principally by molecular decomposition of the hydroperoxide. The non-radical concerted breakdown of hydroperoxide would be unaffected by oxygen. Sagars [49] results also showed a gradual fall in total yield of(hydroperoxide + products) when the oxygen was replaced by nitrogen indicating that other nitrogen containing compounds are formed. The sudden drop in hydroperoxide concentration was shown not to be due to autocatalytic decomposition but marked the onset of intense autoinhibition. He concluded therefore that oxidation was governed by three processes i) the first predominating in the earlier stages, was the chain reaction of the substrate with oxygen, giving an N-alkyl amide hydroperoxide as the primary product, ii) the second, occurring throughout the oxidation was the thermal decomposition of this hydroperoxide and iii) the third, increasing in importance as the reaction progressed, was interference in the oxidation chain by one or more of the products of hydroperoxide fission.

Aston University

Illustration removed for copyright restrictions

Sagar proceeded to study the autoinhibition and influence of the reaction products. The principal volatile products, water, ethanol and propionaldehyde, when bled into the oxygen supply did not inhibit oxidation. A samll amount of acid was also produced during the oxidation but added carboxylic acids were not inhibitors. Autooxidation was only marginally retarded by N-2-hydroxypropylpropionamide, a minor product. Whilst it had been shown by Sagar that amines and isocyanides effectively inhibit autoxidation, by their addition in the oxygen stream into N-n-propylpropionamide at 131°C, neither of these could be detected hence the exact nature of the autoinhibition remained uncertain.

The effects of variable vaency metal salts on autoxidising systems can be extremely complicated and are governed by the reactions with hydroperoxides, probably through formation of complexes which then decompose to give radicals [53]. The influence of traces of transition metal salts on the autoxidation of N-alkyl-amides was therefore only briefly examined by Sagar. He found the effect of small amounts of Co^{2+} very striking (cf. figure 1.14 and 1.9). Oxidation in the presence of Co^{2+} was faster but still autocatalytic. Woodward and Mesrobian [54] showed that the steady rate of oxidation of tetralin was independent of the concentration of cobaltous acetate, in contrast the pseudo-steady rate of autoxidation of N-n-propylpropionamide was increased approximately five to six fold by addition of cobaltous acetate. At higher metal salt concentrations it was suggested that higher rates of overall decomposition of hydroperoxide should result. Indeed, when 50ppm Co^{2+} was added initially, hydroperoxide was not detected at any stage during the oxidation, the stable products, however were rapidly formed.

At a Co^{2+} concentration of 50ppm Sagar observed directly the change in the oxidation state of the metal. During the initial conditioning period under nitrogen the N-alkyl amide solution was pale violet. Within 15 sec. of the start of oxidation the cobalt was converted to the +3 state and the solution became pale green but after about 10 min. the Co^{2+}-Co^{3+} equilibrium favoured the cobaltous state and the solution became blue again. Similar changes in the oxidation state of cations have been observed [55] in many studies of catalysed oxidations of hydrocarbons.

fig 1.12 Kinetic curves for the accumulation of (1) 1-propionamidopropyl hydroperoxide, (2) propionamide, (3) N-propionylpropionamide, (4) N-formylpropionamide, and (5) Σ [(1), (2), (3), and (4)] at 131° in N-n-propylpropionamide (vacuum distilled into quartz receiver before start of the oxidation). Oxygen stream replaced by nitrogen after 135 min.

fig 1.13 Kinetic curves for the accumulation of (1) 1-propionamidopropyl hydroperoxide, (2) propionamide, (3) N-propionylpropionamide, (4) N-formylpropionamide, and (5) Σ [(1), (2), (3), and (4)] at 131° in N-n-propylpropionamide (prep. 1, fraction 10 stored under argon in Pyrex tube for 124 weeks-   Oxygen stream replaced by nitrogen after 60 min. [49]

fig 1.14   Kinetic curves for the accumulation of (1) 1-propionamidopropyl hydroperoxide, (2) propionamide, (3) N-propionylpropionamide, (4) N-formylpropionamide, and (5) Σ [(1), (2), (3), and (4)], in the thermal oxidation at 131° of N-n-propylpropionamide containing initially added 1-propionamidopropyl hydroperoxide (0·006 mole kg.⁻¹) and cobaltous acetate tetrahydrate (6·7 × 10⁻⁶ mole kg.⁻¹) [49]

The metal ions are assumed to catalyse the decomposition of the hydroperoxide by the reactions (1.38 and 1.39) [55], a well established function of metal ions, ie. as radical initiators, previously discussed in this chapter.

$$ROOH + Co^{2+} ----> RO^{\cdot} + Co^{3+} + {}^{\cdot}OH \qquad (1.38)$$

$$ROOH + Co^{3+} ----> RO_2^{\cdot} + Co^{2+} + H^{+} \qquad (1.39)$$
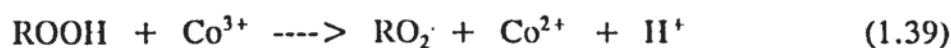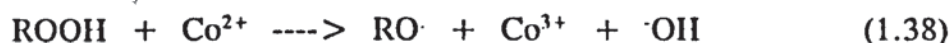
1.5. Previous Investigations into MXD6 Oxygen Scavenging.

1.5.1. Oxygen Scavenging by MXD6 Compounds [56].

Work was undertaken to ascertain which part of the MXD6 compound was responsible for oxygen scavenging and if any other mono/polyamides could produce a similar effect. It seemed likely at the time that cobalt was interacting with the polyamide chain, however interaction with a mono or diamide should be the same and provided an easier method of study. Therefore a range of mono and diamides, MXD6 model compounds (see table 1.4), were synthesised, with varying structures, and their scavenging capabilities, with and without cobalt were measured.

Model Number	Chemical Structure
1	PhCH$_2$NHCOCH$_2$CH$_3$
2	PhCH$_2$NHCO(CH$_2$)$_4$CONHCH$_2$Ph
3	PhNHCO(CH$_2$)$_4$CONHPh
4	CH$_3$CH$_2$CONHCH$_2$(C$_6$H$_4$)CH$_2$NHCOCH$_2$CH$_3$
5	PhCH$_2$CONH(CH$_2$)$_5$CH$_3$
6	CH$_3$CH$_2$CONH(CH$_2$)$_6$NHCOCH$_2$CH$_3$
7	Low m.wt MXD6

Table 1.4 The Range of MXD6 Model Compounds Synthesised for the Oxygen Scavenging Study [56].

The results indicated that from the seven compounds tested only three scavenged oxygen on their own to some extent and vigorously in the presence of cobalt. The three models had in common the structural unit (I).

$$-CO-NH-CH_2 \underset{}{\bigcirc} CH_2-NH-CO- \qquad (I)$$
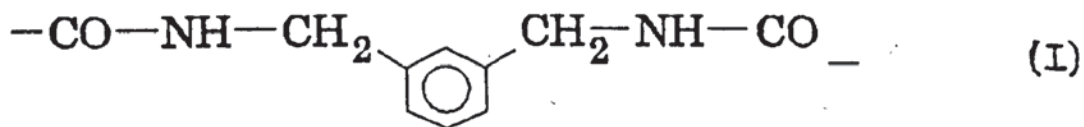
It was therefore believed that scavenging occurs at the benzyl $-CH_2$ sites. A further series of MXD6, model compounds, were prepared (see table 1.5) with a view to clarify he situation further but none of the models showed any activity. However rearrangement of the structures in this precise manner led to the conclusion that for oxygen scavenging to occur there has to be, i) 2 amide links, ii) reactive $-CH_2$ groups adjacent to the benzene ring, iii) the -NH group in the amide link next to the $-CH_2$ group iv) if a disubstituted benzene is involved only the meta isomer is active ie, the scavenging only occurs when the model compound contains the structural unit (I).

Model Number	Chemical Structure
8	$CH_3(CH_2)_2CONH(C_6H_5)NHCOCH_2CH_3$
9	$CH_3(CH_2)_5NHCO(C_6H_4)CONH(CH_2)_5CH_3$
10	$CH_3(CH_2)_5NHCOCH_2(C_6H_4)CH_2CONH(CH_2)_5CH_3$
11	(p)- $CH_3(CH_2)_2CONHCH_2(C_6H_5)CH_2NHCOCH_2CH_3$
12	$PhCH_2CONH(CH_2)_6NHCOCH_2Ph$
13	Adipic Acid
14	m-xylylenediamine

Table 1.5 The Further Range of MXD6 Model Compounds Synthesised for the Oxygen Scavenging Study [56].

1.5.2. Screening of a Range of Metals for Oxygen Scavenging with MXD6 [57].

Low molecular weight MXD6, or model compounds that closely resemble the structure of MXD6, are known [53] to scavenge oxygen when mixed with cobalt. It has also been shown that nylon 6,6/25ppm Cu in a polypropylene matrix exhibits scavenging activity, additionally nylon 3,3, N,N'-dibenzyladipamide and metaxylylene-1,3-dibutanamide scavenge oxygen when mixed with either 200ppm cobalt or 25ppm copper [56,58]. It is also well known that copper in high concentrations acts as an anti-oxidant thereby stabilising polyamides [59,60]. Therefore bearing in mind these effects, work was undertaken [54] to ascertain if any other metals could promote the oxygen scavenging effect with MXD6.

Thirteen different metals were screened for oxygen scavenging effectiveness encorporated in the low molecular weight MXD6 in three different concentrations, 20, 200 and 2000ppm. The metals screened consisted of :- tungsten, cobalt, chromium, copper, lead, molybdenum, manganese, iron, nickel, cerium, palladium, silver and vanadium. The results indicated that cobalt (20,200 & 2000ppm), copper (20ppm) and vanadium (200 & 2000ppm) promoted oxygen scavenging in MXD6. Cobalt and copper more so than vanadium. Most of the other metals did not show any effect. However, some metals stabilised the MXD6 and acted as anti-oxidants. These included: Tungsten (20,200 & 2000ppm), Copper (2000ppm), Palladium (2000ppm) and Silver (200 & 2000ppm). However when mixed with a PET/MXD6 blend only cobalt (200ppm) in the blend was shown to result in material (in the form of bottle containers) with improved oxygen scavenging properties.

1.5.3. Oxygen Scavenging by a Range of MXDn Homologes [61].

Having established the importance of cobalt to the super barrier effect [54], in preference to other metal ions, work was also undertaken [61] to ascertain if other MXDn homologues scavenged oxygen, and if so, what the optimum chain length was. It seemed likely that if coordination between amide and metal does occur, the coordinating site would be the carbonyl moiety in the amide link, forming a ring system as shown in figure 1.15.

Ring Structure
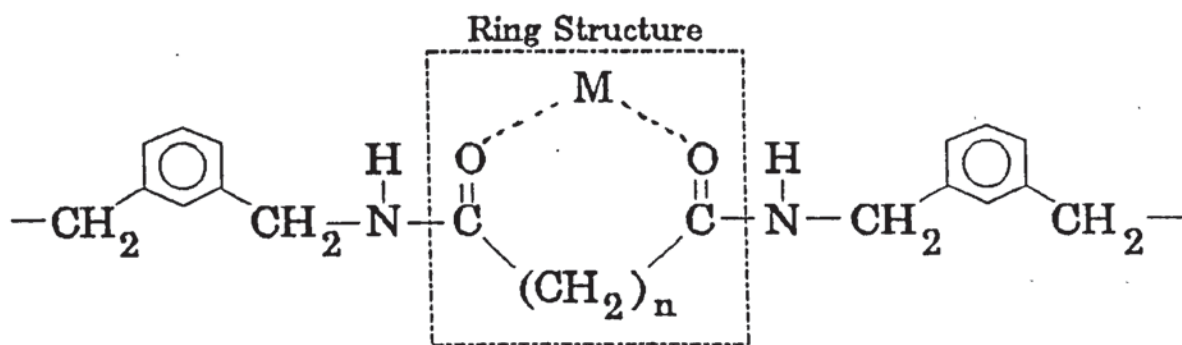
Figure 1.15 Coordination Between Amide and Metal Ion, Via the Carbonyl Group, Resulting in a Ring System.

This type of coordination behaviour is well known for B-diketonate ligands such as acetyl acetonate [62,63]. Fewer members in the ring leads to more strain and therefore chelation will not occur as the ring would be unstable [64,65]. However, too many members in the ring leads to unstability on entropy grounds. A range of MXDn homologues were synthesised with a varying number of carbon atoms in the carboxylic part of the chain (II). The oxygen uptake of each model compound, with and without cobalt, was measured and is summarised in table 1.6.

$$\text{-\{-HNCH}_2 \underset{\bigcirc}{} \text{CH}_2\,\text{NHOC(CH}_2)_n\,\text{CO-\}-}_x \tag{II}$$
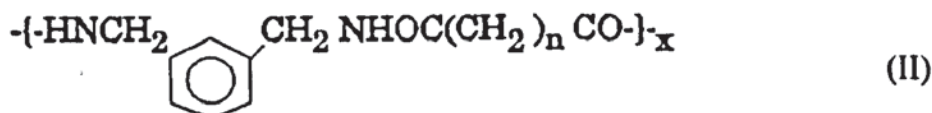
n	MXD_x	Ring Size	O_2-Scavenging Efficiency	
			without cobalt	with cobalt
0	2	5	None	None
1	3	6	Slight	Enhanced
2	4	7	Most Vigorous	Most Vigorous
3	5	8	Vigorous	Vigorous
4	6	9	Slight	Vigorous
6	8	11	None	Vigorous
8	10	13	None	None

Table 1.6 The Oxygen Uptake Assessment of a Range of MXDn Homologues [61].

The polyamides that do exhibit an effect are capable of forming a relatively unstrained bidentate complex with the metal catalyst (see table 1.6). It was shown [61] that MXD2, a short carbon chain, and MXD10, a long carbon chain, produced no scavenging effect possibly due to the steric hindrance associated with a short or very long carbon chain hampering the formation of the chelate ring. The two polyamides that scavenged oxygen vigorously in the pure state, MXD4 and MXD5, still showed a vigorous oxygen uptake when mixed with the metal. Enhanced oxygen scavenging by the polyamide with metal catalyst present was observed for MXD5, MXD6 and MXD8. These results indicate that the optimum ring size is 7 members.

1.5.4. NMR and ESR Investigations [66].

Nuclear magnetic resonance studies were carried out on various polymers and blends relevant to the MXD6/PET scavenging system. The work was directed towards understanding the metal ion/MXD6 interactions in solution. It was found [66] that transition metal ions from the acetates of cobalt, copper, manganese and iron interacted with the carbonyl group of the amide in MXD6. The interaction caused a reduction in the peak height and broadening of the amide carbonyl resonance. However, ^{1}H NMR spectra suggested that Mn, Fe and Cu formed point contacts with the rest of the polymer chain at CH and NH sites and in this respect were different from the cobalt species. Non-transition metal acetates (Ca, Mg and Zn) did not produce these interactions, as was evident from the amide -carbonyl resonance signal. Other possibilities may exsist for the results obtained but the conclusion drawn above may be relevant to the observation that cobalt salts are the most effective catalysts for oxygen scavenging in MXD6 among all the metal ions tested in the above work [66].

Electron spin resonance studies were carried out [67] on various polymers and blends relevant to the MXD6/PET scavenging system. The technique provides chemical information at the molecular level on the basis of the magnetic properties of unpaired electrons. The main result obtained from the ESR investigation was the observation of a free radical signal in samples of MXD6 fibres heavily doped with cobalt salt. This signal could tentatively be assigned to superoxide (O_2^-). Evidence of the superoxide led to the speculation of the reaction mechanism.

1.5.5. Mechanistic Proposal for Oxygen Scavenging in PET/MXD6 System by Cobalt[68].

The results from the investigations dicussed above [66,67], including the results obtained from the MXDn homologues, MXD6 compounds, NMR and ESR investigations, led to the proposal of a reaction mechanism. The initiating species was thought to be a complex formed between the cobalt ions and the MXD6 chain (1.40). This complex interacts with oxygen to form a 'superoxide' (1.41) which then abstracts H-atoms to generate radical species ($\cdot$OH and $\cdot O_2H$), (1.42).

$$2L + Co^{2+} ----> L_2Co^{2+} \qquad (1.40)$$

$$L_2Co^{2+} + O_2 ----> L_2Co^{3+}O_{2\cdot} \qquad (1.41)$$

$$\text{(L= ligand from MXD6)}$$

$$L_2Co^{3+}O_{2\cdot} + RH ----> L_2Co^{2+} + R\cdot + \cdot O_2H \qquad (1.42)$$
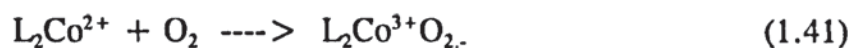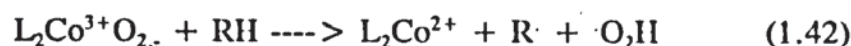
$$\text{(RH = MXD6)}$$

The reaction propagates in the solid phase due to oxygen reacting with reactive sites on the MXD6 which were generated from labile species ($\cdot$OH & $\cdot O_2H$) created in the initiation reactions and subsequent propagation reactions, (1.43-1.49).

$$\cdot O_2H + RH ----> HOOH + R\cdot \qquad (1.43)$$

$$HOOH -----------> 2 HO \qquad (1.44)$$

$$RH + \cdot OH ----> R\cdot + H_2O \qquad (1.45)$$

$$R\cdot + O_2 ----> RO_{2\cdot} \qquad (1.46)$$

$$RO_{2\cdot} + RH ----> RO_2H + R\cdot \qquad (1.47)$$

$$RO_2H -----------> RO\cdot + \cdot OH \qquad (1.48)$$

$$RO\cdot + RH ----> ROH + R\cdot \qquad (1.49)$$
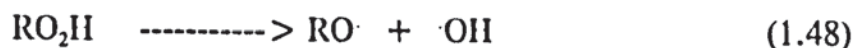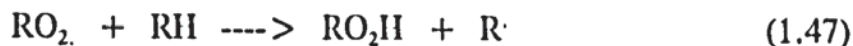
Termination was thought to occur in a number of ways :

$$ROH \text{ or } RO\cdot ----> \text{aldehyde} ---> \text{acid}$$

$$----> \text{primary amide} ---> \text{acid} + \text{ammonia}$$

$$----> \text{cross linked gel (in blends)}$$
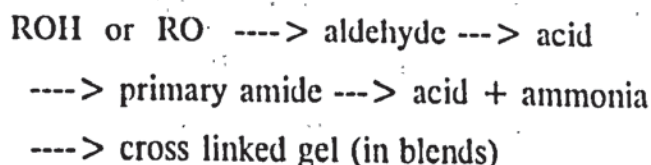
The fundamental question arising from the proposed mechanism however, involved the role of the cobalt. For the oxidation of hydrocarbons in solution, metal catalysts are believed [68] to act in two ways :-

a) in initiating the chain of autoxidation by forming reactive radicals.

b) for the conversion of hydroperoxides to secondary oxidation products.

The questions remaining are, therefore, i) does the cobalt shorten the induction period before scavenging occurs so that the oxidation can propagate at a useful rate, ie, is the cobalt an initiation catalyst or ii) does cobalt increase the rate of the propagation reaction.

1.6. Limitations of Experimental Techniques.

1.6.1. Oxygen Absorption.

The oxidative stability of many materials has been studied using oxygen uptake apparatuses. Numerous oxygen uptake apparatuses were developed for the study of biological samples, rubbers, fats, oils as well as synthetic polymers. Shelton [69] described three types of oxygen absorption studies concerned with the oxidation of rubber. The simplest procedure was based on the measurement of increased weight but this suffers from the disadvantage that small weight increases are difficult to measure accurately. Moreover this method does not take into account the loss of low molecular weight oxidation products. The other two methods, manometric and volumetric, known as replacement techniques, involve measurement of the reduction in oxygen pressure at constant volume and the reduction, at constant pressure, in volume respectively.

Recently the advent of sensitive pressure transducers has made possible the construction of oxygen uptake apparatuses which are capable of monitoring the incipient stage of oxidation at mild temperatures or ultra-violet light intensities. Bigger et al [70] used such an apparatus to help provide useful information, such as the activation energy for the oxidation of polyethylene which, together with data obtained by chemiluminescence, thermogravimetry, melt flow and carbonyl index measurements, enabled a collective assessment of the thermal stability of the materials to be made.

The main problem that occurs with methods relying on measurment of pressure changes is, however, the possible production of volatiles from the degrading compound under analysis. The method is based on the measurement of pressure differences between a sample flask and reference flask. As the sample absorbs oxygen this produces a pressure difference between the two flasks which is recorded as volume of oxygen absorbed. If, however, the sample produces volatiles during degradation this will alter the pressure in the sample flask, with respect to the reference flask, hence distracting the reading of oxygen aborbed.

1.6.2. Spectral Studies.

Infra-red spectroscopy provides a rapid, nondestructive technique for the study of the extent and nature of the reactions involved in the oxidative deterioration of polymers [71-75]. A major attraction of the technique is that it is capable of identifying and following quantitatively the loss or growth of particular functional groups. The growth of carbonyls is a recognised means of following the photooxidation of many polymers, such as PE, PP, PS and PVC [76]. Although IR spectroscopy remains uncontested in importance for the characterisation of polymer structure, it should be emphasized that only limited and partial problems can be solved by the exclusive application of IR spectroscopy. UV spectroscopy has also proved a valuable technique for following the formation of functional groups in autoxidising systems [77]. The limitations of spectral studies however include the inability to pick out non-absorbing groups of importance in autoxidation (eg, ethers, epoxides etc) and the failure to distinguish unequivocally different chemical modifications of the same group (eg, hydroxyl group in alcohols and hydroperoxides, carbonyl groups in esters, ketones etc).

1.6.3. Thermal Analysis.

Thermal methods which are relevant to stability studies include, thermogravimetry (TG), differential thermal analysis (DTA), differential scanning calorimetry (DSC), thermal mechanical analysis (TMA), thermal volatilisation analysis (TVA) and torsional braid analysis (TBA). The general application to polymer studies has been reported elsewhere [78-79]. The listed techniques above that were thought useful and incorporated in this study

included:

i)   Thermogravimetry (TG) : involves a dynamic programmed temperature rise and monitors weight loss as a function of temperature.

ii)   Isothermal weight loss (IWL) : monitors weight loss as a function of time at a specific temperature.

iii)   Differential thermal analysis : differential temperature is monitored as a function of increasing temperature which is raised at a controlled rate.

iv)   Differential scanning calorimetry : differential energy required to maintain the sample and the reference at the same temperature is monitored as a function of increasing temperature which is raised at a controlled rate.

Both TG and DTA/DSC (the former more commonly) have been used to evaluate the apparent kinetic parameters of polymer degradation reactions, namely the activation energy E. The application of TG in polymer degradation studies has been reviewed in detail by Reich and Levi [80] and Flynn and Wall [81]. In addition the application of TG and DTA to the kinetics of decomposition of solids is adequately described in the literature [82-85]. In using TG and isothermal weight loss studies to evaluate kinetic data for stability assessment it should be noted that methods involving a single TG curve for the determination of gradients have been found to be unreliable and not suitable for kinetic analysis of decomposition reactions which proceed via a complex mechanism [81,86]. Therefore in this study (The Oxidation Styudies of Novel Barrier Polymer) a method involving a minimum of three curves, similar to that described by Ozawa [87], was used however it proved to be more time consuming and isothermal studies are not free from problems. The major cause of error in this case being associated with the time taken for the sample to attain the isothermal temperature and the weight loss occuring during this heating up period. This can however be eleviated to some extent by allowing thermal equilibrium to be established with argon/nitrogen flowing over the sample and then changing the gas to oxygen or air.

1.6.4. High Performance Liquid Chromatography.

High performance liquid chromatography (HPLC) has developed into one of the most useful and widely used analytical tools. The simplicity and ease of use, together with its ability to separate complex mixtures has led to the utilisation of HPLC in many branches of chemistry. In this particular study it was used to separate the products of oxidation of a model compound representative of a host polymer. A wide range of columns with vastly different selectivities has been developed. These offer the potential to separate components of increasingly complex mixtures. The problem of developing an HPLC method involves achieving an acceptable degree of separation between all components of interest in a minimum amount of time. However method developement in HPLC is a fairly complex task and an can be fairly time consuming in order to obtain an acceptable chromatographic separation.

The variables to be considered when developing a HPLC method include :-
        i) mode of chromatography
        ii) column packing
        iii) eluent
        iv) detection mode
        v) sample preparation
        vi) physical parameters (temperature, flow rate, column dimension)

The high number of variables involved require careful selection and an ordered appproach to achieve separation particularly of complex samples.

1.7 Objective.

At Carnaud MetalBox Packaging Technology, a polymer system has been identified which is based on a blend of a polyester, poly(ethylene terephthalate) and an aliphatic-aromatic polyamide, MXD6, producing a packaging material which balances properties such as strength, rigidity and cost as well as good oxygen barrier properties. However with the addition of between 50-200ppm of a variable valency metal ion, viz cobalt (Co^{2+} when added), the system was shown to reduce the permeation of molecular oxygen to below limits of detection.

It was proposed that many of the extraordinary properties shown by the blend were due to the behaviour of the oxidisable organic component, the MXD6, which was thought to scavenge oxygen in the walls of the container aided by cobalt behaving as as a catalyst. The main objectives of this study were therefore :-

1. To investigate the mechanism of oxidation of the polyamide component of the blend via the examination of a series of model compounds, having different chemical structures based on the structure of MXD6 and,

2. To examine the effect of different concentrations of cobalt and sodium phosphite (an antioxidant normally present in the MXD6 component) on the oxidation of the model compounds with the aim of identifying the role of the different structural components o f the model on the mechanism of its oxidation in the presence of cobalt.

Kinetic studies of the oxidation process were carried out using oxygen absorption equipment, spectral studies and thermogravimetric analysis at elevated temperatures. The nature of transformation products and intermediates formed during the reaction was paramount to the construction of a reaction mechanism. Identification of these products was achieved by analysing the various samples using spectroscopic and chromatographic techniques, particuarly HPLC.

Chapter 2. Experimental.

2.1 Materials Employed.

2.1.1. Materials Synthesised.

In order to study the mechanism responsible for the super barrier effect it was convenient to prepare a low molecular weight model compounds that accurately represented the repeat unit of the host polymer. By selecting a compound which represented a small part of the polymer chain, the number of separate reactions occuring was greatly reduced. This allowed the reactions to be studied in more detail since it was easier to isolate and identify the transformation products. Models were chosen which represent different sections of the polymer (MXD6) chain, containing two amide groups since the diamide was shown to be nescessary for the absorbtion of oxygen [56].

$$-[-HNCH_2 \underset{\bigcirc}{} CH_2NHOC(CH_2)_4CO-]-_n$$

(MXD6)
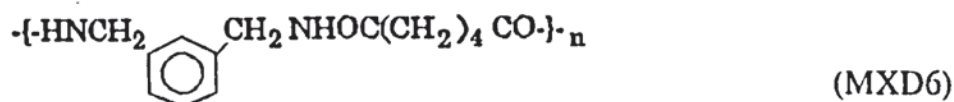
The first model (I) chosen in this work was simlar to model 4 (see section 1.5.1) tested by Carnaud MetalBox and was shown to absorb oxygen. The only difference was the length of the aliphatic chain. Here it was increased to five carbons to mirror the host polymer and represents 1.5 units of the chain.

$$CH_3(CH_2)_4CONHCH_2 \underset{\bigcirc}{} CH_2NHCO(CH_2)_4CH_3$$
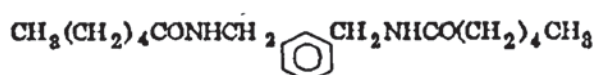
Model I : Benzene-1,3-Dimethyl Hexanamide (I)

The second model (II) represented the aliphatic portion of the chain between the two aromatic rings and was similar to model 12 (section 1.5.1) tested by Carnaud MetalBox. The only difference again was the length of the aliphatic chain which in this case was decreased to four carbons as opposed to six.

$$\underset{\bigcirc}{} CH_2NHCO(CH_2)_4CONHCH_2 \underset{\bigcirc}{}$$
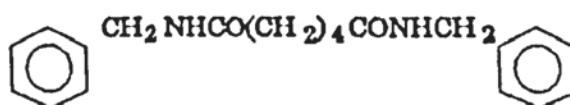
Model II : Hexanedioate-bis-Benzylamide (II)

2.1.1.1. Preparation of Model I : Benzene-1,3-dimethylhexanamide.

Reaction scheme 2.1 details the method first used to produce the first model of MXD6, benzene-1,3-dimethyhexanamide, via a two stage synthesis [88-91]. The first stage involved the formation of methyl hexanoate from hexanoic acid and an exess of methanol (5 times the number of moles of acid) which were pipetted into a suitable round bottom flask. This was placed in a heating mantle and a thermometer and a reflux condenser added. The solution was heated until a gentle reflux was obtained and then concentrated sulphuric acid (1.0 cm^3) was added down the condenser. The mixture was left under reflux overnight and then allowed to cool. The acid was removed from the cold solution by washing with distilled water(3x100 cm^3).The organic layer was then returned to a clean flask and slowly distilled with the product being collected over the range 149" to 152"C.
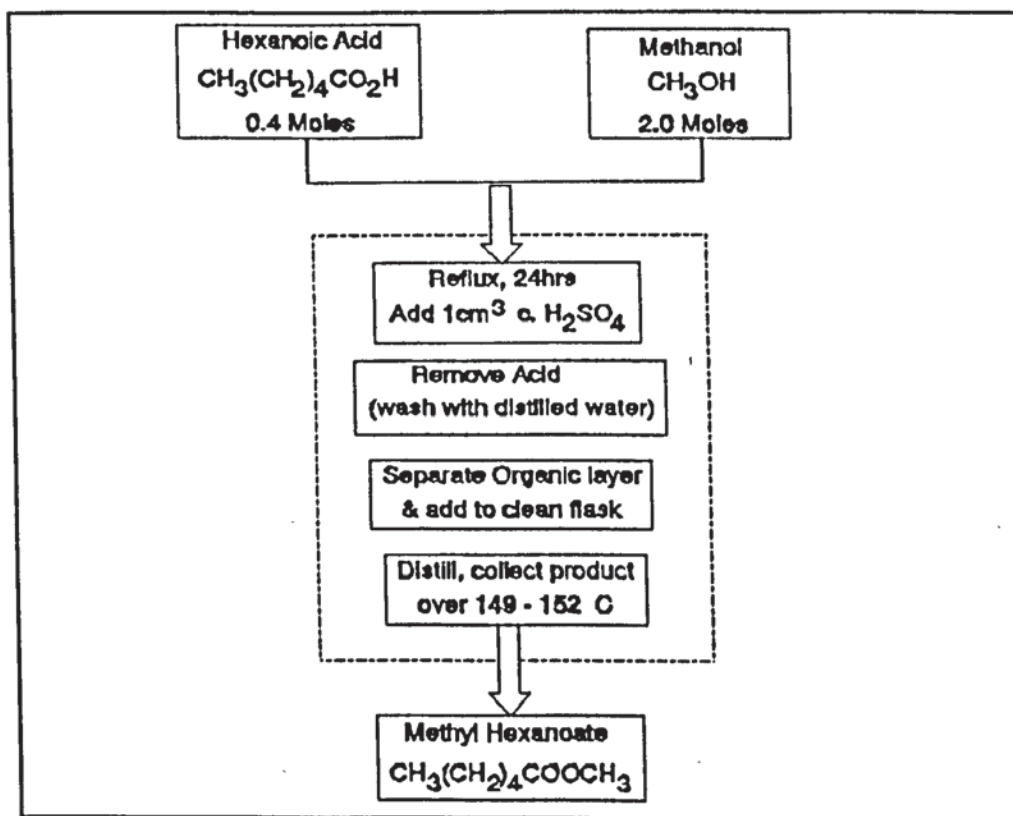
Scheme 2.1. Preparation of Methyl Hexanoate : Esterification of Hexanoic Acid.

The ester was then reacted with m-xylylene diamine to form the corresponding diamide, see scheme 2.2. The ester and a stoichiometric quantity of the diamide (0.48 times the number of moles of ester) were placed in a round bottomed flask and set up under reflux as before. The solution was refluxed gently for four hours where upon a white crystalline solid begen to separate. The mixture was heated for a further 30 minutes before cooling.
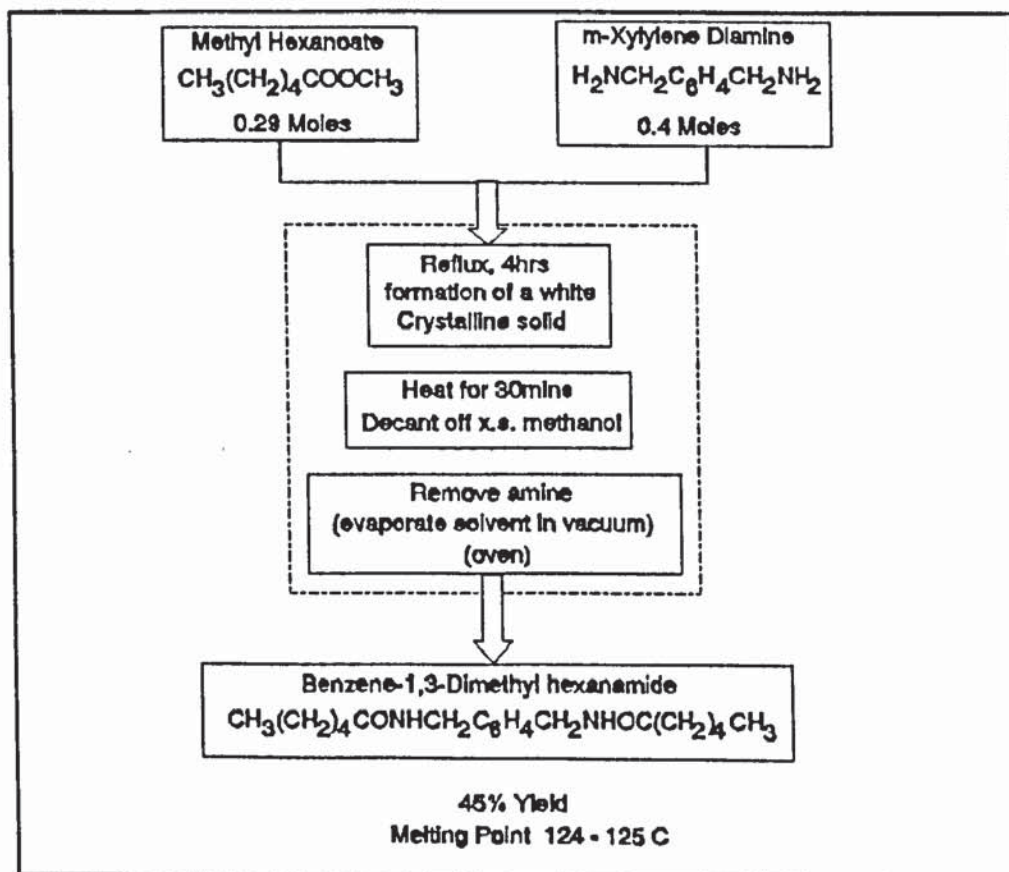
Scheme 2.2. Preparation of Benzene,1,3 Dimethylhexanamide (ModelI) : the Reaction of Methyl Hexanoate and m-Xylylene Diamine.

The diamide was obtained as a soft white powder with a melting range of 124° to 125.5°C. The overall percentage yield with respect to the acid was 45%. The sample was submitted for IR and ^{13}C NMR analysis, see figures 2.1 and 2.2, respectively.
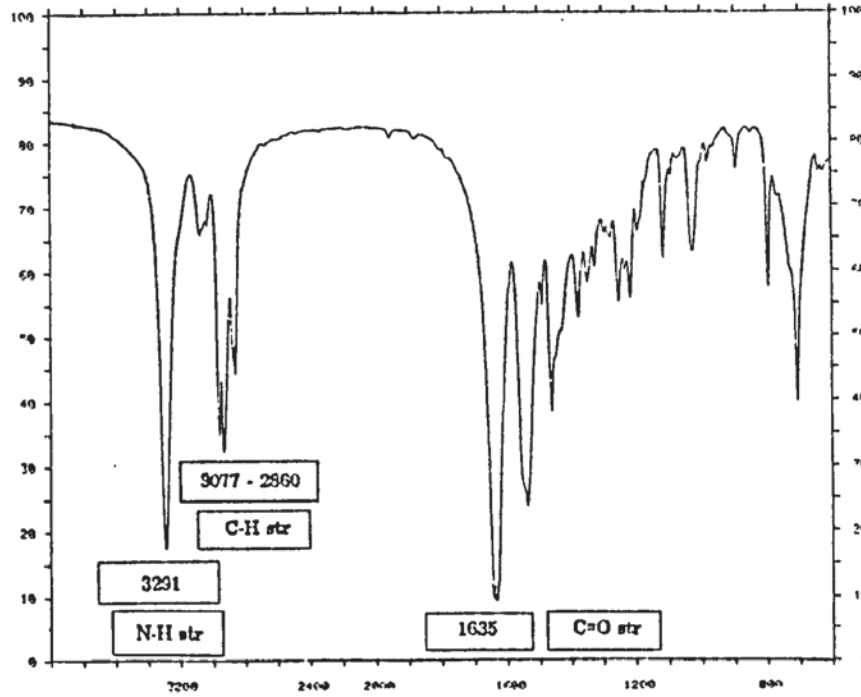
Figure 2.1 FT-IR Spectra of Model I : Benzene 1,3 Dimethylhexanamide (as Kßr Disc).

Carbon N°.	(ppm)	I (%)
1	13 84	5 83
2	21.87	-8 04
3	24 99	-10 84
4	30.94	-8 80
5	35.31	-11.31
6	172.06	-3 99
7	41.90	-12 02
8	139.76	-4 59
9	128.13	5.80
10	125.49	11.33
11	125.91	6.07
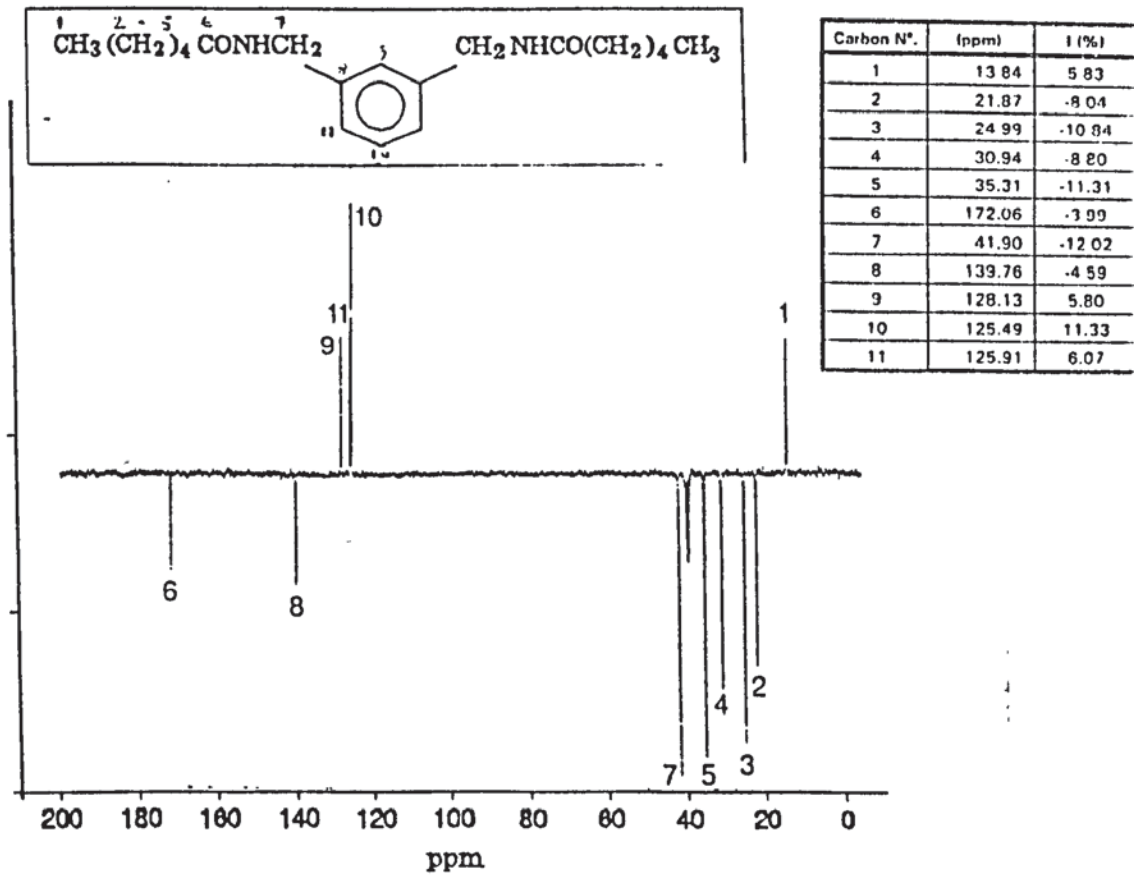
Figure 2.2 ^{13}C NMR Spectra of Model I : Benzene 1,3 Dimethylhexanamide (in DMSO).

2.1.1.2. Preparation of Model II : Hexanedioate-bis-benzylamide.

Model II was synthesised by direct reaction of the two components, dimethyl adipate and benzylamine, to produce the salt. Dimethyl adipate in slight excess (0.15 moles) was added to benzylamine (0.23 moles) in a 100cm^3 round bottomed flask fitted with a reflux condenser and nitrogen purge. This was purged thoroughly for thirty minutes then refluxed gently for four hours before being allowed to cool under nitrogen, see scheme 2.3)
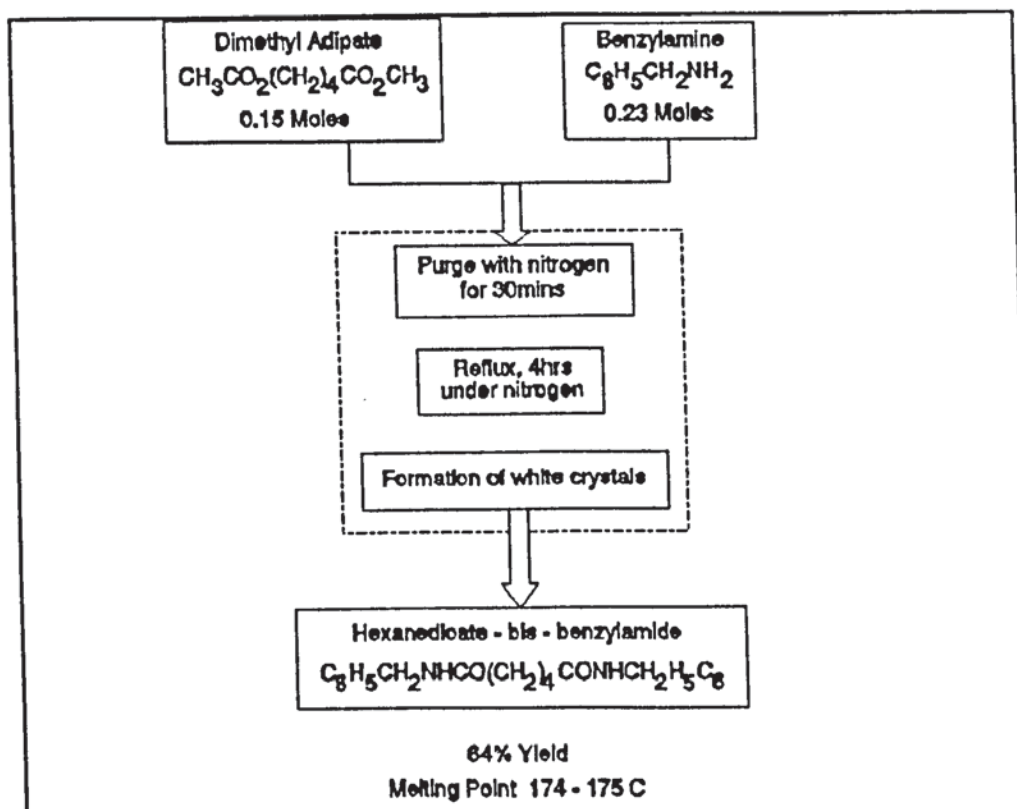
Scheme 2.3. Preparation of Hexanedioate-bis-benzylamide (Model II) : the Direct Reaction of Dimethyl Adipate and Benzylamine.

The product was obtained as a soft white solid with a melting range of 174° to 175°C. The two reactants were soluble in water while the product was insoluble so the separation was relatively easy. Model II was obtained in a 64% yield with characterisation being made by IR and ^{13}C NMR, see figures 2.3 and 2.4, respectively.
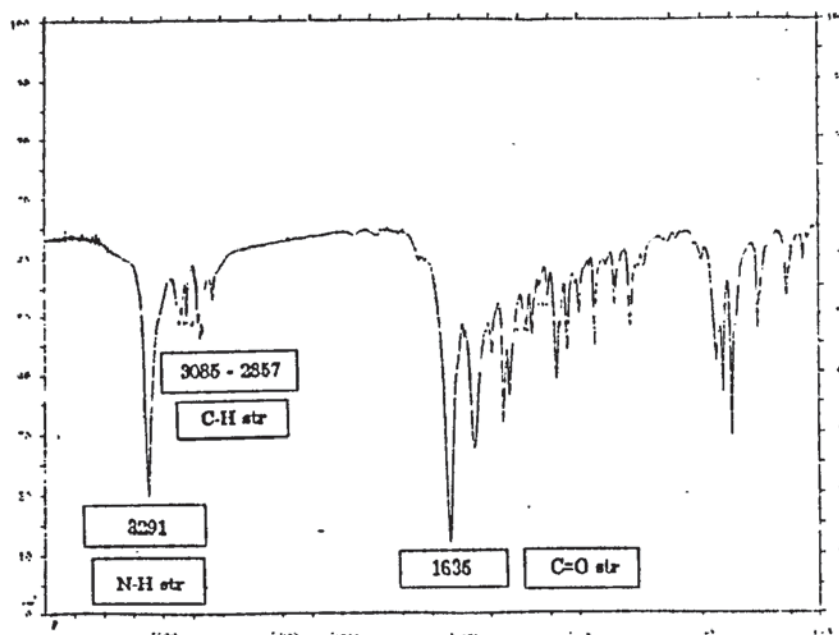
Figure 2.3 FT-IR Spectra of Model II : Hexanedioate-bis-Benzylamide (as KBr Disc).

Carbon N°.	(ppm)	I (%)
1	25 08	-7 01
2	35.18	7.41
3	171.96	-2.75
4	41.96	-8.97
5	139.69	-1 51
6	128.24	12 35
7	127.14	12.14
8	126.66	8.08
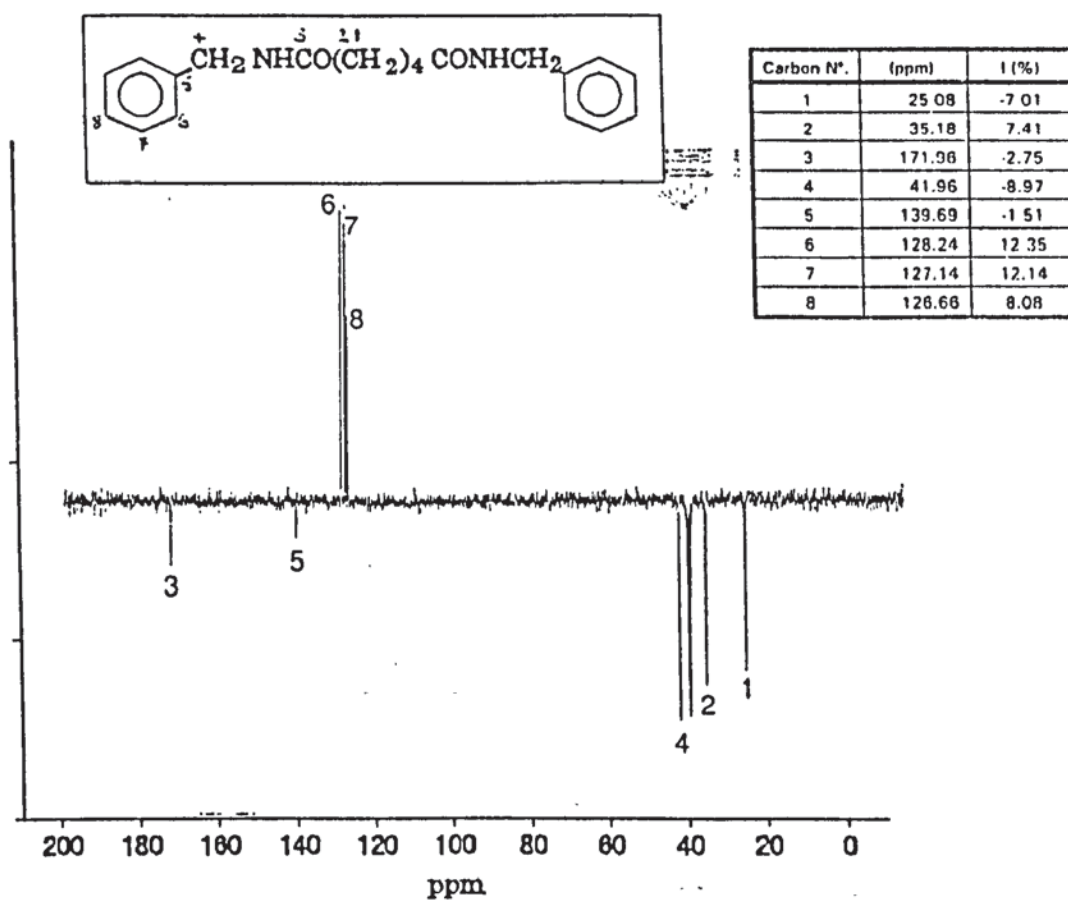
Figure 2.4 ^{13}C NMR Spectra of Model II : Hexanedioate-bis-Benzylamide (in DMSO).

2.1.2. Purification of Commercial Materials.

2.1.2.1. 1,2 Di-Chlorobenzene.

Di-Chlorobenzene (technical grade) was dried over phosphorus pentoxide, filtered and distilled. The fraction boiling at 180.5°C (760 mm hg) was collected and stored in the dark prior to use.

2.1.2.2. Propan-2-ol.

Propan-2-ol (technical grade) was dried over magnesium sulphate, filtered and distilled. The fraction boiling at 82°C (760 mm hg) was collected and stored in the dark prior to use.

2.1.2.3. Acetic Acid.

Acetic acid (technical grade) was dried over magnesium sulphate, filtered and distilled. The fraction boiling at 116-117°C (760 mm Hg) was collected and stored in the dark prior to use.

2.1.3. Other Materials.

2.1.3.1. Acids.

Acid	Grade	Source	Formula
Formic	99%	PSC Analytical Std	HCO_2H
Acetic	99%	PSC Analytical Std	CH_3CO_2H
Propionic	99%	PSC Analytical Std	$CH_3CH_2CO_2H$
Butyric	99%	PSC Analytical Std	$CH_3(CH_2)_2CO_2H$
Valeric	99%	PSC Analytical Std	$CH_3(CH_2)_2CO_2H$
Oxalic	99%	PSC Analytical Std	$HO_2C\text{-}CO_2H$
Malonic	99%	PSC Analytical Std	$HO_2CCH_2CO_2H$
Succinic	99%	PSC Analytical Std	$HO_2C(CH_2)_2CO_2H$
Glutaric	99%	PSC Analytical Std	$HO_2C(CH_2)_3CO_2H$
Adipic	99%	PSC Analytical Std	$HO_2C(CH_2)_4CO_2H$
Isophthalic	99%	PSC Analytical Std	$m\text{-}HO_2CC_6H_4CO_2H$
Benzoic	99%	PSC Analytical Std	$C_6H_5CO_2H$

Table 2.1. Various Carboxylic Acids used in the Characterisation of Degradation Products via HPLC.

2.1.3.2. Aldehydes and Ketones.

Aldehyde/Ketone	Grade	Source	Formula
Formaldehyde	Analar	B.D.H	HCHO
Acetaldehyde	GPR	B.D.H	CH_3CHO
Propionaldehyde	97%	Aldrich	CH_3CH_2CHO
Butyraldehyde	99%	Aldrich	$CH_3CH_2CH_2CHO$
Valeraldehyde	99%	Aldrich	$CH_3(CH_2)_3CHO$
Acetone	Technical	B.D.H	CH_3COCH_3
Butanone	Technical	B.D.H	$CH_3COCH_2CH_3$
Benzaldehyde	99%	Aldrich	C_6H_5COH
Isophthaldehyde	97%	Aldrich	$HOCC_6H_4COH$

Table 2.2. Aldehydes and Ketones used in the Characterisation of Degradation Products via HPLC.

2.1.3.3. Amines.

Amine	Grade	Source	Formula
Methylamine	40% aq.soln.	B.D.H	CH_3NH_2
Ethylamine	70% aq.soln.	Aldrich	$CH_3CH_2NH_2$
Propylamine	98%	Aldrich	$CH_3(CH_2)_2NH_2$
Butylamine	97%	B.D.H	$CH_3(CH_2)_3NH_2$
Pentylamine	90%	B.D.H	$CH_3(CH_2)_4NH_2$
Benzylamine	98%	B.D.H	$C_6H_5CH_2NH_2$
m-Xylylene diamine	99%	Aldrich	$m-H_2NCH_2C_6H_4CH_2NH_2$

Table 2.3. Amines used in the Characterisation of Degradation Products via HPLC.

2.1.3.4. Solvents.

Solvent	Grade	Source
Methanol	IIPLC	Fisons
Water	IIPLC	Fisons
Benzene	99%	B.D.H
DMSO	99%	Aldrich
Toluene	99%	B.D.H

Table 2.4. Solvents used in the Experimentation Involved in this Study

2.1.3.5. Miscellaneous.

Material	Grade	Source
Sodium Iodide	99%	Aldrich
Sodium Thiosulphate	99%	Fisons
Cobalt Neodecanoate	20.5% Cobalt	Shepheard Chemical Company.
2,4 Dinitrophenylhydrazine	Analar	Aldrich
Dansyl Chloride	99%	Aldrich
Ferrous ammonium sulphate	99%	Fisons
Phenanthroline	98%	Aldrich
Phosphoric acid	85wt% (in water)	Aldrich

Table 2.5. Various Other Chemicals used in Experimentation Involved in this Study.

2.2. Experimental Techniques.

2.2.1 Oxygen Absorption.

Oxygen absorption measurements have been shown [69,92] to be useful in the study of oxidation mechanisms for both low molecular weight compounds and polymer systems. Several techniques can be used to monitor oxygen uptake but for the purpose of this study the determination of the resistance of the model compounds to oxidation was carried out using a specially constructed piece of apparatus employing the use of pressure transducers. This allows the rate of absorption and total amount of oxygen absorbed , by the sample, to be measured directly. The apparatus used is shown in figure 2.5.
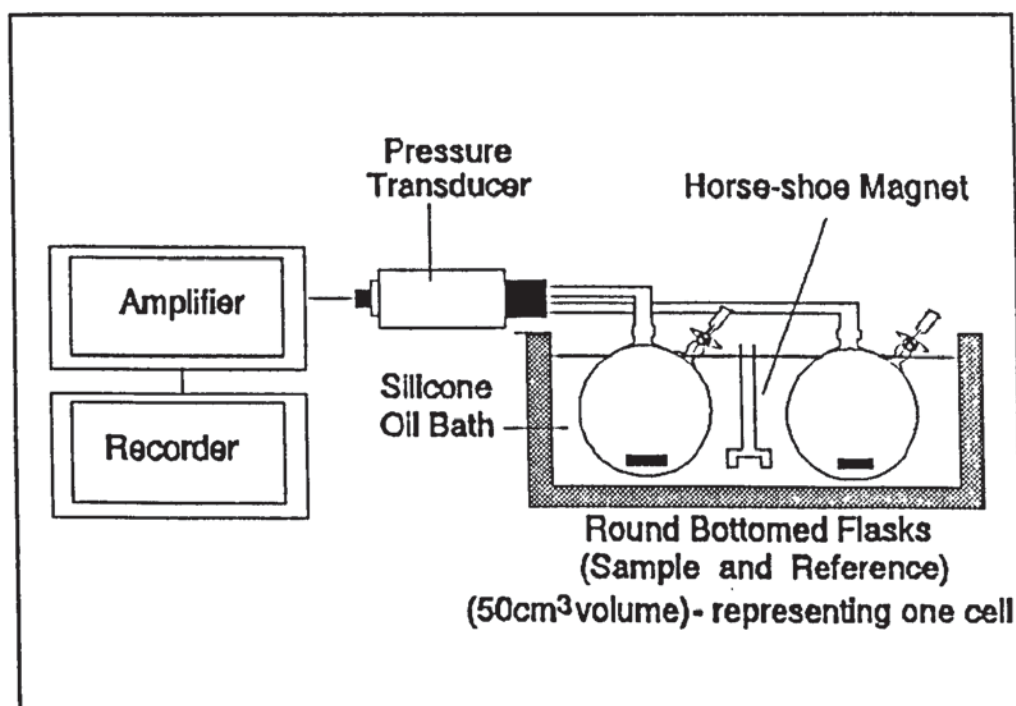
Figure 2.5. Schematic Diagram of the Oxygen Absorption Apparatus used in this Study. Each "cell", capable of measuring one oxidation reaction, consisted of two identical 2-necked 50cm³ round bottomed flasks (a sample flask and a dummy flask), each fitted with a glass tap and stopper. Both flasks were connected, via side arms, to a Pye-Ether pressure transducer (range 5psi), which in turn was wired to a Leeds-Northrup Speedomax 12-channel chart recorder.

The sample flask contained a small sheathed bar magnet for stirring which was controlled by a rotating, speed adjustable horseshoe magnet. The cell was placed in position in a thermostatted bath of silicone oil so that the greased joints (high temperature silicone grease) were just above the level of the oil. The sample flask was so placed as to be in close proximity to the external magnet. Calibration of the system was achieved by withdrawing a 2cm³ sample of air from the sample flask and altering the input voltage to achieve a deflection on the chart of 5 divisions. This allows a full scale deflection equivalent to 40cm³. The sample under study was mixed externally and once introduced, a stream of pure oxygen was passed into the flask for a period of 20s after which the sample flask was stoppered and the overhead stirrer activated. For all oxygen absorption experiments a moderate rate of stirring was aimed for, which eliminated the possibilty of splashing but at the same time ensured a thorough agitation of the solution in the sample flask. As the sample flask warmed up, so the pressure increased slightly, leading to a decrease in the chart reading. Within five minutes, however, the pressure had become constant and the chart reading at this time was taken as the initial deflection. For each sample, the result was obtained as a continuous trace of chart deflection versus oxidation time. The chart deflection (in divisions) was corrected by subtraction of the "initial deflection" and this corrected deflection was converted to cm³ oxygen absorption by multiplying the reading by a factor of 0.4 (deflection of 5 divisions = 2.0cm³). A curve of oxygen absorption vs. oxidation time could then be plotted. In general each system was evaluated at least three times, which resulted in three slightly different oxidation curves. An average curve, based on the average volume of oxygen absorbed at various oxidation times could easily be constructed and errors obtained were within ±15%.

2.2.2 Fourier Transform Infra-red Spectroscopy.

Infra-red spectroscopy was used to follow the changing structure of the model compounds during oxidation. The nature of the products formed from the model compounds is dependent on the mode of decomposition. Measuring the changing area of the product peaks with oxidation time, the degree of oxidation could also be followed.
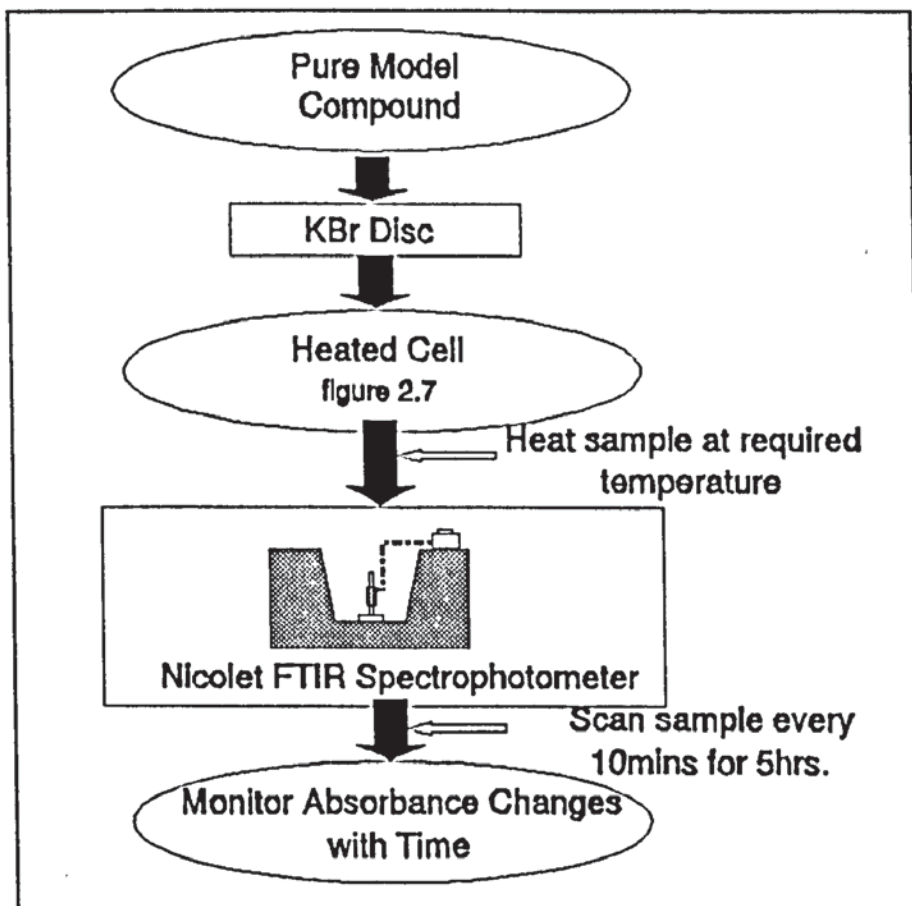
Scheme 2.4. Determination of the Reference Peak for Area Index by FTIR.
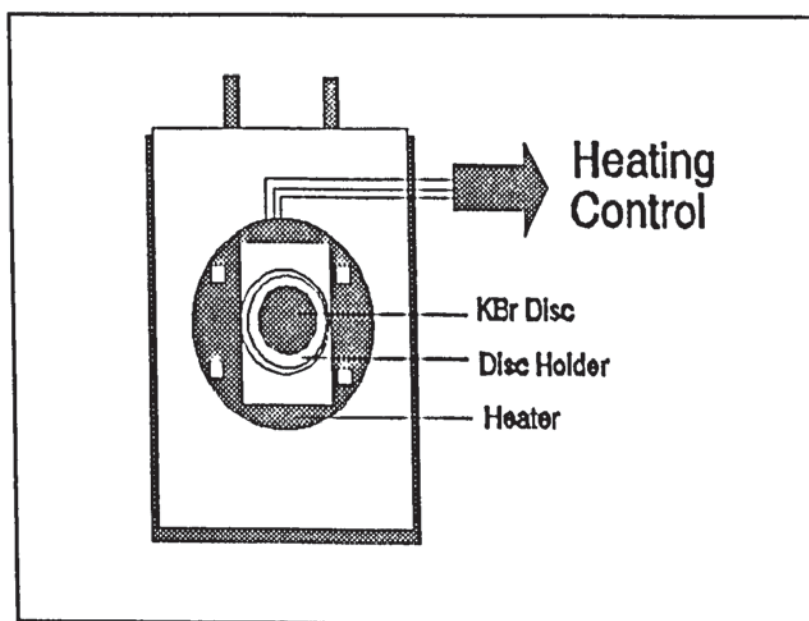
Figure 2.7. The Heated Cell and Holder for use in Determination of the FTIR Reference Peak.

The areas of the product peaks formed were measured and ratioed against a reference peak (wavelength 3000-2890nm) see figure 2.8. The peak areas, after correction against the reference peak, were then plotted against oxidation time. The reference peak was chosen due it's consistency throughout oxidation of the model. It occurs in the C-II stretch region of the IR spectrum corresponding to the aromatic C-II in the model compound which is thought to have no involvement in the oxidation process.
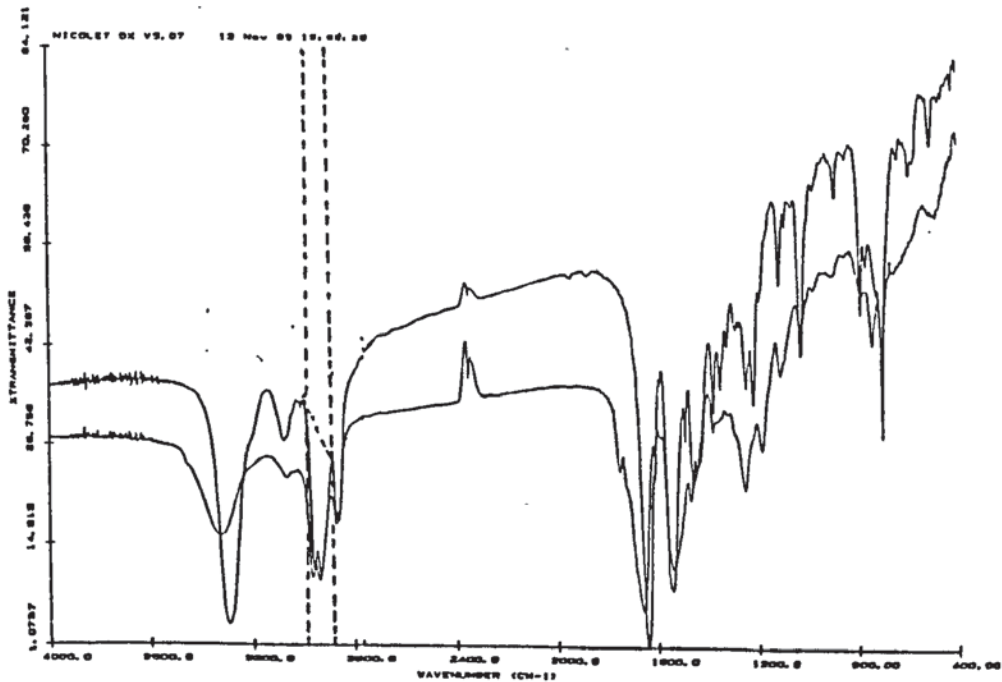
Figure 2.8. A Typical IR Spectra showing the Shaded Reference and Peak for Calculation of Area Index.

$$Area\ Index\ of\ 1635 = \frac{Area\ of\ Shaded\ Peak\ at\ 1635}{Area\ of\ Shaded\ Peak\ at\ 2900}$$
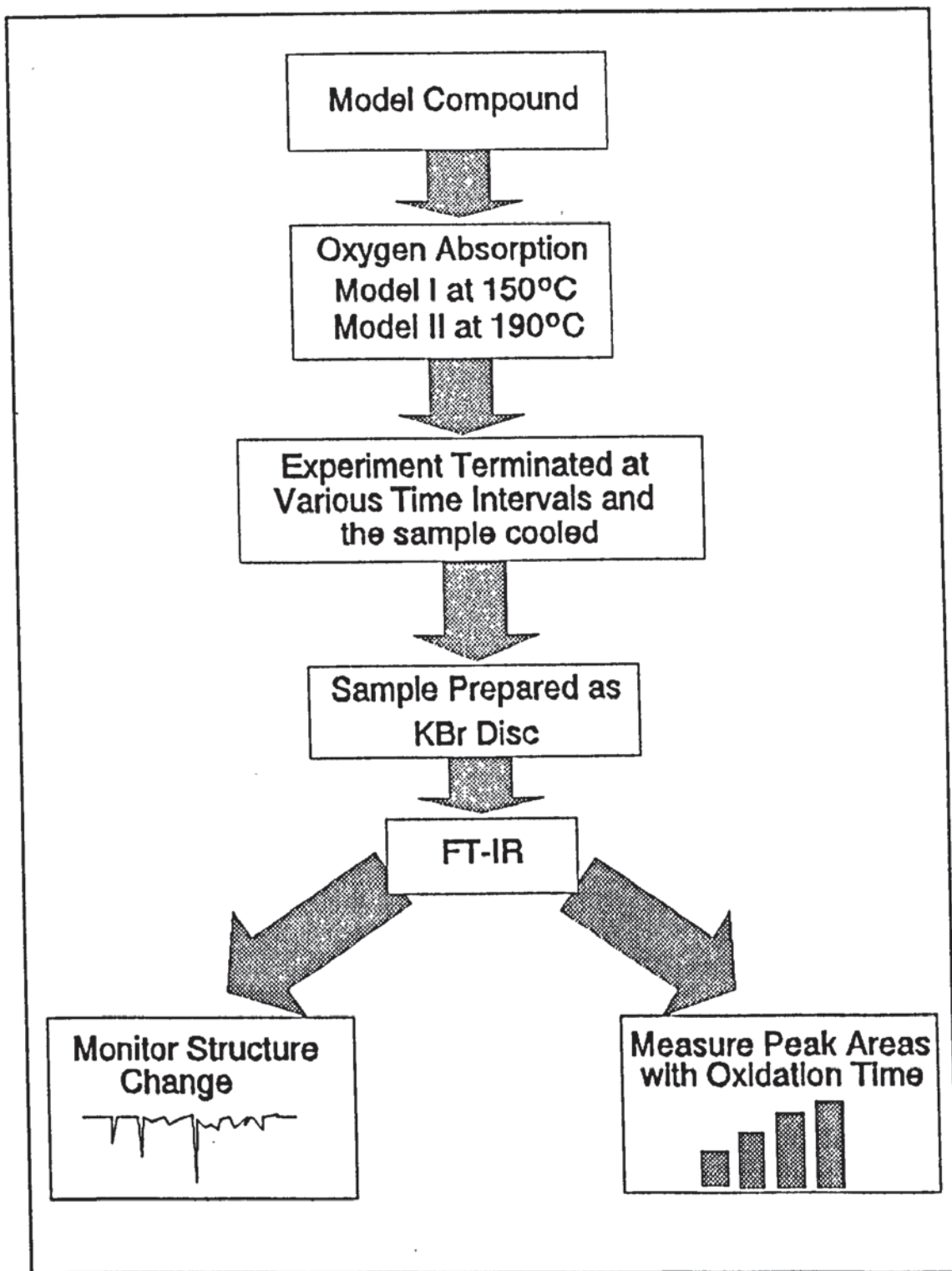
Scheme 2.5 Experimental Outline for the IR Spectroscopic Analysis of the Model Compound.

2.2.3 Ultra-Violet / Visible Spectroscopy.

Ultra-Violet/Visible (UV-Vis) spectroscopy was mainly used to monitor the appearance and growth of the peak at 286nm in the oxidising model (see figure 2.9). It provides a good representation of the extent of oxidation in the model compound and can be directly compared to the oxygen absorption trace. A similar UV spectroscopic technique was used by Russian scientists to investigate the extent of oxidation of polycaproamide [43]. All spectra were measured using a Hewlett-Packard 8452A diode array spectrophotometer incorporating the HP89510A general scanning software and HP89512A kinetics software.
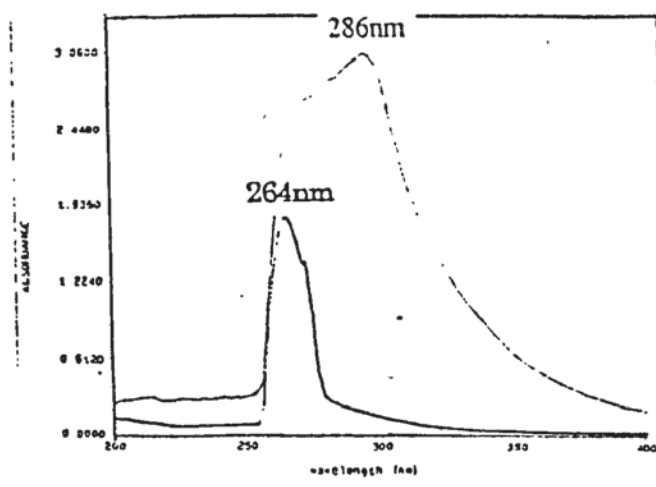
Figure 2.9. UV/Vis Spectrum of Model I with Increasing Oxidation Time at 150°C.

Many reactions can be followed conveniently by UV/Visible spectroscopy with conventional instruments, however it is usually necessary to follow the reaction at one wavelength in order to monitor the reactant concentration. Then to monitor the product formation, it is necessary to change to another wavelength and repeat the experiment. If the system is more complex, with overlapping spectra, it may be very difficult to obtain sufficient information by monitoring only at single wavelengths. This is time consuming and will lead to errors because no two experiments are absolutely identical. One of the advantages of a diode array spectophotometer is that it can measure full spectra very quickly, as little as 0.1sec is required for 190 to 820nm. This means that it is usually only necessary to perform one experimental run to acquire either full spectra, or the specific spectral range of interest.

Initially it was hoped that the experiments could be carried out in the UV-Vis spectrophotometer with the use of a specially constructed heated liquid cell. This required the model being soluble in an appropriate solvent and consequently heated to 150°C, in a quartz cell, and held at this temperature for several hours whilst the changing spectra were monitored. Early experiments using this system were promising but closer examination of the solvent used, DMSO, showed that perhaps the effect upon the system was too unpredictable. Failing to find a further appropiate solvent the model was oxidised in the oxygen absorption apparatus and samples were taken out, cooled and then dissolved in a solvent so the UV-Vis measurements were taken at room temperature. The models were oxidised for periods of 0,5,15,30,45,60,120,300,minutes 0.02g of each sample was taken and dissolved in 10cm^3 of DMSO. The method of sample preparation and analysis is summarised in scheme 2.6.
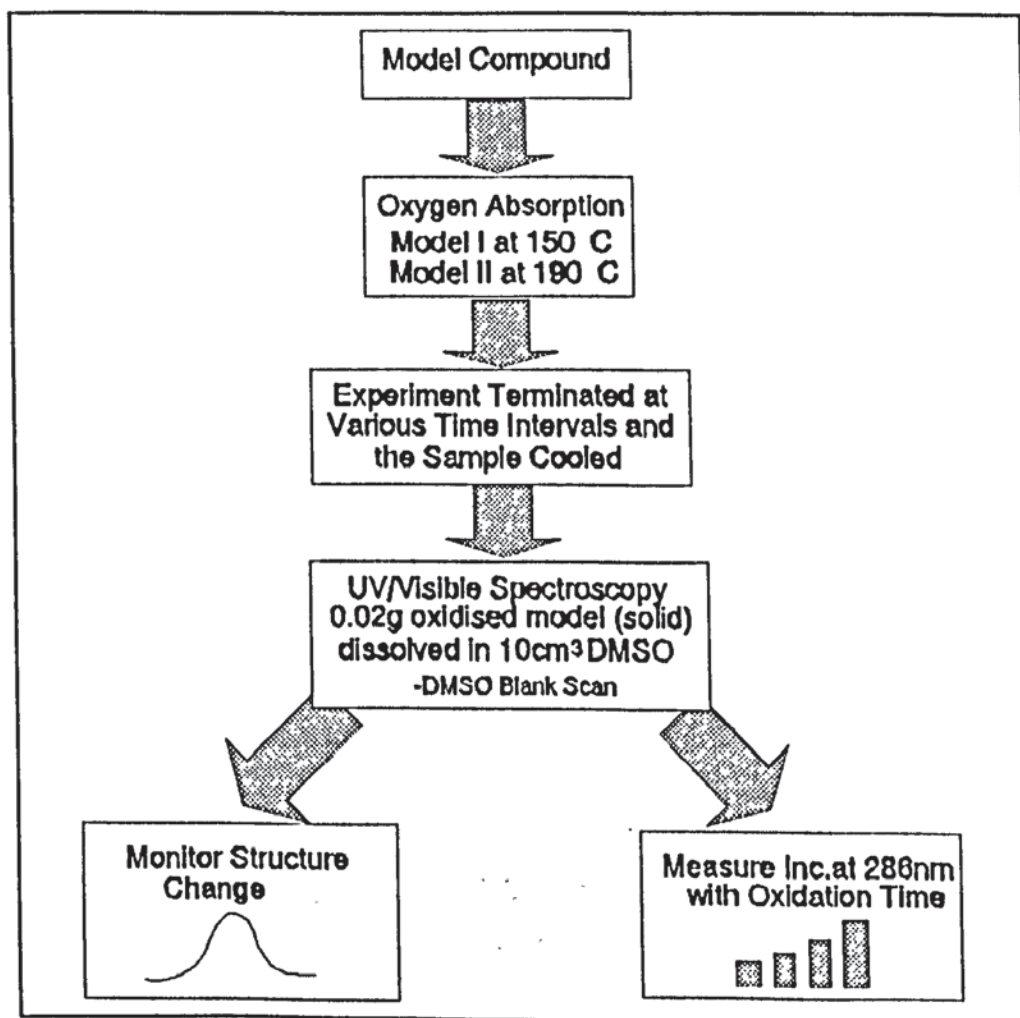
Scheme 2.6 Experimental Outline for UV-Vis Spectroscopic Analysis of the Model Compound.

2.2.4 Hydroperoxide Determination.

It was suggested earlier in this report (Chapter1 section 1.5.5) that one possible role of cobalt, in the oxidation of MXD6/Model compounds, was to decompose the hydroperoxides formed during the initial stages of oxidation, (2.1 and 2.2).

$$ROOH + Co^{2+} -----> RO^{\cdot} + {}^{\cdot}OH + Co^{3+} \qquad (2.1)$$

$$ROOH + Co^{3+} -----> RO_2^{\cdot} + H^+ + Co^{2+} \qquad (2.2)$$
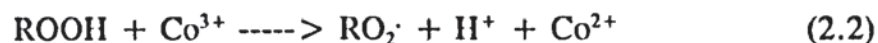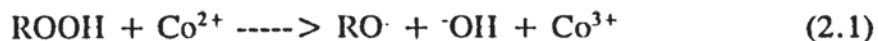
The hydroperoxide concentration during the oxidation of the models I and II at 150°C, in the presence of cobalt, sodium phosphite and cobalt/sodium phosphite was therefore monitored. Two separate methods were used to measure hydroperoxide concentrations:-

1) an iodometric technique [93], and

2) a technique involving the oxidation of a Fe^{2+} salt [94], by the hydroperoxide formed. The amount of Fe^{2+} is determined by the formation of a complex.

The analysis carried out is summarised in scheme 2.7. For the purpose of hydroperoxide determination the model was oxidised in 1,2 di-chlorobenzene at 150°C. 2.0g of the model compound was dissolved in 20cm³ of the solvent and placed in a three-necked round bottomed flask. The flask was fitted with a condenser and an oxygen purge leaving one neck available for the removal of the 1cm³ sample via a pipette. When not in use the neck was sealed with a glass stopper. The flask was inserted into an oil bath at 150°C and samples removed at the required time interval (see figure 2.10).
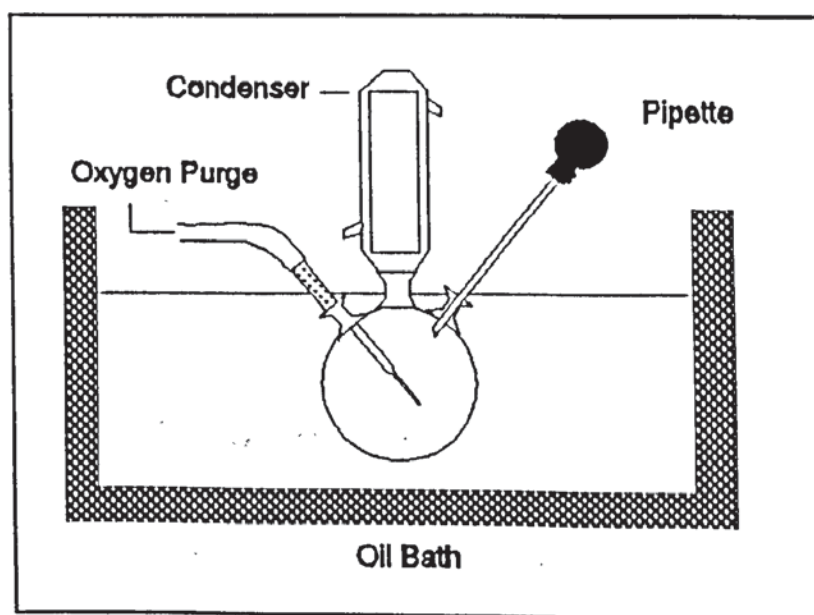
Figure 2.10. Sampling Technique used in the Determination of Hydroperoxide Concentration.

2.2.4.1 Hydroperoxide Determination Using an Iodometric Technique.[93]

A 1cm^3 portion of the reaction mixture, see stage (a) in scheme 2.7, was withdrawn with a pipette and added to a 50cm^3 flat bottomed flask with a ground glass neck. Each flask contained 10cm^3 of each of the following solutions, added prior to the beginning of the hydroperoxide determination.

     i) 2.5% w/v sodium iodide in propan-2-ol

     ii) 10% v/v acetic acid in propan-2-ol

These flasks were wrapped with aluminium foil to prevent photolysis of the sodium iodide. Once the 1cm^3 portion of the reaction mixture had been added, the flask was fitted with a condenser and the contents were heated to reflux, with vigorous stirring, on a hot plate for 6minutes. After this time, the flask was allowed to cool for 2.5mins, and 5cm^3 of distilled water was added. The aluminium foil was then removed and the contents of the flask were titrated, with stirring, with 2x10^{-3} mol/dm^3 solution of sodium thiosulphate in distilled water. The end point was taken as the transformation from yellow to colourless. The iodometric technique described above depends on the oxidation, in acidic solution, of iodide to iodine by any hydroperoxide present, (2.3)

$$RO_2H + 2I^- + 2H^+ ----> ROH + I_2 + H_2O \qquad (2.3)$$

Titration of the yellow solution of iodine produced by the above reaction with sodium thiosulphate solution, proceeded via reaction, (2.4) :-

$$2S_2O_3^- + I_2 ----> S_4O_6^- + 2I^- \qquad (2.4)$$
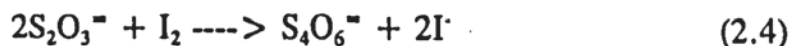
2.2.4.2 Determination of Hydroperoxide Using an Iron Oxidation Technique.[94]

A 1cm^3 portion of the reaction mixture, see stage (b) in scheme 2.7, was withdrawn with a pipette and added to a 25cm^3 volumetric flask followed by 10cm^3 of Analar Benzene. 0.5cm^3 of 0.004M phosphoric acid in methanol was then added followed by 5cm^3 of standardised 0.0005M solution of ferrous ammonium sulphate in methanol.

After down washing the sides of the flask with benzene, the solution was allowed to stand for 15mins before the addition of 1cm^3 of 0.5% solution of phenanthroline in benzene. The sample was then allowed to stand for 30mins and examined in the UV spectrophotometer between wavelengths 490nm and 520nm.

Figure 2.11 shows the UV spectra of the changing absorbance of the iron complex, taken from a typical example, involving the oxidation of model I. Within the initial 60mins of oxidation, of the model, substantial amounts of hydroperoxide were produced, which when added (1cm^3) to the ferous solution resulted in the oxidation of Iron (II), present in the solution, to Iron (III), therefore resulting in a decrease in the amount of iron (II) complex which can form (which produces the absorbance at 510nm), upon addtion of the complex reagent. However after 60mins the amount of hydroperoxide produced during the oxidation reaction begins to decrease, hence less iron (II) is being oxidised resulting in the increase in absorbance at 510nm, due to the increase in iron (II) complex formed. Therefore the absorbance at 510nm (due to the iron II complex) corresponds, indirectly, to the amount of hydroperoxide present in the solution, produced during the oxidation of the sample.

The absorbance of each sample at 510nm was plotted against oxidation time to give a curve as shown in figure 2.12. Finally the absorbance of the sample was then subtracted from the absorbance of a blank sample, ie the ferrous hydroperoxide reagent (+ 1cm^3 Benzene) to give the corresponding hydroperoxide concentration which was also plotted against oxidation time (figure 2.12). Curve (a), in figure 2.12, shows the decrease and subsequent increase in absorbance at 510nm (due to the iron II complex), representing the amount of Fe^{2+} present in the solution, which is determined by the hydroperoxide content of the oxidised model. Curve (b) shows the absorbance after subtraction from the blank (ie, maximum iron II content), representing the amount of hydroperoxide produced during the oxidation of model I.

The standard ferrous solution was made up by dissolving 1.9608g of ferrous ammonium sulphate in methanol and adding 1.38mls of concentrated sulphuric acid and making up to 100ml with methanol, 10ml of this solution was made up to 1L using methanol.
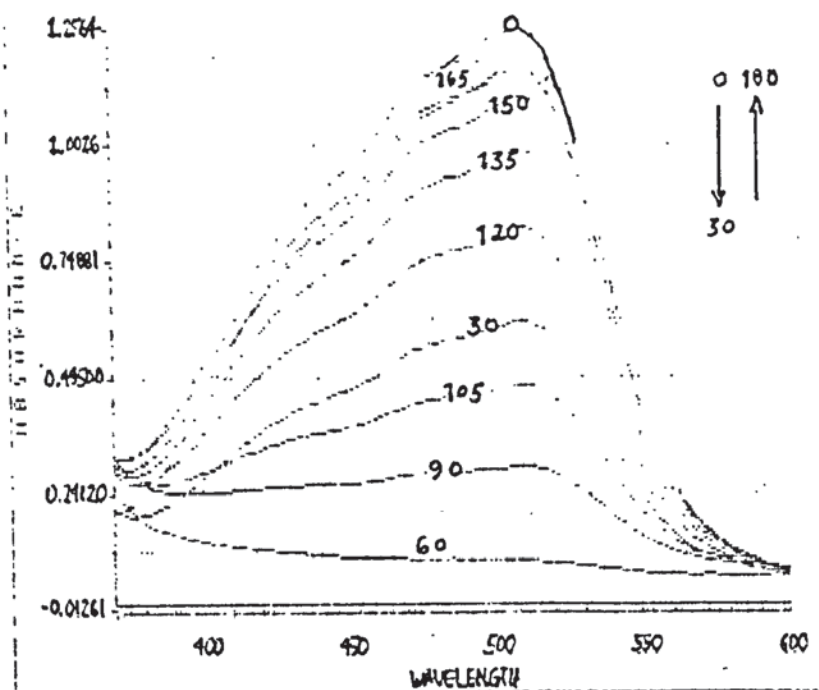
Figure 2.11. UV Spectra of the Changing Absorbance of the Iron Complex with Increasing Oxidation of Model I (Numbers on curves represent the oxidation time of the model which was subsequently added to the ferrous reagent).
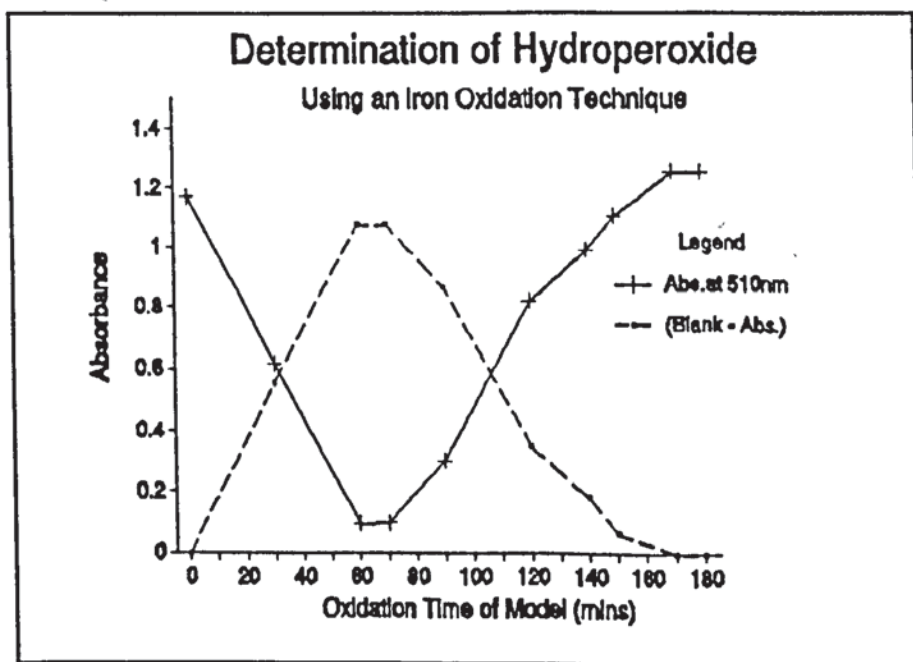
Figure 2.12. Typical Example of the Construction of a Hydroperoxide Curve taken from the Oxidation of Model I in an Oxygen Atmosphere at 150°C.
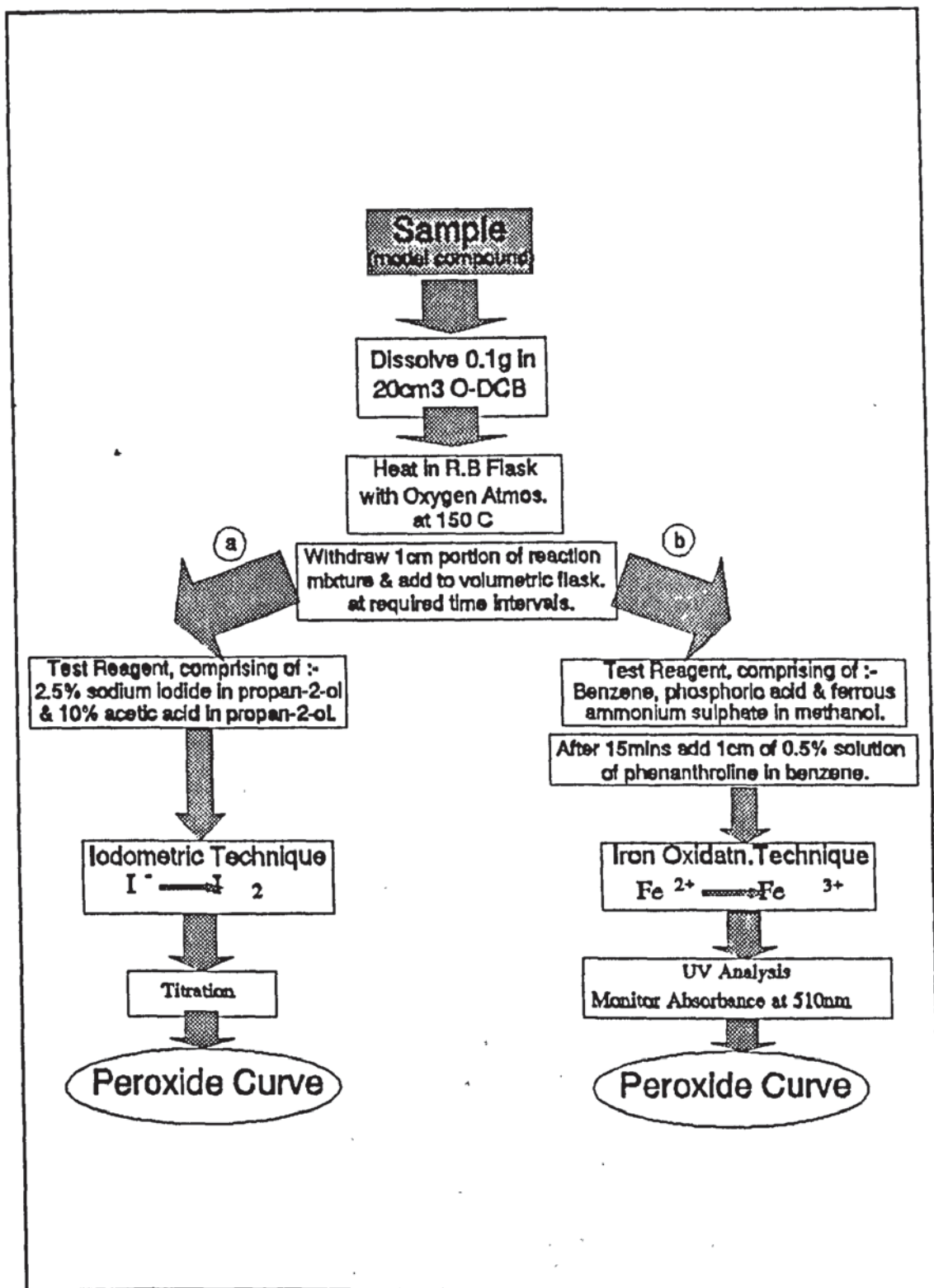
Scheme 2.7 Experimental Outline for the Hydroperoxide Determination of the Model during Oxidation at 150°C.

2.2.5 Thermogravimetric and Differential Thermal Analysis.

Thermogravimetric and Differential thermal analysis were used in two instances, i) in determination of activation energies for the oxidation of the model compounds and, ii) to monitor the effect of differing ratios of sodium phosphite/ cobalt on the degradation (oxidation) exotherm.

2.2.5.1 Determination of Activation Energies.

Based on First order kinetics the activation energies associated with oxidative weight loss, at three different temperatures was estimated. The effect of cobalt, sodium phosphite and cobalt/sodium phosphite was assessed. The TG/DTA equipment used in these experiments was a Linseis, combined thermogravimetric, differential thermal analyser encorporating suitable computer software which enabled comprehensive analysis of the data.

For each sample the weight loss was measured at three different temperatures over a period of 7hrs, in an oxygen rich atmosphere, as described in scheme 2.8. The design of the TG/DTA equipment requires the presence of the sample pan during "ramping" up to the required temperature. In order to avoid oxidation of the sample during temperature ramping, argon gas was flushed through the system, prior to and during the procedure. The "ramping rate used to achieve a rapid constant temperature was as shown in Table 2.6.

140°C Isothermal	150°C Isothermal	160°C Isothermal
10 K/min to 100°C	10 K/min to 110°C	10 K/min to 120°C
5 K/min to 125°C	5 K/min to 135°C	5 K/min to 145°C
2 K/min to 135°C	2 K/min to 145°C	2 K/min to 155°C
1 K/min to 140°C	1 K/min to 150°C	1 K/min to 160°C

Table 2.6. The Ramping Rates used to Achieve the Required Isothermal Temperature for the Analysis of Model I.

190°C Isothermal	200°C Isothermal	210°C Isothermal
10 K/min to 150°C	10 K/min to 160°C	10 K/min to 170°C
5 K/min to 175°C	5 K/min to 185°C	5 K/min to 195°C
2 K/min to 185°C	2 K/min to 195°C	2 K/min to 205°C
1 K/min to 190°C	1 K/min to 200°C	1 K/min to 210°C

Table 2.7. The Ramping Rates used to Achieve the Required Isothermal Temperature for the Analysis of Model II.

Once the temperature had stabilised the argon atmosphere was exchanged for oxygen at a flow rate of 300cc/min. This was indicated on the TG/DTA trace by a rise in the % Mass change and a small endotherm peak. The procedure was repeated for all temperatures and the slopes of the three traces were calculated directly after the onset of weight loss and recorded as rate constant 'K'. Figure 2.13 shows a typical isothermal weight loss trace.
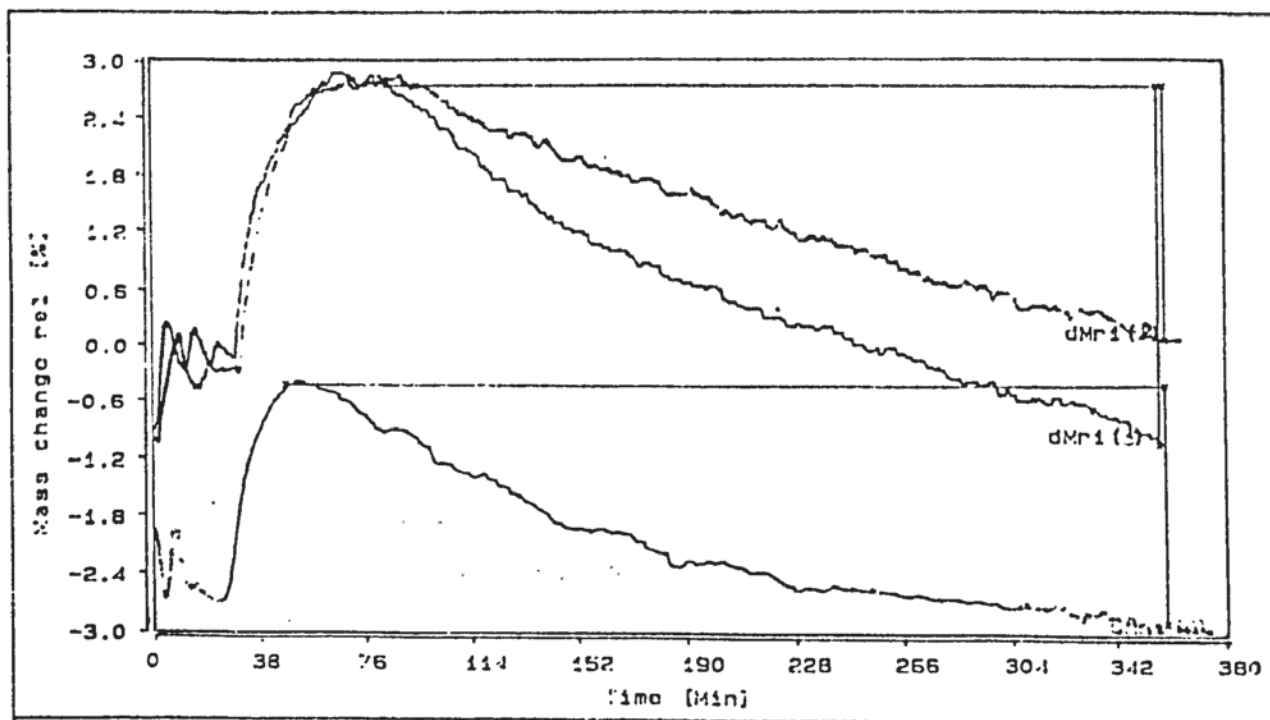
Figure 2.13. T.G.A Trace Obtained from the Isothermal Heating of Model I in an Oxygen Atmosphere.

Using Arrhenius expression :-

$$K = A \exp^{(-\frac{E_a}{RT})}$$

$$LnK = LnA - \frac{E_a}{RT}$$

From a plot of Log of rate constant versus reciprocal of absolute temperature the activation energies were obtained by the slope of the straight line (see figure 2.14)

$$Slope = -\frac{E_a}{R}$$

E_a = activation energy j/mol

R = Gas constant 8.314 j/mol
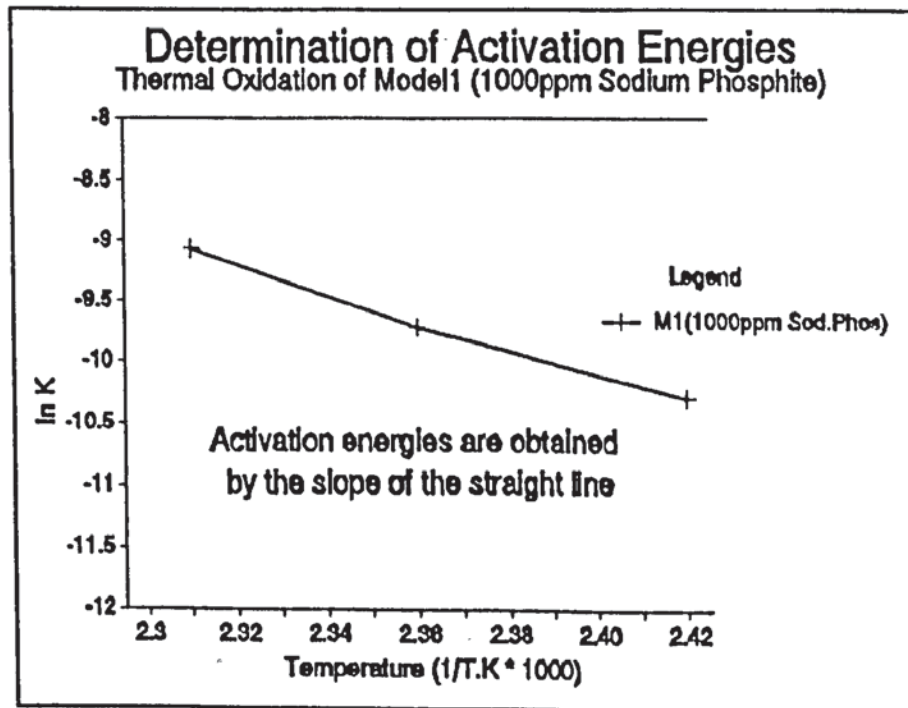
Figure 2.14. Determination of the activation energy for the thermal oxidation of Model1.

2.2.5.2 The Effect of Differing Cobalt/Sodium Phosphite Ratios on the Degradation Exotherm.

The use of TG/DTA analysis enables the degradation exotherm of differing mixtures of sodium phosphite/cobalt to be measured in terms of the maximum temperature at which the exotherm occurs and also the area of the exotherm. This gives an insight into the effect that cobalt and sodium phosphite have upon each other in certain ratios. Analysis was carried out in an oxygen atmosphere at a flow rate of 0.3cc/min with a slight argon pressure preventing back flow into the balance. The cobalt and phosphite were mixed together with a pestle and mortar and approximately 10mg introduced into the aluminium sample pan. An empty pan was used as the reference for which a calibration file had previously been run prior to the analysis. The oven was placed over the sample and reference pan and heated at a rate of 10 /min up to a temperature of 550°C in an oxygen atmosphere. The results were plotted as DTA and % Mass Change against Temperature (0-550°C). The computer software enabled measurement of the exotherm area and peak temperature
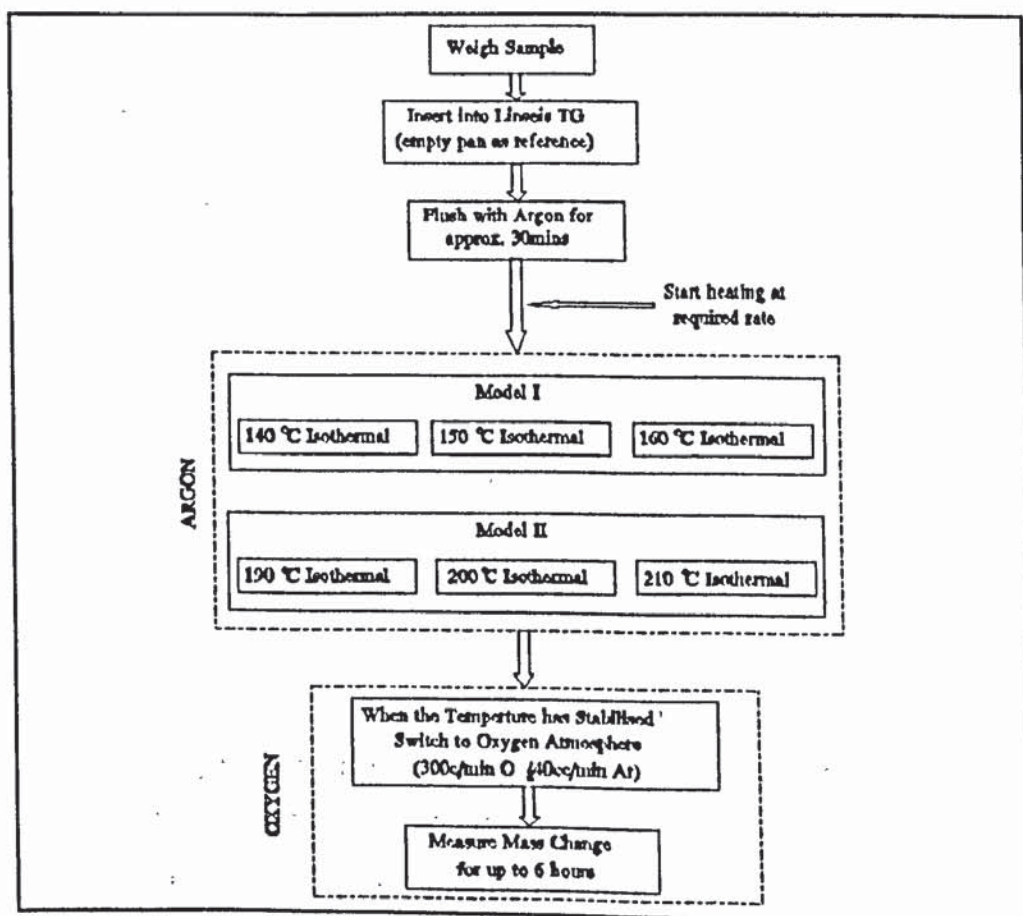
Scheme 2.8 Experimental Outline for the Determination of Activation Energies of the Thermal Oxidation of Models I and II via Isothermal Thermogravimetric Analysis.

2.2.6. Cyclic Voltammetry.

An electrochemical study was initially undertaken to study the effect of the amide models on the redox potential of the cobalt neodecanoate in order to explain the pro-oxidant/anti-oxidant inversion. Cyclic Voltammetry was the technique chosen to carry out this study, use of such equipment being provided by Carnaud MetalBox Packaging Technology at its laboratories in Wantage. Cyclic voltammetry provides an "electrochemical spectrum" indicating the potentials at which processes occur. Hence by obtaining a cyclic voltammogram of the cobalt(II) salt and comparing subsequent voltammograms, with the addition of model compound, useful mechanistic information is provided. Figure 2.15 shows a typical cyclic voltammogram for a reversible reaction. The electrode potential is swept between limits E1 and E2 at a known sweep rate V, on reaching the potential E2 the sweep is reversed, hence completing the cycle. Measurement of the "electrochemical spectrum" was carried out using the apparatus shown in figure 2.16.
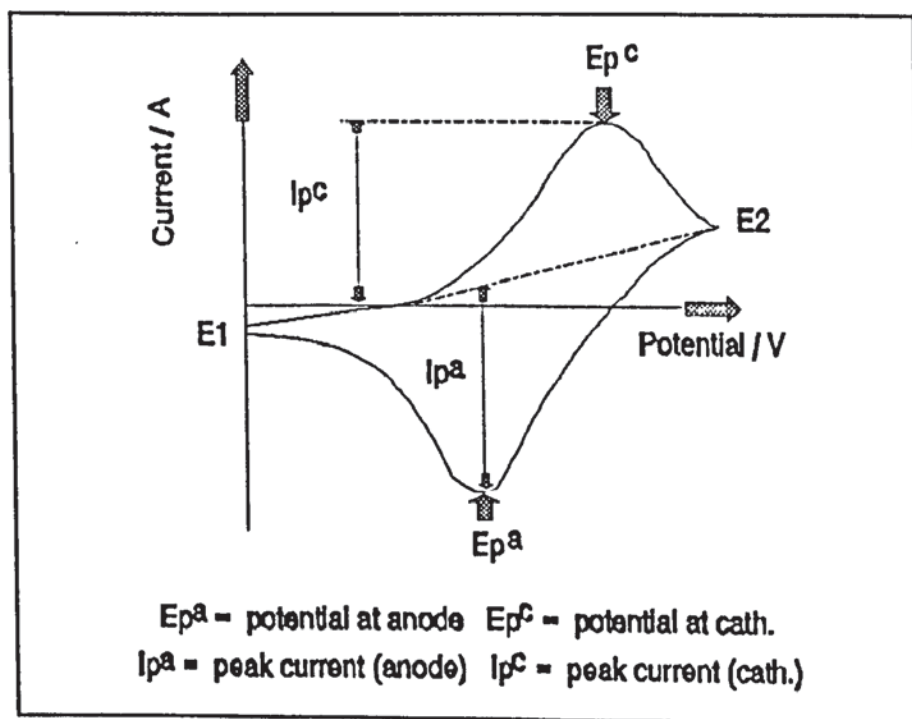
Figure 2.15. A typical Cyclic Voltammogram for a Reversible Reaction.
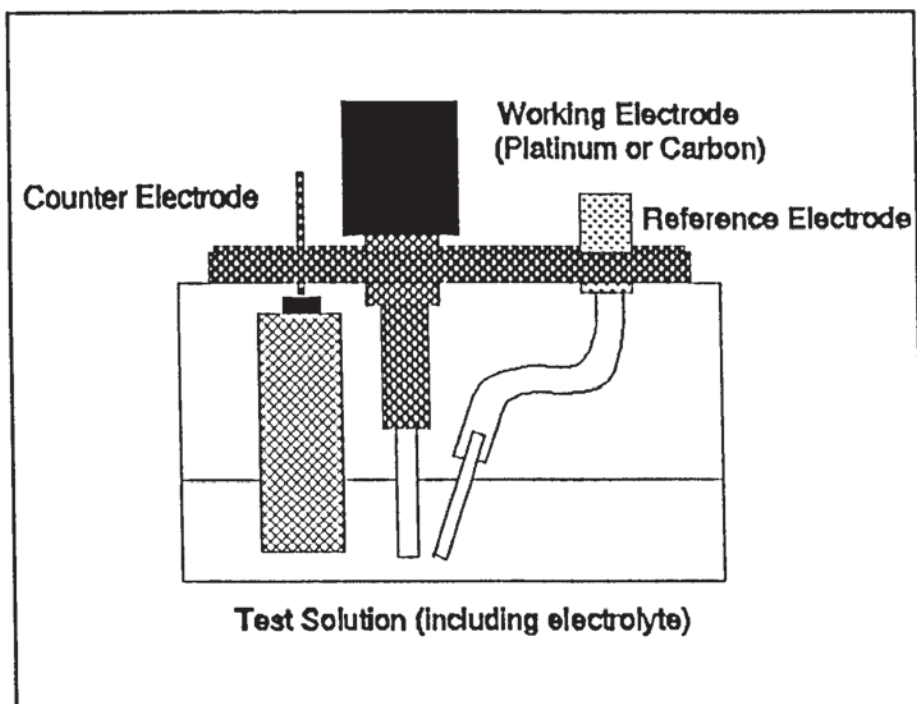
Figure 2.16. Electrochemical Cell used in the Cyclic Voltammetry Experiments.

The cobalt salt was dissolved in an appropiate solvent and placed in the container along with the electrolyte solution. The solution was purged with nitrogen prior to, and blanketed during, measurement to prevent ingress of oxygen into the test solution. The counter electrode and the platinum or carbon working electrode, along with a calomel reference, were connected to the control box and initially voltammograms were recorded over wide sweep rates and for various values of E1 and E2. By observing how the peaks appear and disappear an optimum sweep rate and potential range was obtained. The cyclic voltammogram was then recorded between the set values of E1 and E2 and at the desired sweep rate enabling the following values to be measured :-

Ep^c = potential at cathode

Ep^a = potential at anode

Ip^c = peak current at cathode

Ip^a = peak current at anode

These values, for the cobalt salt, were then compared with subsequent values of cobalt with the addition of model, sodium phosphite or both and hence their effect on the redox potential of the cobalt salt measured.

2.2.7. High Performance Liquid Chromatography.

High performance liquid chromatography was used as the principal technique for the separation and detection of degradation products. Identification of the products was achieved via comparison with the retention times obtained from a series of standard possible products, as shown in scheme 2.9. Possible products included carboxylic acids, aldehydes/ketones and amines. The various conditions used in the analysis of these compounds are shown in table 2.8, the eluent employed was greatly dependent on the organic species to be characterised. Characterisation of all analyses were performed using a Gilson HPLC system incorporating a Spherisorb ODS-2 (100x4.6mm) reverse phase column.

Compound	Mobile Phase	U.V Detection Wavelength (nm)	Flow Rate ml/min
Aliphatic Mono-Carboxylic Acids	Water pH 2.5	210	0.6
Aliphatic Di-Carboxylic Acids	Water : Methanol (98:2) pH 2.5	210	0.6
Aromatic Acids	Water : Methanol (70:30) pH 3.5	254	0.6
Aldehyde and Ketone Derivs.	Methanol : Water (70:30) pH 3.5	360	0.6
Amine Derivatives	Methanol : Water (70:30)	254	0.6

Table 2.8. Conditions used for the Characterisation of the Various Organic Species by H.P.L.C.
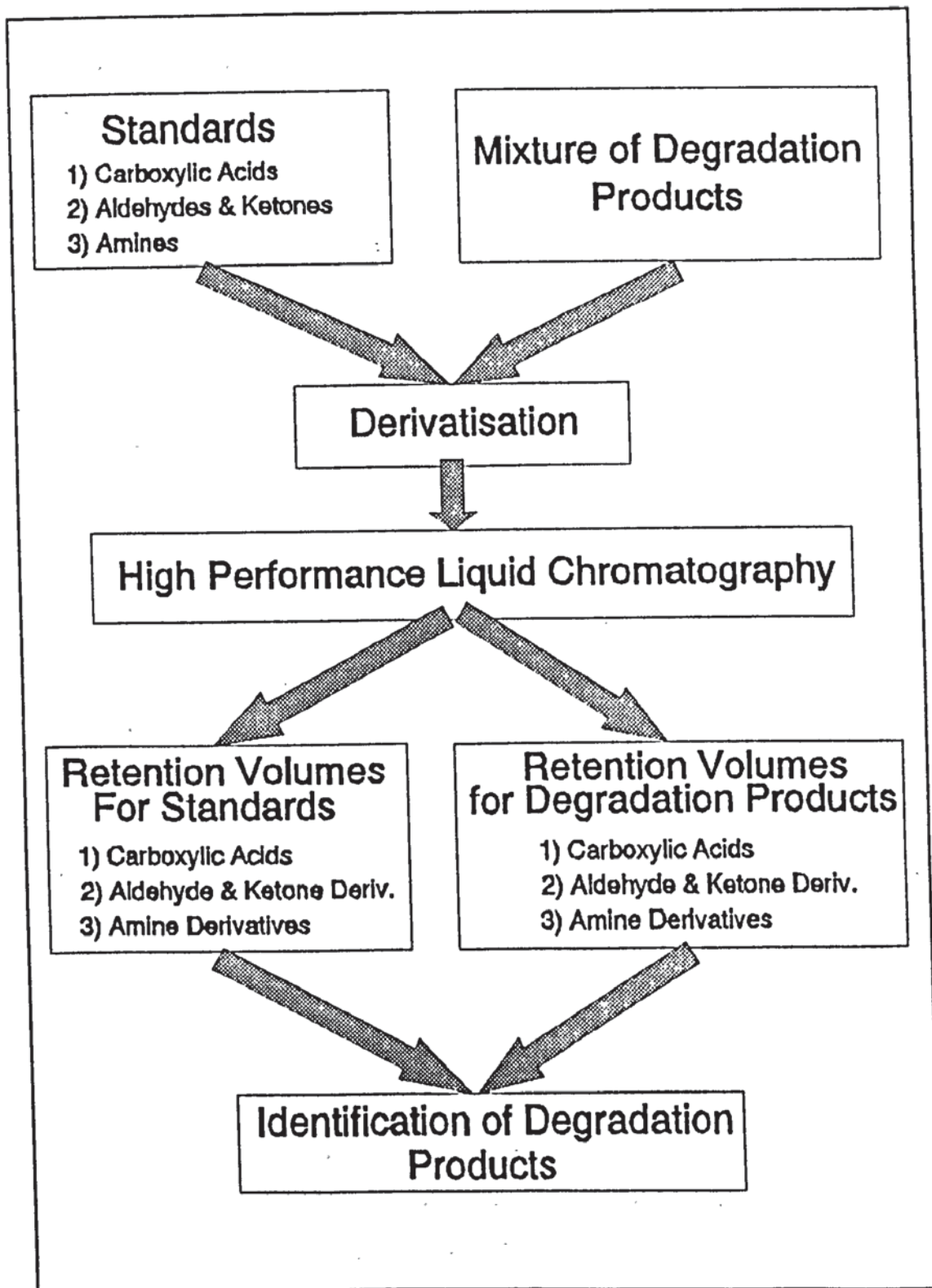
Scheme 2.8 Experimental Outline for the Identification of Degradation Products Via H.P.L.C.

2.2.7.1. H.P.L.C. of Carboxylic Acids.

Derivatisation of the monocarboxylic, dicarboxylic and aromatic acids was not necessary so the required concentration was prepared in HPLC grade water and injected directly onto the column.

2.2.7.2 H.P.L.C. of Aldehydes and Ketones [95].

Derivatives in liquid chromatography are invariably prepared to improve the response of a substance towards a particular detector. Other applications include aiding in the isolation of a substance or improving the chromatographic separation obtained with mixtures having overlapping peaks. Aldehydes and ketones may be selectively derivatised with either 2,4-dintrophenylhydrazine [96] or p-nitrobenzylhydroxylamine hydrochloride [96] without affecting other functional groups present in the molecule. In this particular study identification and separation of aldehydes and ketones using HPLC was carried out in the form of their respective 2,4-dinitrophenylhydrazine (D.N.P.H) derivatives. The reaction (2.5) is a familar one used in qualitative analysis for the characterisation of aldehydes and ketones by physical means [97].

$$O_2N-C_6H_3(NO_2)-NHNH_2 \xrightarrow[H^+]{RCHO} RCH=NNH-C_6H_3(NO_2)-NO_2 + H_2O$$

2,4-Dinitrophenylhydrazine   2,4-Dinitrophenylhydrazone   (2.5)
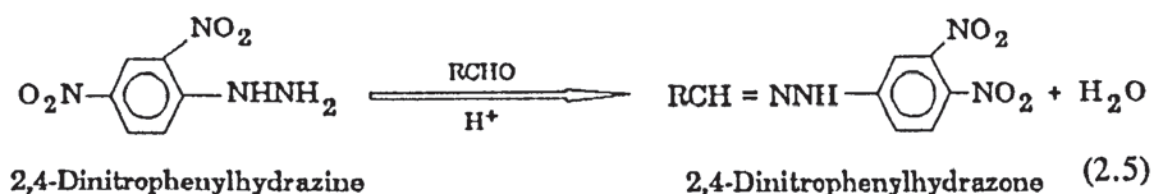
The D.N.P.H solution was prepared by gently warming 0.25g of the D.N.P.H in 5ml of methanol and 0.5ml of concentrated sulphuric acid. The warm solution was clarified by filtration and then treated with 0.1g of the carbonyl compound, dissolved in a minimum volume of methanol or ether. The mixture was boiled for two minutes, then cooled to room temperature which normally separated the D.N.P.H derivative from solution however, if this was not the case, the solution was cautiously treated with dilute sulphuric acid dropwise [98]. The filtered and washed derivative was then recrystallised from ethanol, acetic acid or xylene.

2.2.7.3. H.P.L.C. of Amines.[99]

Amines are usually derivatised via the acid chlorides to form phenyl-substituted amides [96]. Sanger introduced the use of 2,4-dinitro-1-fluorobenzene for the identification of N-terminal amino acid residues in proteins [100]. This reagent has also been widely used for the derivatisation of amine containing compounds in general, reaction (2.6). N-succinimidyl-p-nitrophenylacetate can also be used to derivatise amines under mild conditions without the use of a catalyst, reaction (2.7). However determination of amines produced from the thermal oxidation of models I and II, in this particular study, was carried out through pre-column derivatisation with dansyl chloride (5-dimethylamino-naphthalene-1-sulphonylchloride)(I) which formed the corresponding amide characterised by high absorptivity. Dansyl chloride is the most widely used of a selection of derivatives for fluorescence detection [96]. The measurement of fluoresence has certain advantages as a detection technique for liquid chromatography. The most important of these are high sensitivity, wide linear response and relatively high substance specificity. Dansyl chloride forms derivatives with primary and secondary amines readily, less readily with phenols and imidazoles and very slowly with alcohols, reaction 2.8.
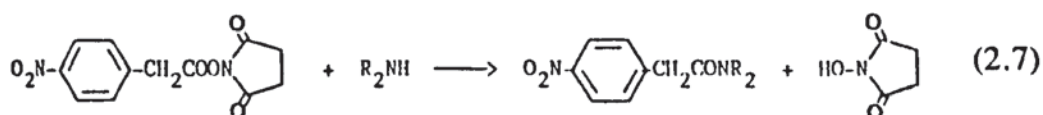
Derivatives were prepared by heating in a sealed vessel, 5.0ml of 0.25M sodium hydrogen carbonate solution with 1.0ml of 0.02M dansyl chloride solution, 0.5ml of each amine solution and 10.5ml of acetone. This was then heated at 60°C for 20mins.
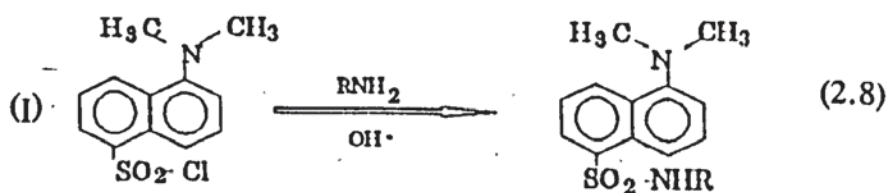
Chapter 3. Oxidation Studies of Benzene-1,3-Dimethyl Hexanamide (Model I)

3.1 Object and Methodology.

Benzene,1,3,Dimethyl hexanamide, see table 3.1, is used here as a hydrocarbon model (model I) to represent the repeat unit of the Nylon polymer MXD6, see table 3.1, in the oxidation experiments. The commercial polymer, MXD6, contains sodium phosphite added as an antioxidant at a very low concentration of about 1000ppm. Therefore as a direct comparison to the MXD6, sodium phosphite was added to the model compound and its effect on the model, at different concentrations, was examined.The work described in this chapter deals with the oxidation characteristics of Model I in the presence and absence of the antioxidant sodium phosphite and cobalt neodecanoate present in the polymer as an impurity (see table 3.1 for structures). Analysis of the results of this study was conducted with the help of a number of analytical and spectroscopic techniques viz, oxygen Absorption, ft-ir analysis, ultra violet/visible analysis, hydroperoxide determination and thermogravimetric/differential thermal analysis, see scheme 3.1.

The complementary information obtained from these different techniques has lead to a better understanding of the oxidation process of the model compound. The oxygen uptake was monitored through oxygen absorption techniques and the change in structure, associated with the oxygen uptake, was monitored by infra-red and ultra-violet/visible spectroscopy. The amount and rate of hydroperoxide formation during the oxidation process is also related to the oxygen absorption characteristics of the model and this has lead to an insight into the mechanism of the reactions involved. Activation energies of the oxidation process were obtained from thermogravimetric and differential thermal analysis. Therefore the effects of addition of sodium phosphite and cobalt on the oxidising system could be studied in the same way without modification to any of the techniques.

Molecular Weight	Chemical Structure and Name	Abbreviation
332.49	$CH_3(CH_2)_4CONHCH_2$ ⬡ $CH_2NHCO(CH_2)_4CH_3$ Benzene 1,3 Dimethyl Hexanamide	Model I (white powder) m.p $= 125°C$
	$-\{-HNCH_2$ ⬡ $CH_2NHOC(CH_2)_4CO-\}-_n$ poly(m-xylylene adipamide)	MXD6
465.46	$Co(C_{10}H_{19}O_2)_2 \cdot 4H_2O$ Cobalt Neodecanoate	Cobalt (purple pellets) m.p,$-4H_2O,140°C$
216.04	$Na_2HPO_3.5H_2O$ Sodium Phosphite	Sodium Phosphite (white crystals) m.p,$-5H_2O,150°C$

Table 3.1. Various Chemicals used in the Oxidation Study of Model I.

3.2 Results.

3.2.1 Effect of Cobalt Neodecanoate (cobalt) and Sodium Phosphite on the Oxidation of Model I : Oxygen Absorption Study.

The oxidation of model I alone and with varying concentrations of cobalt has been assessed by oxidising the model in an atmoshere of pure oxygen in the melt phase at 150°C, inside the oxygen absorption apparatus. The oxidation was carried out in the oxygen absorption apparatus as described in Section 2.4.1. The effect of additions of sodium phosphite to the model and model/cobalt systems was studied in the same way without modification to the oxygen absorption technique.
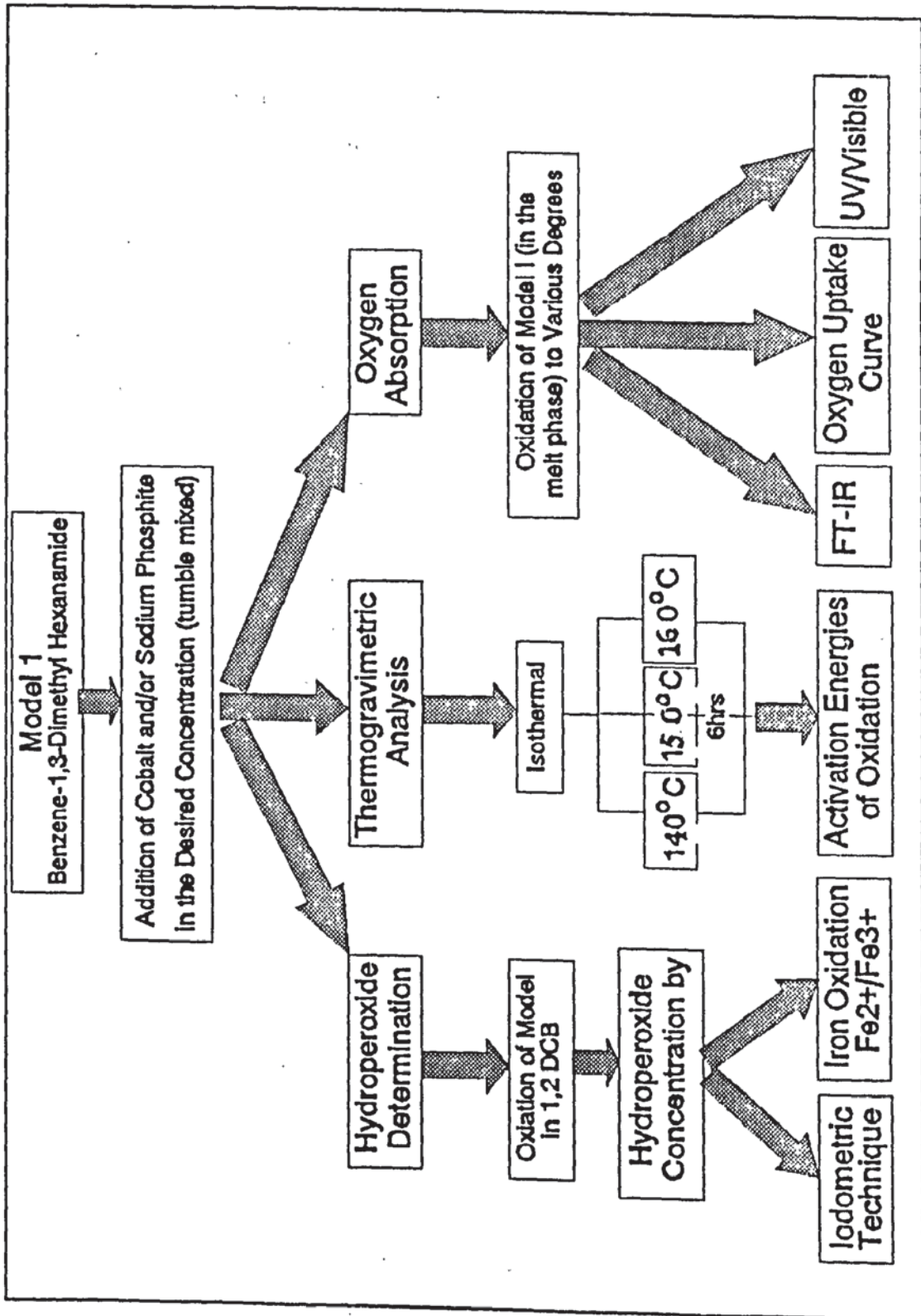
Scheme 3.1 Experimental Outline of the Oxidation Study of Model1.

3.2.1.1 Oxidation of Model I.

The oxidation curve of model I in the melt phase is shown in figure 3.1 After a very short induction period of less than five minutes, the rate of oxygen uptake was rapid particularly during the initial 2hrs. In the later stages of oxidation (>2hrs) oxygen uptake slowed down increasing at a constant rate up to 20hrs.

3.2.1.2 Oxidation of Model I in the Presence of Cobalt.

The effect of different concentrations of cobalt neodecanoate on the oxidation of model I is shown in figure 3.2a. It is clear from the oxygen absorption traces that the cobalt salt has the ability to slightly increase the oxidation of the model compound. However, after the initial 5hrs of oxidation the rates of oxidation of all samples proceeded at a similar rate (see figure 3.2b). The major difference in oxidation rates occurred in the initial 1hr as shown in figure 3.2b which compares the oxidation rates of the model containing varying concentrations of cobalt over time periods of 1, 5 and 20hrs. All different cobalt concentrations used produced very short induction period of less than 5mins except for the 200ppm cobalt, whereby the induction period is increased to approximately 15mins. Results revealed that increasing cobalt concentration increases the volume of oxygen absorbed up to a critical cobalt concentration of 200ppm cobalt, see figure 3.2a.

3.2.1.3 Oxidation of Model I in the Presence of Sodium Phosphite.

The oxidation of model I in the presence of 500, 1000 and 2000ppm sodium phosphite at 150°C is shown in figure 3.3a. The small quantities of sodium phosphite were tumble mixed with the model compound over a period of several hours to ensure thorough mixing of the two solids. Sodium phosphite acted as an inhibitor of the oxidation of model I at 150°C in the melt phase. Inhibition increased with increasing concentration of sodium phosphite, see figure 3.3b. Furthermore, the use of higher concentrations of sodium phosphite has led to an increase in the length of the induction period which was followed by a gradual auto-retarding uptake of oxygen. This contrasts the rapid oxidation of model I alone after a very short induction period, (see figure 3.3a).

3.2.1.4 Oxidation of Model I in the Presence of Cobalt and Sodium Phosphite.

The effect of various concentrations of cobalt upon the oxidation of model I in the presence of a constant concentration of sodium phosphite (1000ppm) is shown in figure 3.4. It is clear from the previous oxygen absorption traces (figure 3.3) that sodium phosphite has the ability to inhibit the oxidation of the model compound. However in the presence of cobalt the catalytic behaviour of the metal ion overcomes the inhibiting effect of the sodium phosphite hence increasing the overall oxidation of the model, see figure 3.4a. The catalytic effect of the cobalt increases with increasing its concentration up to a value of 200ppm. At higher cobalt concentrations (eg, 400 and 800ppm), the catalytic effect of the cobalt subsides, see figure 3.4b. Figure 3.4b shows clearly that the major oxidation of model I which occurs in the presence of sodium phosphite (1000ppm) and varying concentrations of cobalt (optimum at 200ppm) takes place within the initial hours of the oxidation process (more pronounced within the first 60mins). This behaviour is similar to that shown earlier, see figure 3.4c, for a comparison of the oxidation rates of this model with cobalt in the presence or absence of sodium phosphite).

3.2.2 Infra-red Spectroscopic Analysis of Model I During Thermal Oxidation.

By studying the Infra-Red spectra of the oxidised model at certain wavelengths, mainly $3600-3200cm^{-1}$ and $1800-1550cm^{-1}$ the effect of continuous oxidation upon the model structure could be followed aiding in the construction of the oxidation reaction mechanism. The analysis was carried out as described in section 2.4.2. The main IR peak changes in the model systems oxidised, with and without cobalt (& sodium phosphite), appeared at five distinct wavelength regions, carbonyls : $1746cm^{-1}$, $1705cm^{-1}$, $1683cm^{-1}$ and $1635cm^{-1}$, N-H region $3291cm^{-1}$, see figure 3.6 (also Fig.3.5 for the IR of the neat model) which is a typical example showing the changes in the FTIR spectra of model I with increasing oxidation time, up to 300 mins, in both the carbonyl and N-H- regions. The changes in the areas of the wavelength ranges, (although suprisingly small), was measured with respect to a reference peak at $3000-2890\ cm^{-1}$, and plotted against oxidation time (figures 3.8 & 3.9).

One of the most distinctive bands in an infra-red spectrum is the one arising from the carbonyl stretching mode. The procedure of detection and direct correlation of various types of carbonyl group is largely based on the frequency and intensity of one band, that due to the stretching of the C=O link. The precise position of this band, over a range 1800-1600cm^{-1}, is dependent on a number of factors. For example hydrogen bonding and conjugation effects can each lower the (C=O) frequency by as much as 50-100cm^{-1}. Electron release from a substituent nitrogen is also effective in lowering the (C=O) frequency, since it results in greater C-O single bond character (I), as in the case of amides, (C=O str 1650cm^{-1}). Therefore any breakdown of the amide group, resulting in the formation of aldehydes, ketones or carboxylic acids, would produce an increase in the (C=O) frequency, ie. from 1635cm^{-1} upto 1750cm^{-1}. The positions of C=O absorption for aldehydes, ketones, carboxylic acids, esters and amides are listed in table 1.2. This, therefore appears to be case in the oxidation of model I, in which the absorbances at 1746, 1705 and 1683cm^{-1} correspond to the formation of aldehydes, aromatic aldehydes and aromatic carboxylic acids, respectively (more definite characterisation is made later in this chapter). These arise from the decomposition of the amide group characterised by absorbances at 1635 and 3291cm^{-1}.

(I)
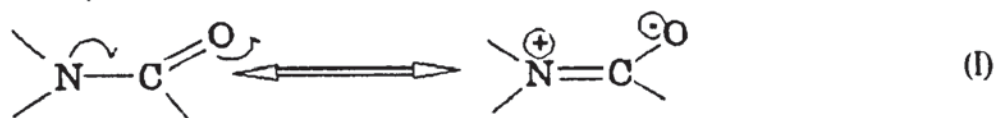
Type of Compound	Position of Absorption (cm^{-1})
aldehyde	1720-1740 (aliphatic) 1695-1715 (aromatic)
ketone	1705-1725 (aliphatic) 1680-1700 (aromatic)
carboxylic acid	1700-1720 (aliphatic) 1680-1700 (aromatic)
ester	1735-1745 (aliphatic) 1715-1725 (aromatic)
amide (C=O) (N-II)	1670-1630 3500-3200

Table 1.2 Stretching Vibrations for Some Carbonyl Compounds.

3.2.2.1 The Oxidation of Model I Alone.

The oxidation of the model alone (figure 3.6 and 3.8) revealed the increase of three absorbances in the carbonyl region at 1746, 1705 and $1683cm^{-1}$ (figure 3.8A) due to the formation of new products and a decrease in absorbance, with oxidation time, at $3291cm^{-1}$ and $1635cm^{-1}$ in the N-II and C-O stretch regions of the ir spectra respectively (figure 3.9A). The decrease in the two absorbancs (ie, negative curve) at 3291 (N-II) and $1635cm^{-1}$ (C=O), figure 3.9a, represent the decomposition of the amide (-NII-CO-) function of model I.

3.2.2.2 Oxidation of Model I in the Presence of Cobalt.

The effect of various concentrations of cobalt upon the FTIR spectra of the oxidised model compound can be seen in figure 3.7, 3.8 & 3.9. It is apparent that the same five points of interest exist ie, the increase of the absorbances at 1746, 1705 and $1683cm^{-1}$, and the decrease of the absorbances at 3291 and $1635cm^{-1}$. Additions of 50ppm and 100ppm cobalt (figs.3.8B & C) resulted in the immediate production of all three product peaks ie, 1746, 1705 & $1683cm^{-1}$. The peak at $1683cm^{-1}$, due to aromatic carboxylic acids, grew most rapidly reaching a relatively high proportion after 120 minutes of oxidation, before decreasing. The remaining two peaks increased at a similar rate but at a higher rate than in the absence of cobalt (fig.3.8A). The decrease in peak area due to the amide group is also apparent in the presence of 50ppm and 100ppm cobalt.

Addition of 200ppm cobalt (fig.3.8D) produced an induction period of 30 minutes after which all three product peaks developed at a fast rate. The loss in area due to the amide group (3291 & 1635) is still of a higher magnitude compared to the product peak formation but appears to be slower in the presence of 200ppm cobalt. 400ppm and 800ppm cobalt (figs.3.8E & F) produced a slightly different trace to the previous ones. Initially all three product peaks grew rapidly but after approximately 30 minutes the peak at $1683cm^{-1}$, after reaching a higher proportion compared to the other two, began to decrease almost reaching zero after 300 minutes of oxidation while the remaining two peaks, 1746 and $1705cm^{-1}$, leveled off at a high value. 400ppm cobalt produced a large peak loss due the amide group (fig 3.9E) but 800ppm cobalt showed the least loss of the amide functionality (fig 3.9F).

3.2.2.3 Oxidation of Model I in the Presence of Sodium Phosphite.

The effect of sodium phosphite upon the peak formation produced from the oxidation of model I can be seen in figure 3.10, 3.12 & 3.13 . Again the five maximum absorptions are observed (1750, 1705, 1683, 1635 & 3291cm^{-1}) only the rate at which these peaks change is different. Figure 3.12A and 3.13A provides a graphical representation of the increase or decrease of these peaks with increasing oxidation time. It is very clear from figure 3.12 that the production of the three product peaks , particularly 1683cm^{-1}, and loss of the amide peaks, at 3291cm^{-1} and 1635m^{-1}, are inhibited in the presence of sodium phosphite (compare with figs 3.8A & 3.9A). The peak at 1705cm^{-1} appears almost immediately but grows relatively slowly. There is a period of 120 minutes before the production of any peaks in the region 1705 and 1683 cm^{-1}.

3.2.2.4 Oxidation of Model I in the Presence of Sodium Phosphite and Cobalt.

In the presence of 50ppm cobalt (& 1000ppm Sodium Phosphite) only the peak at 1746cm^{-1} is visible and its rate of production was very slow, see figure 3.12B. The loss of area due to the amide group (3291 & 1635cm^{-1}), figure 3.13 was also unusually retarded compared to the same experiment in the absence of sodium phosphite. Addition of 100ppm cobalt resulted in a slight increase of rate of peak formation but only after a 200ppm addition did the production of all three product peaks begin to grow rapidly, see figures 3.12C & D. The loss of peak area due to the amide (fig 3.13) began to increase with the addition of 100ppm and 200ppm cobalt. 400 and 800ppm cobalt produced a very high increase in the rate of production of all three product peaks and increase in peak loss within the initial 30 minutes. However both rates slow down after 30 minutes and again after 120 minutes with a slight decrease in area of the peak 1683cm^{-1}, see figures 3.12E & F.

3.2.3 UV-Vis Spectroscopic Analysis of Model I During Thermal Oxidation.

Similarly, UV-Vis spectral analysis of oxidation of the model in the absence or presence of cobalt or sodium phosphite is expected to lead to information which help clarify the understanding of the model oxidation mechanism. Method of analysis was carried out as described in section 2.4.3.

3.2.3.1 UV-Vis Analysis of Model I Alone.

Figure 3.14 shows the UV-Vis spectrum of Model I alone with a prominent absorbance at 264nm. However oxidation of the model generally leads to to an increase in absorbance of the band at 286nm, see figure 3.15 as an example. Therefore monitoring the growth of the band at 286nm provides a good representation to the extent of oxidation in the model compound. The increase in absorbance of this band was therefore measured and plotted against increasing oxidation time, as shown in figure 3.16. The growth of the band was very fast within the initial 120 mins before slowing down substantially.

3.2.3.2 UV-Vis Analysis of Model I in the Presence of Cobalt.

The uv-vis spectra of model I in the presence of cobalt (200ppm) with increasing oxidation is shown in figure 3.17. It was a typical uv-vis spectra of a series of spectra analysed in the presence of several concentrations of cobalt ranging from 50pm to 800ppm. Figure 3.17 shows similar increases in the 286nm absorption to that shown for model I alone (see fig.3.15). This increase was measured for each cobalt concentration with increasing oxidation time and can be seen in figure 3.18. The overall rate of increase in the 286nm absorption band with oxidation time was very similar for each concentration of cobalt used. The rate of increase resembled the rates of increasing oxygen uptake, rapid increase at the beginning of oxidation, slowing down after the initial 2hrs. Inhibition periods appeared to be very short with absorbances increasing within 5mins. The increase in absorbance of the 286nm band with time over a 20hr and 1hr period can be seen in figure 3.18.

3.2.3.3 UV-Vis Analysis of Model I in the Presence of Sodium Phosphite.

Figure 3.19 shows the uv-vis spectra of model I, in the presence of 1000ppm sodium phosphite with increasing oxidation time. Again it highlights the growth of the band at 286nm which is noticably smaller in comparison to that of the model alone (fig.3.15) and model I in the presence of cobalt (fig.3.17). The effect of different concentrations of sodium phosphite (500ppm, 1000ppm and 2000ppm) upon the increase absorbance of the 286nm band over a 1hr (insert) and 20hr oxidation period are shown graphically in figure 3.20.

Sodium phosphite acts to inhibit the developing absorbance of the 286nm band, the inhibiting effect increasing with increasing concentration of sodium phosphite. This behaviour is comparable with that observed for the oxidation curves (from oxygen absorption study see section 3.2.1.3). The effect of the sodium phosphite can be seen more clearly in the initial 60mins of oxidation, see insert of figure 3.20. In its absence the absorbance rises rapidly auto-accelerating in the initial hour but addition of 500ppm of sodium phosphite slows down this rapid change and delays the onset of the auto accelerating effect. Addition of 1000ppm sodium phosphite increases this effect but this change levels off at 2000ppm.

3.2.3.4 UV-Vis Analysis of Model I in the Presence of Sodium Phosphite and Cobalt.

The uv-vis spectra of model I in the presence of sodium phosphite (1000ppm) and cobalt (200ppm) with increasing oxidation is shown in figure 3.21. It was a typical uv-vis spectrum of a series of spectra analysed in the presence of several concentrations of cobalt ranging from 50pm to 800ppm. The extent of oxidation was monitored by the change in the uv/visible spectra particularly the increase in absorbance of the 286nm band over a 20hr and 1hr(insert) oxidation period, see figure 3.22. The absorbance at 286nm increased at a similar rate to the oxygen uptake of the model (cf figure 3.4). The growth of the 286nm band indicates the potential of the cobalt to overcome the inhibiting effect of the sodium phosphite. All additions of cobalt with the exception of 50ppm produce very rapid absorbance changes before slowing down after 2hrs of oxidation.

A comparison of the four separate experiments is summarised in figure 3.23. It shows the increase in absorbance at 286nm during the increasing oxidation of model I, alone and in the presence of a typical concentration of cobalt, sodium phosphite and a combination of both cobalt and sodium phopshite.

3.2.4 Effect of Cobalt and Sodium Phosphite on Peroxide Formation During the Oxidation of Model I.

The hydroperoxide concentration during the oxidation of the model compound, at 150°C, in the presence of cobalt, sodium phosphite and cobalt/sodium phosphite was monitored. Two separate methods were used to measure the hydroperoxide concentration:-

1) an iodometric technique, which depends on the oxidation, in acidic solution, of iodide to iodine by any hydroperoxide present and

2) a technique involving the oxidation of a Fe^{2+} salt, by the hydroperoxide formed, and monitoring the absorbance of the unoxidised iron via a complex formation using UV spectroscopy. Both techniques and the analysis carried out are described in section 2.4.4.

3.2.4.1 Effect of Oxidation of Model I on Hydroperoxide Formation.

The hydroperoxide formed during the oxidation of model I in 1,2 dichlorobenzene at 150°C in an oxygen atmosphere is shown in figure 3.24. The hydroperoxide curve, via iodometric titration for Model I alone (fig.3.24) suggested an inhibition period of approximately 15mins followed by a steady build up of hydroperoxide reaching a maximum after 70mins of oxidation. The curve obtained via the iron oxidation method for model I alone suggested an inhibition period of approximately 5mins followed by a steady build up of hydroperoxide reaching a maximum also after 70mins, figure 3.25.

3.2.4.2 The Effect of Sodium Phosphite on Hydroperoxide Formation in the Oxidising Model.

Sodium Phosphite was added to the model in concentrations of 1000ppm and 2000ppm. The hydroperoxide curves were then compared with that of the model after oxidation for 250mins (Figure 3.26 & 3.27). In the presence of 1000ppm sodium phosphite, as measured by Iodometric titration (fig 3.26), the induction period, before the commencement of hydroperoxide formation, is increased to approximately 45mins. Peak concentration occurs at 75mins.

In the presence of 2000ppm sodium phosphite hydroperoxide formation begins after 70mins of oxidation reaching a peak concentration at approx. 100mins, as measured by Iodometric titration (fig3.26) and begins after 15mins, reaching a maximum at 100mins, as measured by the iron oxidation technique, see figure 3.27. The overall effect of sodium phosphite is therefore seen to delay the onset of hydroperoxide formation in the oxidising model, see inset figure 3.26 & 3.27.

3.2.4.3 The Effect of Cobalt on the Hydroperoxide Formation in the Oxidising Model.

Cobalt Neodecanoate was added to the model in concentrations of 50, 200 and 800ppm and the hydroperoxide formation compared to that of Model1 alone after oxidation for 250mins (Figure 3.28 & 3.29). None or very little hydroperoxide was detected during the oxidation of Model I in the presence of all concentrations of cobalt examined using both the iodometric titration technique (fig 3.28) and the iron oxidation technique (fig 3.29).

3.2.4.4 The Effect of Sodium Phosphite and Cobalt on the Hydroperoxide Formation in the Oxidising Model.

Sodium Phosphite in a concentration of 1000ppm was added to the model in addition to 200ppm and 800ppm cobalt. The effect of the combination of cobalt and phosphite upon the hydroperoxide formation was examined and the results were compared to those of model1(sodium phosphite) (Figure 3.30 & 3.31). The presence of 200ppm and 800ppm cobalt in combination with sodium phosphite produced no or very little hydoperoxide detectable by the iodometric titration technique (fig3.30) or the iron oxidation technique (fig.3.31).

3.2.5 Further Investigation of the Effect of Cobalt on Peroxide Formation during the Oxidation of Model I.

Results for the previous section showed clearly that cobalt supresses the formation of hydroperoxide in the model, (both in the presence and absence of sodium phosphite), at all concentrations and when measured by two different peroxide determination techniques (iodometric and colormetric). The lack of hydroperoxide formed during the oxidation of the model, in the presence of cobalt, is therefore possibly due to the breakdown of the peroxide by the cobalt salt.

However to prove this possibility, and eliminate any experimental interference from the methods used for peroxide determination, a simple experiment was conducted where-by the cobalt was added during the oxidation of the model compound, as opposed to the oxidation of a cobalt-model mixture from time zero. The experimental outline is summarised in scheme 3.2.
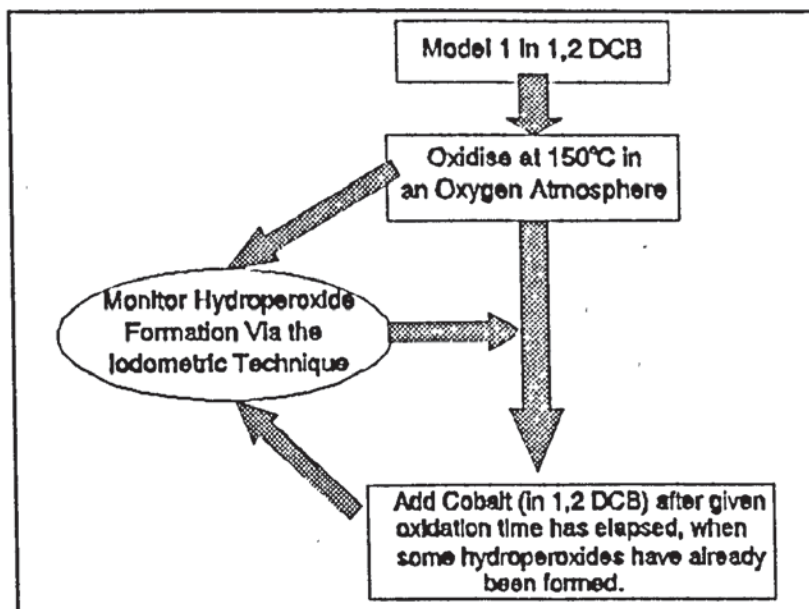
Scheme 3.2 Experimental Outline for the Investigation of the Effect of Cobalt on Peroxide Formation During the Oxidation of Model I at 150°C in 1,2 DCB, (nos. on curves are conc.(ppm) of cobalt added after 50mins oxidation time).

Hydroperoxide concentration was monitored using the Iodometric technique described in section 2.4.4. The model compound was dissolved in 1,2 Dichlorobenzene and oxidised under an oxygen atmosphere at 150°C. The hydroperoxide build up was monitored during oxidation of the model only and the cobalt was added after 50 minutes oxidation when the hydroperoxide concentration in the model started to rise (see figure 3.32). Figure 3.32 shows clearly that the addition of cobalt to the model, after the model's initial oxidation (for approx 50 mins) and build up of hydroperoxide concentration, leads to prevention of further hydroperoxide formation and to decomposition of all peroxide already formed in the model. It is also clear from figure 3.32 that 200ppm cobalt has a stronger inhibition effect in the peroxide formation than 800ppm.

3.2.6 The Effect of Cobalt and Sodium Phosphite on the Oxidation of Model I : Thermogravimetric Study.

A totally different way of assessing the effect of cobalt, sodium phosphite and a combination of cobalt-sodium phosphite on the oxidation of the model compound is to measure the activation energies required for the different oxidation experiments. By measuring the weight loss of the model, at fixed temperatures, assuming the weight loss is due to loss of volatile products formed during the oxidation, the effect of cobalt and sodium phosphite additions can be monitored. Samples of model I, in the absence and presence of various concentrations of sodium phosphite and cobalt were heated isothermally in an oxygen atmosphere at 140°, 150° and 160°C for 6 hours inside the thermal balance, according to the procedure described in section 2.4.5.

3.2.6.1 The Effect of Cobalt on the Oxidation of Model I : Thermogravimetric Study.

The isothermal traces showing the effect of different concentrations of cobalt on the thermal oxidation of model I can be seen in the figures listed :-

a) ModelI Alone at 140, 150 & 160°C (figure 3.33a)
b) ModelI + 200ppm Cobalt at 140, 150 & 160°C (figure 3.33b)
c) ModelI + 5000ppm Cobalt at 140, 150 & 160°C (figure 3.33c)
d) ModelI + 10000ppm Cobalt at 140, 150 & 160°C (figure 3.33d)

Based on first order kinetics, it was possible to calculate the activation energies associated with the oxidative weight loss of model I, with and without cobalt. The slope of each trace was calculated directly after the onset of weight loss and recorded as rate constant 'k', see table 3.3.

Sample (ppm Co)	Degradation Temp.(°C)	Rate Constant 'k' (s⁻¹)	ln 'k'
Model1	140	1.68×10^{-4}	-8.69
	150	2.29×10^{-4}	-8.38
	160	3.21×10^{-4}	-8.04
200ppm	140	9.83×10^{-5}	-9.23
	150	1.14×10^{-4}	-9.02
	160	1.62×10^{-5}	-8.77
5000ppm	140	7.84×10^{-4}	-7.15
	150	8.72×10^{-4}	-7.04
	160	9.30×10^{-4}	-6.92
10000ppm	140	7.95×10^{-4}	-7.14
	150	9.17×10^{-4}	-6.99
	160	1.11×10^{-3}	-6.82

Table 3.3 Rate Constants Derived for the Thermal Oxidation (via isothermal TGA) of Model I with and without Cobalt.

From the plots of the logarithms of the rate constants versus the reciprocal of the absolute temperature at which the analysis was conducted, the activation energies were obtained by the slope of the straight line (figure 3.35). Slope of the straight line $= -E_a/R$ where $E_a=$ activation energy (J mol⁻¹) and R= gas constant 8.314 (J K⁻¹ mol⁻¹), see table 3.4

Sample (ppm Cobalt)	Straight Line Equation	Activation Energy (kJ mol⁻¹)
Model1 (0ppm)	y = 5.82 - 6.0x	49.8
200ppm	y = 0.93 - 4.2x	34.9
5000ppm	y = -2.07 - 2.1x	17.5
10000ppm	y = -0.36 - 2.8x	23.3

Table 3.4 Activation Energies Calculated for the Oxidative Degradation of Model I, with and without Cobalt.

3.2.6.2 The Effect of Cobalt and Sodium Phosphite on the Oxidation of Model I :
Thermogravimetric Study.

The traces derived from isothermally heating model I (1000ppm sodium phosphite) in the
presence of cobalt, at 140, 150, 160°C are shown in figure 3.34 and listed below :-

a) ModelI (sodium phosphite) at 140, 150 & 160°C (figure 3.34a)

b) ModelI (sodium phosphite) + 200ppm Cobalt at 140, 150 & 160°C (figure 3.34b)

c) ModelI (sodium phosphite) + 5000ppm Cobalt at 140, 150 & 160°C (figure 3.34c)

d) ModelI (sodium phosphite) + 10000ppm Cobalt at 140, 150 & 160°C (figure 3.34d)

Sample (ppm Co)	Degradation Temp.(°C)	Rate Constant 'k' (s⁻¹)	ln 'k'
Model I	140	2.41×10^{-5}	-10.64
	150	4.36×10^{-5}	-10.04
	160	1.15×10^{-4}	-9.07
200ppm	140	2.98×10^{-4}	-8.12
	150	2.96×10^{-4}	-8.12
	160	3.05×10^{-4}	-8.10
5000ppm	140	5.25×10^{-4}	-7.55
	150	5.81×10^{-4}	-7.45
	160	6.66×10^{-4}	-7.32
10000ppm	140	6.35×10^{-4}	-7.36
	150	7.60×10^{-4}	-7.18
	160	8.93×10^{4}	-7.02

Table 3.5 Rate Constants Derived for the Thermal Oxidation of Model I, in the Presence
of 1000ppm Sodium Phosphite, with and without Cobalt.

Again the slope of each trace (fig 3.36) was calculated directly after the onset of weight loss and recorded as rate constant 'k', see table 3.5. From the plots of the logarithms of the rate constants versus the reciprocal of the absolute temperature at which the analysis was conducted, the activation energies were obtained by the slope of the straight line (figure 3.36) and are shown in table 3.6.

Sample (containing 1000ppm sodium phosphite (ppm Cobalt)	Straight Line Equation	Activation Energy (kJ mol⁻¹)
Model1	y = 21.78 - 13.4x	111.4
200ppm	y = -7.18 - 0.4x	3.3
5000ppm	y = -2.71 - 2.0x	16.7
10000ppm	y = 0.12 - 3.1x	25.7

Table 3.6 Activation Energies Calculated for the Oxidative Degradation of Model I, in the Presence of 1000ppm Sodium Phosphite, with and without Cobalt.

The isothermal weight change curves derived from the samples produced two characteristic points of interest. Initially some degree of oxidation in the form of weight gain was observed followed by a lengthy period of weight loss. The gain in weight occurred for up to 8,000 secs, depending on the sample, before commencement of the weight loss (figure 3.37).
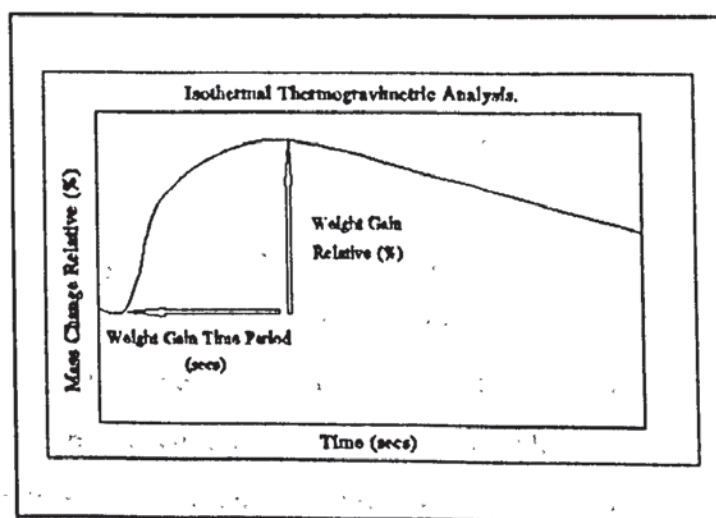
Figure 3.37 A Schematic Representation of a Typical Isothermal Thermogravimetric trace showing the Calculation of Initial Weight Gain Followed by Weight Loss of the Sample During Oxidation.

An increase in temperature and an increase in the cobalt concentation generally resulted in the weight gain being concentrated over a shorter period of time, see figure 3.38. The relative weight gain was also found to be dependent on both the temperature of oxidation and the concentration of the cobalt catalyst in the model compound. At lower temperaures and low levels of cobalt ion, the weight gain was more apparent, see figure 3.39. This initial weight gain is thought to be related to the oxygen uptake of the model compound. Oxidation results in the formation products (eg, hydroperoxide, carbonyl groups) which decompose to form volatiles ejected from the model as, for example, carboxylic acids, aldehydes & ketones. The weight loss proceeded the weight gain and continued throughout the analysis of the sample. At higher temperatures the rate of weight loss was greater than at lower temperatures and generally greater in the presence of cobalt. Therefore the initial weight gain is thought to be caused by oxygen reacting with the model and the weight loss due to the emission of the oxidation by-products.

3.3 Discussion.

The five techniques used in the study of the thermal oxidation of model I, each in their own unique way reveal something about the effect that heat, oxygen, cobalt and sodium phosphite had upon the model compound. In different ways they have assessed the extent of increasing degradation of the model and hence individually led to an insight into the mechanism of the thermal oxidation of the model in absence and presence of the antioxidant (sodium phosphite) and the catalytic impurity (cobalt neodecanoate).

3.3.1 The Thermal Oxidation of Model I Alone.

The primary and sole use of the oxygen absorption technique was to study the oxygen uptake of the model. The other techniques, (hydroperoxide determination, ir and uv/vis spectroscopy and thermogravimetric analysis), although providing an assessment of the extent of oxidation this was secondary to gaining an insight into the model breakdown and mechanism of thermal oxidation.

Oxygen absoption showed clearly that model I readily absorbs oxygen at 150°C, in the melt phase. This absorption was particularly dramatic in the initial 2 hours of oxidation after which point the oxygen absorption curve began to 'level' out (figure 3.40). Important observations can be made from the shape of the oxygen absorption curve. Firstly the absence of any induction period is an important factor. The exposure of a polymer to oxygen is usually charaterised by an induction period, during which the polymer does not show any obvious changes and therefore there is no evidence of oxygen absorption. However, it is during this stage that small amounts of hydroperoxide are formed and initiate the subseqent rapid autoxidation of the polymer. The absence of such an induction period in model I therefore suggests a rapid formation of hydroperoxide resulting in the rapid autoxidation of the model compound. Peroxide analysis of the model did in fact show an immediate production of hydroperoxide which proceeded to build up over a 70 minute period, see figure 3.40. The second important observation, concerning the oxygen absorption curve, was the levelling off period, ie, the decline in the rate of oxygen uptake. It was thought that this could perhaps be due to the production of volatile degradation products, which are apparent from the thermogravimetric isothermal study on the degradation of model I (fig3.33a).

The method of oxygen absorption measurement is based on the changes of pressure within a sample and reference flask, therefore production of volatiles in the sample flask would make a slight difference to the oxygen absorption measurement. However it is thought that the levelling off period is more likely to be due to the saturation of the active sites in the model compound. Support for this proposal arises from evidence of the UV/Vis experiments which also produces a levelling off period due to the decline in the rate of increase in the absorbance at 286nm (fig.3.16). Other alternatives may involve the depletion of oxygen in the sample flask or the formation of products with inhibitive activity as investigated by Denisov [101] and experienced by Sagar [49] during the study of alkylamides, but the possibility of saturated active sites was also proposed by Patel [102] after his study of the oxidation of MXD,6(+200ppm cobalt) at 100°C for 100mins.

The spectroscopic study, to a certain extent, supports the oxygen absorption results by providing an alternative measure to the extent of oxidation of model I. The FT-IR study followed the build up of reactant products, and the disappearance of the amide functional group (-NH-CO-), in the oxidising model (fig3.8a). The peaks formed at $1746cm^{-1}$, $1705cm^{-1}$ and $1683cm^{-1}$ are typical of aliphatic aldehydes (eg.acetaldehyde), aromatic aldehydes (isophthalaldehyde) and aromatic carboxylic acids (isophthalic) respectively, see figure 3.41 and 3.42, maybe resulting from the breakdown of the amide functional group which was very apparent. Therefore in following the formation and disappearance of these functional groups provided an alternative assessment to the extent of degradation of the model. However, FT-IR spectroscopic analysis is unlikely to detect the complete range of products formed from the oxidation of model I. Possible products of oxidation include aliphatic and aromatic amines which produce characteristic absorbances at approximately $1605cm^{-1}$, see figure 3.43 for typical examples. An absorbance in this region would be difficult to identify in the FT-IR spectra of the oxidised model. A combination of analysis by both FT-IR and UV/Vis spectroscopy may help in some respect for the identification of amines, but TG analysis also showed a large percentage of products were lost as volatiles during the oxidation of model I. These are likely to include low molecular weight carboxylic acids and aldehydes/ketones, hence avoiding detection by spectroscopic analysis (FT-IR & UV/Vis) on the non-volatile part of the sample. Ideally, in conjunction with the isothermal thermogravimetric study, analysis should also include evolved gas analysis.

The formation of functional groups as monitored by FT-IR spectroscopy are more defined and easily recognisable. However in the uv-vis spectra particualar functional groups are not so easily recognisable. It was apparent that during oxidation of the model the absorbance at 286nm increased with increasing oxidation. Measuring this increase with increasing oxidation time provided an assessment of the extent of oxidation of the model, which compared favourably with the oxygen absorption curves. However, it was important to investigate the origins of this absorbance from a mechanistic point of view. It is likely that this increase is due to the formation of a particular functional group associated with an aromatic ring due to the absorbance at a high wavelength. The FT-IR study has already suggested that the breakdown of the model is occurring via the amide function resulting in the formation of aldehydes, and carboxylic acids.

The formation of these different functionalities and the breakdown of the amide group must involve the break down of several bonds in the model compound. Kamerbeek et al [37] and Mortimer [38] asserted that the CH_2-NH bond was responsible for initial polyamide cleavage. Their arguments were based on the assumption that the weakest bond would break more easily than the stronger bond. For polyamides, the next theoretically weakest bond is the CH_2-CO bond. Fission of the CH_2-NH bond results in the formation of an amido and alkyl radical (3.1), and fission of the CH_2-CO bond results in the formation of an alkyl and hydroisocyanate radical (3.2).

i) $\wedge CH_2$-CO-NH-$CH_2 \vee$ ------> $\wedge CH_2$-CO-NH· + ·$CH_2 \vee$ (3.1)

ii) $\wedge CH_2$-CO-NH-$CH_2 \vee$ --------> $\vee \wedge CH_2$· + ·CO-NH $CH_2 \vee$ (3.2)

Both breakages lead to the formation of radicals from which the oxidation reaction may propagate. However radical formation is also likely to occur by loss of a reactive hydrogen atom (alpha to the NH group) due to external forces, such as shear or heat. Peroxide studies of the oxidation of model I (section 3.2.4) suggest the formation of substantial quantities of hydroperoxide via which the propagation step of the oxidation reaction is likely to take place, see scheme 3.3. Decomposition of the hydroperoxide would lead to the formation of isophthaldehyde (and subsequently isophthalic acid), and m-xylylene diamine via reaction scheme 3.4 and 3.5 respectively.

The uv-vis spectra of these three possible products (isophthalaldehyde, isophthalic acid and m-xyxlylene diamine), with increasing concentration, is shown in figures 3.44, 3.45 and 3.46 respectively. It appears that m-xylylene diamine was the likely cause of the increase in absorbance at 286nm during the oxidation of model I. The formation of the aromatic aldehyde and aromatic acid is also likley, as is apparent in the FT-IR analysis, but their presence in the uv spectra, as with the formation of any aliphatic product, is masked by the broad absorption due to the formation of m-xylylene diamine. The main absorption of m-xylylene diamine in the FT-IR spectra occurs at 1607cm^{-1} (see fig 3.43), making detection during the FTIR analysis extremely difficult. In Summary due to the action of heat on the model, formation of radical species occur with the subsequent absorption of oxygen and hydroperoxide formation. Decomposition of these hydroperoxides, through a series of reactions, leads to the formation of aldehydes, carboxylic acids and amines (scheme 3.6).

Model I

CH₃(CH₂)₄CONHCH₂ — CH₂NHCO(CH₂)₄CH₃

Heat (150°C)

-CH-NHCO-

(loss of reactive hydrogen atom due to external forces)

(bond fission)
-CH₂ NH- or -CO-CH₂ -

-CH₂ + NH-   -CO + CH₂·

RH ⟸ model absorbs oxygen
(oxygen absorption study)

Hydroperoxide Formation
(detected by peroxide determination
using iodometric or colormetric
technique).
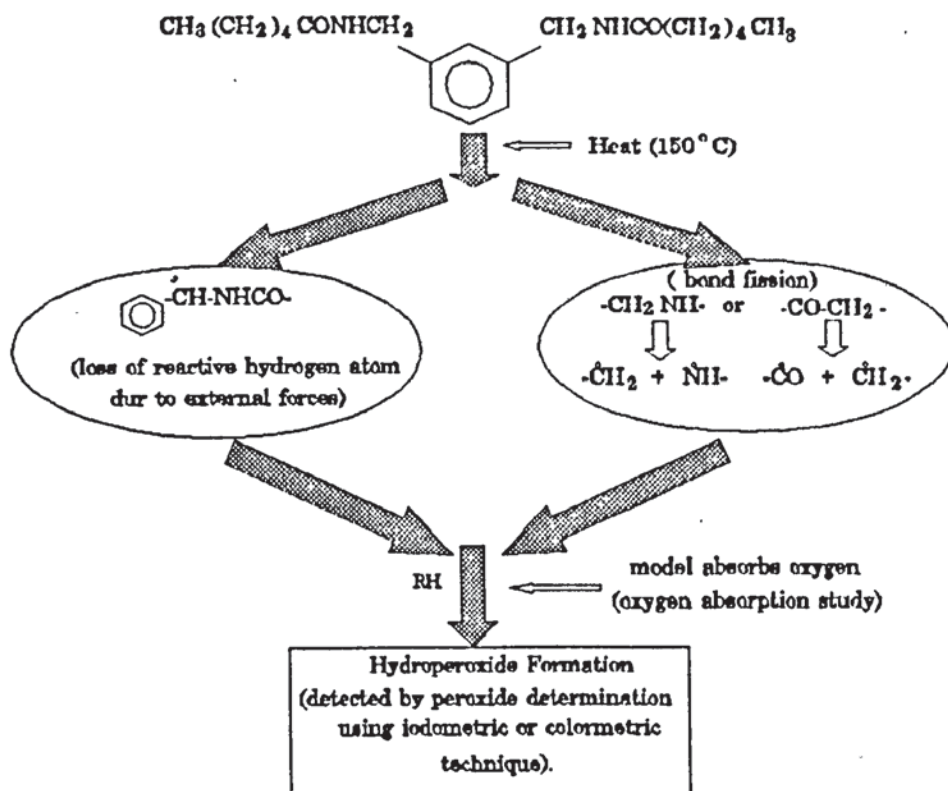
Scheme 3.3 Oxidation Mechanism of Model I Outlining the Possible Breakdown of the Model Via Loss of a Reactive Hydrogen or Bond Fission Reslting in Hydroperoxide Formation.

Scheme 3.4 Oxidation Mechanism of Model I Outlining the Formation of Isophthalaldehyde and Isophthalic Acid.
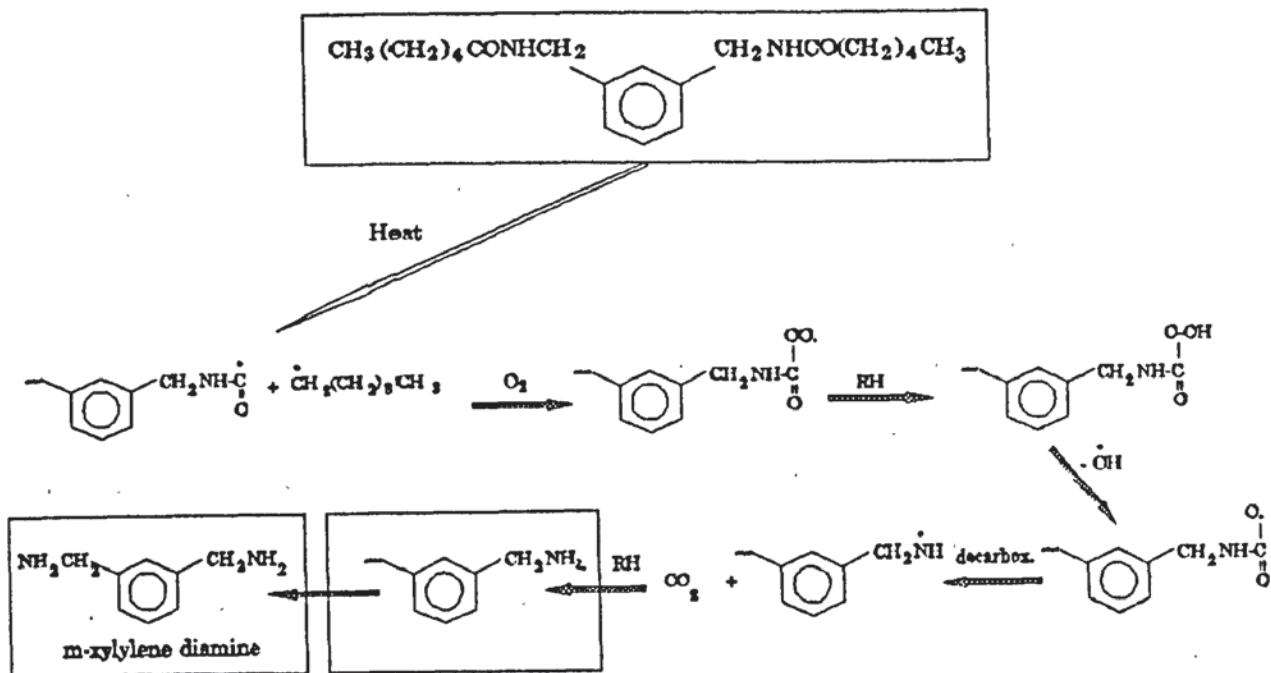
Scheme 3.5 Oxidation Mechanism of Model I Outlining the Formation of m-Xylylene Diamine.
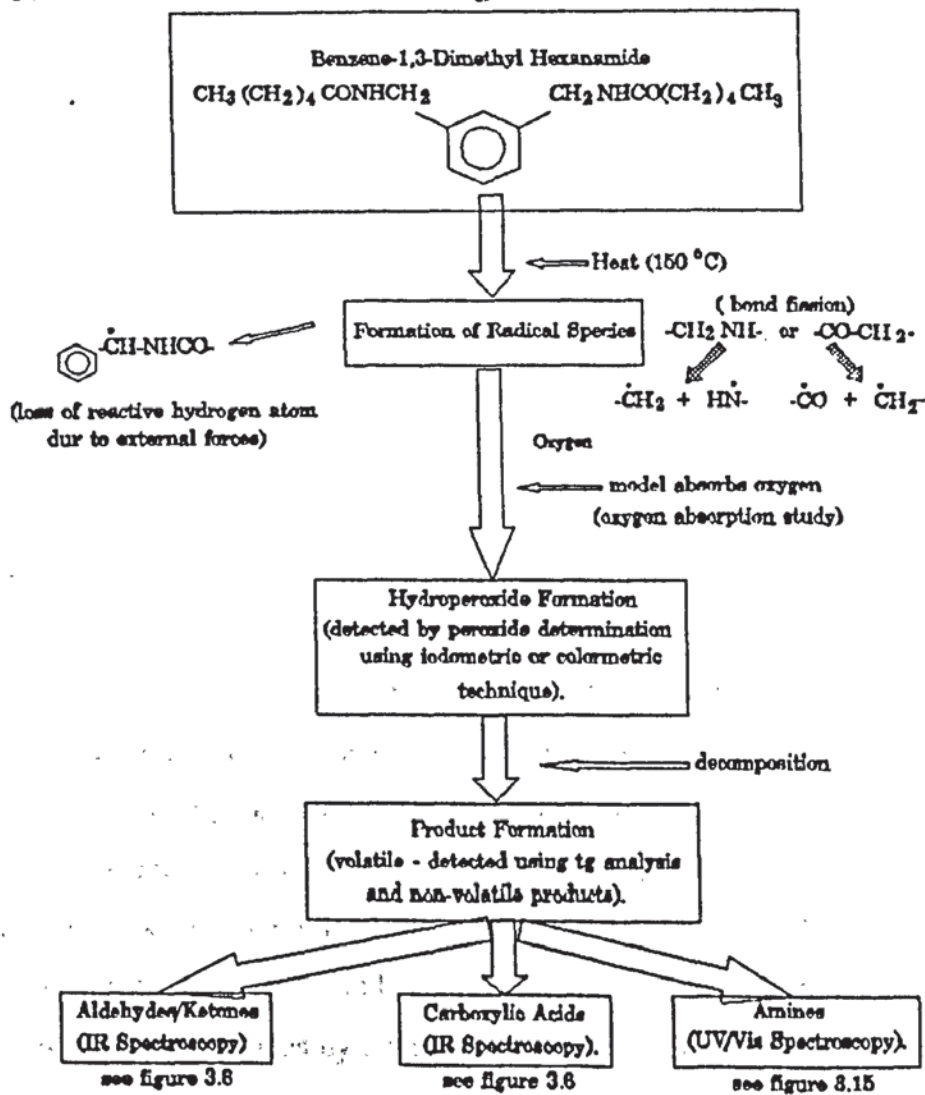
Scheme 3.6 Oxidation Mechanism of Model I Outlining the Possible Breakdown of the Model Via Loss of a Reactive Hydrogen or Bond Fission Resulting in Hydroperoxide Formation with Subsequent Decomposition to form a Series of Aldehydes, Carboxylic acids and Amines.

3.3.2 The Thermal Oxidation of Model I in the Presence of Cobalt.

The effect of cobalt on the oxidation of model I at 150°C is summarised in scheme 3.7. It was found that in all oxidation studies of model I that the unmodified model readily absorbs oxygen alone, however the addition of cobalt (0-800ppm) did not dramatically increase the amount of oxygen absorbed. This was confirmed by Infrared and UV-visible spectroscopic techniques which followed the build up of products and decomposition of the model structure during thermal oxidation . It is now apparent that the uv-vis analysis monitored, at least in part, the formation of m-xylylene diamine in the oxidising model. Similar findings were also encoutered by Carnaud MetalBox [56] when studying the oxygen uptake potential of a series of model compounds for the polymer, MXD6. However, additions of cobalt (0-200ppm) to the MXD6 polymer and the 'ideal' polymer blend (96%PET, 4% MXD,6) was shown to greatly increase the potential of the substrate to absorb oxygen. Patel [102] showed (figure 3.47 & 3.48) that the rate of oxidation of the blend and the polymer alone increased with catalyst (cobalt) concentration until the catalyst concentration reached a critical concentration of 200ppm (in case of the blend) where the most effective oxygen uptake results were recorded. There after further small incremental increases in cobalt concentration resulted in the oxygen uptake rate suffering a catastrophic decline.

Many other investigators [16,28] have observed a similar decline in the rate of oxidation of polymers as the concentration of transition metal ions, such as cobalt, is increased beyond a critical value. The experiments conducted in this work on model I, with a cobalt range from 0-800ppm, failed to show a critical concentration of cobalt, in contrast to the behaviour described by the afore mentioned workers. The general trends of the oxygen absorption curves showed an initial absorption followed by a levelling off period, ie, a decline in the rate of oxygen uptake, similar to the model alone. Again it is thought that this levelling off period is more likely to be due to the saturation of the active sites in the model compound. In the study of model I alone, the importance of hydroperoxide formation in the oxidation process is clearly indicated. Similarly, as was discovered in a study of the autoxidation of N-alkyl amides by Sagar [49], when cobalt was added initially to the amide, hydroperoxide was not detected at any stage during the oxidation, however, the model was shown to absorb oxygen (figure 3.49) with the continuing formation of stable products.

Sagar assumed, in his work, that the metal ions catalysed the decomposition of the hydroperoxide by the reaction sequence (3.3 and 3.4) [49].

$$R'OOH + Co^{2+} \longrightarrow R'O\cdot + Co^{3+} + \cdot OH \quad (3.3)$$

$$ROOH + Co^{3+} \longrightarrow RO_2\cdot + Co^{2+} + H^+ \quad (3.4)$$

and further that, after the very rapid initial conversion of cobaltous to cobaltic, reaction (3.4) is probably rate determining in the early stages of oxidation. Further investigation of the effect of cobalt on peroxide formation during the oxidation of model I, as caried out in section 3.2.5, confirms that cobalt has the ability to decompose the hydroperoxide, resulting in a slight increase in the oxidation of the model compound.

The spectroscopic study, carried out on the model in the presence of cobalt, revealed that the reaction mechanism, in respect to the pathway of formation of degradation products, is unaltered in the presence of cobalt. Similarly the products formed are aldehydes, carboxylic acids and amines. The only difference which may occur, in the presence of cobalt, may involve the initiation process. In the model alone there are two possibilities for initiation to occur, as discussed in section 3.3.1. However in the presence of cobalt a third possibility must be considered. For the oxidation of hydrocarbons, metal catalysts have been known to initiate the chain of autoxidation by forming reactive radicals. Therefore initiation may occur via a favourable complex formation between the cobalt and amide chain, resulting in the abstraction of the most reactive hydrogen atom, which is the hydrogen atom in the alpha position to the NH group, which is also made more reactive by being alpha to the benzene ring. To explain this complex formation, it is suggested that the carbonyl groups of the amide donate a lone pair of electrons to the cobalt in preference to electron pair donation via the N-H groups (II).
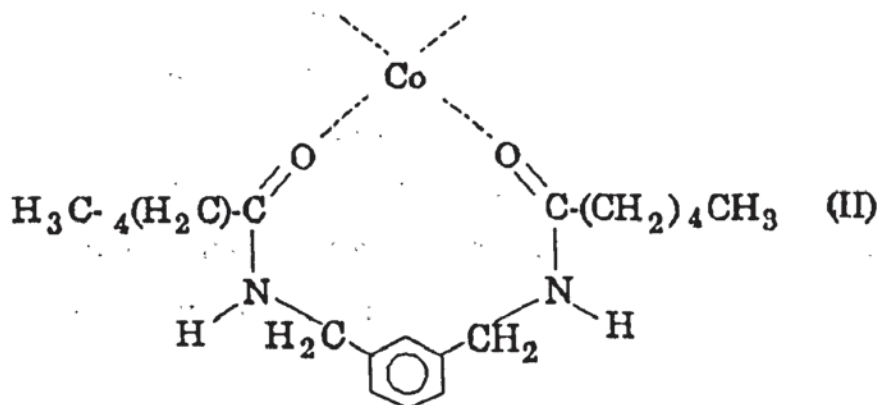
The complex is thought to activate the oxygen present thus creating a superoxide radical anion (III) which may be a very reactive centre,
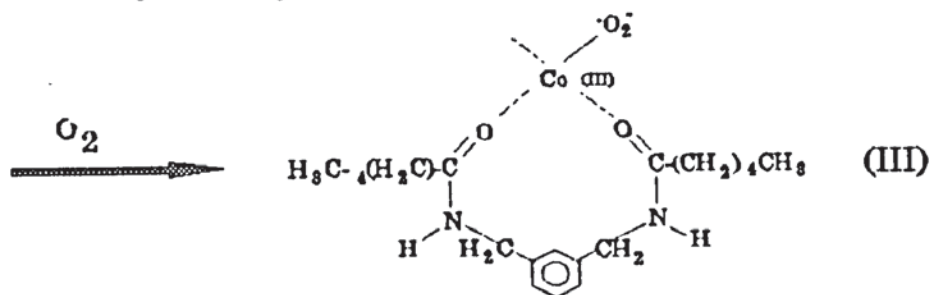
which in turn may abstract the most readily available hydrogen atom (IV) from a neighbouring amide chain, ie, alpha to the N-H group.
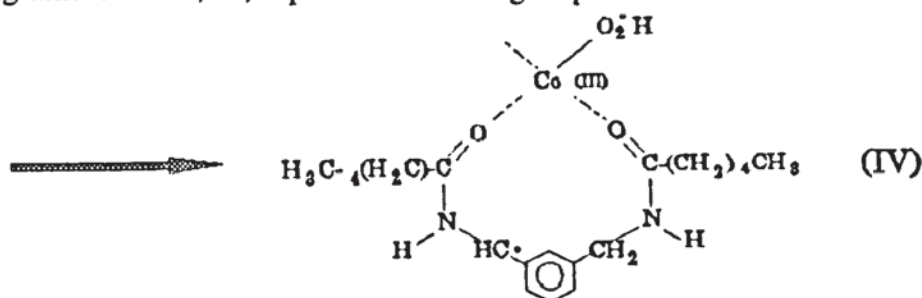
Disproportionation of the latter leads to a conjugated species having a high degree of resonance stabilization (V,VI).
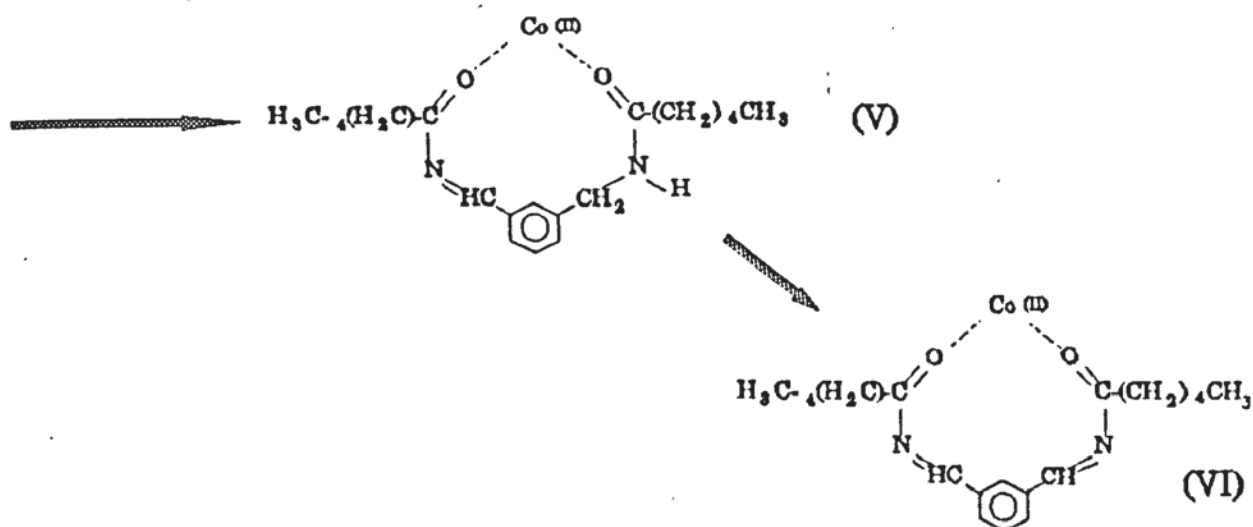
Thus duing the course of initiation, the radicals R., $.O_2H$ and .OH have been formed. It is therefore pssible that these radicals are responsible for the latter stages of oxidative propagation. This, therefore, does not necessitate that the cobalt play any further part in the oxidation process and implies that it acts principally as a reaction initiator. If this was the case, hydroperoxide formation would be detected during the oxidation of model I in the presence of cobalt, however the absence of any such hydroperoxide formation, as discussed earlier in figure 3.49, was clearly illustrated.
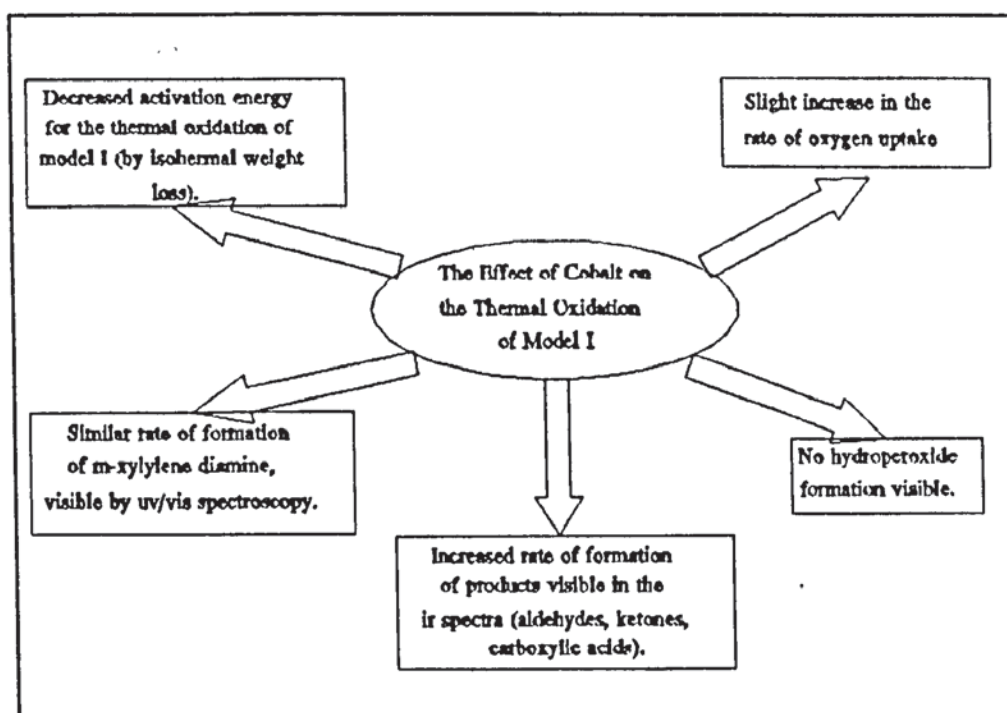
Scheme 3.7 A Summary of the Effect of Cobalt on the Oxidation of Model I at 150°C.

3.3.3 The Thermal Oxidation of Model I in the Presence of Sodium Phosphite.

The effect of sodium phosphite on the oxidation of model I at 150°C is summarised in scheme 3.8. The antioxidant found in the MXD6 (by Carnaud MetalBox), sodium phosphite, in a concentration of 1000ppm is therefore the likely reason for the conflict in results between the model and the MXD6 polymer blend. In this work, experiments were conducted where similar concentrations of sodium phosphite to that normally present in the polymer were added to the model and the antioxidant activity was clearly displayed (fig.3.3). The antioxidant effect was increased with increasing concentration, resulting in a lower total of oxygen absorbed (fig.3.3) and delaying the onset of degradation products which were visible by IR and UV/visible spectroscopy (figures 3.12 and 3.20 respectively). Monitoring the hydoperoxide formation in the oxidising model also gave a clear indication of the antioxidant effect of the sodium phosphite. When added to the model compound, sodium phosphite delayed the onset of the hydroperoxide formation, which is reflected in the reduced oxygen uptake performance of the model, see figure 3.50. Finally the sodium phosphite was shown to behave as an inhibitor for the amide oxidation, increasing the activation energy, calculated by isothermal weight loss curves (figure 3.52 & table 3.6).
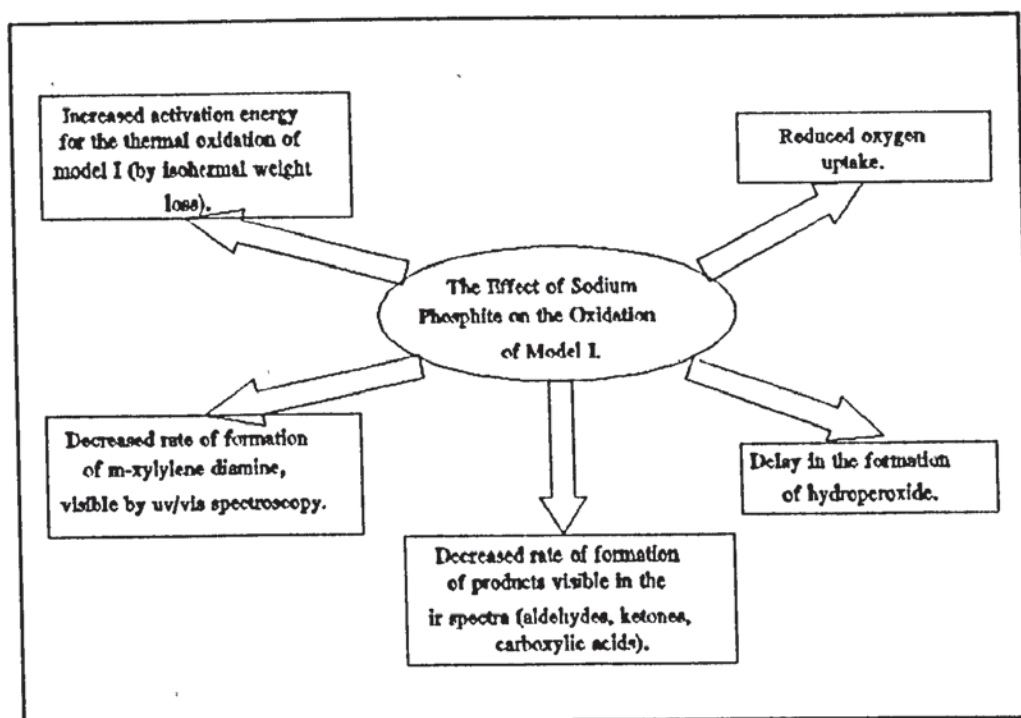
Scheme 3.8 A Summary of the Effect of Sodium Phosphite on the Oxidation of Model I at 150°C.

3.3.4 The Thermal Oxidation of Model I in the Presence of Cobalt and Sodium Phosphite.

The effect of sodium phosphite and cobalt on the oxidation of model I at 150°C is summarised in scheme 3.9. When cobalt is added to the model, in the presence of sodium phosphite, the results obtained are more comparable with those of the MXD6 and the 'ideal blend'. The oxidation of the model in the absence of cobalt was shown to be somewhat retarded but in its presence oxidation proceeded rapidly (fig.3.4). However a critical concentration of cobalt was not reached, in the oxygen absorption study, above which the level of oxygen uptake should fall (fig. 3.4).

However, the determination of activation energies for the thermal oxidation of model, via an isothermal weight loss technique (section 3.2.6), revealed that the use of cobalt at 5000ppm and 10000ppm, concentrations in excess of those used in the oxygen absorption study, lead to an increasing activation energy, in comparison to that of 200ppm cobalt (figure 3.52 and table 3.6) but was still lower than that of the model, particularly the model in the presence of 1000ppm sodium phosphite.

The hydroperoxide results show an absence of any hydroperoxide (fig3.30), which suggests that the cobalt is still likely to be responsible for their decomposition, as discussed earlier. The spectroscopic analysis follows the same trend as the oxygen absorption, with analysis in the IR and UV-Vis spectra (figures 3.12 & 3.22 respectively), revealing that increasing the cobalt concentration increased the rate of product formation, with respect to the model plus 1000ppm sodium phosphite. The nature of products formed were similar to that of the model alone only the rate of formation has changed.
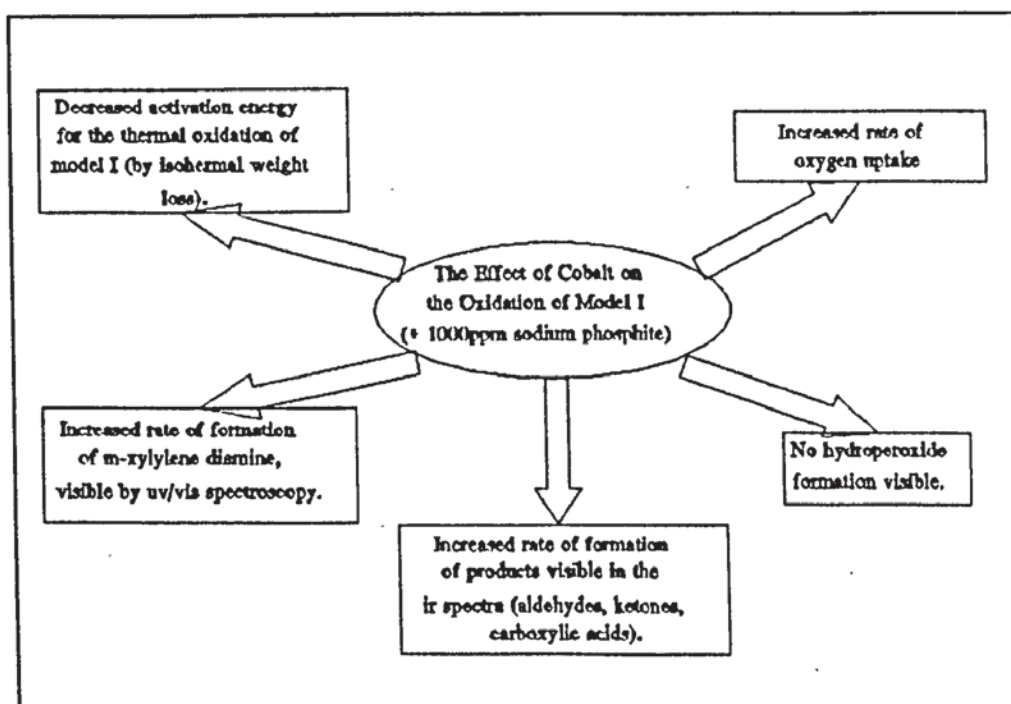
Scheme 3.9 A Summary of the Effect of Sodium Phosphite and Cobalt on the Oxidation of Model I at 150°C.
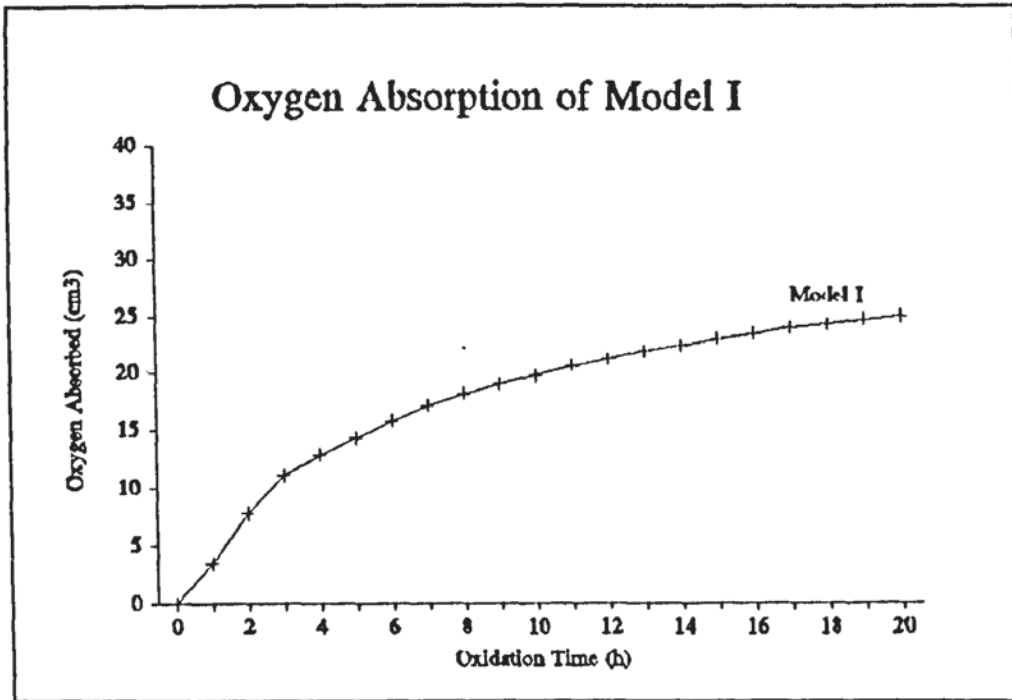
Figure 3.1 Oxygen Absorption of Model I in the Melt Phase at 150°C (curve represents volume of oxygen absorbed per 0.5g of sample).
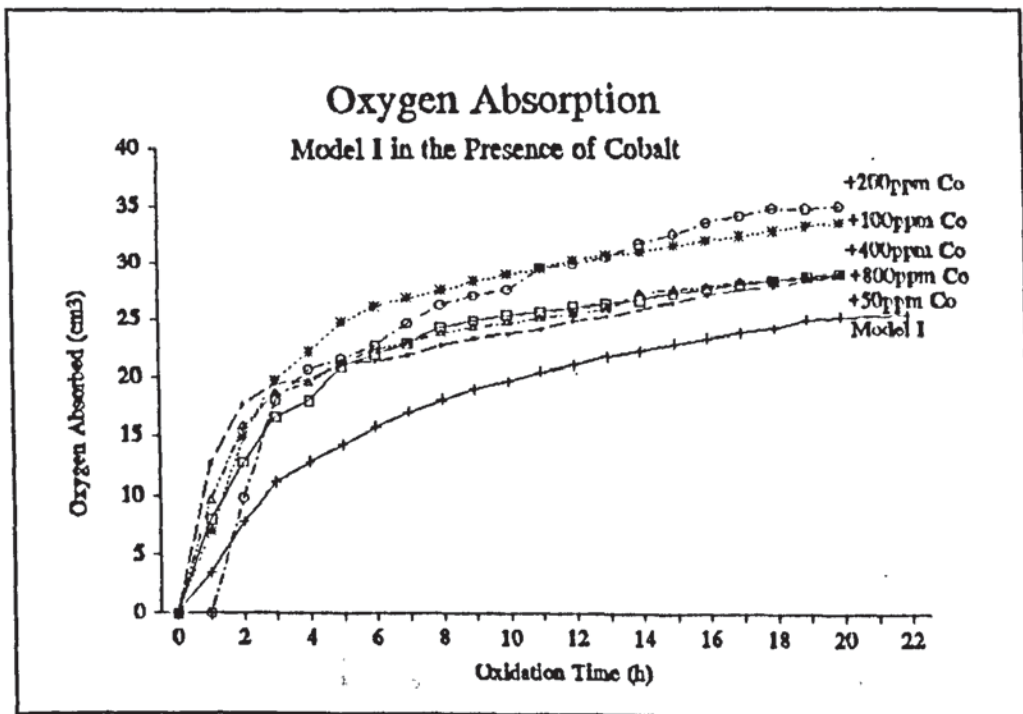
Figure 3.2a Oxygen Absorption of Model I in the Melt Phase at 150°C in the Presence of Different Cobalt Concentrations (curve represents volume of oxygen absorbed per 0.5g of sample).

Rates of Oxidation

Model I : Effects of Cobalt Concentration
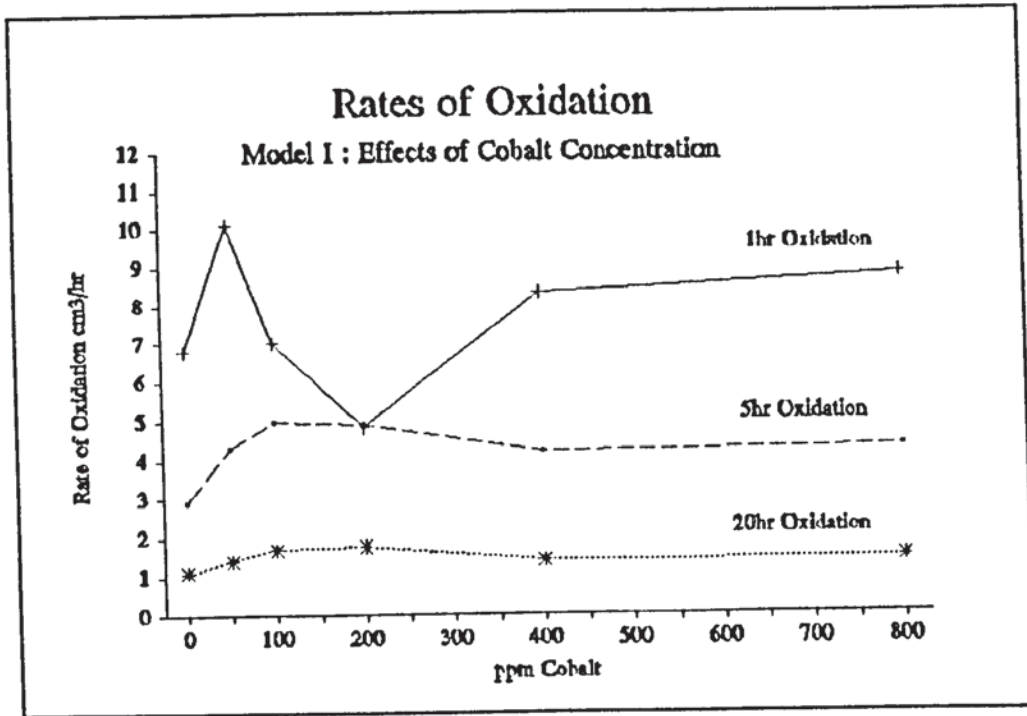
Figure 3.2b The Effect of Cobalt Concentration on the Rate of Oxidation of Model I, at 150°C (in the melt), over a 1hr, 5hr and 20hr Period (rates obtained from oxygen absorption curves).

Oxygen Absorption

Model I + Various Conc.of Sodium Phosphite
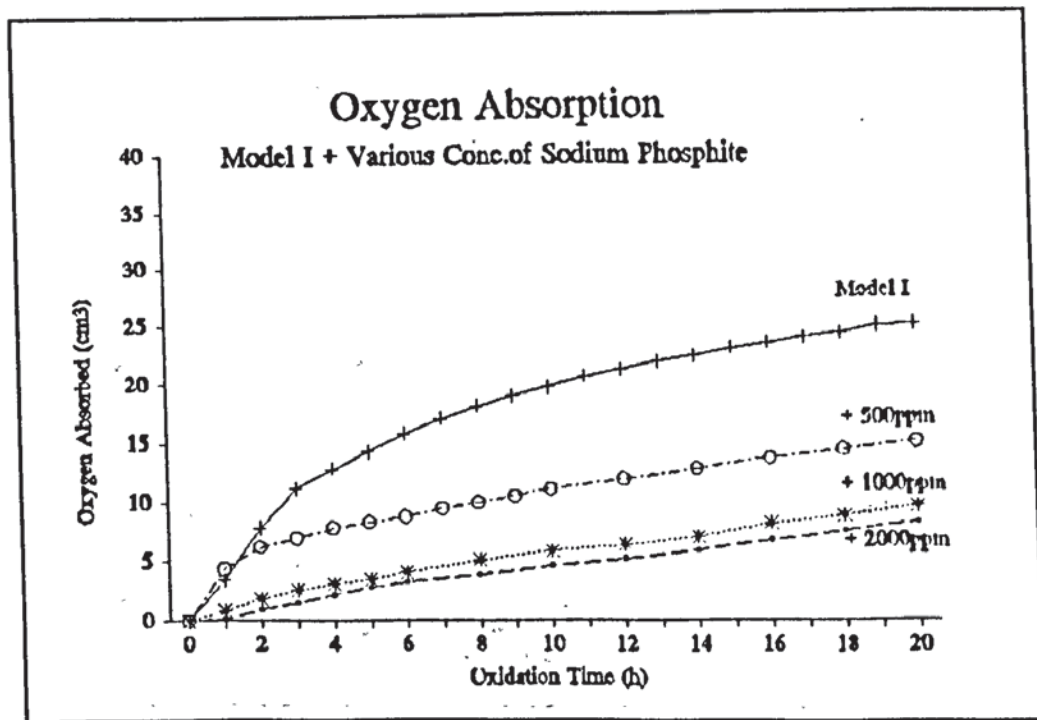
Figure 3.3a Oxygen Absorption of Model I in the Melt Phase at 150°C in the Presence of Different Sodium Phosphite Concentrations (curve represents volume of oxygen absorbed per 0.5g of sample).

Rates of Oxidation

Model I : Effect of Sodium Phosphite Concentration
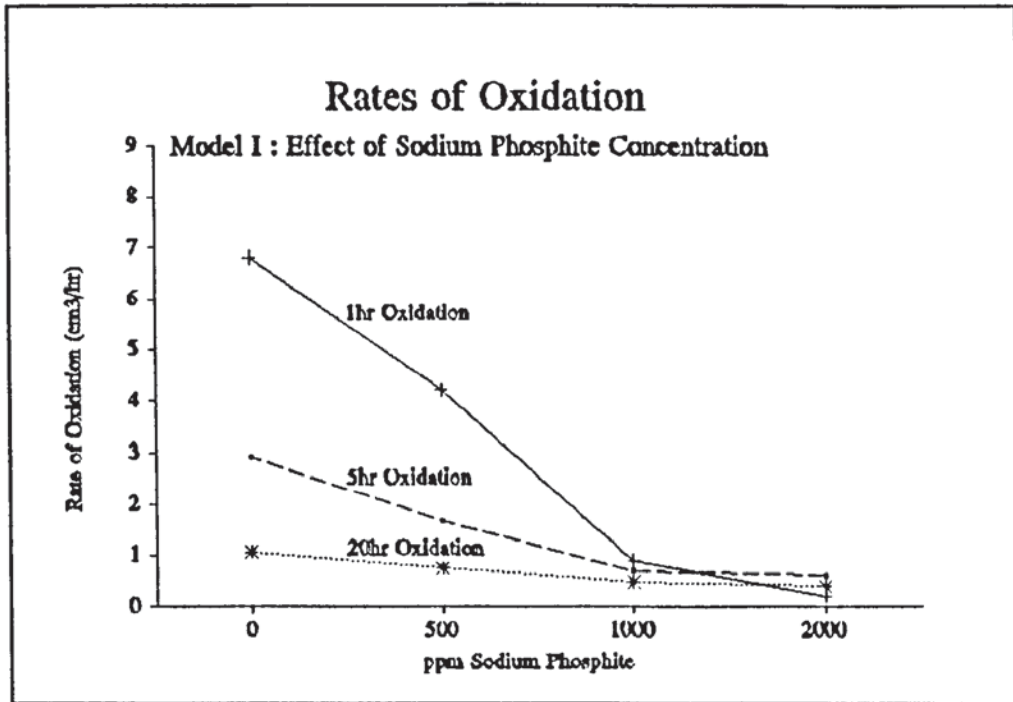
Figure 3.3b The Effect of Sodium Phosphite Concentration on the Rate of Oxidation of ModelI, at 150°C (in the melt), over a 1hr, 5hr and 20hr period (rates obtained from oxygen absorption curves).

Oxygen Absorption

Model I in the Presence of Sodium Phosphite (1000ppm)
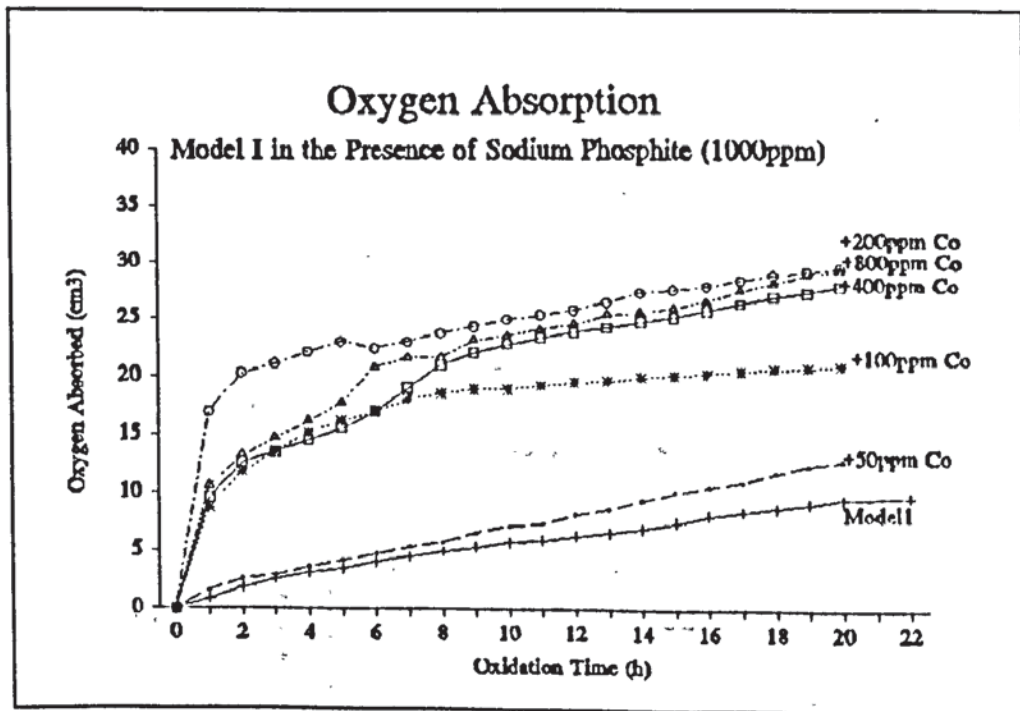
Figure 3.4a Oxygen Absorption of Model I in the Melt Phase at 150°C, in the Presence of 1000ppm Sodium Phosphite and Different Concentrations of Cobalt (curve represents volume of oxygen absorbed per 0.5g of sample).
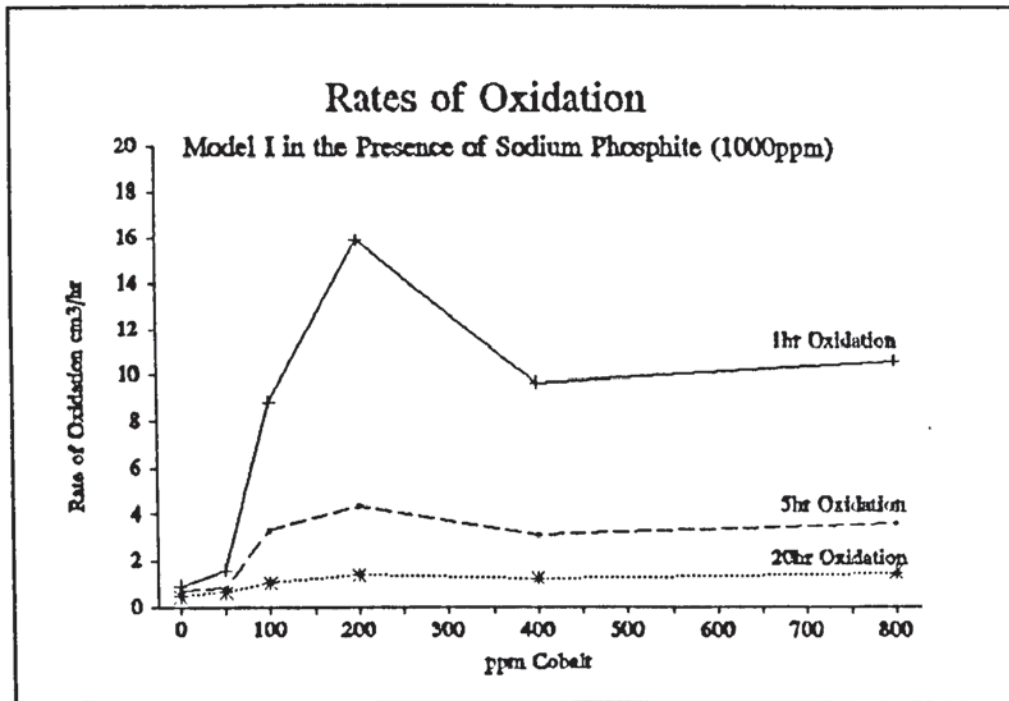
Figure 3.4b The Effect of Cobalt Concentration on the Rate of Oxidation of Model I plus 1000ppm Sodium Phosphite, at 150°C (in the melt), over a 1hr, 5hr and 20hr period (rates obtained from oxygen absorption curves).
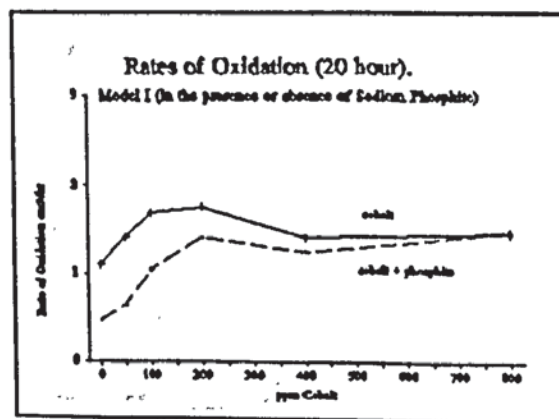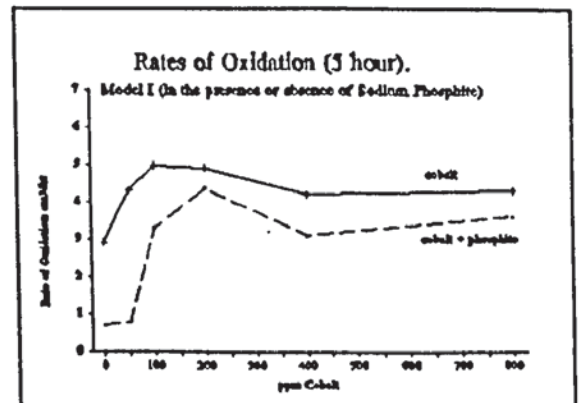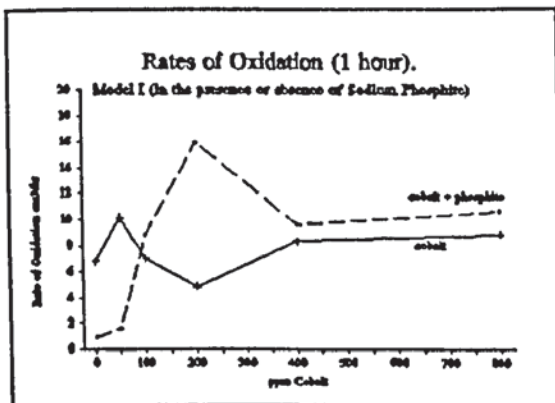
Figure 3.4c A Comparison of the Effect of Cobalt & Cobalt/Sodium Phosphite (1000ppm) on the Rate of Oxidation of Model I, at 150°C, over a 1hr(i), 5hr(ii) and 20hr(iii) period.
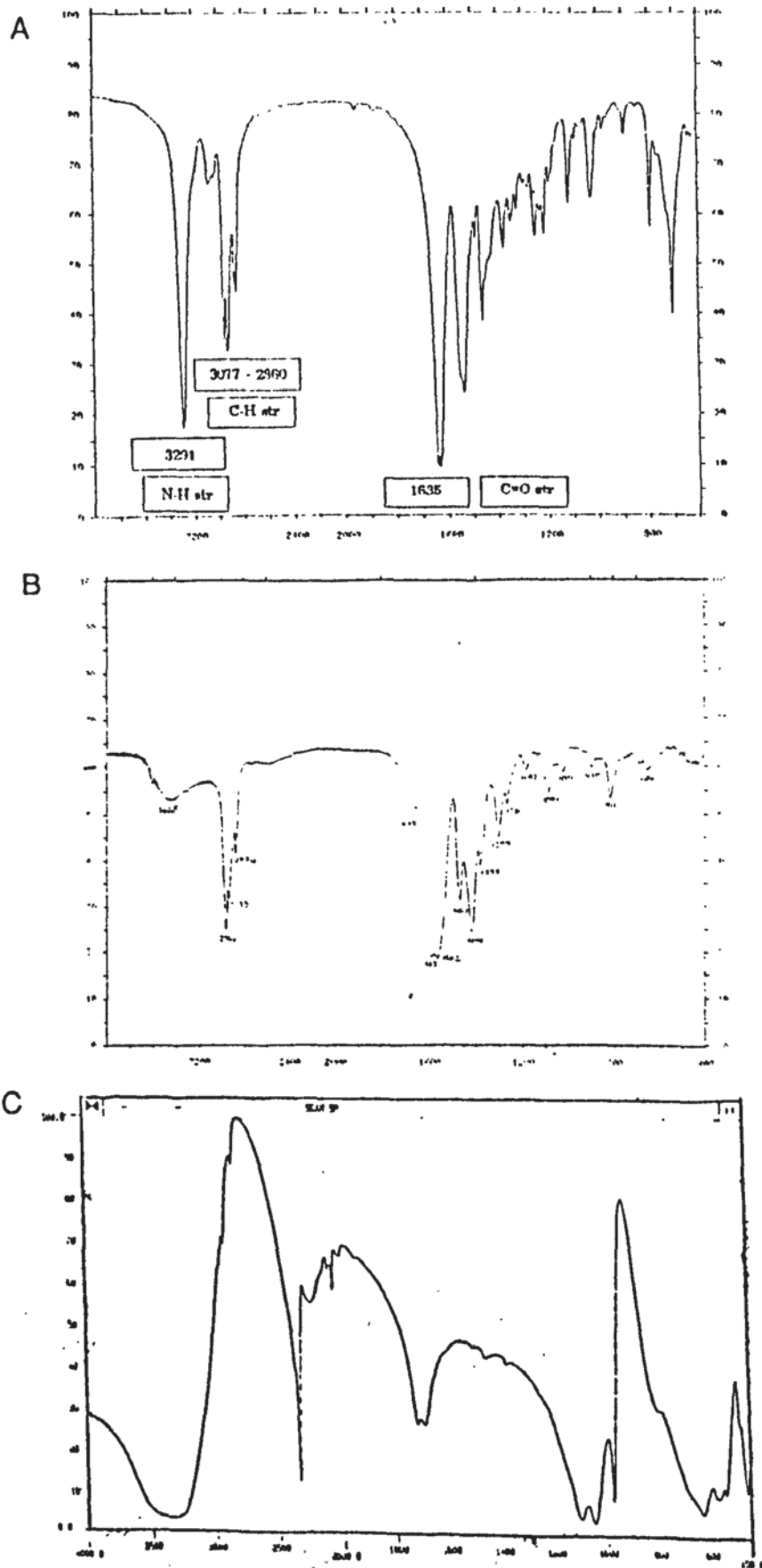
Figure 3.5   The FT-IR Spectra of A) Model I, B) Cobalt Neodecanoate and C) Sodium Phosphite, Prepared as KBr Discs.
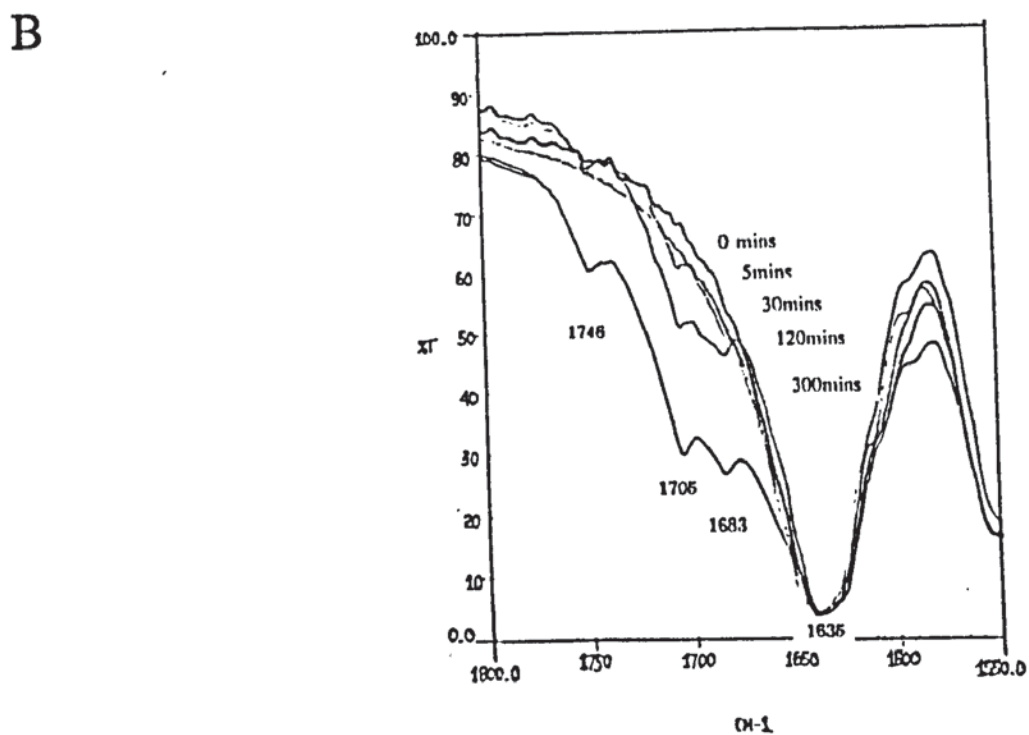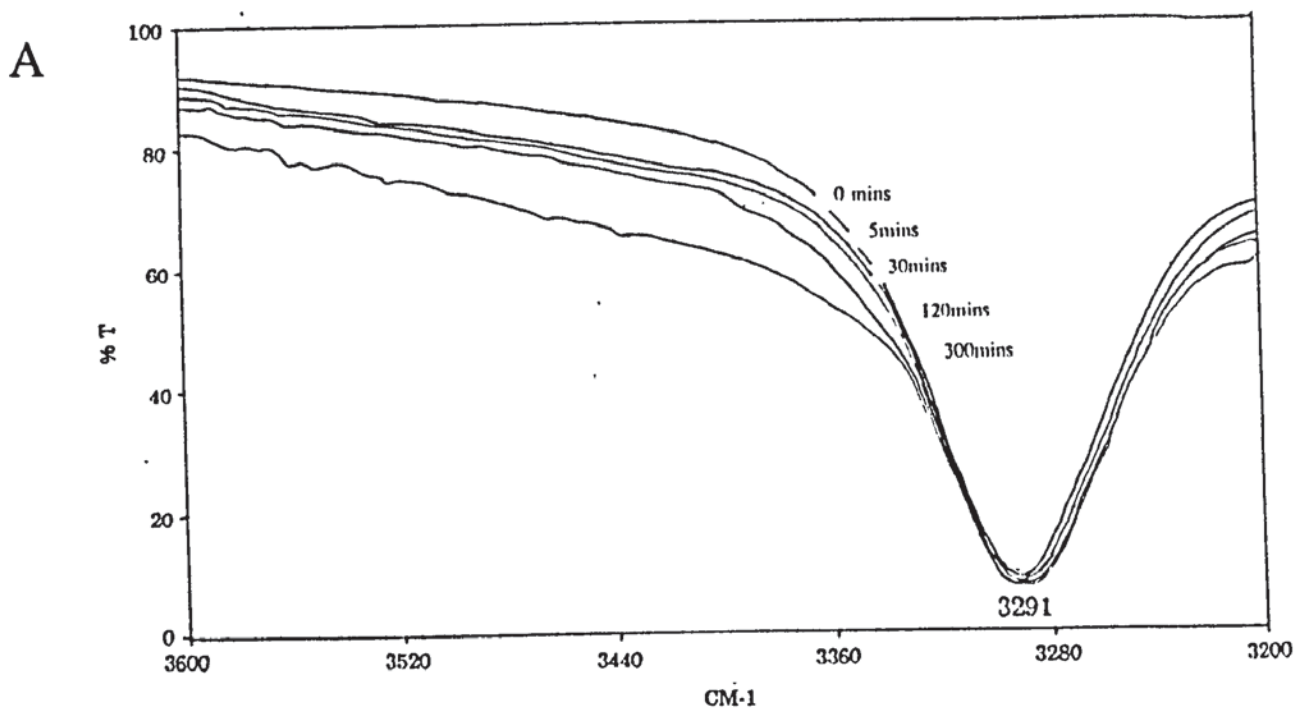
Figure 3.6 The Changing FT-IR Spectra of Model I with Increasing Oxidation Time, at 150°C, in the Regions 3600-3200cm⁻¹ (A) and 1800-1550cm⁻¹ (samples taken out from the oxygen absorption experiments).
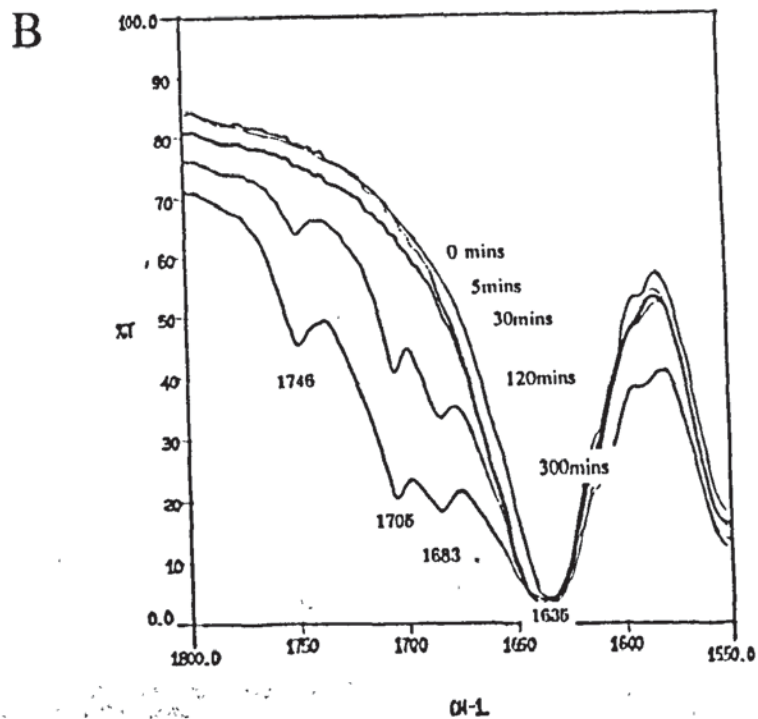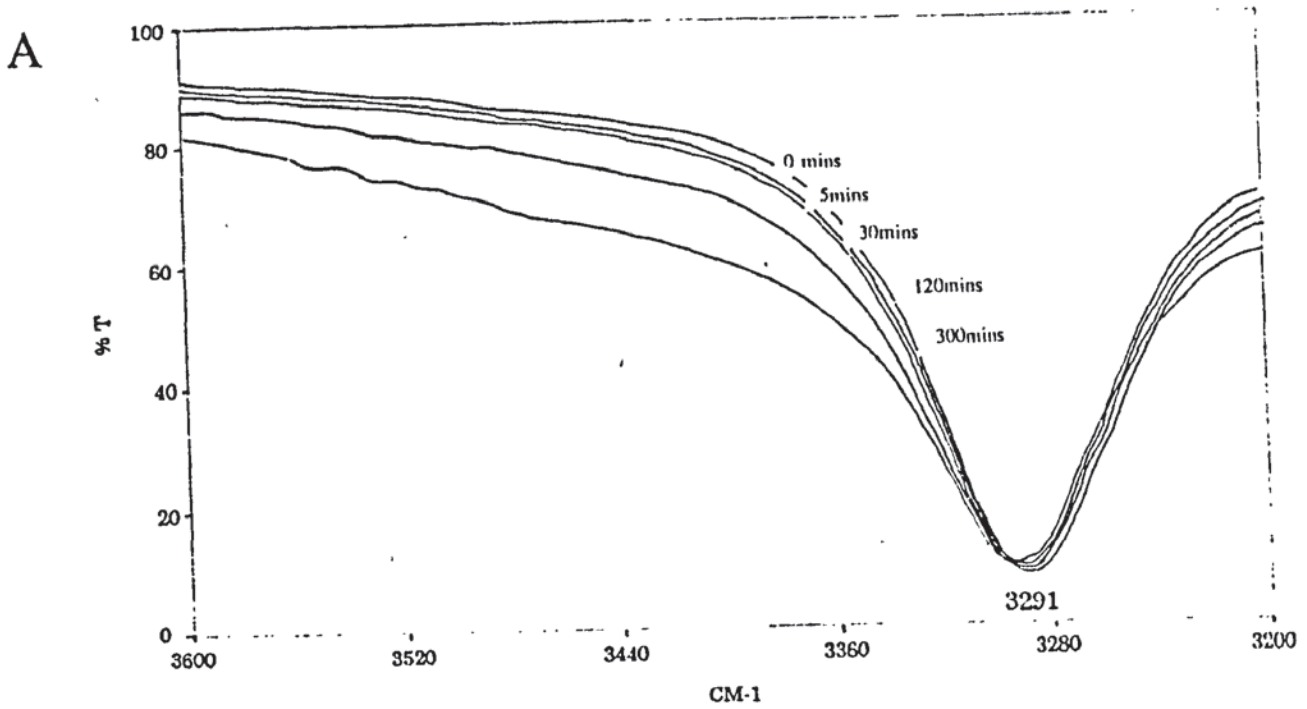
Figure 3.7   The Changing FT-IR Spectra of Model I, in the Presence of 200ppm Cobalt, with Increasing Oxidation Time, at 150°C, in the Regions 3600-3200cm⁻¹ (A) and 1800-1550cm⁻¹ (samples taken out from the oxygen absorption experiments).
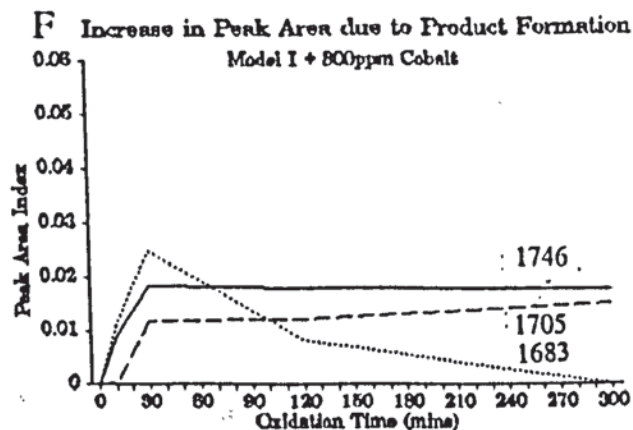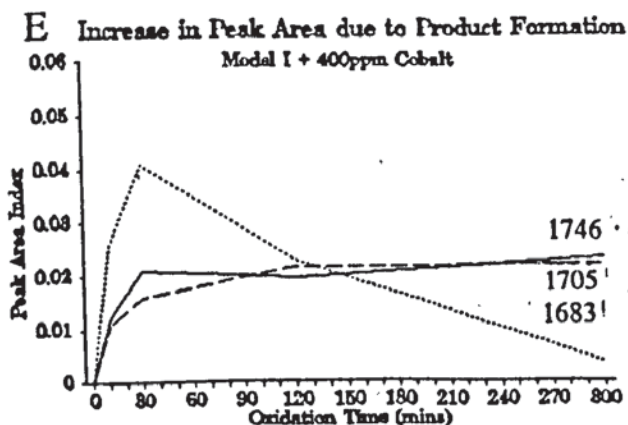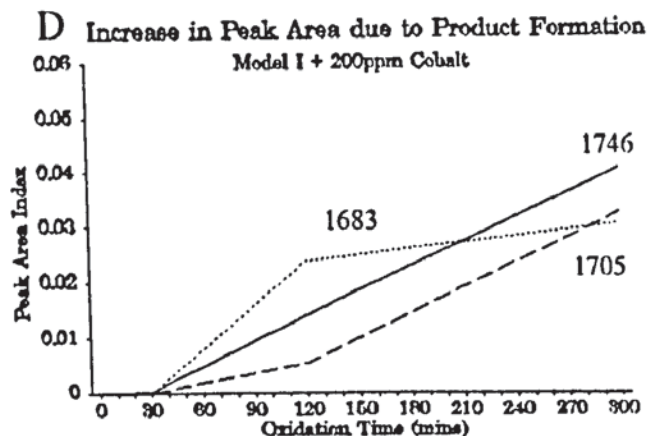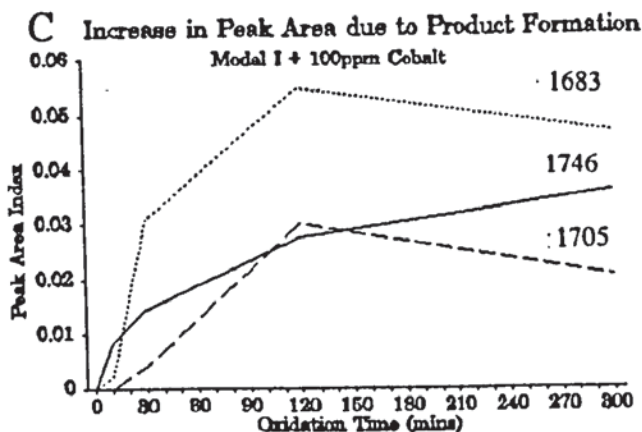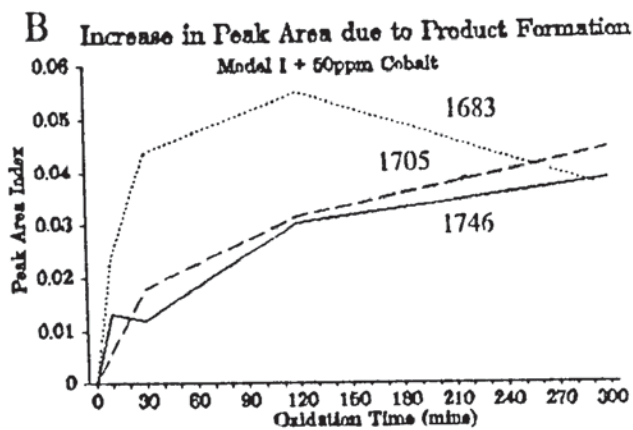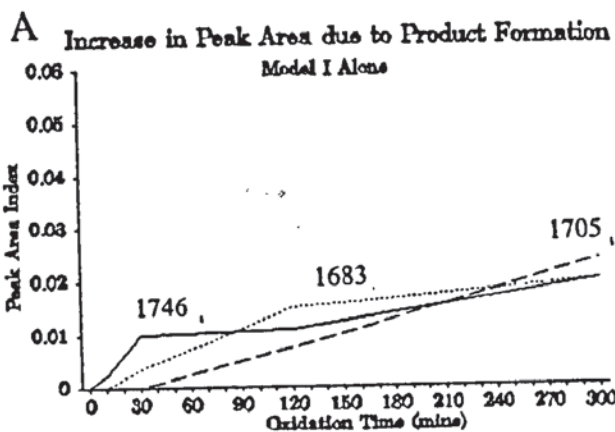
Figure 3.8 The Effect of Various Concentrations of Cobalt on the FT-IR of Model I During Oxidation at 150°C, (sampled out from the oxygen absorption experiments and analysed as KBr discs at room temperature), Showing the Growth of Various Product Peaks at 1746, 1705 & 1683cm^{-1}.
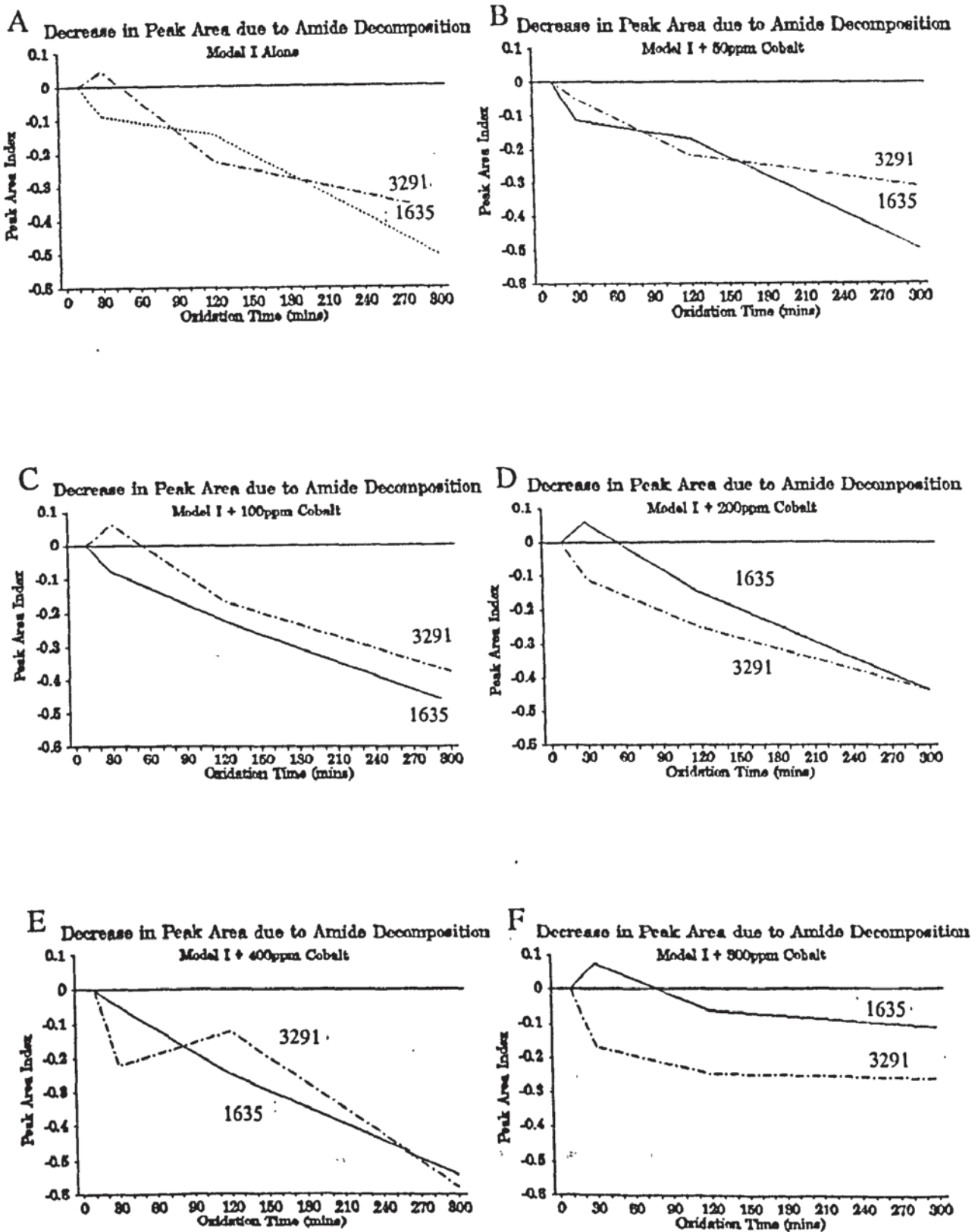
Figure 3.9   The Effect of Various Concentrations of Cobalt on the FT-IR of Model I During
Oxidation at 150°C, (sampled out from the oxygen absorption experiments and
analysed as KBr discs at room temperature), Showing the Decomposition of the
Amide Peaks at 3291 & 1635cm⁻¹.
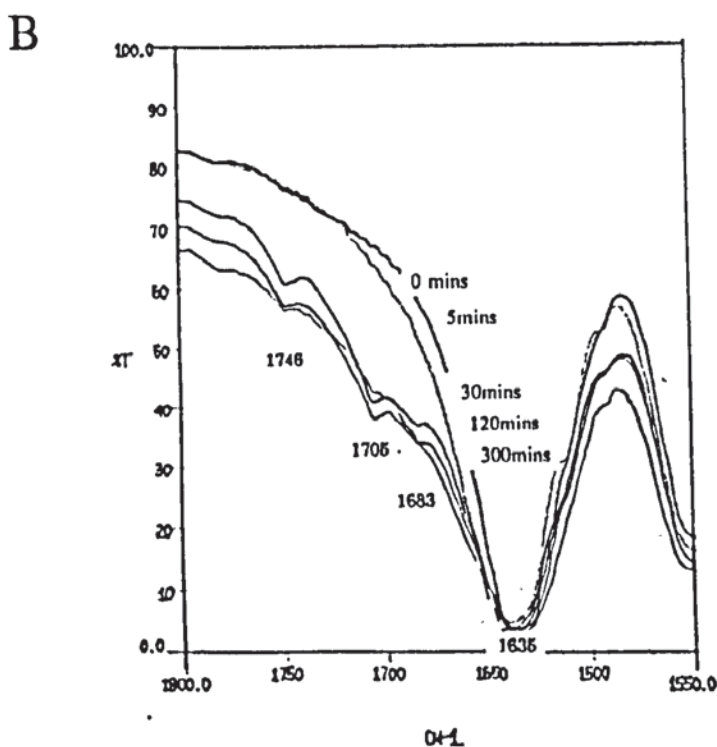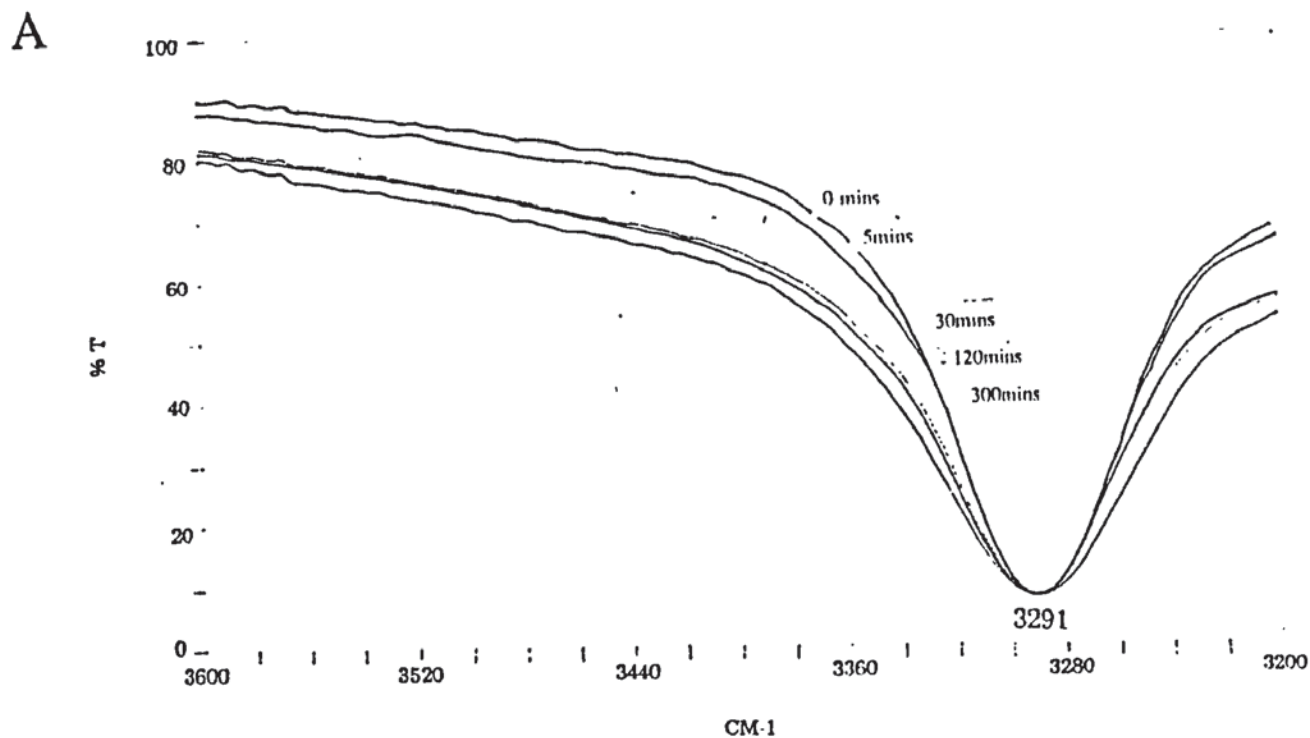
Figure 3.10 The Changing FT-IR Spectra of Model I, in the Presence of 1000ppm Sodium Phosphite, with Increasing Oxidation Time, at 150°C, in the Regions 3600-3200cm^{-1} (A) and 1800-1550cm^{-1} (samples taken out from the oxygen absorption experiments).
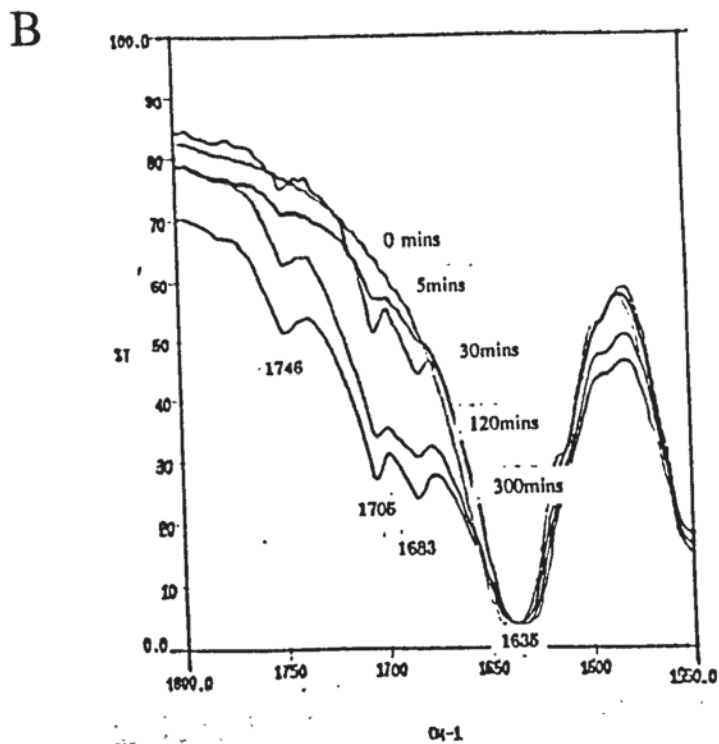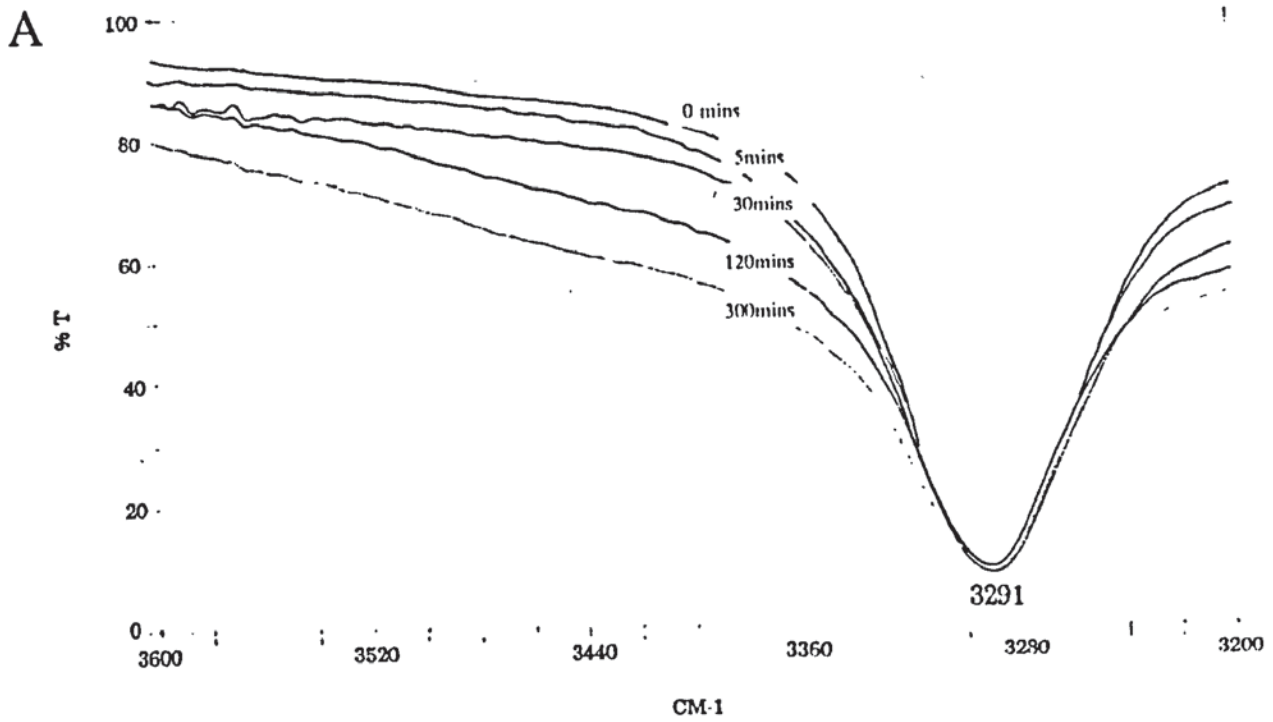
Figure 3.11 The Changing FT-IR Spectra of Model I, in the Presence of 200ppm Cobalt & 1000ppm Sodium Phosphite, with Increasing Oxidation Time, at 150°C, in the Regions 3600-3200cm⁻¹ (A) and 1800-1550cm⁻¹ (samples taken out from the oxygen absorption experiments).
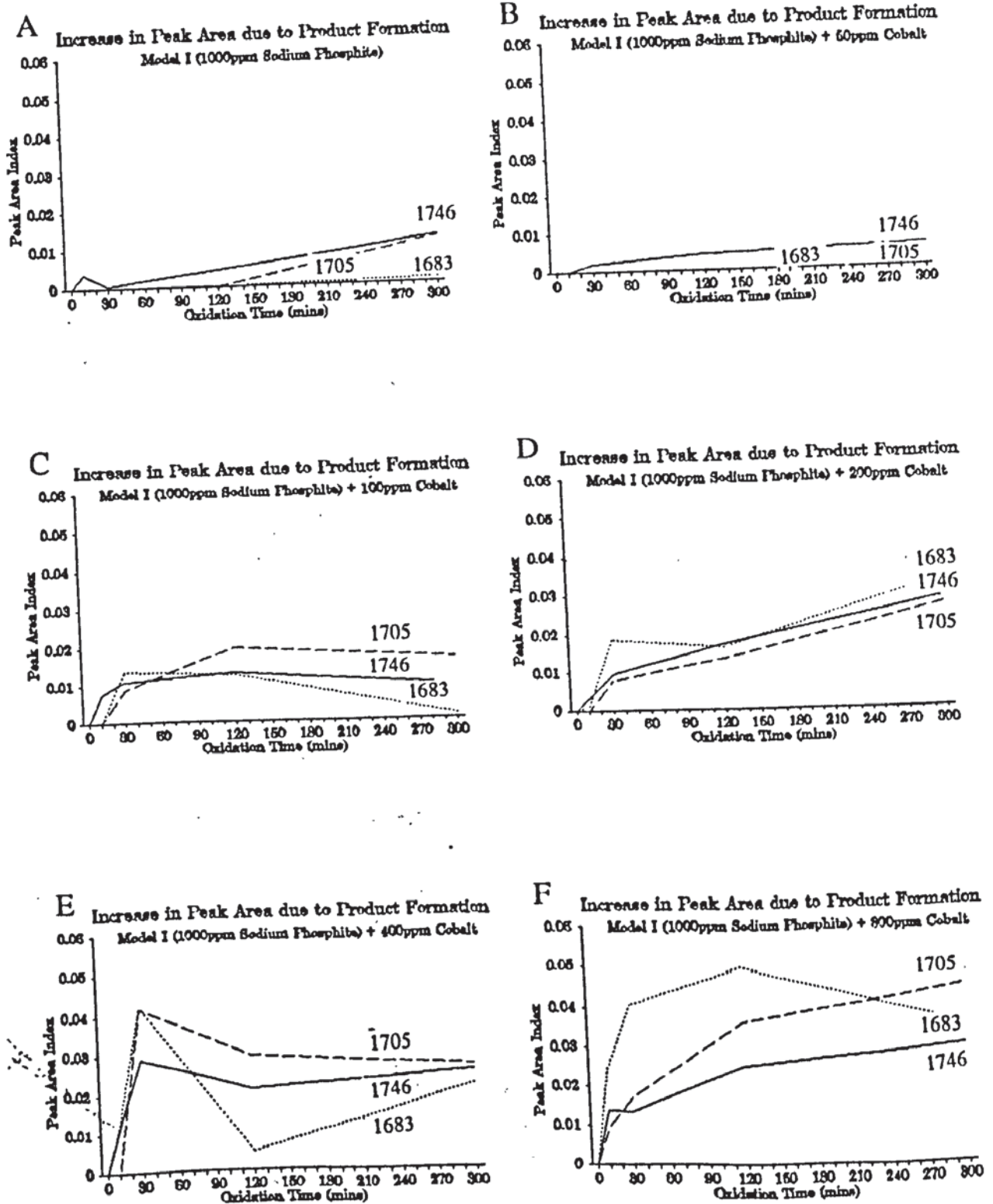
Figure 3.12 The Effect of Various Concentrations of Cobalt on the FT-IR of Model I (+ 1000ppm Sodium Phosphite) During Oxidation at 150°C, (sampled out from the oxygen absorption experiments and analysed as KBr discs at room temperature), Showing the Growth of Various Product Peaks at 1746, 1705 & 1683cm⁻¹.
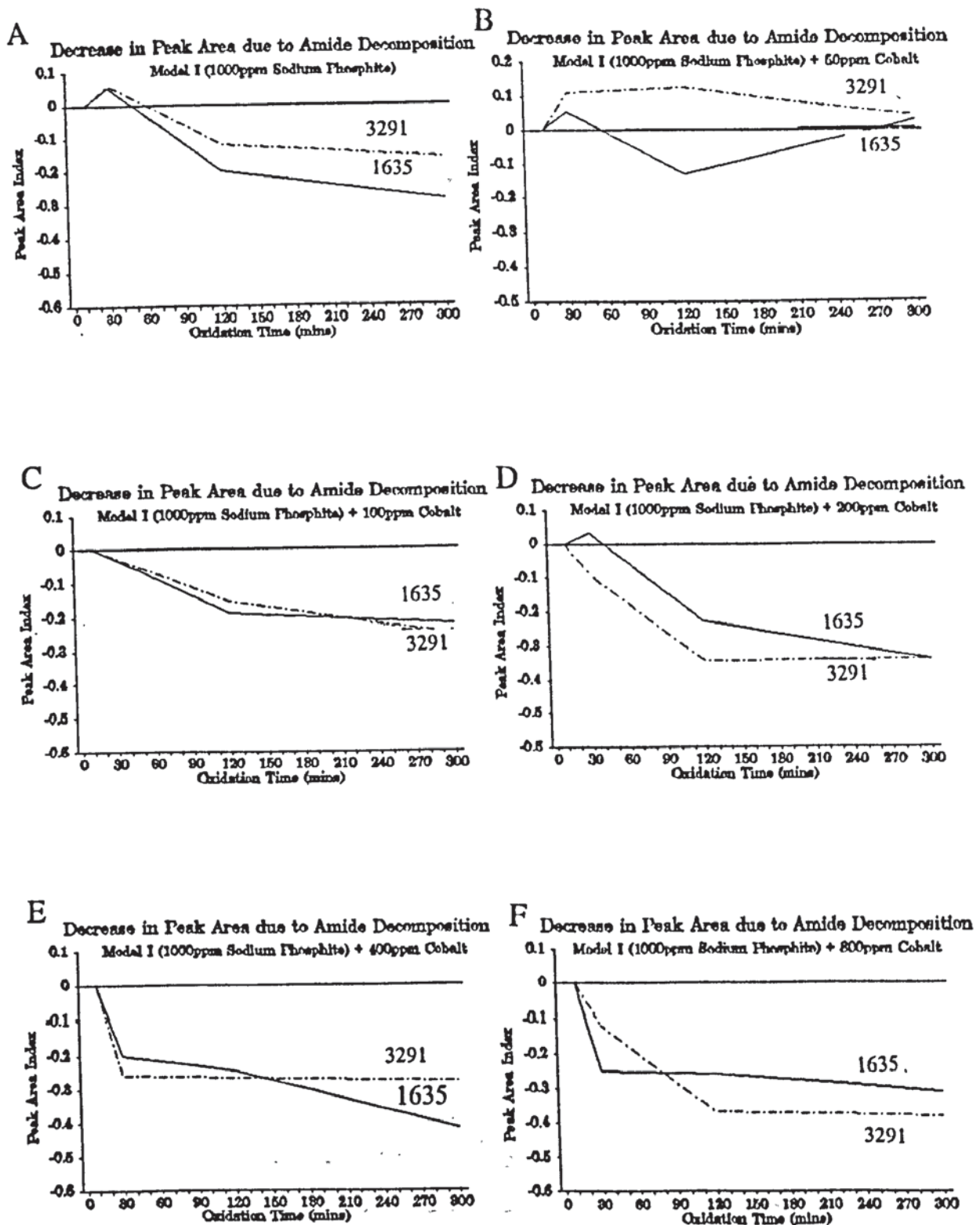
Figure 3.13 The Effect of Various Concentrations of Cobalt on the FT-IR of Model I (+ 1000ppm Sodium Phosphite) During Oxidation at 150°C, (sampled out from the oxygen absorption experiments and analysed as KBr discs at room temperature), Showing the Decomposition of the Amide Peaks at 3291 & 1635cm⁻¹.
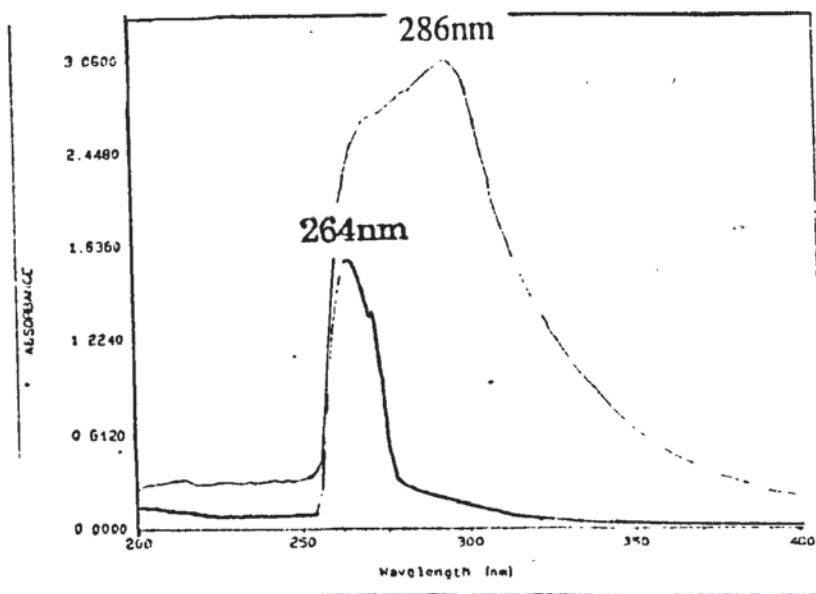
Figure 3.14 The UV-Vis Spectra of Model I, Measured in DMSO, Before and After Oxidation at 150°C in the Oxygen Absorption Apparatus.
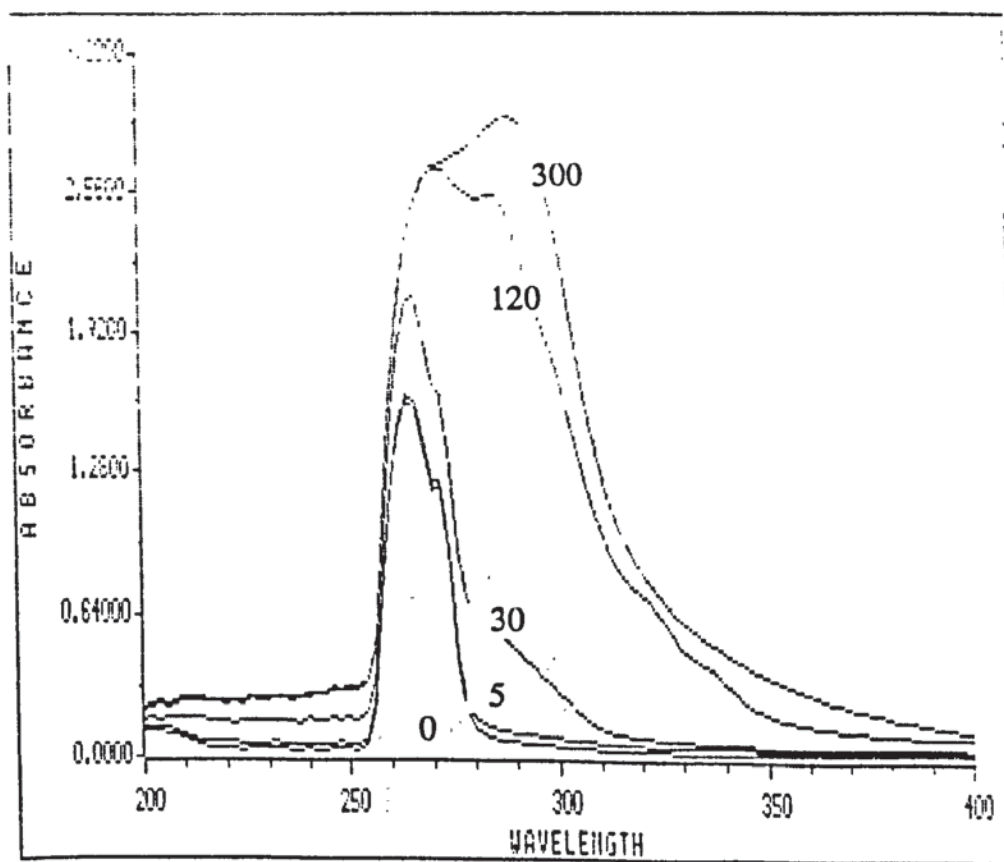
Figure 3.15 The Changing UV-Vis Spectra of Model I, after Increasing Oxidation at 150°C, in DMSO (sampled out from the oxygen absorption experiments and run at room temperature).
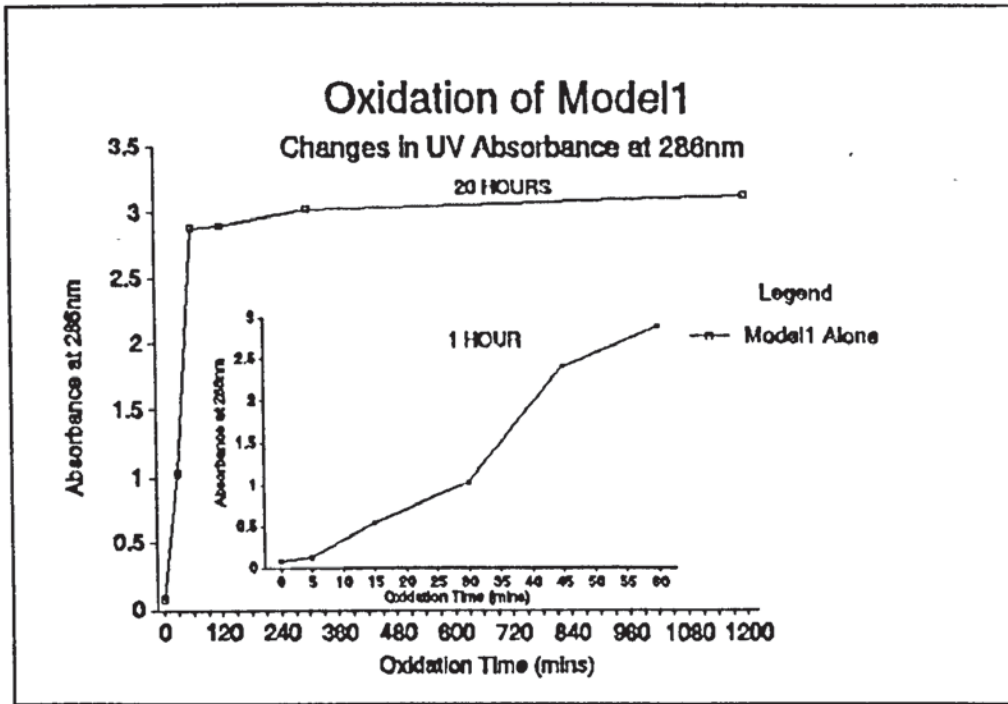
Figure 3.16 Changes in the UV-Vis, 286nm, Absorption Band During Oxidation of Model I, at 150°C, in DMSO (sampled out from the oxygen absorption experiments and run at room temperature).
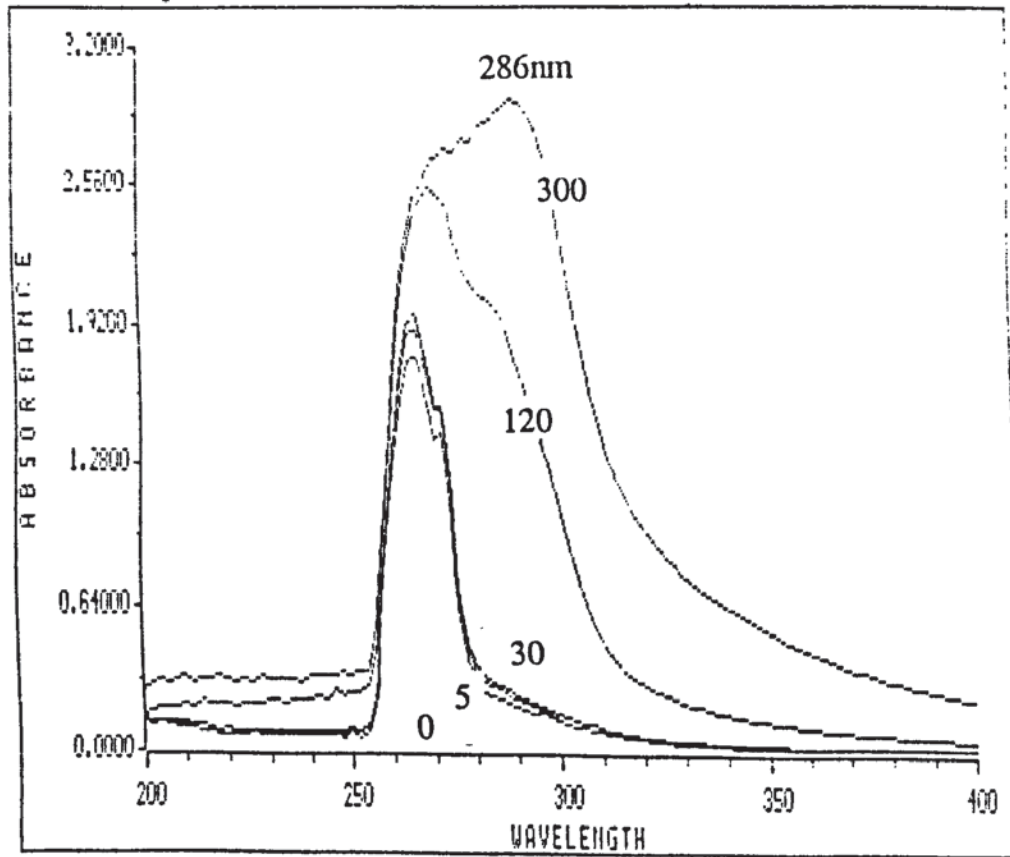
Figure 3.17 The Changing UV-Vis Spectra of Model I in the Presence of 200ppm Cobalt, after Increasing Oxidation at 150°C, in DMSO (sampled out from the oxygen absorption experiments and run at room temperature).
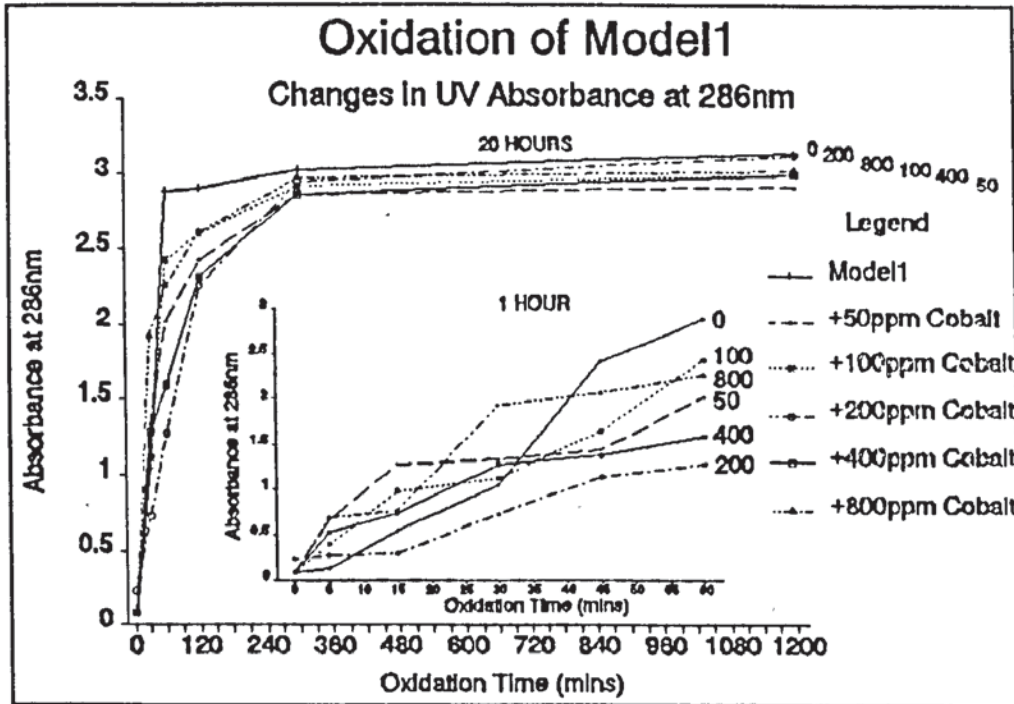
Figure 3.18 Changes in the UV-Vis, 286nm, Band During Oxidation of Model I in the Presence of Different Concentrations of Cobalt, at 150°C, in DMSO (sampled out from the oxygen absorption experiments and run at room temperature).
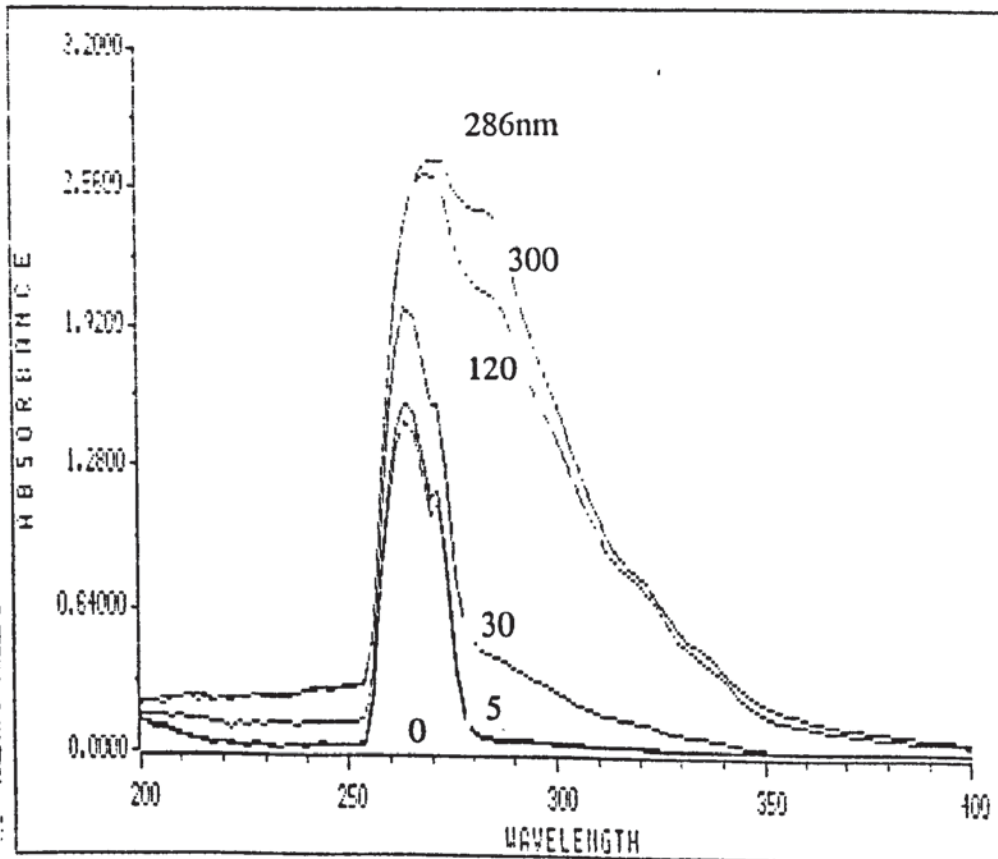
Figure 3.19 The Changing UV-Vis Spectra of Model I in the Presence of 1000ppm Sodium Phosphite, after Increasing Oxidation at 150°C, in DMSO (sampled out from the oxygen absorption experiments and run at room temperature).
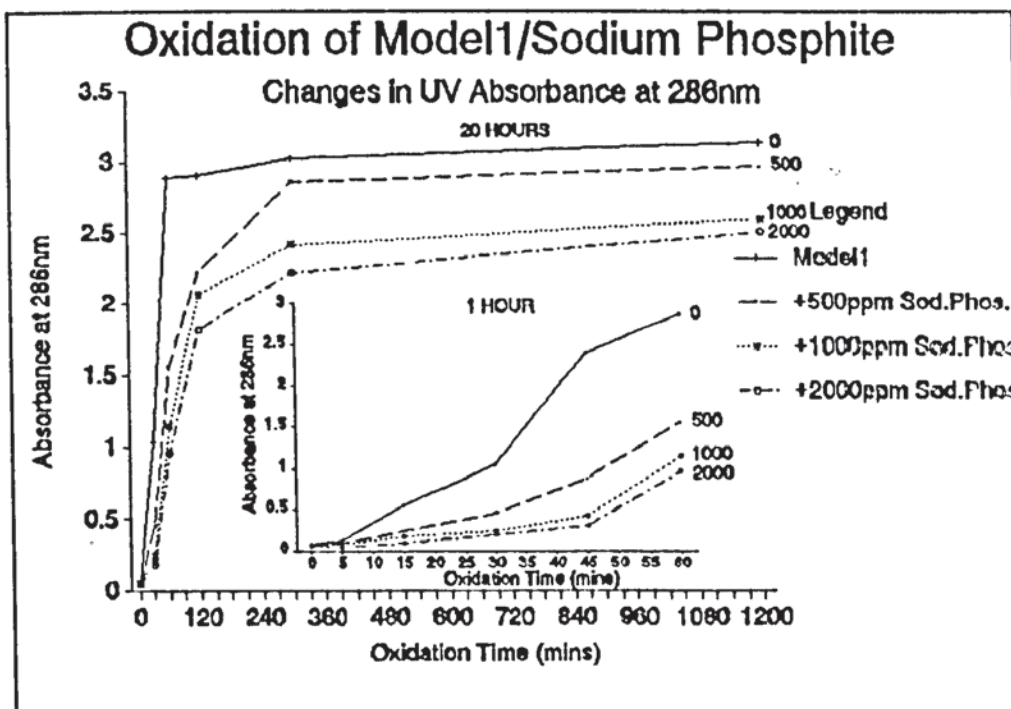
Figure 3.20 Changes in the UV-Vis, 286nm, Absorption Band During Oxidation of Model I in the Presence of Different Concentrations of Sodium Phosphite, at 150°C, in DMSO (sampled out from the oxygen absorption experiments and run at room temp).
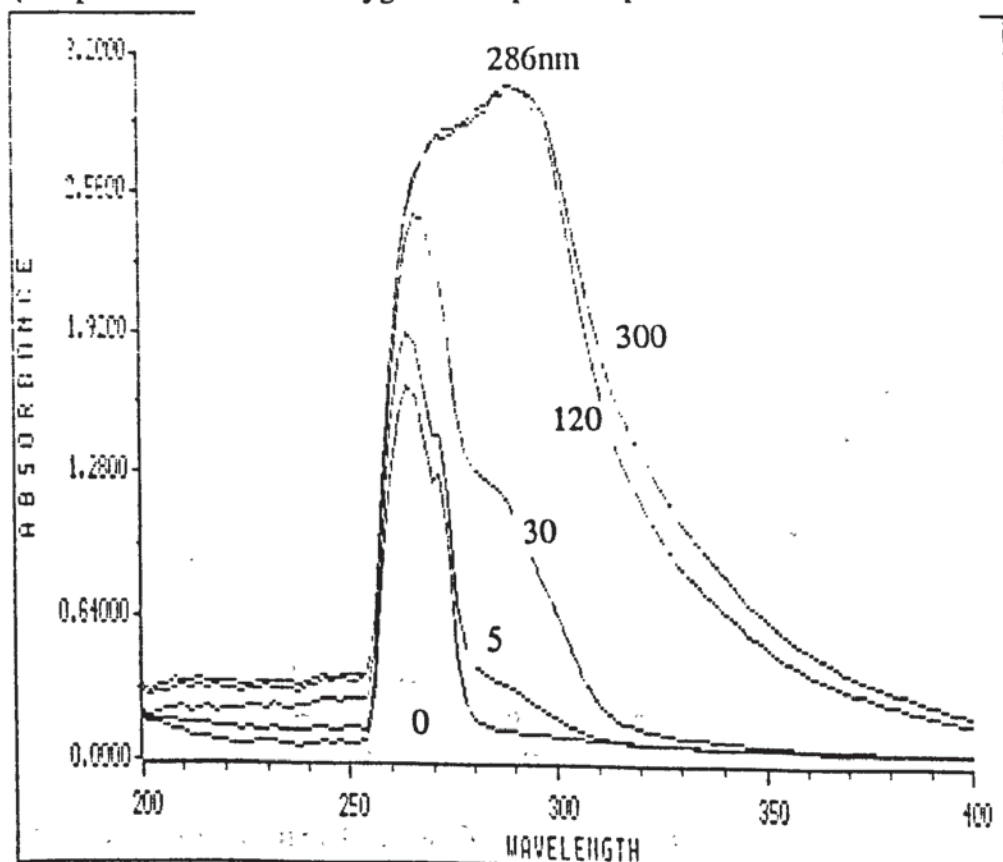
Figure 3.21 The Changing UV-Vis Spectra of Model I (+ 1000ppm Sodium Phosphite) in the Presence of 200ppm Sodium Phosphite, after Increasing Oxidation at 150°C, in DMSO(sampled out from the oxygen absorption experiments and run at room temp)
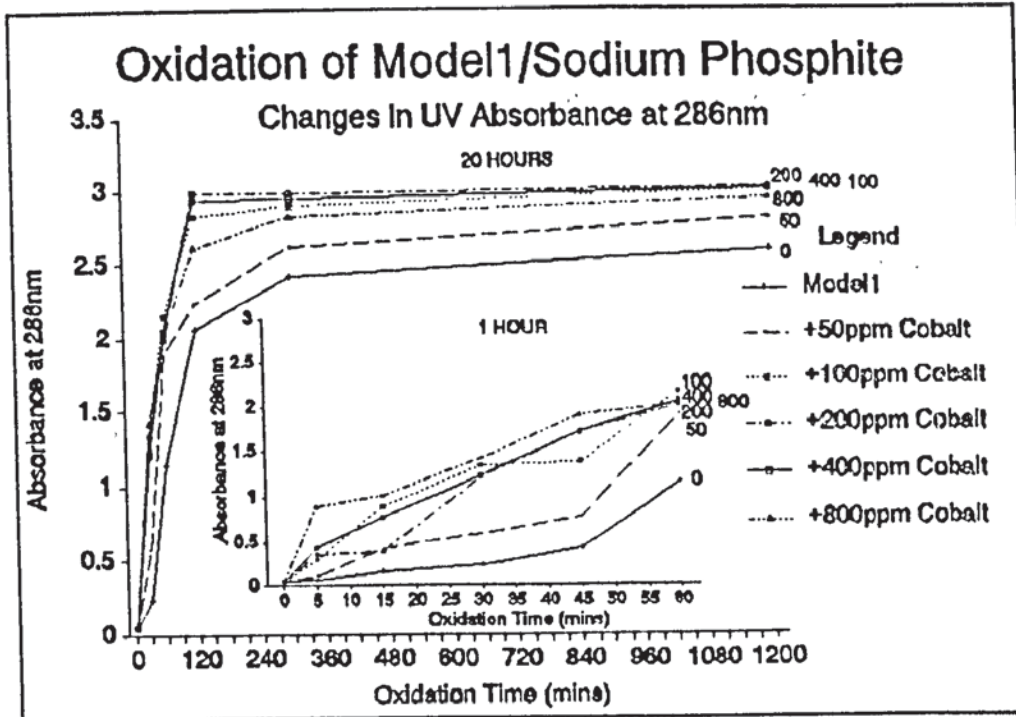
Figure 3.22 Changes in the UV-Vis, 286nm, Absorption Band During Oxidation of Model I (+1000ppm Sodium Phosphite) in the Presence of Different Concentrations of Cobalt, at 150°C, in DMSO (sampled out from the oxygen absorption experiments and run at room temperature).
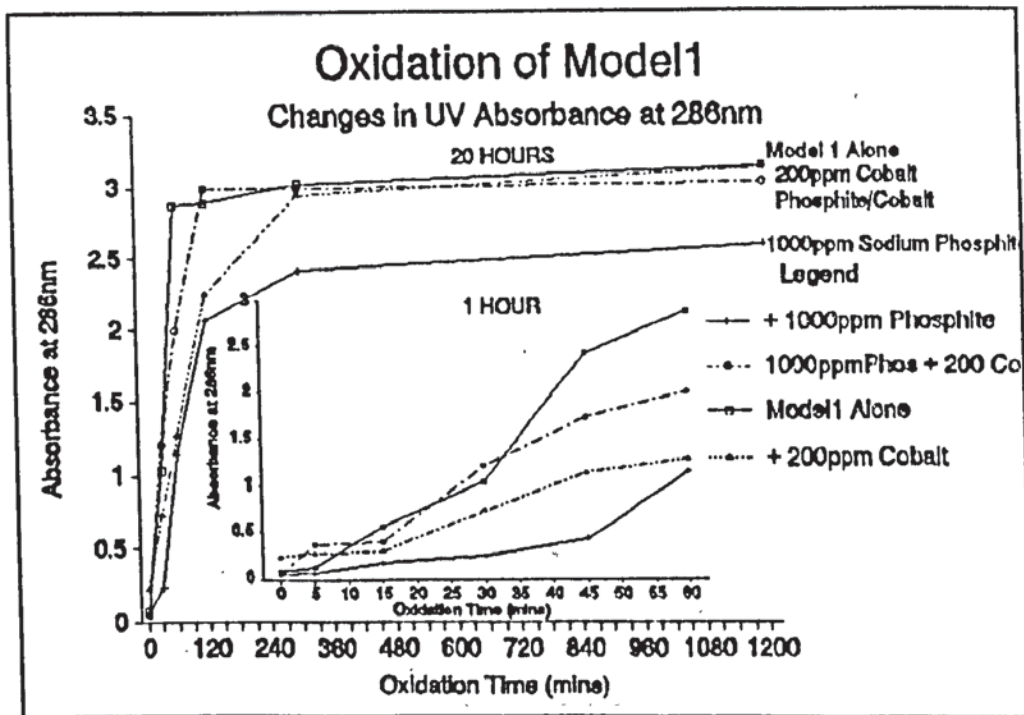
Figure 3.23 A Comparison of the Effect of Cobalt, Sodium Phosphite and a Combination of the Two Upon the Changes in the UV-Vis, 286nm, Absorption Band During the Oxidation of Model I, at 150°C, (sampled from the oxygen absorption experiment and measured at room temperature in DMSO).
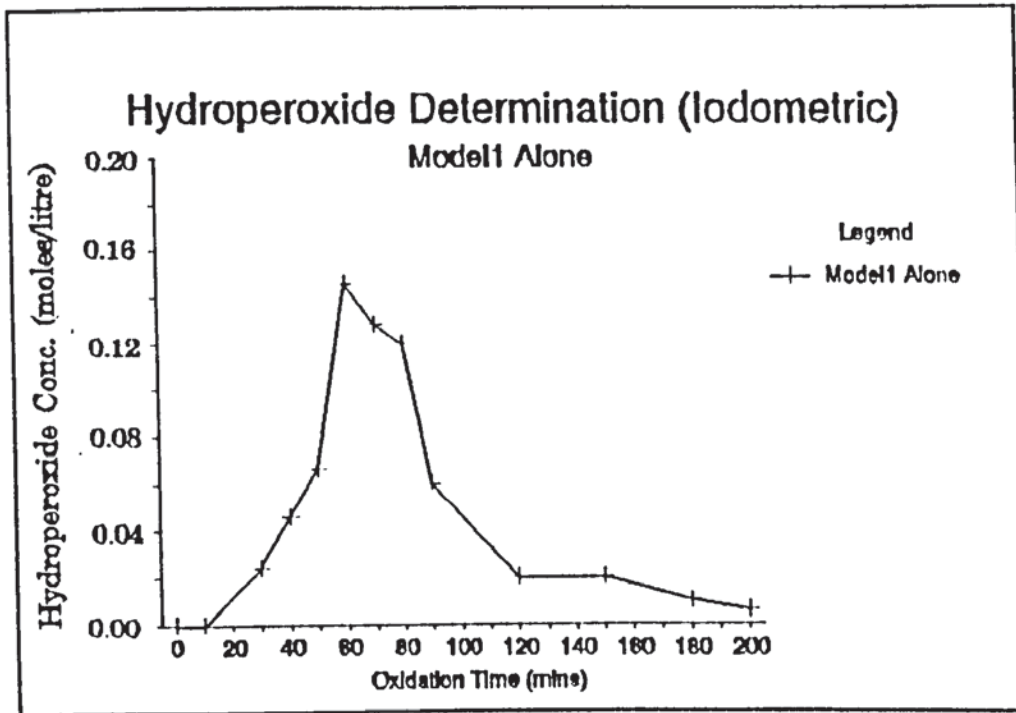
Figure 3.24 Hydroperoxide Formation During the Oxidation of Model I, in 1,2 DCB, at 150°C Using the Iodometric Titration Technique.
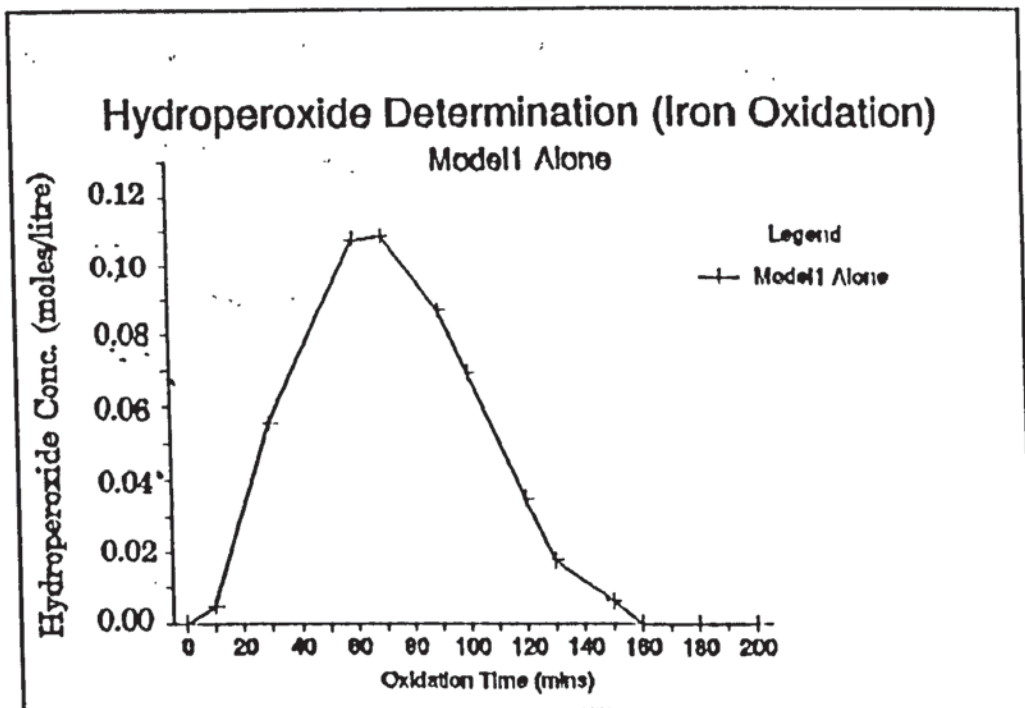
Figure 3.25 Hydroperoxide Formation During the Oxidation of Model I, in 1,2 DCB, at 150°C Using the Iron Oxidation Technique.
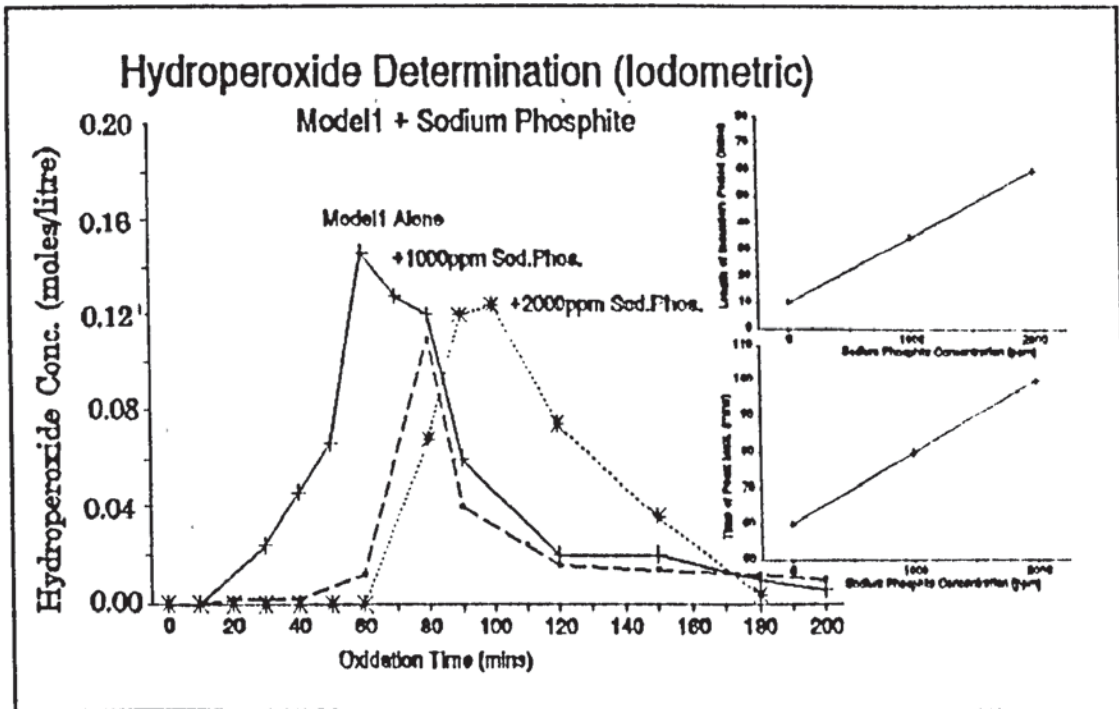
Figure 3.26 Hydroperoxide Formation During the Oxidation of Model I in the Presence of Different Concentrations of Sodium Phosphite, at 150°C, in 1,2 DCB Using the Iodometric Titration Technique.
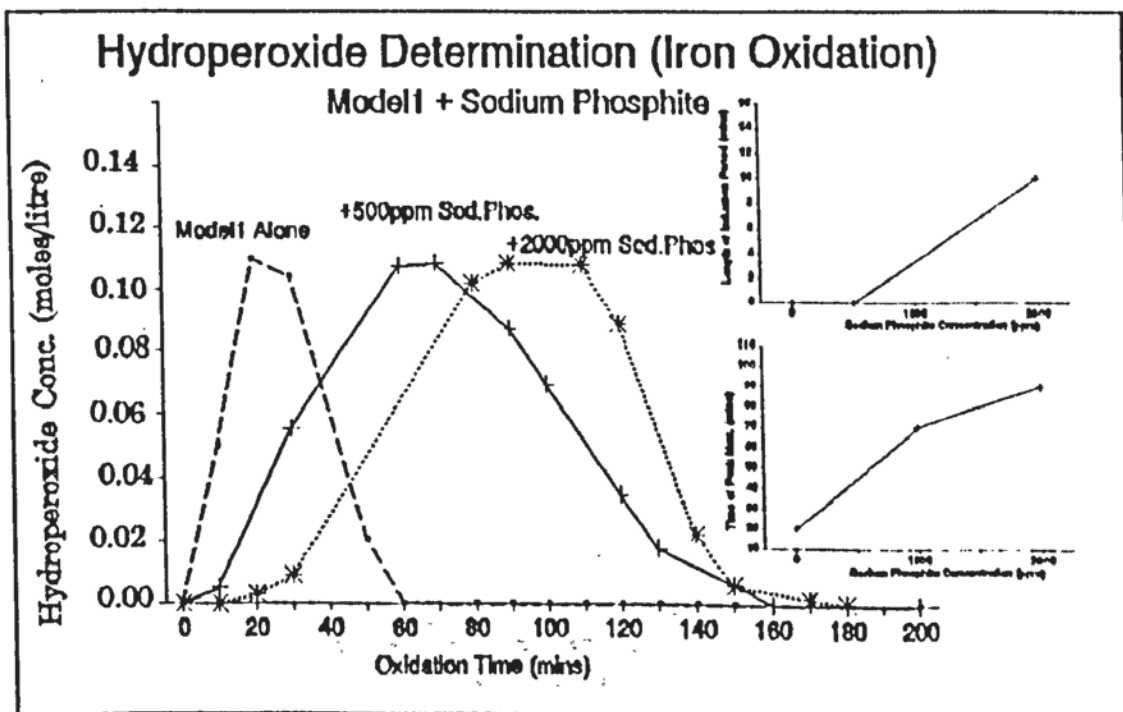
Figure 3.27 Hydroperoxide Formation During the Oxidation of Model I in the Presence of Different Concentrations of Sodium Phosphite, at 150°C, in 1,2 DCB Using the Iron Oxidation Technique.
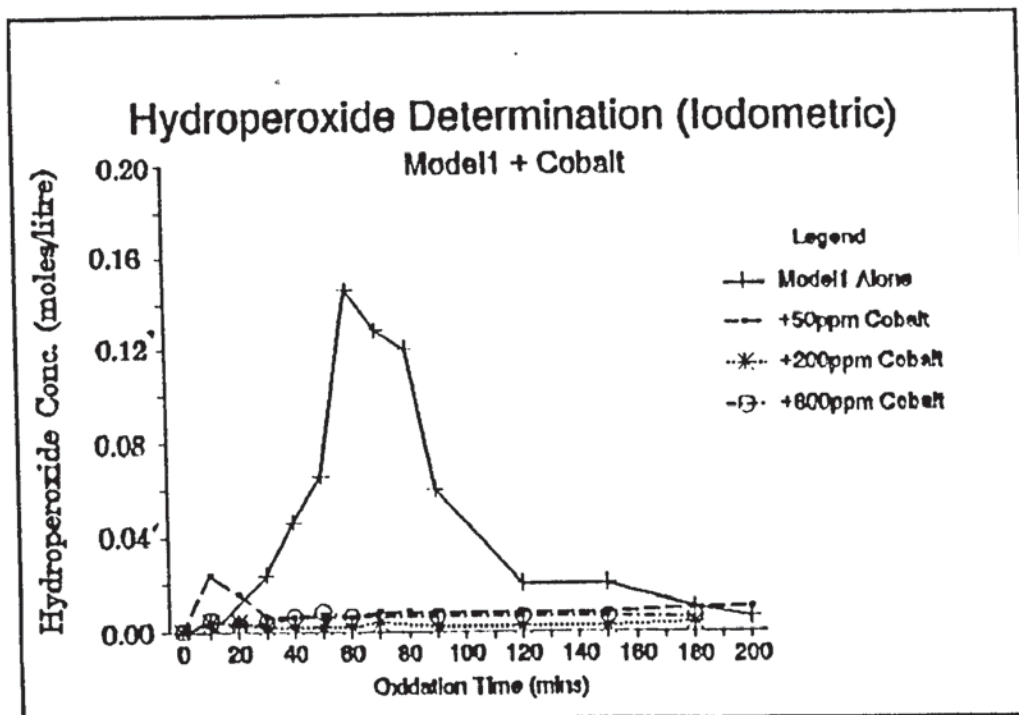
Figure 3.28 Hydroperoxide Formation During the Oxidation of Model I in the Presence of Different Concentrations of Cobalt, at 150°C, in 1,2 DCB Using the Iodometric Titration Technique.
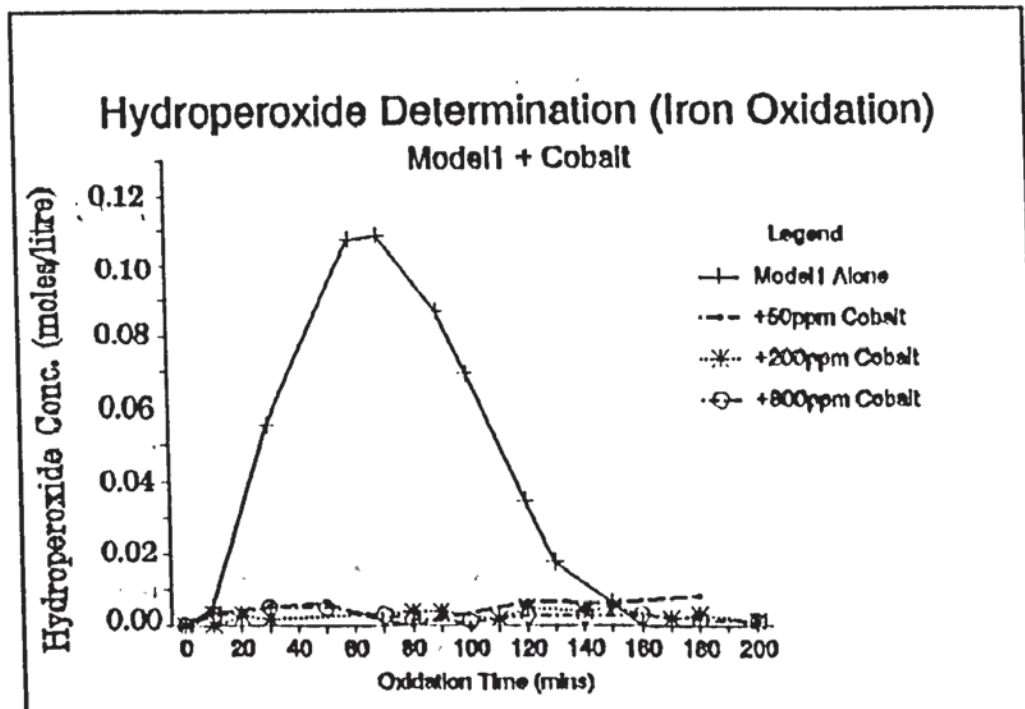
Figure 3.29 Hydroperoxide Formation During the Oxidation of Model I in the Presence of Different Concentrations of Cobalt, at 150°C, in 1,2 DCB Using the Iron Oxidation Technique.

Hydroperoxide Determination (Iodometric)
Model1/2000ppm Sod.Phos. + Cobalt
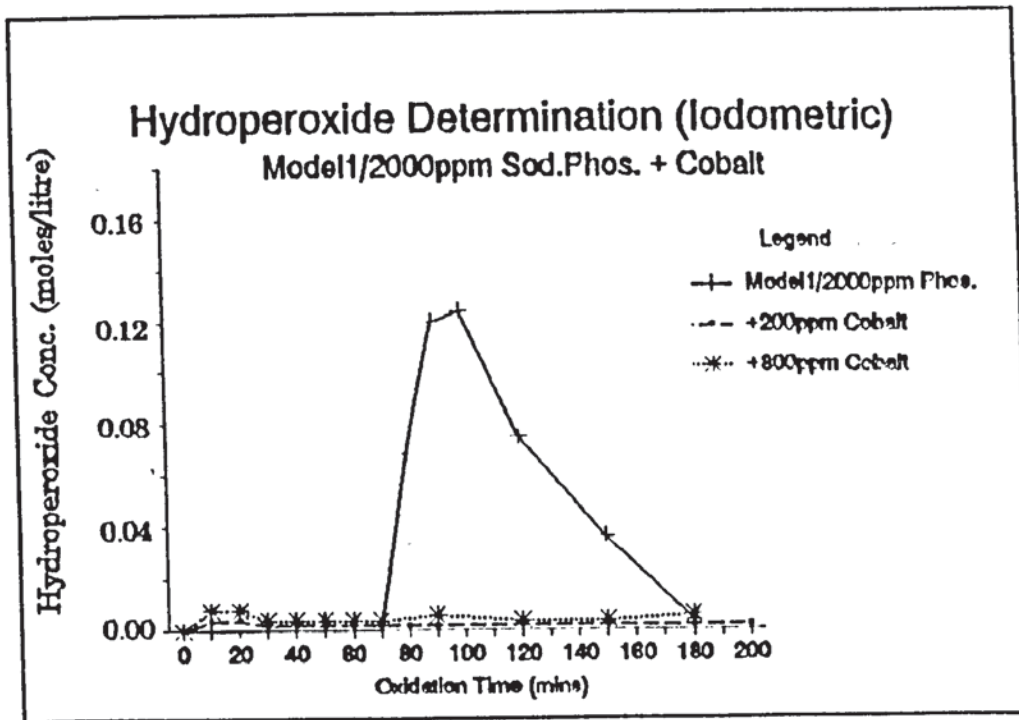
Figure 3.30 Hydroperoxide Formation During the Oxidation of Model I (+ 2000ppm Sodium Phosphite) in the Presence of Different Concentrations of Cobalt, at 150°C, in 1,2 DCB Using the Iodometric Titration Technique.

Hydroperoxide Determination (Iron Oxidation)
Model1/2000ppm Sod.Phos. + Cobalt
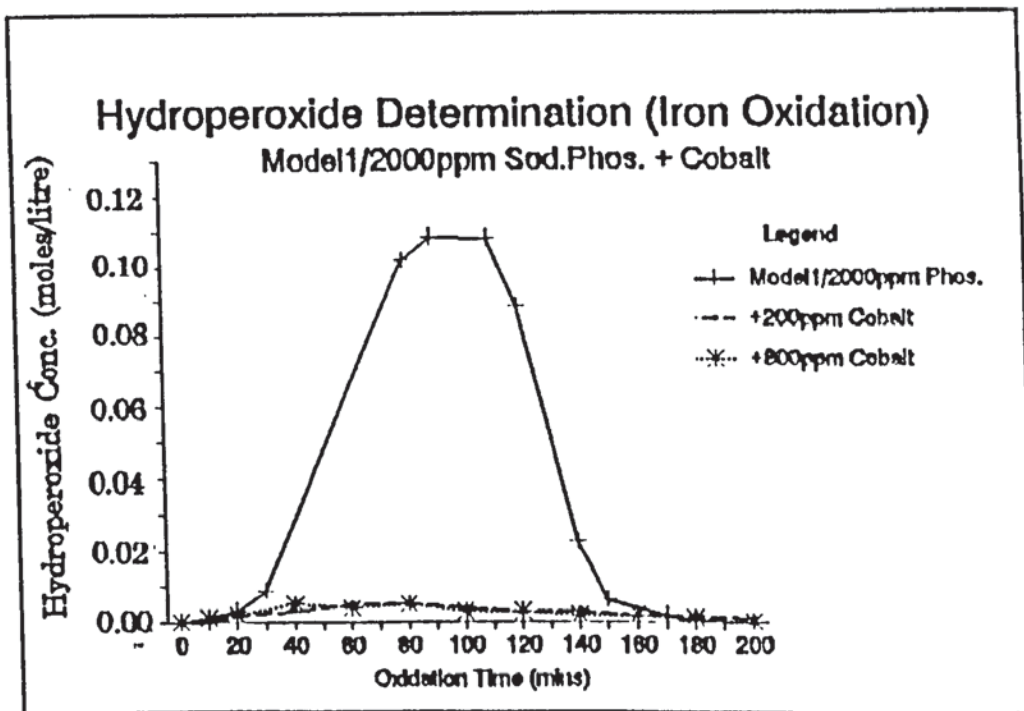
Figure 3.31 Hydroperoxide Formation During the Oxidation of Model I (+ 2000ppm Sodium Phosphite) in the Presence of Different Concentrations of Cobalt, at 150°C, in 1,2 DCB Using the Iron Oxidation Technique.
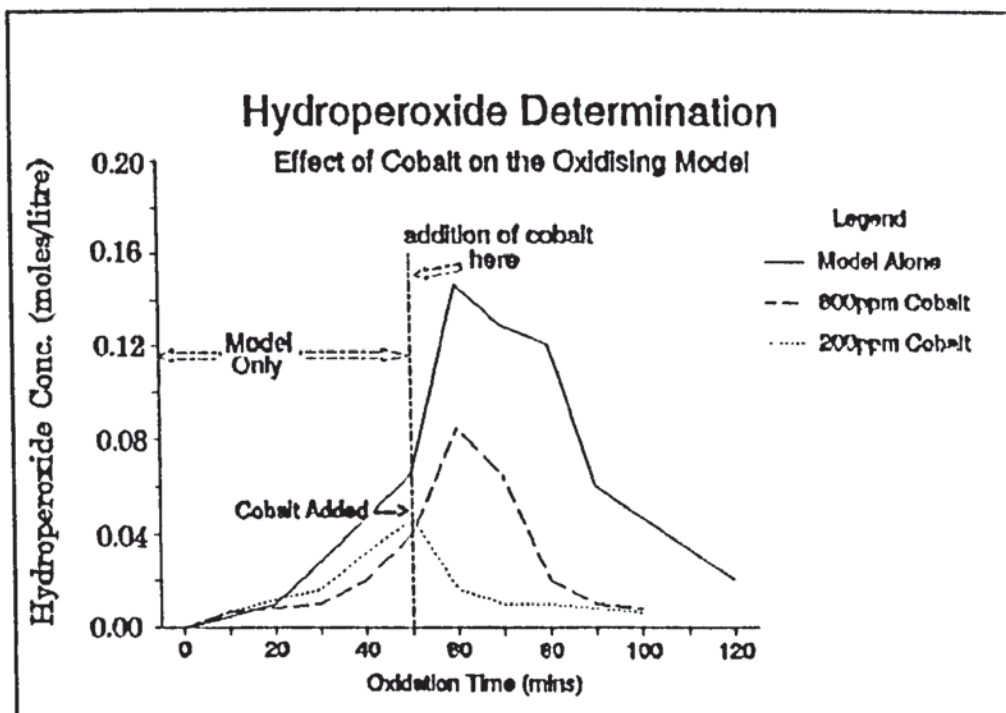
Figure 3.32 The Effect of Cobalt Addition to the Hydroperoxide Formation of the Oxidising Model, in 1,2 DCB, at 150°C (Nos.on curves are conc (ppm) of cobalt added after 50 mins oxidation time).
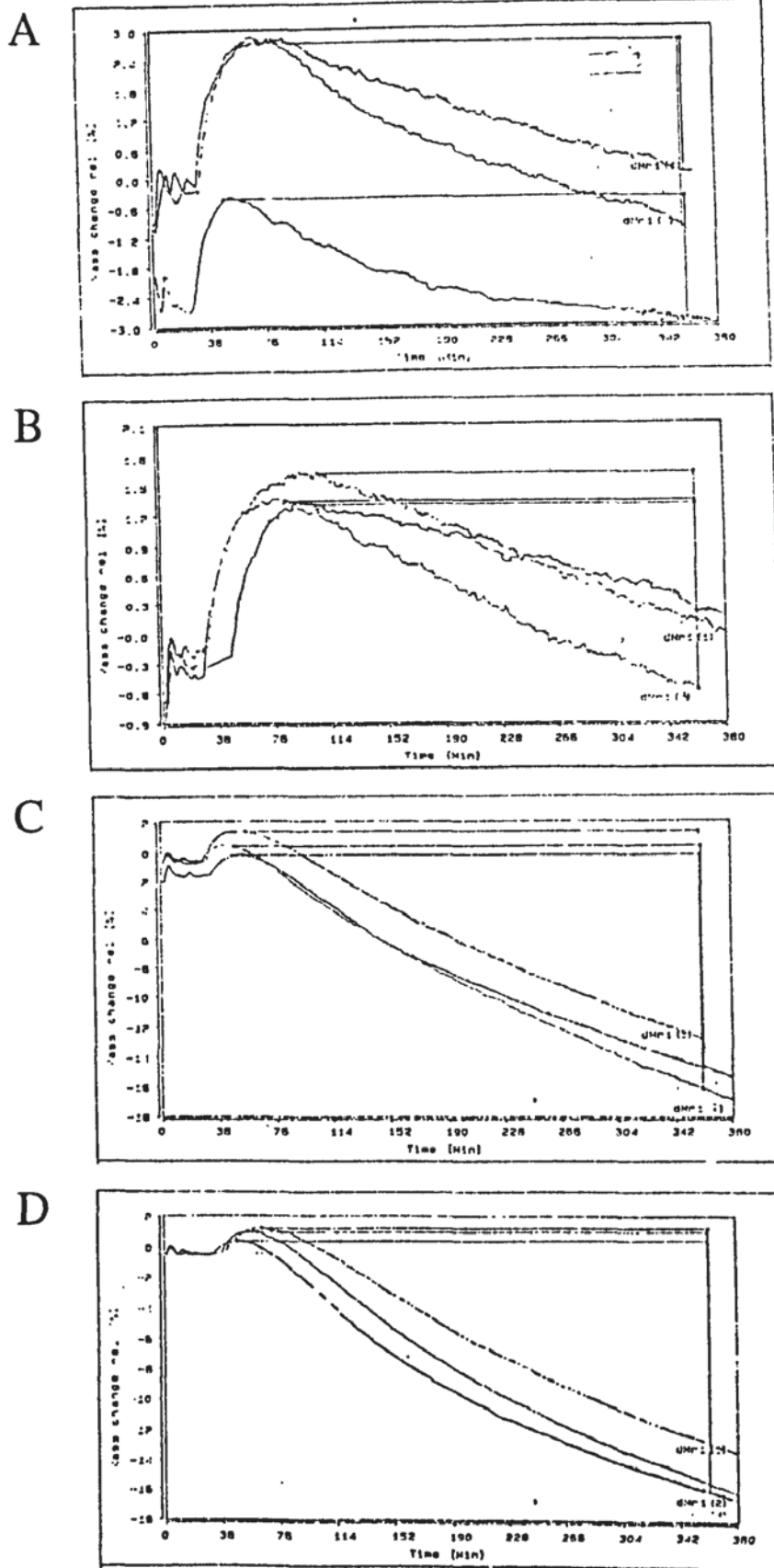
Figure 3.33 T.G.A Traces Obtained From the Isothermal Heating of Model I Alone (A) and in the Presence of 200ppm Cobalt (B), 5000ppm Cobalt (C) and 10000ppm Cobalt (D). Analysis was Carried Out at 140, 150 and 160°C in an Oxygen Atmosphere.
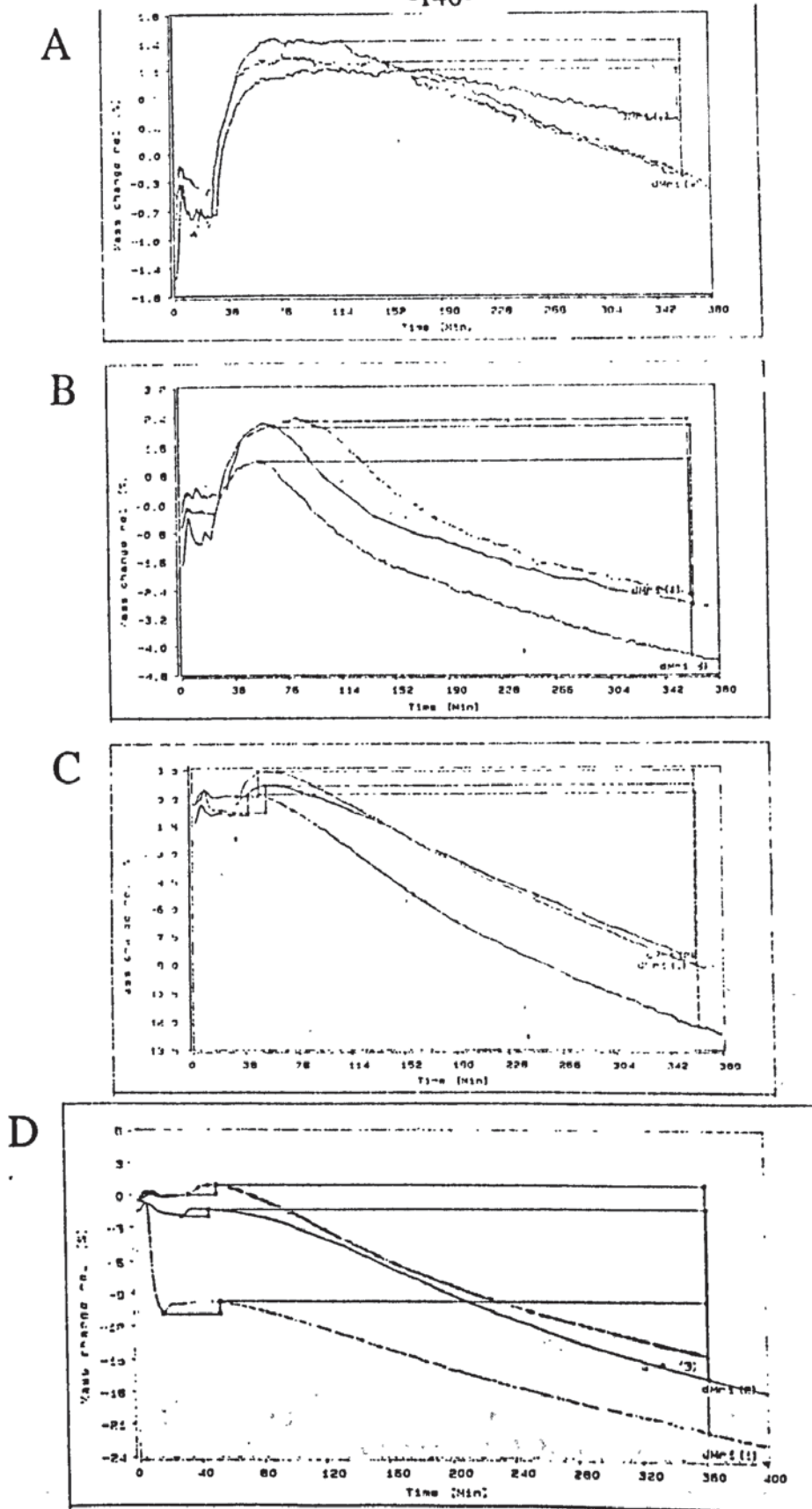
Figure 3.34 T.G.A Traces Obtained From the Isothermal Heating of Model I + 1000ppm Sodium Phosphite (A) and in the Presence of 200ppm Cobalt (B), 5000ppm Cobalt (C) and 10000ppm Cobalt (D). Analysis was Carried Out at 140, 150 and 160°C in an Oxygen Atmosphere.
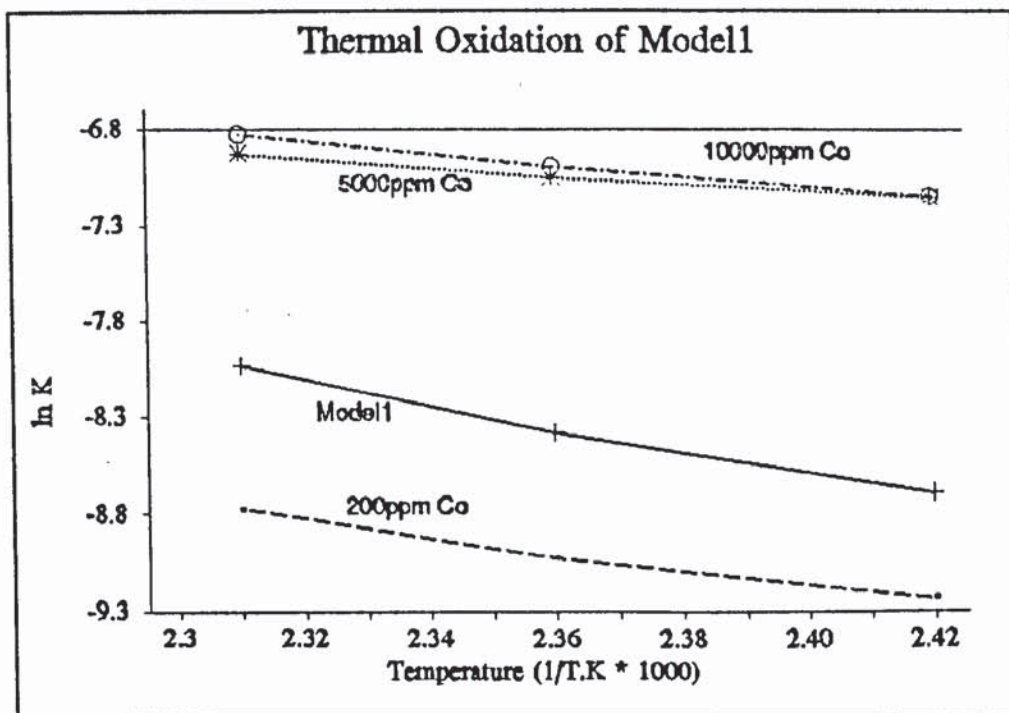
Figure 3.35 Determination of Activation Energies for the Thermal Oxidation of Model I in the Presence of Different Concentrations of Cobalt by Isothermal Thermogravimetric Analysis.
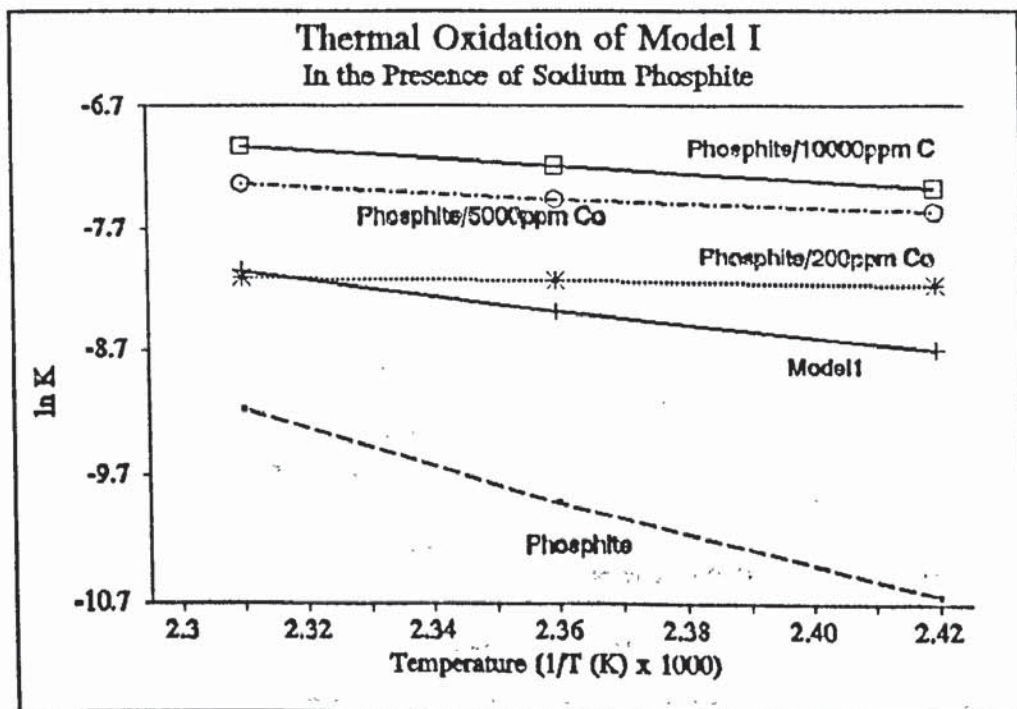
Figure 3.36 Determination of Activation Energies for the Thermal Oxidation of Model I (+ 1000ppm Sodium Phosphite) in the Presence of Different Concentrations of Cobalt by Isothermal Thermogravimetric Analysis.
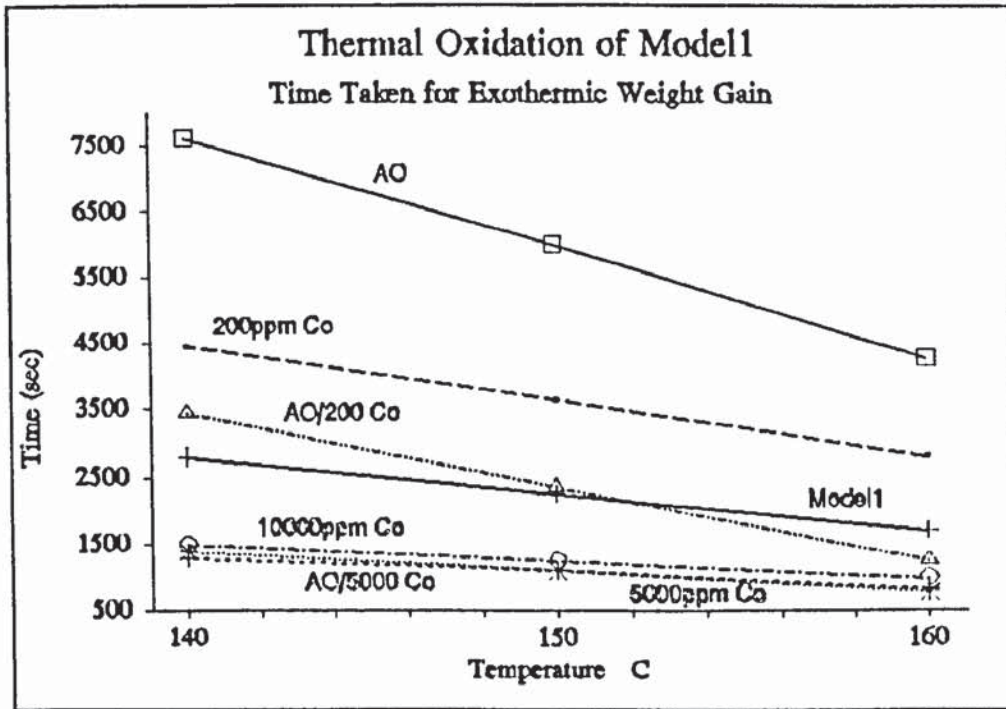
Figure 3.38 The Effect of Temperature and Cobalt Concentration on the Time Taken for the Formation of the Initial Weight Gain Produced During the Isothermal Thermogavimetric Analysis of Model I at 140, 150 and 160°C.
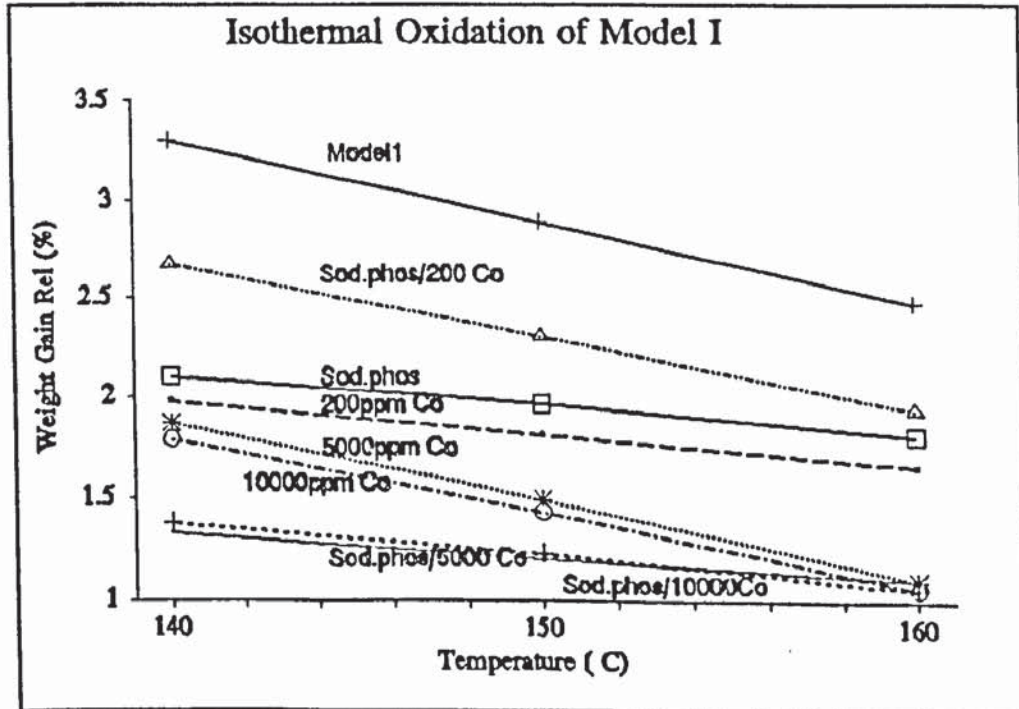
Figure 3.39 The Effect of Temperature and Cobalt Concentration on the Initial Weight Gain Produced During the Isothermal Thermogavimetric Analysis of Model I at 140, 150 and 160°C.
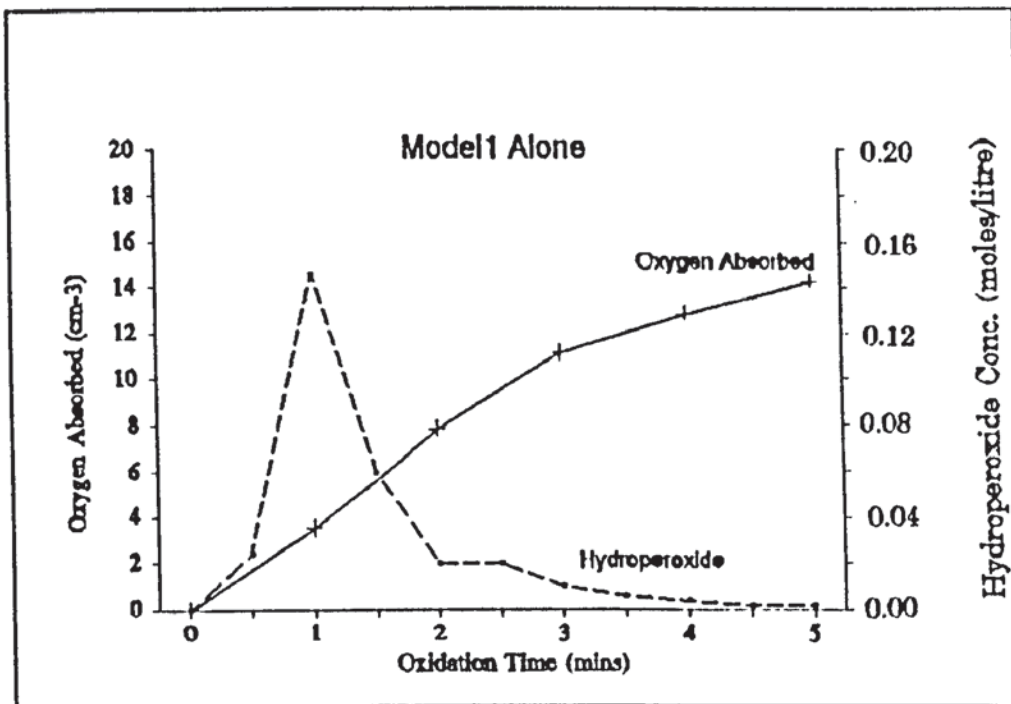
Figure 3.40 A Comparison of the Oxygen Absorbed and the Hydroperoxide Produced During the Thermal Oxidation of Model I at 150°C, in the melt phase.
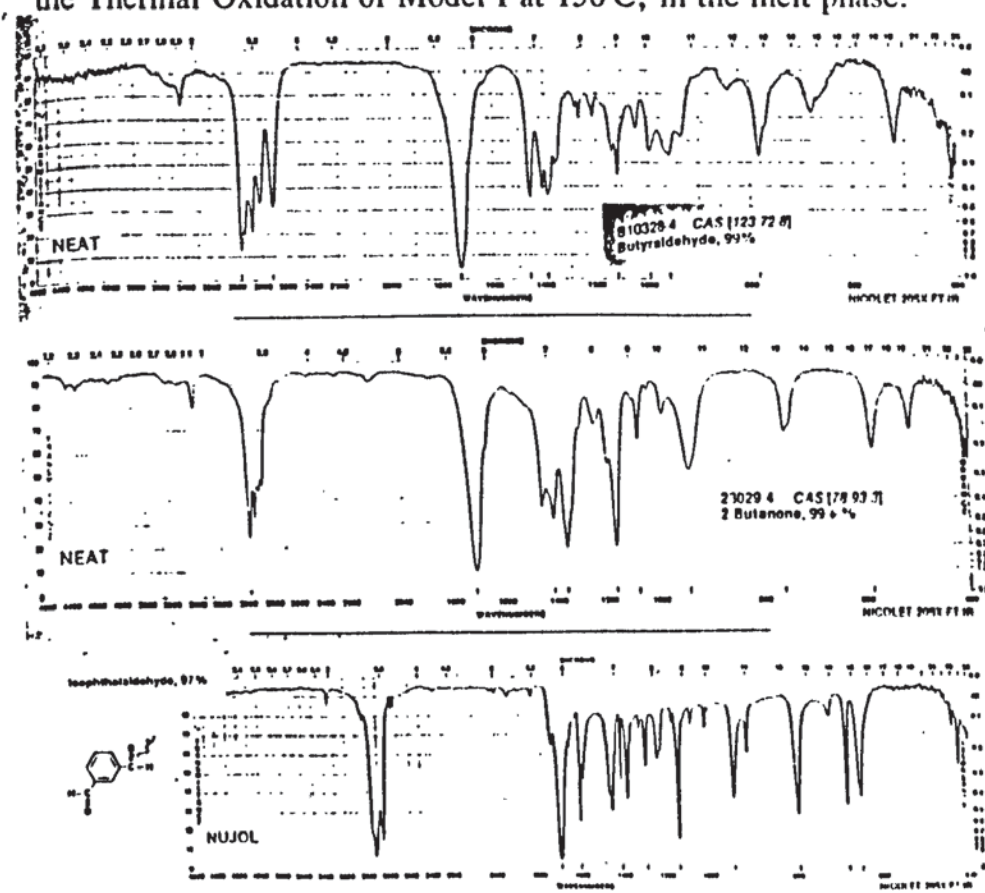
Figure 3.41 The FT-IR Spectra of Various Aldehydes and Ketones likely to be Formed as Products of Oxidation of Model I at 150°C (reproduced from the Aldrich Library of IR Spectra).
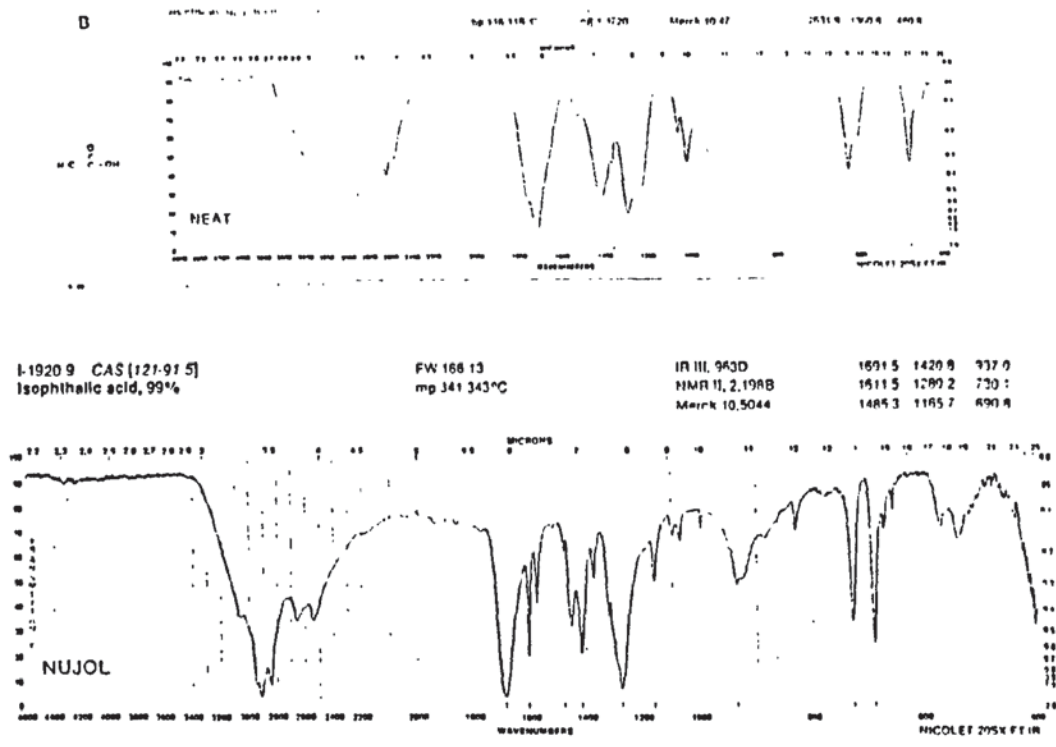
Figure 3.42 The FT-IR Spetra of Various Carboxylic acids likely to be Formed as Products of Oxidation of Model I, at 150°C (reproduced from the Aldrich Library of IR Spectra).
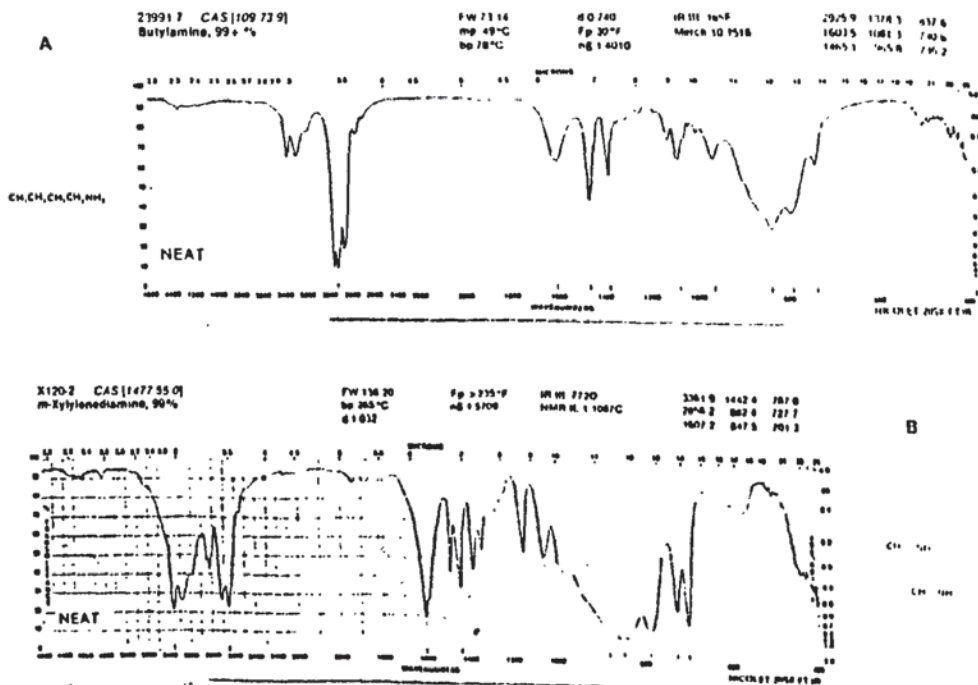
Figure 3.43 The FT-IR Spetra of Various Amines likely to be Formed as Products of Oxidation of Model I, at 150°C (reproduced from the Aldrich Library of IR Spectra).
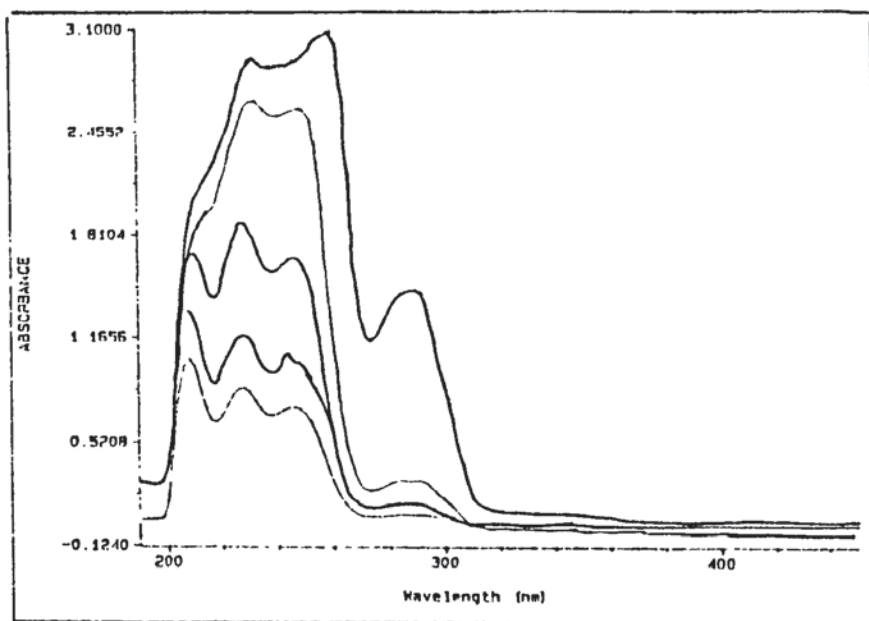
Figure 3.44 The UV-Vis Spectra of Isophthaldehyde, in Methanol, with Increasing Concentration.
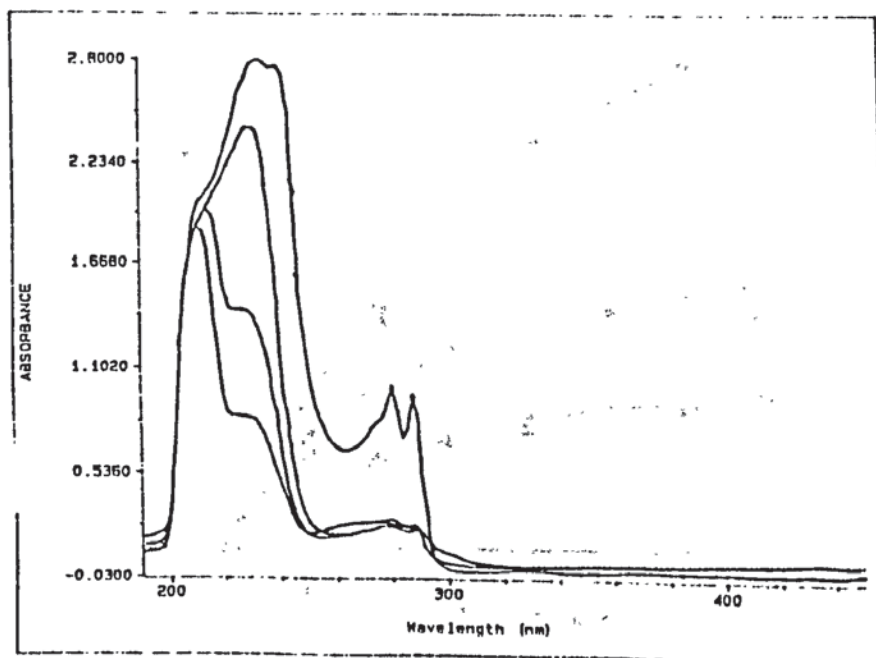
Figure 3.45 The UV-Vis Spectra of Isophthalic acid, in Methanol, with Increasing Concentration.
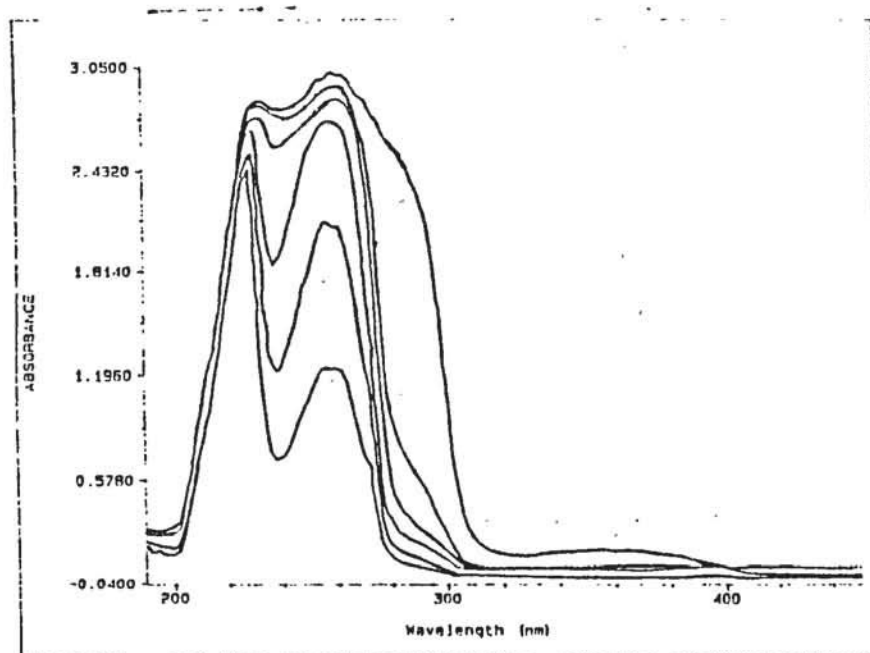
Figure 3.46 The UV-Vis Spectra of m-Xylylene diamine, in Methanol, with Increasing Concentration.

Aston University

Illustration removed for copyright restrictions

Figure 3.47 Curves relating the rate of Oxygen Uptake to the Concentration of Cobalt in MXD6 at 100°C.(taken from " The Thermal and Oxidative Degradation of an Aromatic Polyamide, by S.N.Patel (Thesis Leeds Univ. 1992))[102].

Figure 3.48 Curves relating the Rate of Oxygen Uptake to the Concentration of Cobalt in a Blend of 96% Polyester and 4% MXD6, at 100°C. (taken from " The Thermal and Oxidative Degradation of an Aromatic Polyamide, by S.N.Patel (Thesis Leeds Univ.1992))[102].
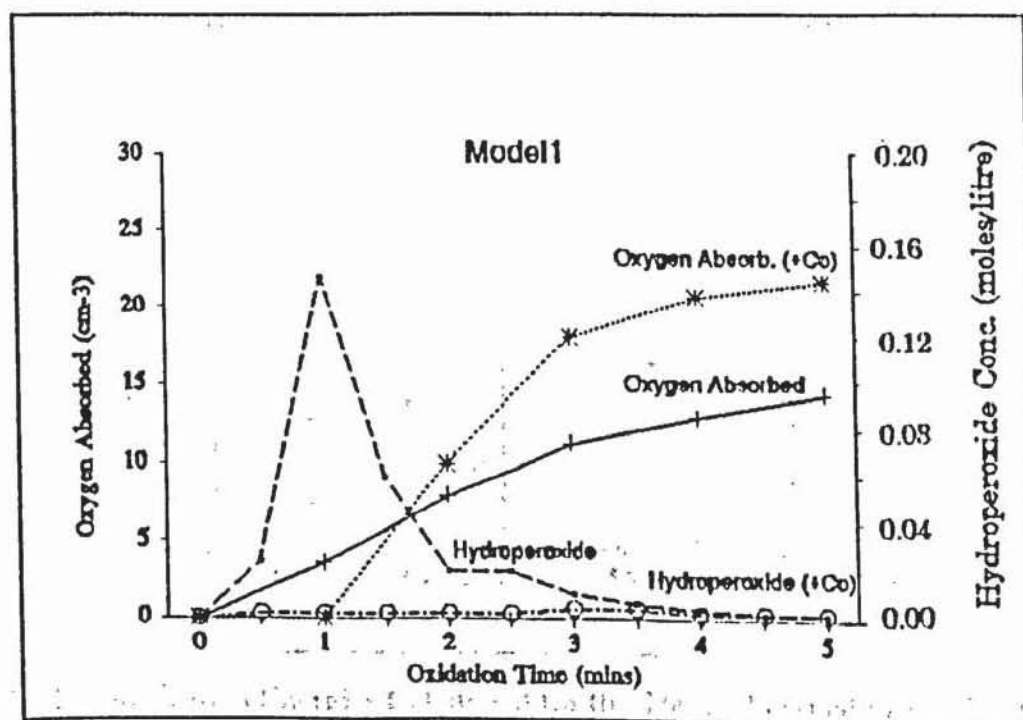
Figure 3.49 A Comparison of the Oxygen Absorbed and the Hydroperoxide Produced During the Thermal Oxidation of Model I in the Presence of 200ppm Cobalt at 150°C, in the melt phase.
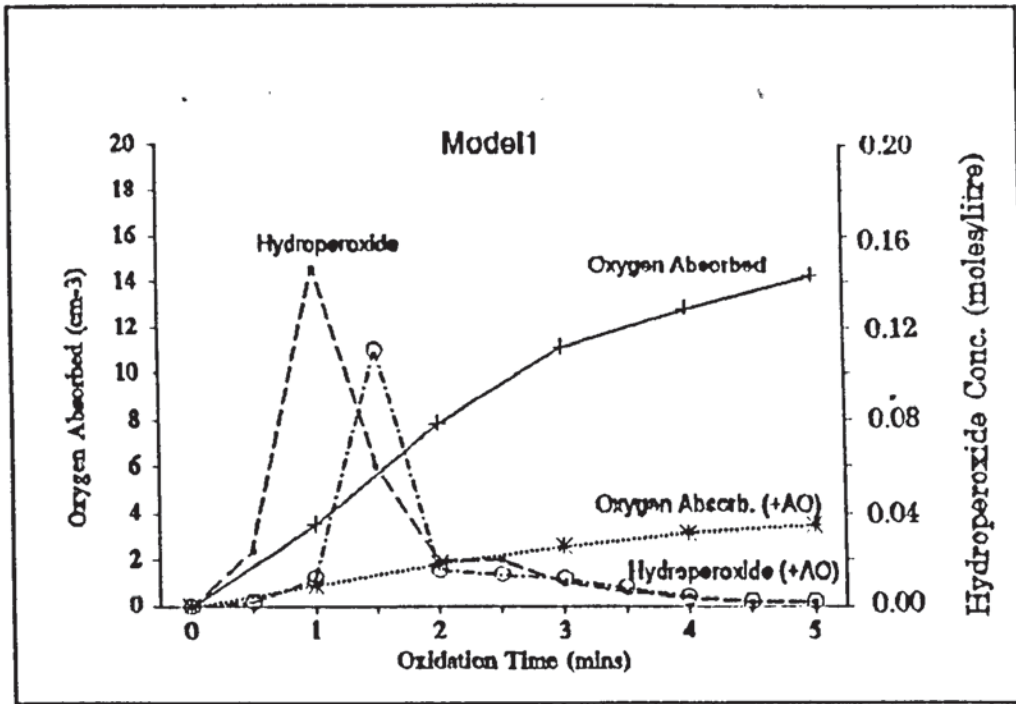
Figure 3.50 A Comparison of the Oxygen Absorbed and the Hydroperoxide Produced During the Thermal Oxidation of Model I in the Presence of 1000ppm Sodium Phosphite at 150°C, in the melt phase.
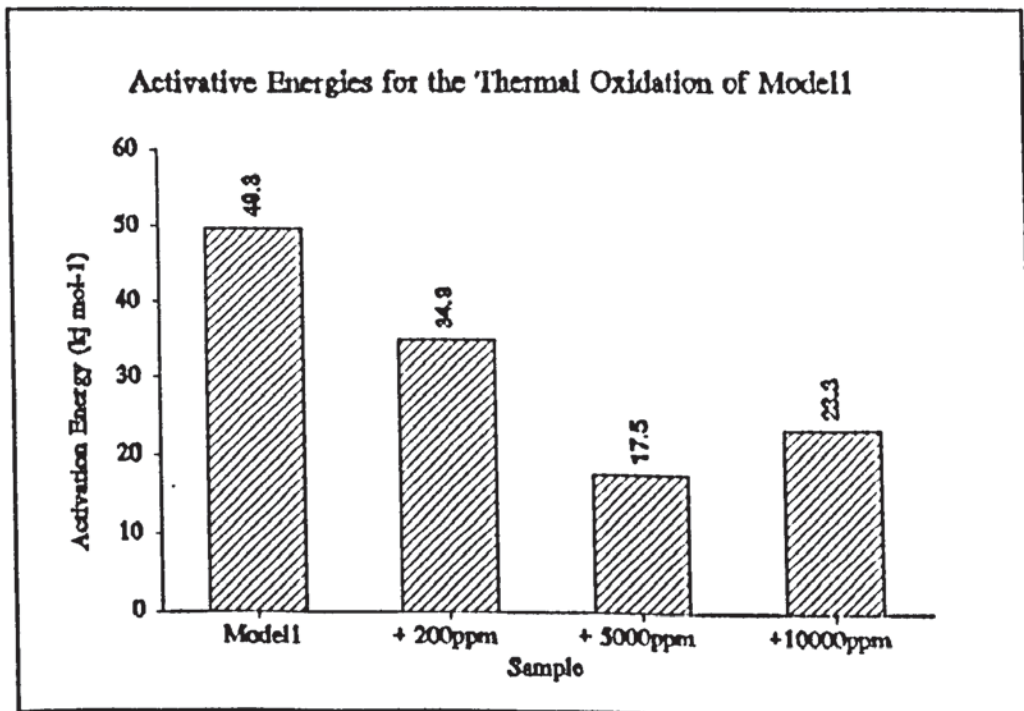
Figure 3.51 The Activation Energies Calculated for the Thermal Oxidation of Model I, with and without Cobalt.
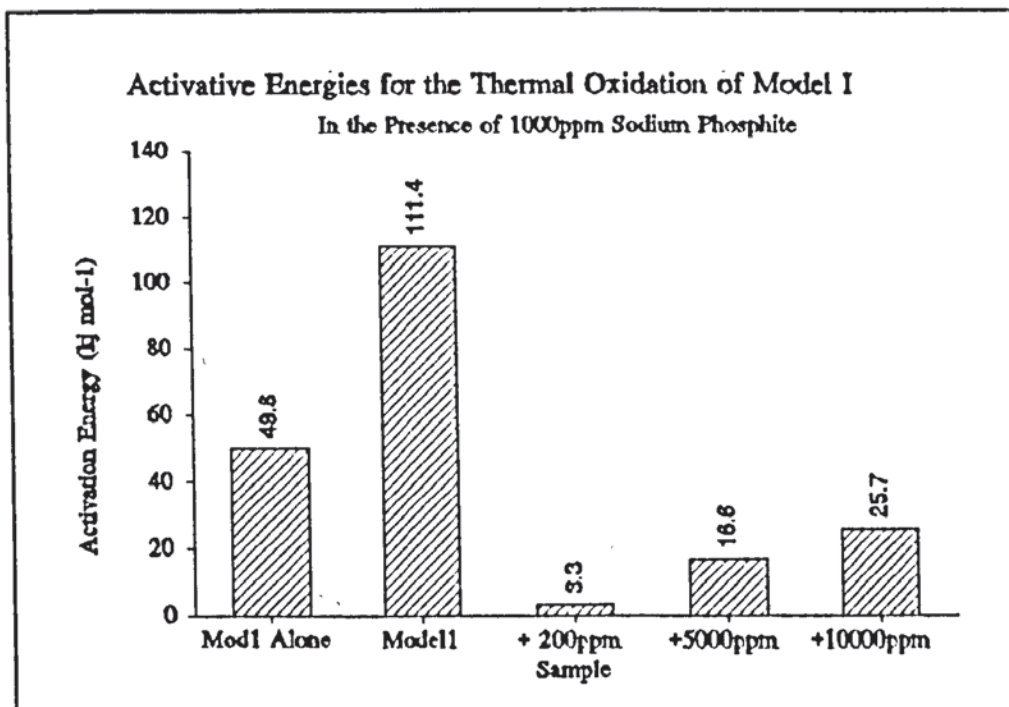
Figure 3.52 The Activation Energies Calculated for the Thermal Oxidation of Model I, in the Presence of 1000ppm Sodium Phosphite, with and without Cobalt.

Chapter 4. Oxidation Studies of Hexanedioate-bis-Benzylamide (Model II).

4.1 Object and Methodology.

Model II, Hexanedioate-bis-benzylamide, see table 4.1, is used here as the second hydrocarbon of the repeat unit of the Nylon polymer MXD6, see table 4.1, representing the aliphatic portion of the chain between the two aromatic rings. In this Chapter the oxidation characteristics of Model II in the presence and absence of sodium phosphite and cobalt neodecanoate are determined (see table 4.1 for structures). Methods used for this determination, the same used for the study of Model I in the previous Chapter, are summarised in scheme 4.1 and include:-

1. Oxygen Absorption
2. FT-IR Analysis
3. Ultra Violet/Visible Spectroscopic Analysis
5. Hydroperoxide Determination
6. Thermogravimetric/Differential Thermal Analysis

These techniques provided valuable information concerning the oxidation of Model I in the previous chapter complementing one other and assisting in the insight to the function of the cobalt neodecanoate and sodium phosphite. The oxygen uptake can be monitored through oxygen absorption techniques and the change in structure, associated with the oxygen uptake, can be monitored by infra-red and ultra-violet/visible spectroscopy. The oxygen absorption study of model I proved particularly useful when studying the effect of different concentrations of cobalt neodecanoate, and sodium phosphite, on the system, whereas hydroperoxide formation depicted clearly the effect of sodium phosphite and also gave an insight into the reaction mechanism.
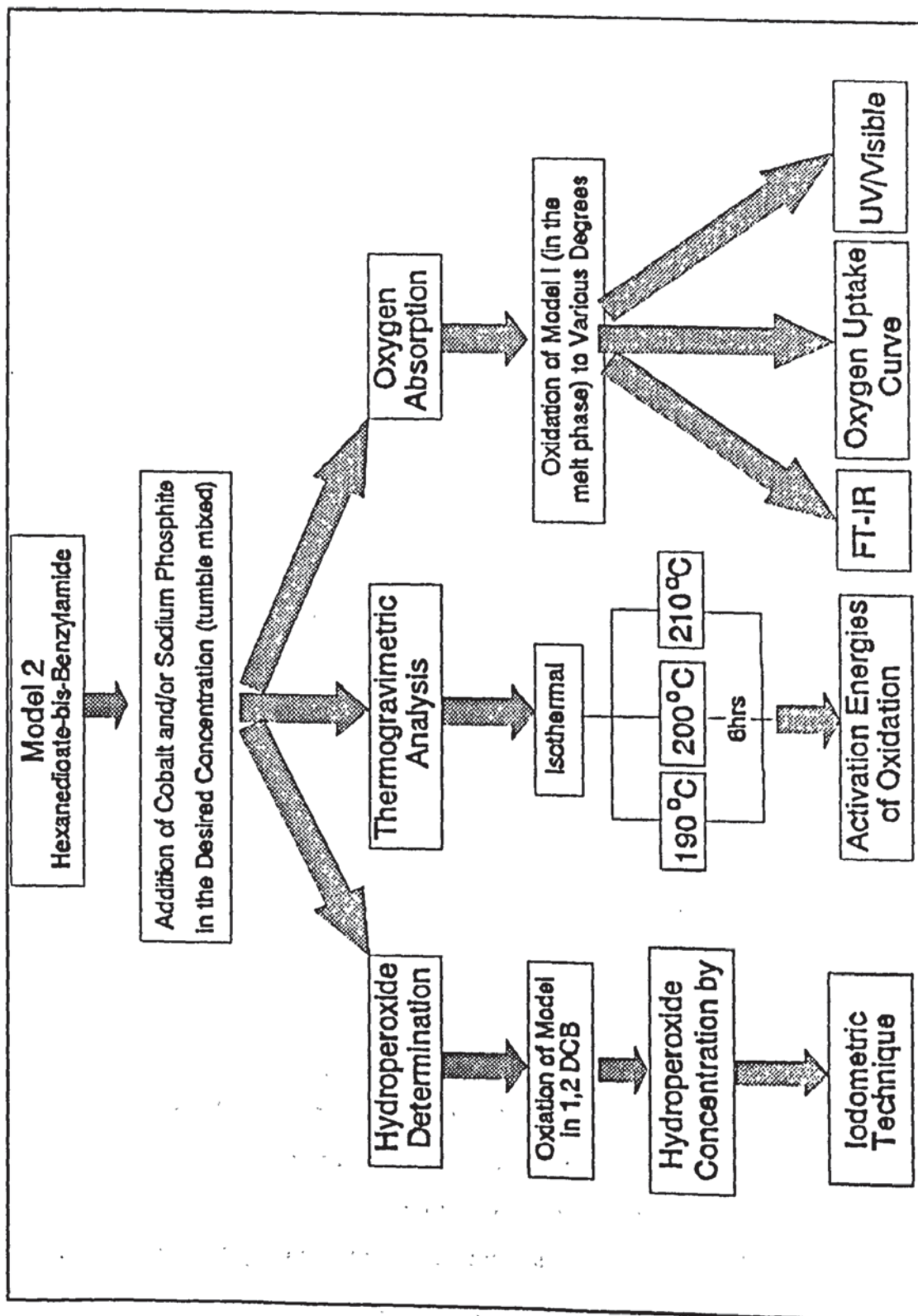
Scheme 4.1 Experimental Outline of the Oxidation Study of Model II.
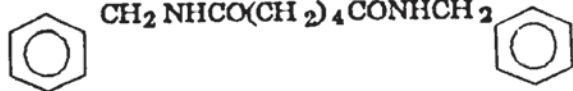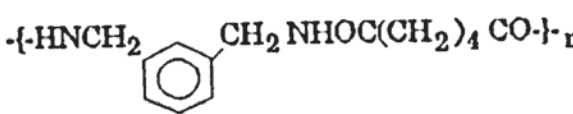
Molecular Weight	Chemical Structure and Name	Abbreviation
356.41	CH_2 NHCO$(CH_2)_4$CONHCH$_2$ Hexanedioate-bis-Benzylamide	Model II (white powder) m.p = 175°C
	-{-HNCH$_2$ CH$_2$ NHOC$(CH_2)_4$ CO-}-$_n$ poly(m-xylylene adipamide)	MXD6
302	Co$(C_{10}H_{19}O_2)_2 \cdot 4H_2O$ Cobalt Neodecanoate	Cobalt (purple pellets) m.p, -4H$_2$O, 140°C
216.04	$Na_2HPO_3.5H_2O$ Sodium Phosphite	Sodium Phosphite (white crystals) m.p, -5H$_2$O, 150°C

Table 4.1 Various Chemicals used in the Oxidation Study of Model II

4.2 Results.

4.2.1 The Effect of Cobalt Neodecanoate (cobalt) and Sodium Phosphite on the Oxidation of Model II : Oxygen Absorption Study.

The oxidation of model II alone and with varying concentrations of cobalt has been assessed by oxidising the model in an atmosphere of pure oxygen in the melt phase at 190°C, inside the oxygen absorption apparatus. The oxidation was carried out in the oxygen absorption apparatus as described in section 2.4.1. The effect of addition of sodium phosphite to the model and model/cobalt system is studied in the same way without modification to the oxygen absorption technique.

4.2.1.1 Oxidation of Model II.

The oxidation of model II in the melt phase is shown in figure 4.1. After a very short induction period of less than five minutes, the rate of oxygen uptake was rapid particularly during the initial 2hours. In the later stages of oxidation oxygen uptake slowed down increasing at a constant rate up to 20 hours.

4.2.1.2 Oxidation of Model II in the Presence of Cobalt.

The effect of different concentrations of cobalt neodecanoate on the oxidation of model II is shown in figure 4.2a. It is clear from the oxygen absorption traces that cobalt, in all concentrations has very little effect on the model compound. Over a 20 hour period the amount of oxygen absorbed by the model in the presence of cobalt is less than in its absence, particularly with the addition of 50ppm. The only difference in oxidation rates occurs in the initial 1 hour , as shown in figure 4.2b, which compares the oxidation rates of the model with a range of cobalt concentrations over time periods of 1, 5 and 20hrs. All the different cobalt concentrations used produce very short induction periods of less than 5mins which is comparable with the model alone.

4.2.1.3 Oxidation of Model II in the Presence of Sodium Phosphite.

The oxidation of model II in the presence of 500, 1000 and 2000ppm sodium phosphite at 190°C is shown in figure 4.3. Sodium phosphite only slightly inhibited the oxidation of model II but had a greater effect when used used in larger concentrations. Oxidation was auto-accelerating but slower in the initial period (<5hrs) in comparison to model II alone. Figure 4.3b shows clearly that the sodium phosphite inhibited the oxidation more profoundly in the early stages, ie in the first 60 minutes. It was during these initial stages that model II alone had the greatest intake of oxygen before encountering a gradual auto-retarding stage. The higher the concentration of sodium phosphite used the greater the inhibiting effect in the first 60 minutes of oxidation.

4.2.1.4 Oxidation of Model II in the Presence of Cobalt and Sodium Phosphite.

The effect of various concentrations of cobalt upon the oxidation of model II in the presence of a constant concentration of sodium phosphite of 1000ppm is shown in figure 4.4. It is clear from the previous oxygen absorption traces (figure 4.3) that sodium phosphite, particularly at a 2000ppm level, has the ability to slightly inhibit the oxidation of the model compound. However, in the presence of cobalt the catalytic behaviour of the metal ion overcomes the inhibiting effect of the sodium phosphite hence increasing the overall oxidation of the model, see figure 4.4a. Figure 4.4b shows clearly that the major oxidation of model II, which occurs in the presence of sodium phosphite (1000ppm) and varying concentrations of cobalt, takes place within the initial hours of the oxidation time (more pronounced within the first 60 minutes). The behaviour is similar to that shown earlier, see figure 4.2, for oxidation of this model in the presence of cobalt only (ie, absence of sodium phosphite). The rate of oxidation particularly in the initial 60 minutes increases with increasing cobalt concentration, the greatest increase between 0 and 100ppm, see figure 4.4b and 4.4c, for a comparison of the oxidation rates of this model with cobalt in the presence or absence of sodium phosphite.

4.2.2 Infra-red Spectroscopic Analysis of Model II During Thermal Oxidation.

By studying the Infra-red spectra of model I, after oxidation, at certain wavelengths the effect of continuous oxidation upon the model structure could be followed, see chapter 3.2.2. Analysis in the 3600-3200cm^{-1} region showed a decrease in intensity of the N-H stretch, due to the amide group, suggesting a breakdown of the functional group to various components. However in the region 1800-1550cm^{-1} analysis showed the appearance of additional peaks suggesting the formation of new compounds due to the oxidation of the model compound. Therefore in order to gain a similar picture of the the effect of oxidation upon model II the analysis was carried out as described in section 2.4.2. Monitoring the differences obtained in the FT-IR spectra of model II upon oxidation at 190°C with increasing oxidation time reveals four main points of interest :-

1) an increase in absorbance at 1743cm^{-1} (possibly an aliphatic aldehyde).

2) an increase in absorbance at 1701cm^{-1} (aromatic aldehyde or ketone).

3) a decrease in absorbance at 3291cm^{-1} (N-H of amide).

4) a decrease in absorbance at 1635cm^{-1} (C=O of amide).

4.2.2.1 Oxidation of Model II.

These are displayed in figure 4.5 which shows the FT-IR spectra of model II with increasing oxidation at 190°C between wavelength ranges 3600-3200cm^{-1} and 1800-1550cm^{-1}. The increase in absorbances (1743 & 1701cm^{-1}) are due to the formation of new products whose functional group absorbs in this region of the Infra-red spectrum (fig.4.7A). The decrease in absorbances at 3291 and 1635cm^{-1} represent the amide part of model2 (-NH-CO-) which during oxidation maybe considerably affected breaking down to form new products possibly associated with the product growth observed (fig.4.7A). During the oxidation of model I the formation of aliphatic, aromatic aldehydes/ketones and an aromatic carboxylic acid were thought to be responsible for the production of three peaks in the IR spectra at 1746, 1705 and 1683cm^{-1} respectively. Similarly, comparing the new absorbances produced during the oxidation of model II with the stretching vibrations of a range of carbonyl compounds (table 3.2), it seems likely that the absorbance at 1743cm^{-1} and 1701cm^{-1} are typical of an aliphatic aldehyde and an aromatic aldehyde (or carboxylic acid) respectively.

4.2.2.2 Oxidation of Model II in the Presence of Cobalt.

The effect of cobalt on the model compound was also assessed by monitoring the FT-IR spectra of the oxidising model with increasing oxidation time, see figure 4.6. In particular the areas of the four changing absorbances were measured with respect to a reference peak and plotted against oxidation time. Figure 4.7 shows the growth or disappearance of these peaks during the oxidation of model II with increasing concentrations of cobalt from 0 to 800pm. Generally formation of new products is considerably less than the decrease associated with the loss of absorbances at 3291 & 1635cm^{-1}. The growth of peak 1743cm^{-1} is more pronounced than the peak at 1701cm^{-1}, however this peak becomes more prominent in the later stages of oxidation.

Increasing the cobalt concentration from 50ppm (B) to 800ppm (F) results in a greater loss of the N-H and C=O absorbances, at $3291cm^{-1}$ and $1635cm^{-1}$ respectively. However the greatest loss of the two absorbances occurs during the oxidation of model II alone (fig.4.7A).

4.2.2.3 Oxidation of Model II in the Presence of Sodium Phosphite.

The effect of sodium phosphite upon the peak formation produced from the oxidation of model II can be seen in figures 4.8 and 4.10. Again the four maximum absorptions are observed (1743, 1701, 1635 & $3291cm^{-1}$) only the rate at which these peaks change is different. Figure 4.10A provides a graphical representation of the increase or decrease of these peaks with oxidation time. It is clear from this figure that the production of the peak at $1701cm^{-1}$ and the loss of the amide peaks, at 3291 and $1635cm^{-1}$ are slightly inhibited in the presence of sodium phosphite (compare with figure 4.7A).

4.2.2.4 Oxidation of Model II in the Presence of Sodium Phosphite and Cobalt.

Figure 4.9 shows the effect sodium phosphite in combination with cobalt has upon the FT-IR spectra of the oxidised model. Again it is apparent that the same four points of interest exsist, however, the rates at which they progress is different. Figure 4.10 shows the growth of the product peaks and the decrease in size of the peaks due to the amide function during the oxidation of model II in the presence of 1000ppm sodium phosphite and the effect of different concentrations of cobalt upon these peak areas. The presence of 1000ppm sodium phosphite highlights the differences due to the increasing cobalt concentration on the oxidation of model II more so than in it's absence. The loss in area of the N-H and C=O absorbance is still more pronounced than any gain in area due to product formation. Increasing the concentration of cobalt, particularly from 0 (A) to 200ppm (D), increases the loss of these two absorbances and increases the overall growth of the product peak at $1743cm^{-1}$. The peak at $1701cm^{-1}$ developed during the later stages of oxidation.

4.2.3 UV-Vis Spectroscopic Analysis of Model II During Thermal Oxidation.

Similarly, UV-Vis spectral analysis of the oxidation of model II in the absence or presence of cobalt or sodium phosphite is expected to lead to information which can help clarify the understanding of the model oxidation mechanism. Method of analysis was carried out as described in section 2.4.3.

4.2.3.1 UV-Vis Analysis of Model II Alone.

Figure 4.11 shows the UV-Vis spectrum of model II alone with a prominent absorbance at 264nm. However oxidation of the model generally leads to an increase in absorbance of the band at 280nm, see figure 4.12 as an example. Therefore monitoring the growth of the band at 280nm provides a good representation to the extent of oxidation in the model compound. The increase in absorbance of this band was therefore measured and plotted against increasing oxidation time, as shown in figure 4.13. The growth of the band was very fast within the initial 120 mins before slowing down substantially.

4.2.3.2 UV-Vis Analysis of Model II in the Presence of Cobalt.

The uv-vis spectrum of model II in the presence of cobalt (200ppm) with increasing oxidation is shown in figure 4.14. It was a typical uv-vis spectrum of a series of spectra analysed in the presence of several concentrations of cobalt ranging from 50ppm to 800ppm. Figure 4.15 shows similar increases in the 280nm absorption to that shown for model II alone (see figure 4.12). This increase was measured for each cobalt concentration with increasing oxidation time and can be seen in figure 4.15. Generally all additions of cobalt produced an initial rapid increase in absorbance, indicating a very short inhibition period, i.e less than 5mins for the oxidation of model II to begin. However in the later stages of oxidation slight differences in the rates of increase of the 280nm band were noticable. An increase in cobalt from 50-200ppm produced a slight rise in the rate of increase of the 280nm band between 30 and 300mins oxidation.

4.2.3.3 UV-Visible Analysis of Model II in the Presence of Sodium Phosphite.

Figure 4.16 shows the uv-vis spectrum of model II, in the presence of 1000ppm sodium phosphite with increasing oxidation time. Again it highlights the growth of the band at 280nm which is noticably smaller in comparison to that of the model alone (fig.4.12) and the model in the presence of cobalt (fig.4.14). The effect of sodium phosphite, in a concentration of 500ppm, 1000ppm and 2000ppm, upon the increase in absorbance at 280nm during the oxidation of model II at 190°C over a 1hour (insert) and 20 hour period are shown in figure 4.17. Sodium phosphite acts to inhibit the developing absorbance of the 280nm band, the inhibiting effect increasing slightly with increasing concentration of sodium phosphite. This behaviour is comparable with that observed for the oxygen uptake curves (from oxygen absorption study, see section 4.2.1.3).

4.2.3.4 UV-Vis Analysis of Model II in the Presence of Sodium Phosphite and Cobalt.

The uv-vis spectrum of model II in the presence of sodium phosphite (1000ppm) and cobalt (200ppm) with increasing oxidation is shown in figure 4.18. This is a typical uv-vis spectrum of a series of spectra analysed in the presence of several concentrations of cobalt ranging from 50ppm to 800ppm. The extent of oxidation was monitored by the change in the

uv/visible spectra particularly the increase in absorbance of the 280nm band over a 20hr and 1hr (insert) oxidation period, see figure 4.19. The absorbance at 280nm increases with increasing concentrtion of cobalt (0-800ppm). The initial absorbance increase is very rapid, particularly in the presence of higher concentrations of cobalt (200, 400 & 800ppm). This indicates the increasing potential of the cobalt to overcome the inhibiting effect of the sodium phosphite. The overall general trend of increasing absorbance of the oxidising model with increasing cobalt concentration is similar to the oxygen uptake curve of the model (see oxygen absorption study, figure 4.4).

A comparison of the four separate experiments is summarised in figure 4.20. It shows the increase in absorbance at 280nm during the increasing oxidation of model II, alone and in the presence of a typical concentration of cobalt, sodium phosphite and a combination of both cobalt and sodium phosphite.

4.2.4 Effect of Cobalt and Sodium Phosphite on Peroxide Formation During the Oxidation of Model II.

In chapter 3.2.4 the formation of peroxide during the oxidation of model I was monitored using two different techniques, iodometric and iron oxidation. Both techniques enabled the amount of hydroperoxide formed during oxidation to be measured consistently and accurately. The results obtained from both techniques were very similar and contributed towards providing an insight into the reaction mechanism and also depicting clearly the effect of sodium phosphite. Therefore hydroperoxide determination was also carried out on model II but due to the similarity in results obtained from both techniques used in the determination of model I it was decided that only one technique was required for assesment of model II. The iodometric technique was chosen to conduct the analysis mainly because it provides a measurement of the hydroperoxide content of the sample that much quicker. The analysis of hydroperoxide using the iodometric technique is described in section 2.4.4, however analysis of model II proved more difficult due to insolubility of the model in 1,2 dichlorobenzene at low temperatures. In order to avoid precipitation of the model a heated syringe was used to withdraw the sample from the flask for subsequent analysis.

4.2.4.1 Effect of Oxidation of Model II on Hydroperoxide Formation.

The hydropeoxide formed during the oxidation of model II in 1,2 dichlorobezene at 150°C in an oxygen atmosphere can be seen in figure 4.21. The hydroperoxide curve suggests an inhibition period of approximately 30mins followed by a steady build up of hydroperoxide reaching a maximum after 120mins of oxidation.

4.2.4.2 The Effect of Sodium Phosphite on Hydroperoxide Formation in the Oxidising Model.

Sodium phosphite was added to the model in concentrations of 1000ppm and 2000ppm. The hydroperoxide curves were then compared with that of model II after oxidation for 200mins (figure 4.22). In the presence of 1000ppm sodium phosphite the induction period, before the commencement of hydroperoxide formation, was increased to approximately 45mins. Peak concentration occured at 130mins. In the presence of 2000ppm sodium phosphite, hydroperoxide formation begins after 55mins reaching a maximum at 140mins.

The overall effect of sodium phosphite is therefore seen to delay the onset of hydropeoxide formation in the oxidising model, see inset figure 4.22.

4.2.4.3 The Effect of Cobalt and Cobalt/Sodium Phosphite on the Hydroperoxide Formation in the Oxidising Model.

Cobalt alone and cobalt in addition to 1000ppm sodium phosphite was added to the model and the concentration of hydroperoxide compared to that of model II alone after oxidation for 200mins (figure 4.23). Similarly to the oxidation of model I, under the same conditions, none or very little hydroperoxide was detected.

4.2.6 The Effect of Cobalt and Sodium Phosphite on the Oxidation of Model II : Thermogravimetric Study.

The previous chapter examined the effects of cobalt and sodium phosphite on the oxidation of model I. Of particular interest was the comparison of the activation energies of the model compound, in the presence of sodium phosphite and cobalt, required for the thermal oxidation of the amide. The results showed clearly the catalytic effect of the cobalt and the inhibition properties of the sodium phosphite. The activation energies were calculated by measuring the weight loss of the model, at fixed temperatures, the weight loss being due to loss of volatlie products formed during the oxidation. Therefore by analysing model II in a similar manner the effect of cobalt and sodium phosphite upon the thermal oxidation of model II can be monitored and also a comparison of the activation energy for both model I and model II can be obtained.

The analysis of model I was carried out at 140, 150 and 160°C, however due to the higher melting point of model II, the analysis was carried out at 190, 200 and 210°C. Samples of unmodified model II, and model II with various concentrations of sodium phosphite and cobalt, were heated isothermally in oxygen at these temperatures for 6 hours, according to the procedure described in section 2.4.5.

<u>4.2.6.1 The Effect of Cobalt on the Oxidation of Model II : Thermogravimetric Study.</u>

The isothermal traces showing the effect of different concentrations of cobalt on the thermal oxidation of model II can be seen in the figures listed :-

a) Model II Alone at 190, 200 & 210°C (figure 4.24a)

b) Model II + 200ppm Cobalt at 190, 200 & 210°C (figure 4.24b)

c) Model II + 5000ppm Cobalt at 190, 200 & 210°C (figure 4.24c)

d) Model II + 10000ppm Cobalt at 190, 200 & 210°C (figure 4.24d)

Based on first order kinetics, it was possible to calculate the activation energies associated with the oxidative weight loss of model II, with and without cobalt. The slope of each trace was calculated directly after the onset of weight loss and recorded as rate constant 'k', see table 4.2.

Sample (ppm Co)	Degradation Temp.(°C)	Rate Constant 'k' (s^{-1})	ln 'k'
Model II	190	1.58×10^{-4}	-8.75
	200	2.04×10^{-4}	-8.50
	210	2.56×10^{-4}	-8.27
200ppm	190	7.99×10^{-5}	-9.43
	200	9.71×10^{-5}	-9.20
	210	1.28×10^{-4}	-8.96
5000ppm	190	2.53×10^{-4}	-8.28
	200	2.63×10^{-4}	-8.24
	210	2.70×10^{-4}	-8.22
10000ppm	190	3.79×10^{-4}	-7.88
	200	4.10×10^{-4}	-7.80
	210	4.38×10^{-4}	-7.73

Table 4.2 Rate Constants Derived for the Thermal Oxidation (via isothermal TGA) of Model II with and without Cobalt.

From the plots of the logarithms of the rate constants versus the reciprocal of the absolute temperature, at which the analysis was conducted, the activation energies were obtained by the slope of the straight line (figure 4.26). Slope of the straight line $= -E_a/R$ where $E_a =$ activation energy (J mol^{-1}) and R$=$ gas constant 8.314 (J K^{-1} mol^{-1}), see table 4.3.

Sample (ppm Cobalt)	Straight Line Equation	Activation Energy (kJ mol^{-1})
0ppm	y = 1.86 - 4.8x	39.9
200ppm	y = 1.60 - 5.0x	41.6
5000ppm	y = -6.84 - 0.7x	5.49
10000ppm	y = -4.28 - 3.4x	28.7

Table 4.3 Activation Energies Calculated for the Oxidative Degradation of Model II, with and without Cobalt.

4.2.6.2 The Effect of Cobalt and Sodium Phosphite on the Oxidation of Model II : Thermogravimetric Study.

The traces derived from isothermal heating model II (containing 1000ppm sodium phosphite) in the presence of cobalt, at 190, 200 and 210°C are shown in figure 4.25 and listed below :-

a) Model II (sodium phosphite) at 190, 200 & 210°C (figure 4.25a)

b) Model II (sodium phosphite) + 200ppm Cobalt at 190, 200 & 210°C (figure 4.25b)

c) Model II (sodium phosphite) + 5000ppm Cobalt at 190, 200 & 210°C (figure 4.25c)

d) Model II (sodium phosphite) + 10000ppm Cobalt at 190, 200 & 210°C (figure 4.25d)

Again the slope of each trace (fig 4.27) was calculated directly after the onset of weight loss and recorded as rate constant 'k', see table 4.4.

Sample (ppm Co)	Degradation Temp.(°C)	Rate Constant 'k' (s⁻¹)	ln 'k'
Model2	190	9.69×10^{4}	-9.24
	190	1.21×10^{-4}	-9.02
	200	1.51×10^{4}	-8.80
200ppm	180	6.88×10^{5}	-9.58
	190	9.69×10^{5}	-9.24
	200	1.36×10^{-4}	-8.90
5000ppm	190	2.36×10^{-4}	-8.35
	200	2.54×10^{4}	-8.28
	210	2.80×10^{-4}	-8.18
10000ppm	180	3.10×10^{4}	-8.08
	190	3.43×10^{-4}	-7.98
	200	3.70×10^{4}	-7.90

Table 4.4 Rate Constants Derived for the Thermal Oxidation of Model II, in the Presence of 1000ppm Sodium Phosphite, with and without Cobalt.

From the plots of the logarithms of the rate constants versus the reciprocal of the absolute temperature, at which the analysis was conducted, the activation energies were obtained by the slope of the straight line (figure 4.27) and are shown in table 4.5.

Sample(containing 1000ppm sod.phos) (ppm Cobalt)	Straight Line Equation	Activation Energy (kJ mol⁻¹)
0ppm	y = 2.58 - 5.5x	45.7
200ppm	y = 5.45 - 6.8x	56.5
5000ppm	y = -4.27 - 1.9x	15.6
10000ppm	y = -3.76 - 2.0x	16.63

Table 4.5 Activation Energies Calculated for the Oxidative Degradation of Model II, in the Presence of 1000ppm Sodium Phosphite, with and without Cobalt.

Similarly to the thermal oxidation of model I, the isothermal weight change curves of model II were characterised by a short period of weight gain, due to oxygen reacting with the model, followed by a longer period of weight loss, due to the emission of the oxidation products. The weight loss was used in the calculation of the activation energies, however the initial weight gain is also an important factor in the oxidation of the model compound. This period is affected by both the temperature of the reaction and the cobalt concentration. The size and time period of the weight gain decreased with increasing temperature as shown in figures 4.28 and 4.29. The effect of cobalt concentration is also shown in these figures, it appears that cobalt, when present in larger concentrations (>200ppm), also decreases the size of the initial weight gain.

4.3 Discussion.

The five techniques used in the study of the thermal oxidation of model I (chapter 3) were used in the same context for the thermal oxidation study of model II. Again, in different ways they assessed the extent of increasing degradation of the model and have individually led to an insight into the mechanism of the thermal oxidation of the model in the absence and presence of the anti-oxidant (sodium phosphite) and the catalytic impurity (cobalt neodecanoate).

4.3.1 The Thermal Oxidation of Model II Alone.

The exposure of a polymer to oxygen is usually characterised by an induction induction period, the importance of which was discussed in chapters 1 and 3. The oxygen absorption characterisitics of model II, at 190°C, show an immediate uptake of oxygen with no apparent induction period. This suggests therefore a rapid formation of hydroperoxide resulting in the rapid autoxidation of the model compound. Peroxide analysis of model II does in fact show an immediate production of hydroperoxide, even at the slightly lower oxidation temperature of 150°C, which then proceeds to build up over a 2hour period, see figure 4.30. In the later stages of oxidation, oxygen uptake appears to level off. Similarly to the oxygen absorption characteristics of model I their could be several possibilities for this decrease in rate of oxygen uptake , i) sufficient production of volatiles in the sample flask of the oxygen absorption apparatus to affect the pressure readings, ii) formation of

transformation products likely to inhibit the oxidation of the model compound, iii) oxygen starvation ie, lack of oxygen in the sample flask, iv) saturation of the model compound. The most likely reason is the saturation of the model compound. Due to the high initial intake of oxygen the available sites for further oxidation become less and less hence a leveling off period on the oxygen absorption curve, see figure 4.30.

The spectral studies generally reflect the results obtained from the oxygen absorption studies. Infra-red analysis of the oxidising model, at various time intervals, suggests the breakdown of the amide bond, highlighted by the decrease in peak areas due to the (N-H str) and (C=Ostr) of the amide functional group (-NH-CO-) represented by absorbances at 3291cm^{-1} and 1635cm^{-1}, see figure 4.7a. The subsequent formation of peaks at 1743cm^{-1} and 1701cm^{-1} (fig.4.7a) are typical absorbances of a range of aldehydes/ketones and carboxylic acids that are likely to be formed, see figure 4.31 and 4.32 respectively. Definite characterisation is difficult from carbonyl absorbances alone but the peak at 1743cm^{-1} is possibly due to an aliphatic aldehyde (eg, acetaldehyde). The absorbance at 1701cm^{-1} could, however be characteristic of both an aromatic aldehyde (eg, benzaldehyde) and a dicarboxylic acid (eg, glutaric). The limitations of spectroscopic analysis were outlined in chapter 3. The loss of volatlie products during the oxidation of model II were probably more pronounced compared to model I, due to the higher temperatures involved. Therefore, low molecular weight carboxylic acids, aldehydes/ketones and amines (fig.4.33) may avoid detection by the spectroscopic analysis.

During the thermal oxidation of model I (chapter3) the growth of the absorbance band at 286nm, in the UV-Vis spectra was monitored with increasing oxidation time. This had some reflection on the extent of oxidation of the model compound. This increase in absorbance was due to the increasing concentration, in the model, of the aromatic amine m-xylylene diamine, formed as by product of oxidation. Similarly during the thermal oxidation of model II, UV-Vis analysis detected the growth of an absorbance band at 280nm (fig.4.12), with increasing oxidation time of the model compound, which again reflected the extent of oxidation of the model.

Therefore based on the same reaction scheme postulated for the formation of m-xylylene diamine, in model I, the likely by product of thermal oxidation of model II, producing this absorbance at 280nm, would be benzylamine (fig.4.34), via reaction scheme 4.2 which involves scission of the CH_2-CO bond (as dicussed in ch.3 section 3.3.1). The resulting formation of the hydroisocyanate radical proceeds to react with oxygen, present in the system with subsequent formation and decomposition of the hydroperoxide followed by decarboxylation resulting in the formation of benzylamine. The overall oxidation cycle for model II is outlined in scheme 4.3, which similarly to the oxidation of model I, describes the breakdown of the model via loss of a reactive hydrogen or bond fission resulting in the formation of hydroperoxide. This subsequently decomposes to form aldehydes/ketones and carboxylic acids (for example, benzaldehyde & benzoic acid, see scheme 4.4), detectable by IR analysis and amines (for example, benzylamine, see scheme 4.2), detectable by UV-Vis spectroscopy.
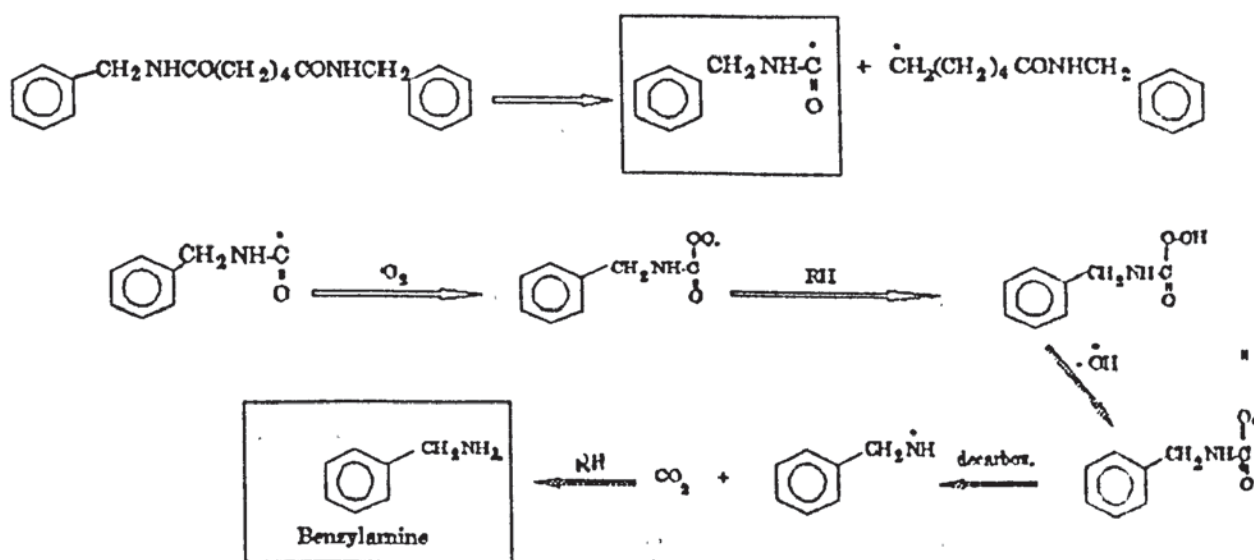
Scheme 4.2 The Reaction Scheme for the Oxidation of Model II, at 190°C, Resulting in the Formation of Benzylamine.

Model II
Hexanedioate-bis-Benzylamide

$CH_2 NHCO(CH_2)_4 CONHCH_2$

Heat (190 °C)

Formation of Radical Species

(bond fission)
$-CH_2 NH-$ or $-CO-CH_2-$

$\cdot CH-NHCO-$

(loss of reactive hydrogen atom due to external forces)

$\dot{C}H_2 + HN-$ $\qquad$ $\dot{C}O + \dot{C}H_2-$

Oxygen

model absorbs oxygen
(oxygen absorption study)

Hydroperoxide Formation
(detected by peroxide determination
using iodometric or colormetric
technique).

decomposition

Product Formation
(volatile - detected using tg analysis
and non-volatile products).

Aldehydes/Ketones
(IR Spectroscopy)
see figure 4.6

Carboxylic Acids
(IR Spectroscopy).
see figure 4.6

Amines
(UV/Vis Spectroscopy).
see figure 4.13

Scheme 4.3 The Oxidation Cycle of Model II, Outlining the Formation of Radicals Via Loss of a Reactive Hydrogen or Bond Fission Resulting in the Formation and Subsequent Decomposition of Hydroperoxides and the Formation of Aldehydes/ketones, Carboxylic Acids and Amines.

$CH_2 NHCO(CH_2)_4 CONHCH_2$

Heat

$CHNHOO(CH_2)_4 CONHCH_2$

O_2

$CHNHOO(CH_2)_4 CONHCH_2$

RH

$CHNHCO(CH_2)_4 CONHCH_2$

$\cdot OH$

$CHNHOO(CH_2)_4 CONHCH_2$

$HNCO(CH_2)_4 CONHCH_2$ +

Benzaldehyde

$R\cdot$

Benzoic Acid

O_2 $\qquad$ RH $\qquad$ $-OH$ $\qquad$ RH
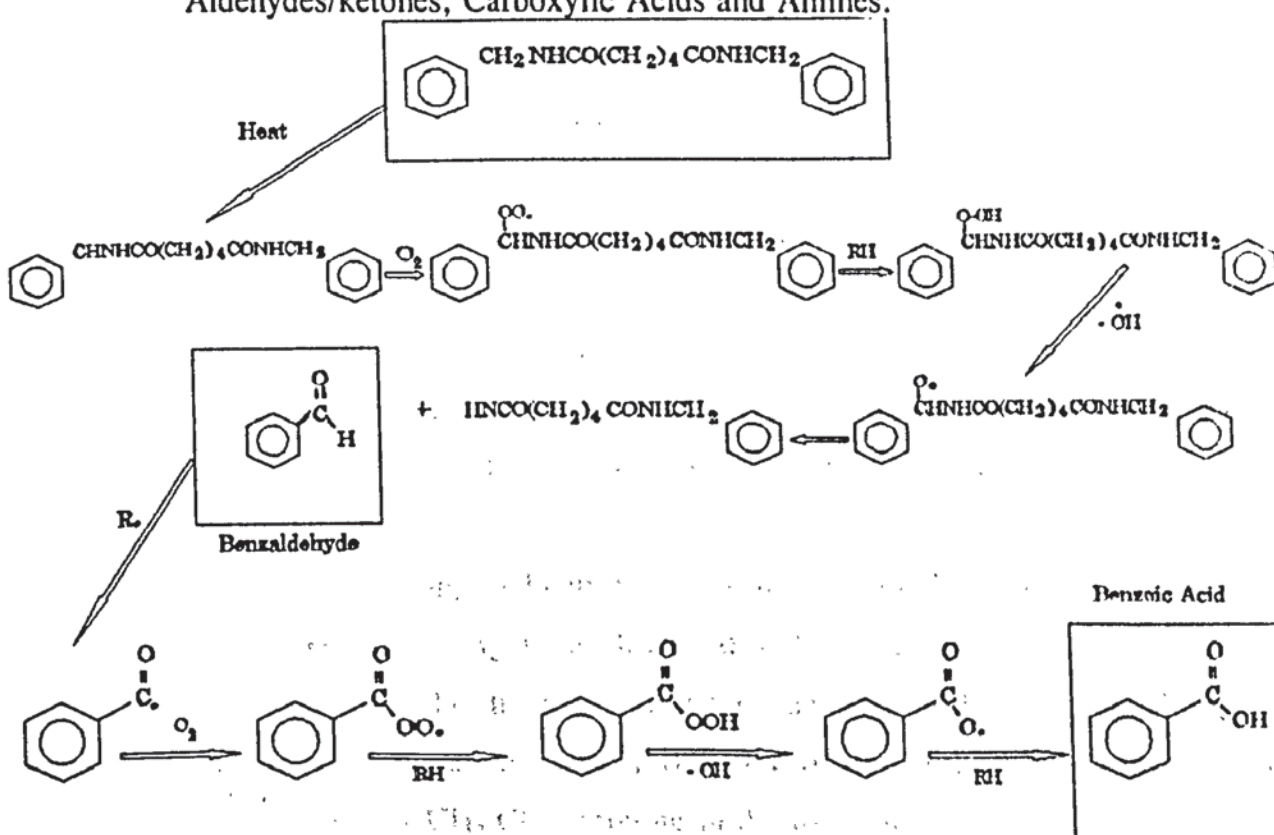
Scheme 4.4 The Reaction Scheme for the Oxidation of Model II, at 190°C, Resulting in the Formation of Benzaldehyde and Benzoic Acid.

4.3.2 The Thermal Oxidation of Model II in the Presence of Cobalt.

The addition of cobalt to the model, in arange of concentrations (50-800ppm), does not increase the already dramatic oxygen uptake of the model. The effect of cobalt slightly lowers the rate of oxygen uptake at 190°C over a 20hr period, the greatest difference occuring during the initial period. The peroxide analysis of the oxidising model in the presence of cobalt appears to suggest an immediate breakdown of peroxide upon formation, see figure 4.35, which was also discussed in chapter 3, due to a similar finding with model I, with reference to the work of Sagar. It was proposed that metal ions, in this case cobalt, catalysed the decomposition of the hydroperoxide, hence were not detected at any stage during the oxidation. However, during the thermal oxidation of model I, this catalysed decomposition of the hydroperoxide led to a slight increase in the oxidation of the model, but this was not so for model II. Even though cobalt appeared to catalyse the decomposition of the hydroperoxide at 150°C the oxygen absorption results showed a decreased oxygen uptake of model II, at 190°C. It therefore seems likely that the cobalt would catalyse the oxidation of model II at the lower temperature of 150°C but at the higher temperature of 190°C the functionality of the cobalt changes.

The limiting effect of the cobalt on the oxidation of model II was also confirmed by infrared and UV-visible spectroscopic techniques which followed the build up of products and decomposition of the model structure during thermal oxidation, see figures 4.7 and 4.15. It is now apparent that the uv-vis analysis monitored, at least in part, the formation of benzylamine in the oxidising model. The spectroscopic study, carried out on the model in the presence of cobalt, also revealed that the reaction mechanism, in respect to the pathway of formation of degradation products is unaltered in the presence of cobalt.

Similarly the products that appear likely to be forming are aldehydes/ketones, carboxylic acids and amines, see figures. Again, as discussed in the same context for model I (chp3), the presence of cobalt may alter the initiation step of the reaction. In the model alone there are two possibilities for initiation to occur i) fission of the weakest bonds in the amide chain ie, CH_2-NH bond or CH_2-CO, resulting in the formation of the respective radicals, or ii) loss of a reactive hydrogen atom (alpha to the NH group) due to external forces, such

as shear or heat, again resulting in radical formation. In the presence of cobalt a third possibility may be considered in which initiation may occur via a favourable complex formation between the cobalt and amide chain, resulting in the abstraction of the most reactive hydrogen atom. Such complex formation in model I relied on the donation of a lone pair of electrons by the carbonyl groups of the amide to the cobalt in preference to electron donation via the N-H groups (see chp3 section 3.3.2).

Similarly model II also has the availability of two carbonyl groups for which to donate a lone pair of electrons. However the resulting coordination is likely to take place around the aliphatic part of chain (I), as opposed to the aromatic part in model I.
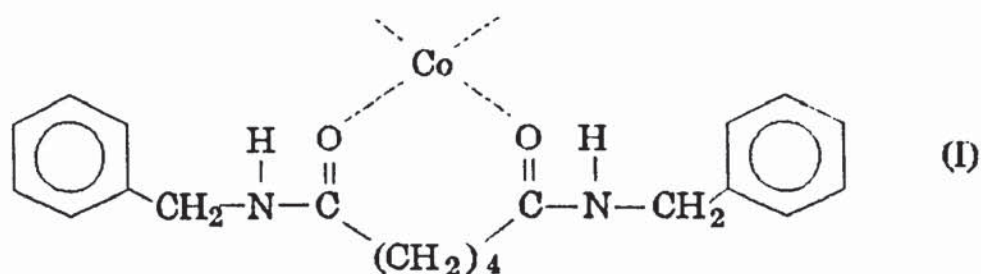
The complex is thought to activate the oxygen present (c.f model I), thus creating a superoxide radical anion (II),
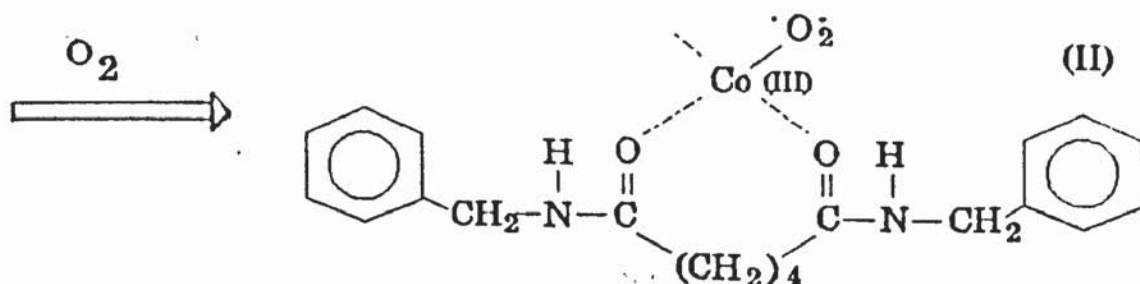
which may in turn abstract the most readily available hydrogen atom from a neighbouring amide chain, ie alpha to the N-H group (III).
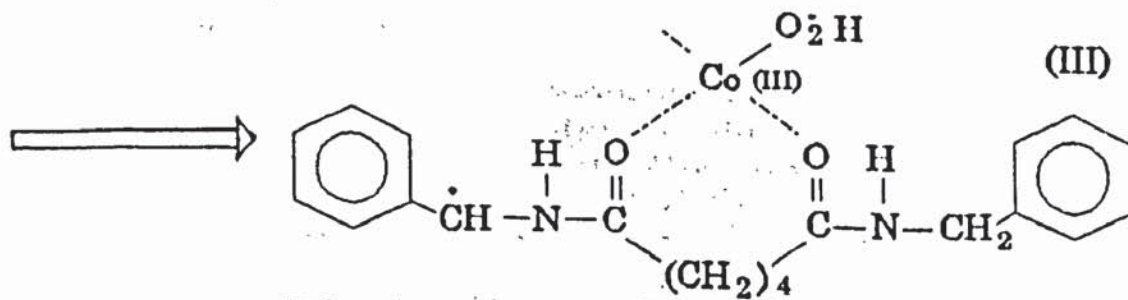
Disproportionation of the latter leads to a conjugated species having a high degree of resonance stabilization (IV & V).
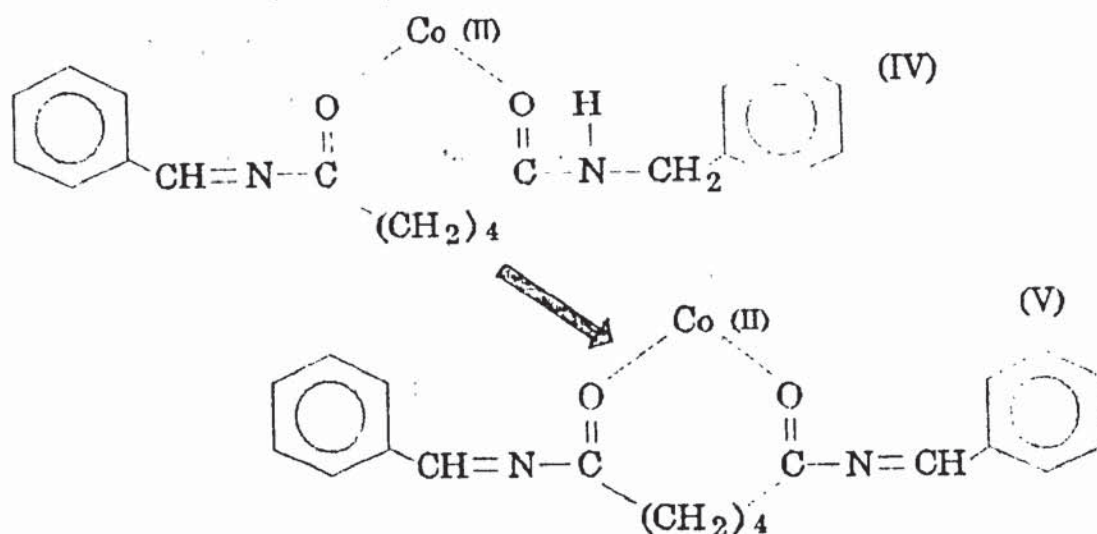
The radicals formed during this series of reactions are responsible for the latter stages of oxidative propagation. Complex formation of this nature in both models I and II therefore suggests that cobalt acts principally as a reaction initiator, but as discussed in chapter 3 if this was the case hydroperoxide formation would be detected during the oxidation of model I and model II in the presence of cobalt, however the absence of any such hydroperoxide formation, see figures 3.24 (MI) and 4.23 (MII) was clearly illustrated. A summary of the effect of cobalt upon the oxidation of model II is shown in scheme 4.5.
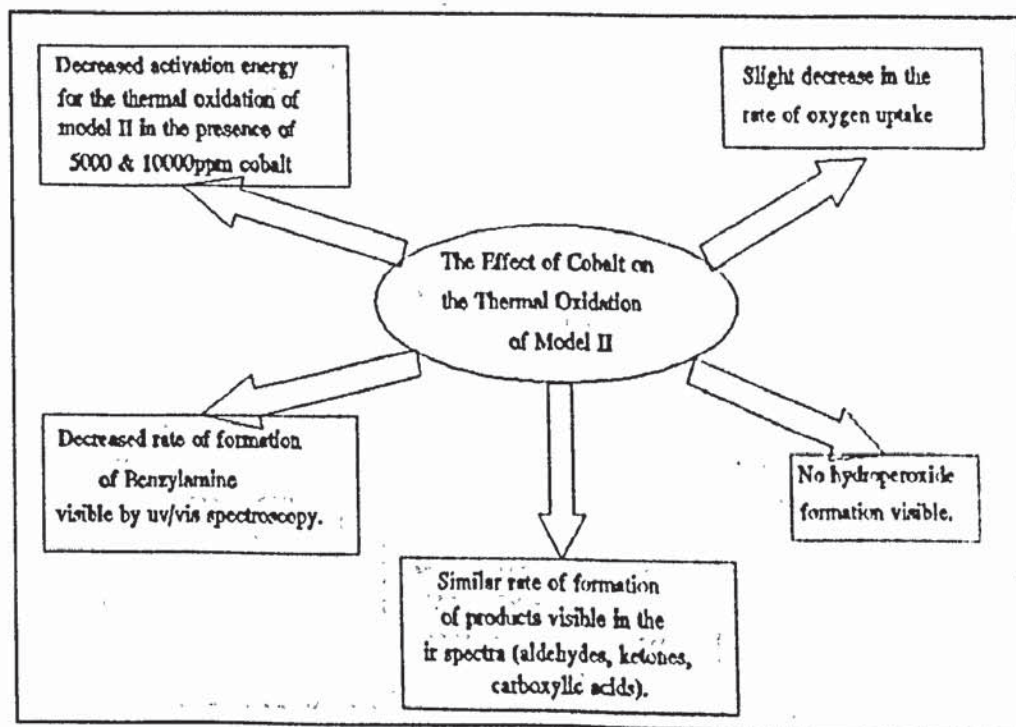
Scheme 4.5 A Summary of the Effect of Cobalt on the Oxidation of Model II.

4.3.3 The Thermal Oxidation of Model II in the Presence of Sodium Phosphite.

Sodium phosphite is known antioxidant used in the manufacture of MXD6. The addition of antioxidants to an oxidising polymer inhibits the reaction of oxygen with the substrate, this is reflected by an induction period on an oxygen absorption curve. This is comparable to the effect of sodium phosphite on the oxidation of model II. Although no clearly defined induction period is observed the rate of oxidation is definitely inhibited by the addition of the anti-oxidant. This was apparent in al studies conducted on the thermal oxidation of model II. A summary of the effect of sodium phosphite upon the oxidation of model II is shown in scheme 4.6. The antioxidant effect was increased with increasing concentration, resulting in a lower total of oxygen absorbed (fig.4.3) and delaying the onset of degradation products which were visible by IR and UV-Visible spectroscopy (figure 4.10 and 4.16 respectively). Monitoring the hydroperoxide formation in the oxidising model also gave a clear indication of the antioxidant effect of the sodium phosphite. When added to the model compound, sodium phosphite delayed the onset of the hydroperoxide formation, which was reflected in the reduced oxygen uptake performance of the model, see figure 4.36. Finally the sodium phosphite was shown to behave as an inhibitor for the amide oxidation, increasing the activation energy, calculated by isothermal weight loss curves (figure 4.38 and table 4.5).
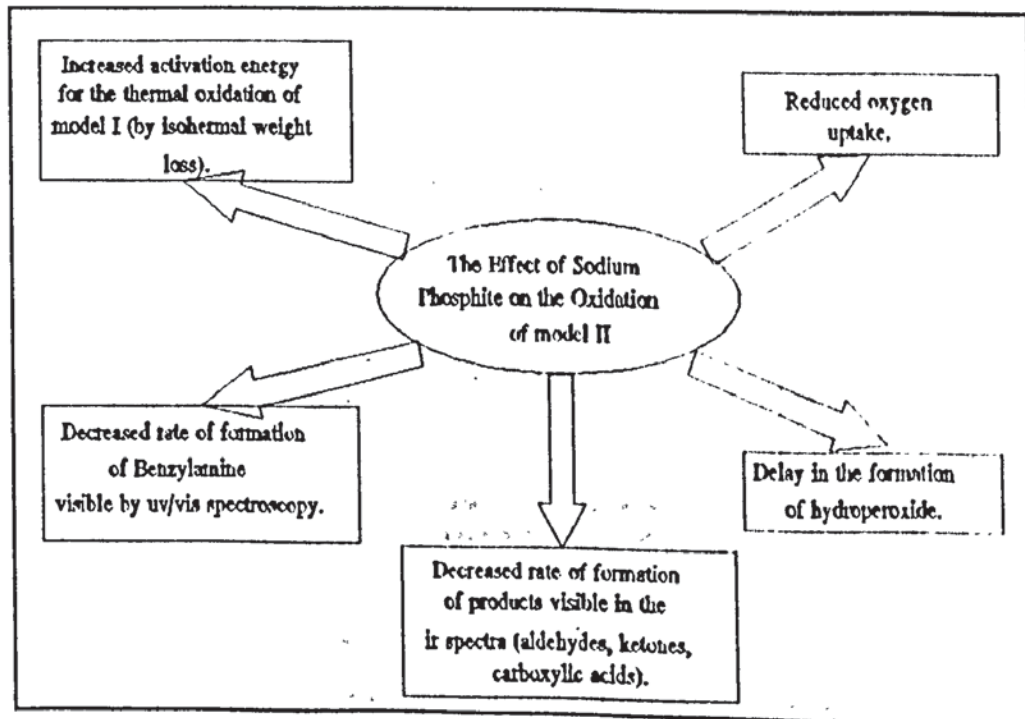
Scheme 4.6 A Summary of the Effect of Sodium Phosphite on the Oxidation of Model II.

4.3.4 The Thermal Oxidation of Model II in the Presence of Cobalt and Sodium Phosphite.

The addition of sodium phosphite (1000ppm) to the model is therefore more representative of the MXD6 used in the initial studies responsible for the superbarrier effect. Consequently the effect of cobalt on the model compound, in the presence of sodium phosphite, was monitored. The addition of cobalt slightly increased the oxygen uptake of the model. Cobalt appeared to have a greater effect during the initial stages of oxidation. The hydroperoxide study of the oxidising model again suggested the immediate decomposition by the transition metal ion but in this instance oxygen absorption studies suggest cobalt is acting as a pro-oxidant, see figure 4.39. The spectroscopic analysis follows the same trend as the oxygen absorption, with analysis in the ir and uv-vis spectra (figures 4.10 and 4.19 respectively), revealing that increasing the cobalt concentration increased the rate of product formation, with respect to the model plus 1000ppm sodium phosphite. The nature of products formed were similar to that of the model alone only the rate of formation has changed. A summary of the effect of cobalt and sodium phosphite upon the oxidation of model II is shown in scheme 4.7.
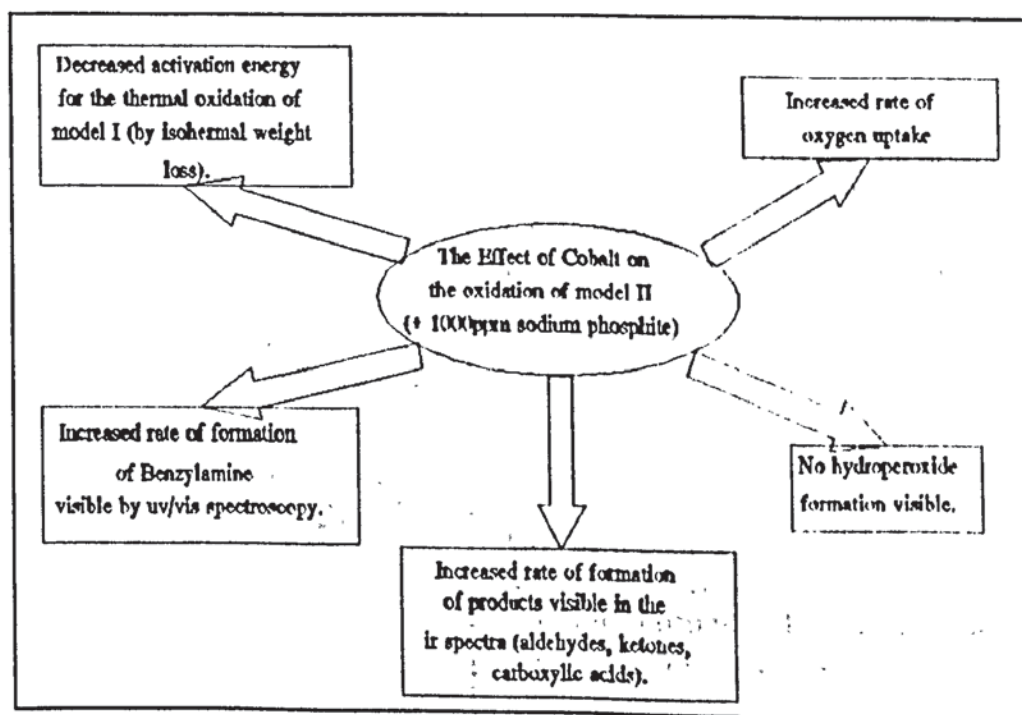
Scheme 4.7   A Summary of the Effect of Sodium Phosphite and Cobalt on the Oxidation of Model II.

4.3.5 A Comparison of the Thermal Oxidation of Model I with Model II, Via the Oxygen Absorption Study at 150°C and 190°C respectively.
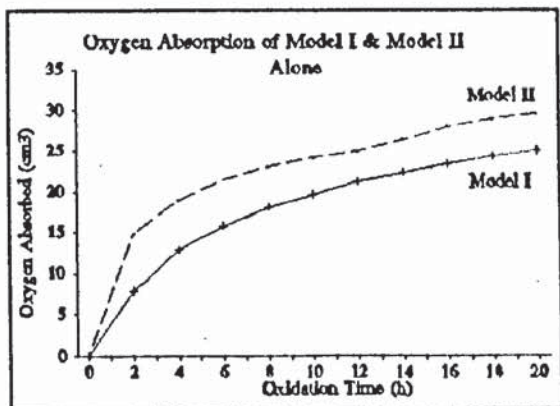
Initial oxidation of model II is slightly faster than that of model I, probably due to the higher temperature at which the oxidation was conducted. With the same amount of oxidisable functional groups in each structure it would be expected that over a period of time both models would absorb similar quantities of oxygen, which is reflected in the oxygen absorption traces.
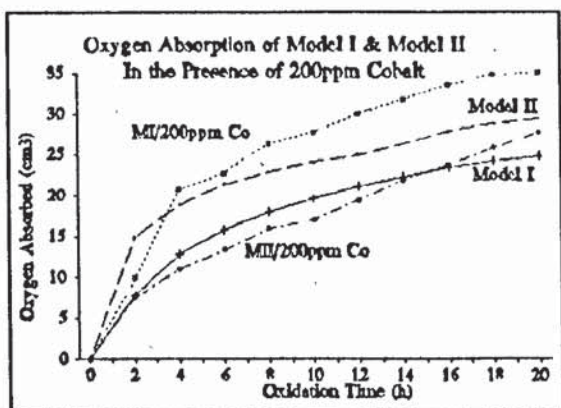
Cobalt has less effect on the oxidation of model II, at 190°C, than was the case for model I, at 150°C. Cobalt decreased the amount of oxygen absorbed during oxidation of model II, however increased the oxidation of model I. Hydroperoxide studies of model II at 150°C, shows that cobalt acts to catalyse the decomposition of the hydroperoxide, therefore suggesting that at this lower tempeature cobalt may well behave in a similar manner to that in model I, ie. by increasing the oxidation.
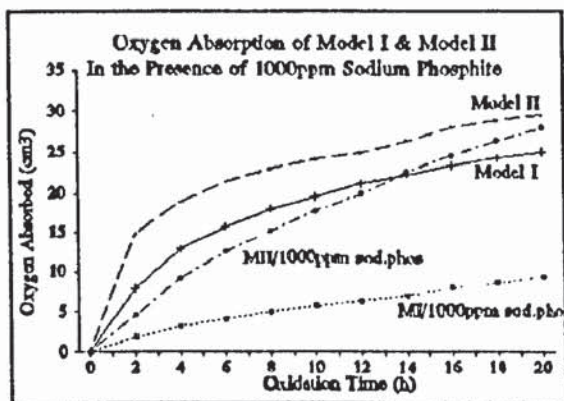
Sodium phosphite acts an antioxidant for the thermal oxidation of both models I and II, but is more efective in model I probably due to the lower temperatures involved, ie 150°C in model I as opposed to 190°C in model II.
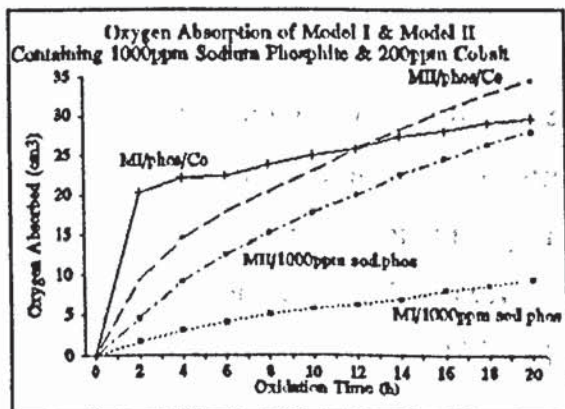
Cobalt increases the oxidation of both model I and model II in the presence of 1000ppm sodium phosphite. The final amount of oxygen absorbed in both cases was very similar

Chapters 3 and 4 provided a study of two model compounds which represented different sections of the polymer (MXD6) chain and both contained two amide groups as a diamide was shown to be necessary for the absorption of oxygen [56]. Model I represented 1.5 units of the polymer whereas model II represented the aliphatic portion of the chain between the two aromatic rings. Both were shown to absorb oxygen readily and in similar amounts. The relatively high temperatures at which these experiments were conducted probably resulted in a high degree of hydroperoxide decomposition, in the absence of cobalt, hence the extensive oxidation of the models alone.

In the presence of cobalt the oxidation of model I is increased to greater extent in comparison to model II. This may suggest that if the slight increase in oxidation is due to complex formation of the cobalt with the model, initiating oxidation, then complexation is more favourable across the aromatic ring (ie, as in model I). However in the presence of sodium phosphite (1000ppm), cobalt increases the oxidation of both models to a similar extent. Therefore, if complex formation takes place between the cobalt and model, via donation of a lone pair of electrons by the carbonyl groups, it appears that ring formation is possible either across the aromatic ring (as for model I) or across the aliphatic chain (as for model II). The analysis of a third model (VII) consisting of a combination of the two previous models would provide four accessible amide groups. This should lead to a theoretical doubling of the rate of absorption of oxygen if the complexing of cobalt takes place more favourably across the ring but it would remain constant if complexing took place on the aliphatic chain.

$$CH_3(CH_2)_4CONHCH_2 CH_2NHCO(CH_2)_4CONHCH_2 CH_2NHCO(CH_2)_4CH_3 (VII)$$
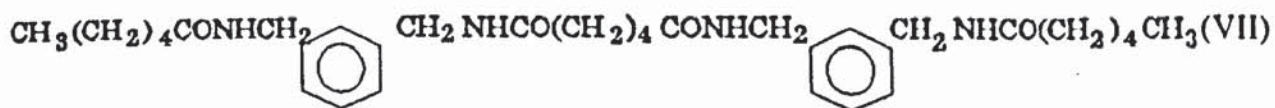
Using the evidence provided from the investigation of the oxidation of MXD6, Patel [102] believed that a mechanism of complex formation between the cobalt the polymer at specific sites seemed to be the most convincing. This initiated the formation of free radicals from which oxidation proceeded. However since the study concentrated on the solid state oxidation of MXD6 fibre, the mobility of the catalyst was highly restricted.

It was therefore proposed that a significant degree of radical formation had already occured in the melt whilst the polymer was being processed and that the cobalt therefore behaved primarily as an initiation catalyst and to a lesser extent a propagation catalyst. The oxidation of model I and II was carried out in the melt, therefore cobalt would have complete mobility and more likely to act primarily as a propagation catalyst, catalysing the decomposition of hydroperoxides.

$$ROOH + Co^{2+} \longrightarrow RO^{\cdot} + {}^{\cdot}OH + Co^{3+}$$
$$ROOH + Co^{3+} \longrightarrow RO_2^{\cdot} + {}^{+}H + Co^{2+}$$
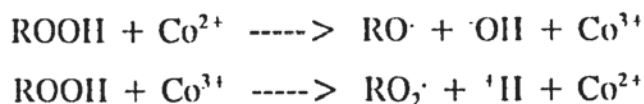
The basis of this proposal is based on the hydroperoxide curves formed during the oxidation of model I and model II. In the presence of cobalt, hydroperoxide was not detected at any stage during the oxidation, however, the model was shown to absorb oxygen with continuing formation of stable products. It appears as though the cobalt decomposed any remaining hydroperoxide resulting in the slight increase in oxidation. The possibility of some cobalt complexation however, should not be ruled out, particularly in consideration of work conducted at Carnaud MetalBox on a range of MXDn homologues, as discussed in the Introduction.

Oxygen Absorption of Model II
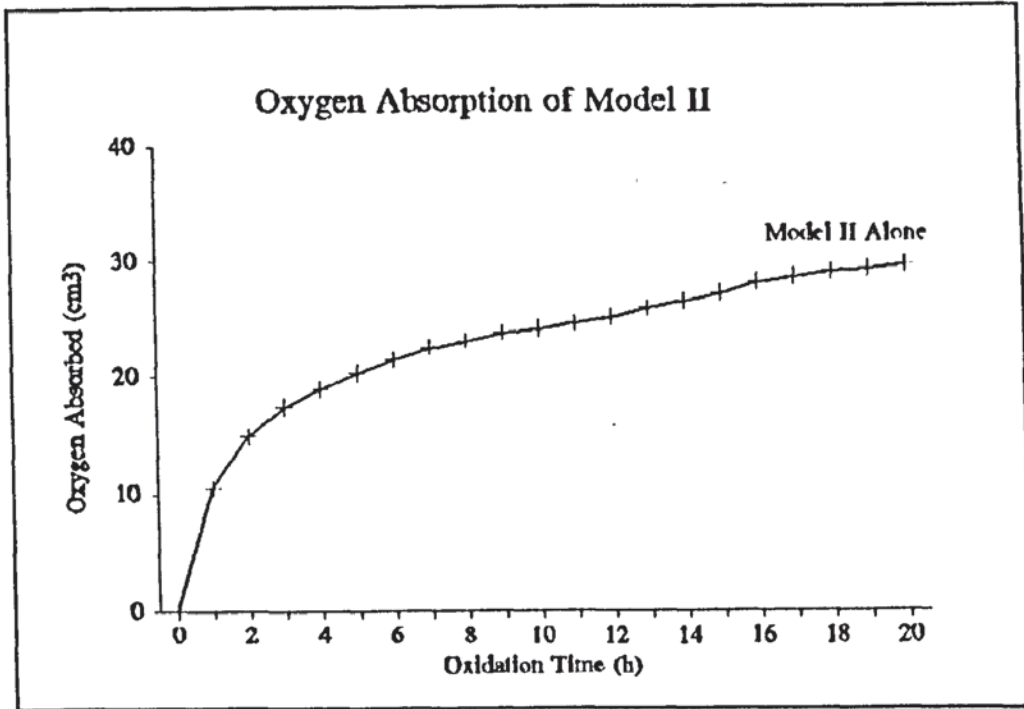
Figure 4.1   Oxygen Absorption of Model II in the Melt Phase at 190°C (curve represents volume of oxygen absorbed per 0.5g of sample).

Oxygen Absorption of Model II
In the Presence of Cobalt
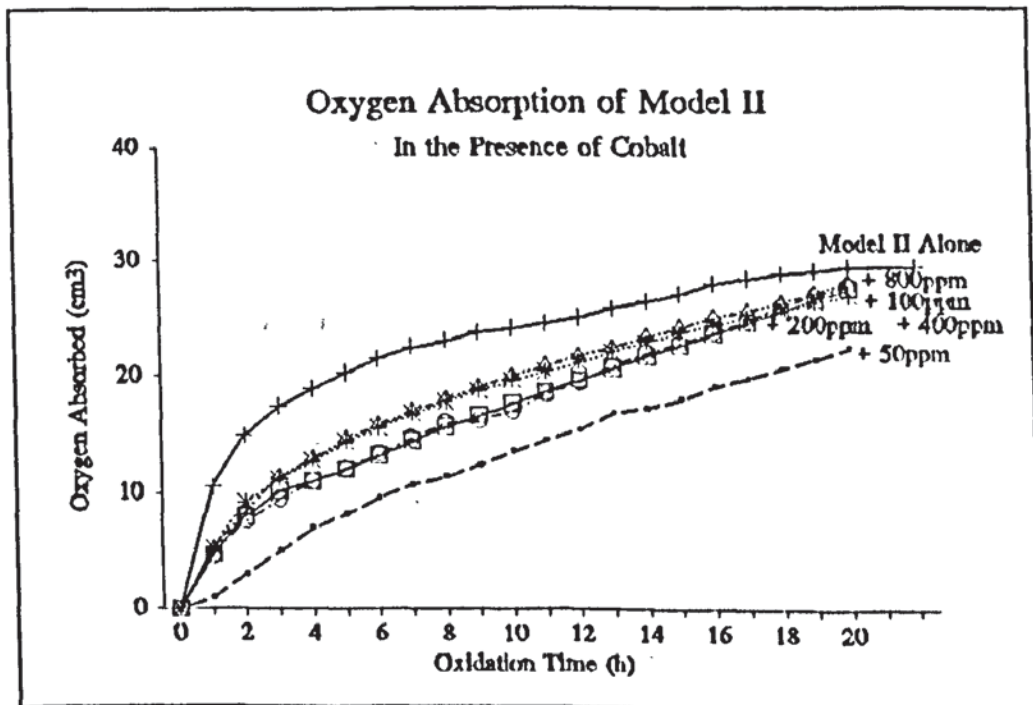
Figure 4.2a   Oxygen Absorption of Model II in the Melt Phase at 190°C in the Presence of Different Cobalt Concentrations (curves represent volume of oxygen absorbed per 0.5g of sample).

Rates of Oxidation

Model II ; Effects of Cobalt Concentration
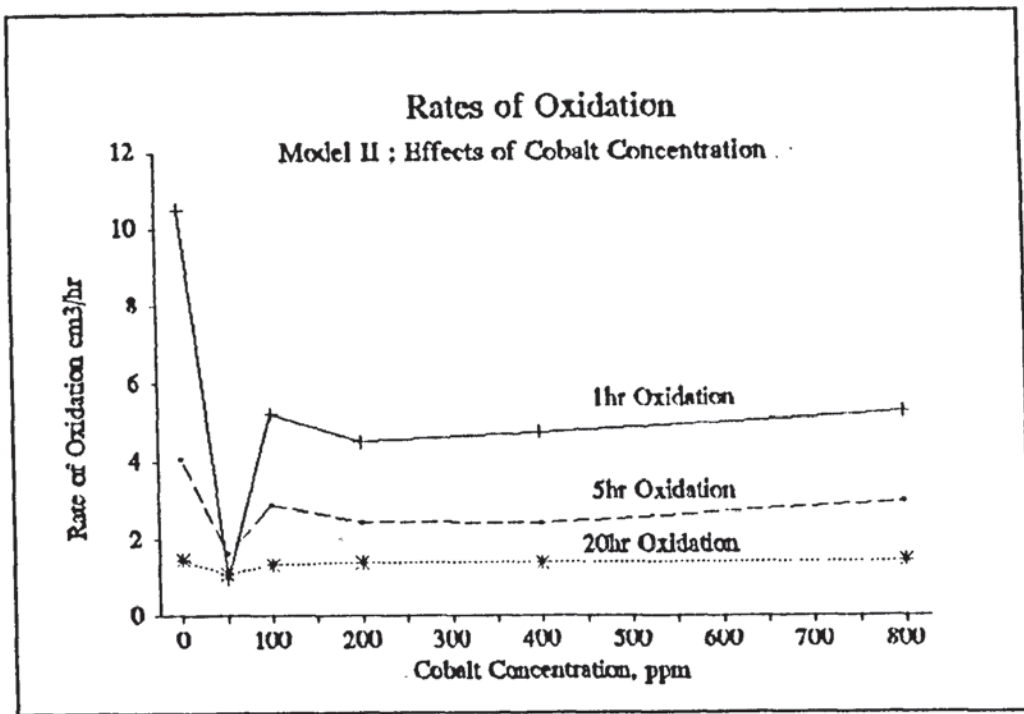
Figure 4.2b The Effect of Cobalt Concentration on the Rate of Oxidation of Model II, at 190°C (in the melt), over a 1hr, 5hr and 20hr Period (rates obtained from oxygen absorption curves).

Oxygen Absorption of Model II

In the Presence of Sodium Phosphite
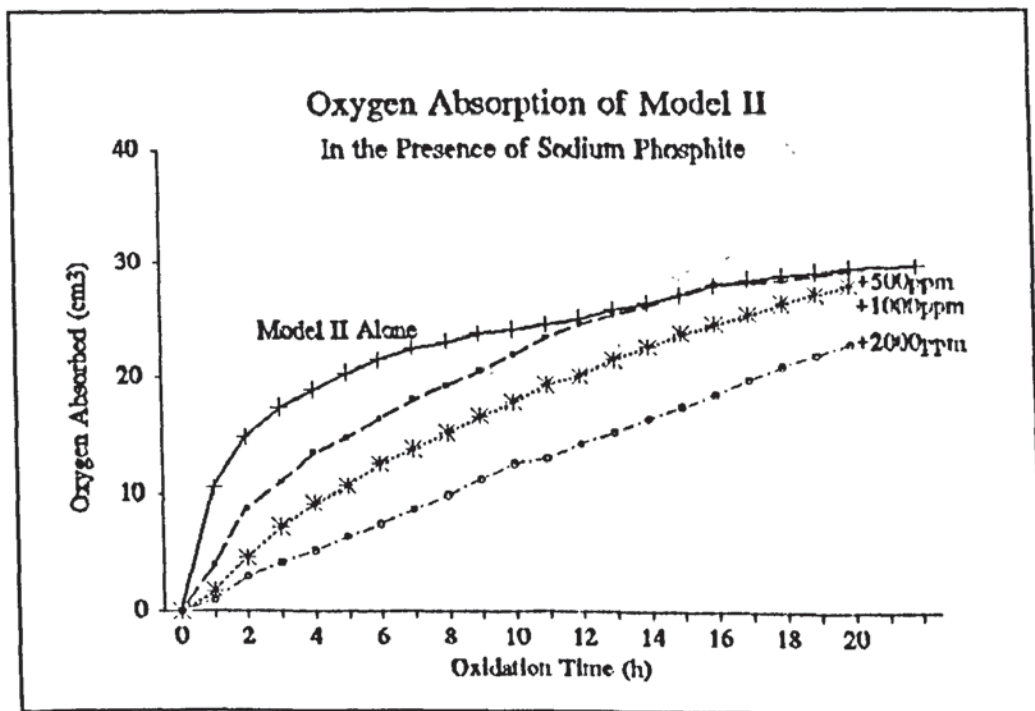
Figure 4.3a Oxygen Absorption of Model II in the Melt Phase at 190°C in the Presence of Different Sodium Phosphite Concentrations (curves represent volume of oxygen absorbed per 0.5g of sample).

Rates of Oxidation

Model II : Effect of Sodium Phosphite Concentration
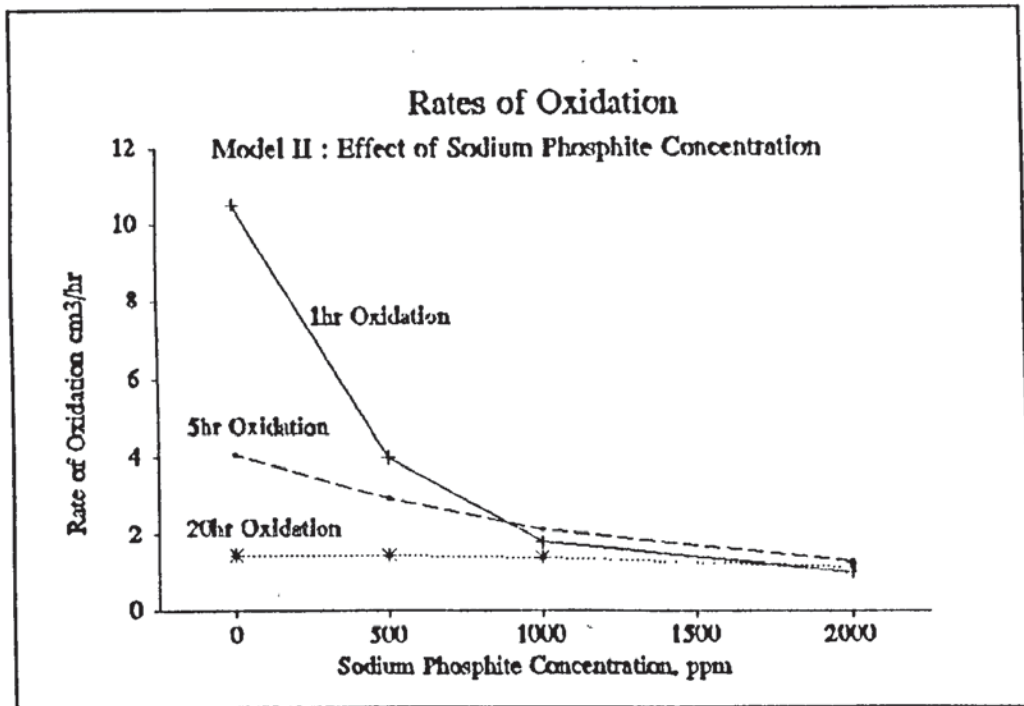
Figure 4.3b The Effect of Sodium Phosphite Concentration on the Rate of Oxidation of Model II, at 190°C (in the melt), over a 1hr, 5hr and 20hr period (rates obtained from oxygen absorption curves).

Oxygen Absorption of Model II

Model II (1000ppm Sodium Phosphite) : Effect of Cobalt Conc.
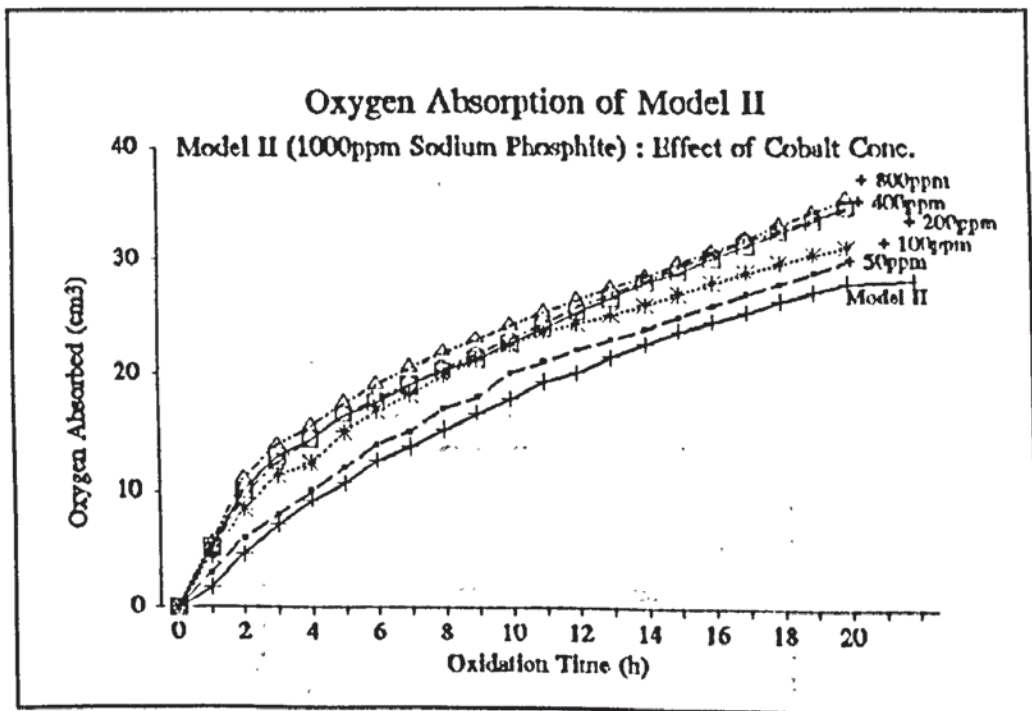
Figure 4.4a Oxygen Absorption of Model II in the Melt Phase at 190°C, in the Presence of 1000ppm Sodium Phosphite and Different Concentrations of Cobalt (curves represent volume of oxygen absorbed per 0.5g of sample).
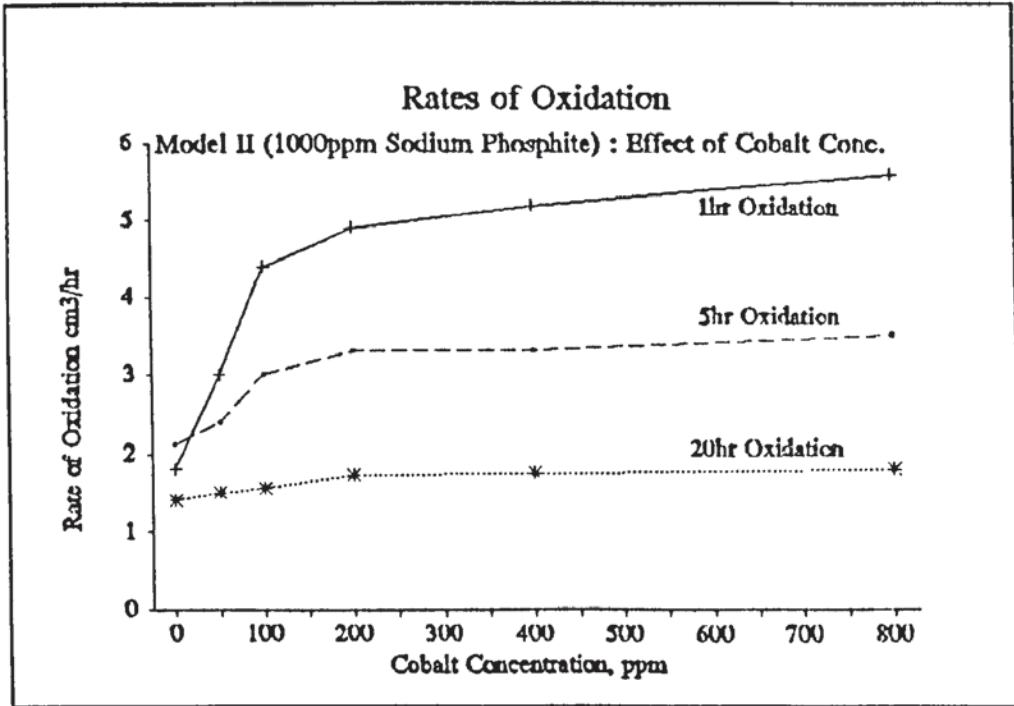
Figure 4.4b The Effect of Cobalt Concentration on the Rate of Oxidation of Model II plus 1000ppm Sodium Phosphite, at 190°C (in the melt), over a 1hr, 5hr and 20hr period (rates obtained from oxygen absorption curves).
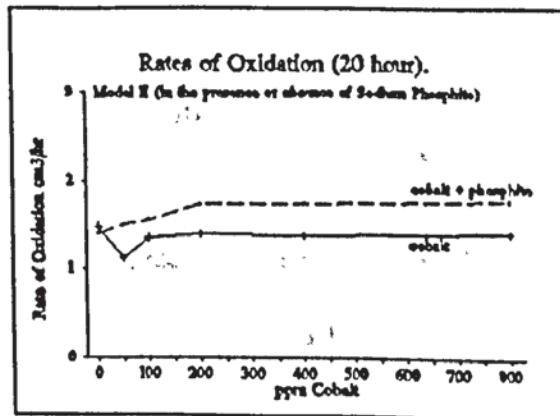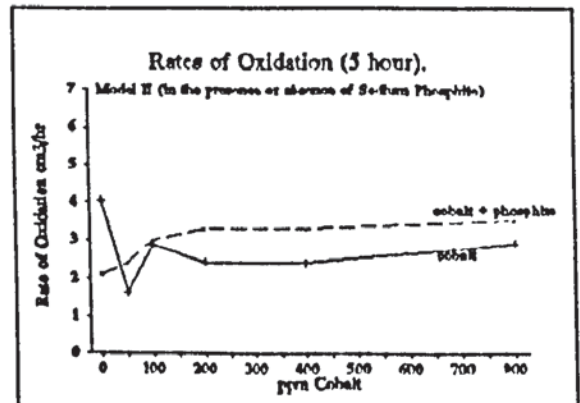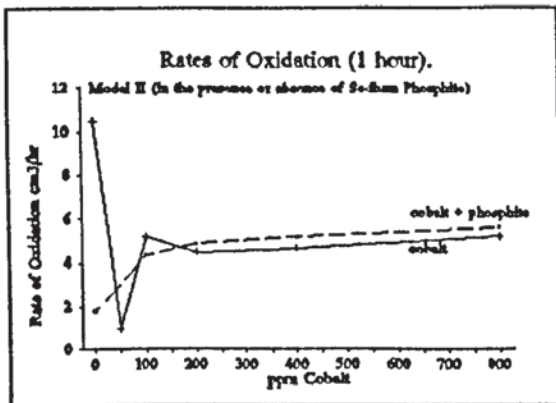
Figure 4.4c A Comparison of the Effect of Cobalt & Cobalt/Sodium Phosphite on the Rate of Oxidation of ModelII, at 190°C, over a 1hr(i), 5hr(ii) and 20hr(iii) period.
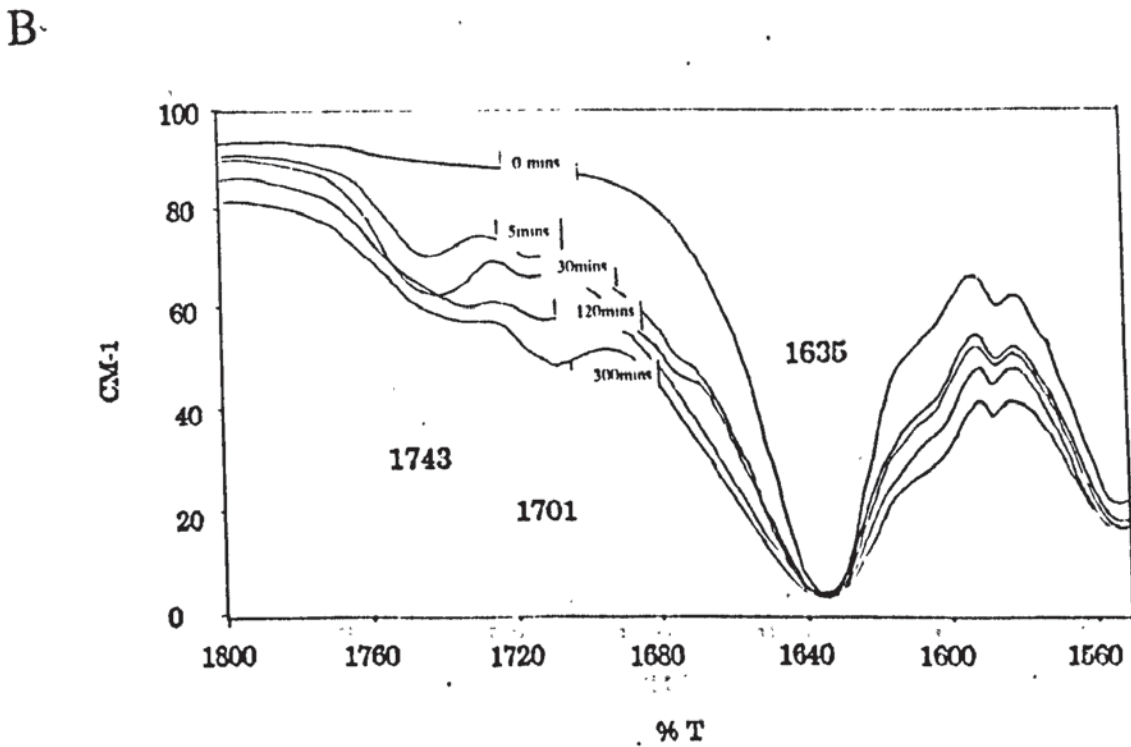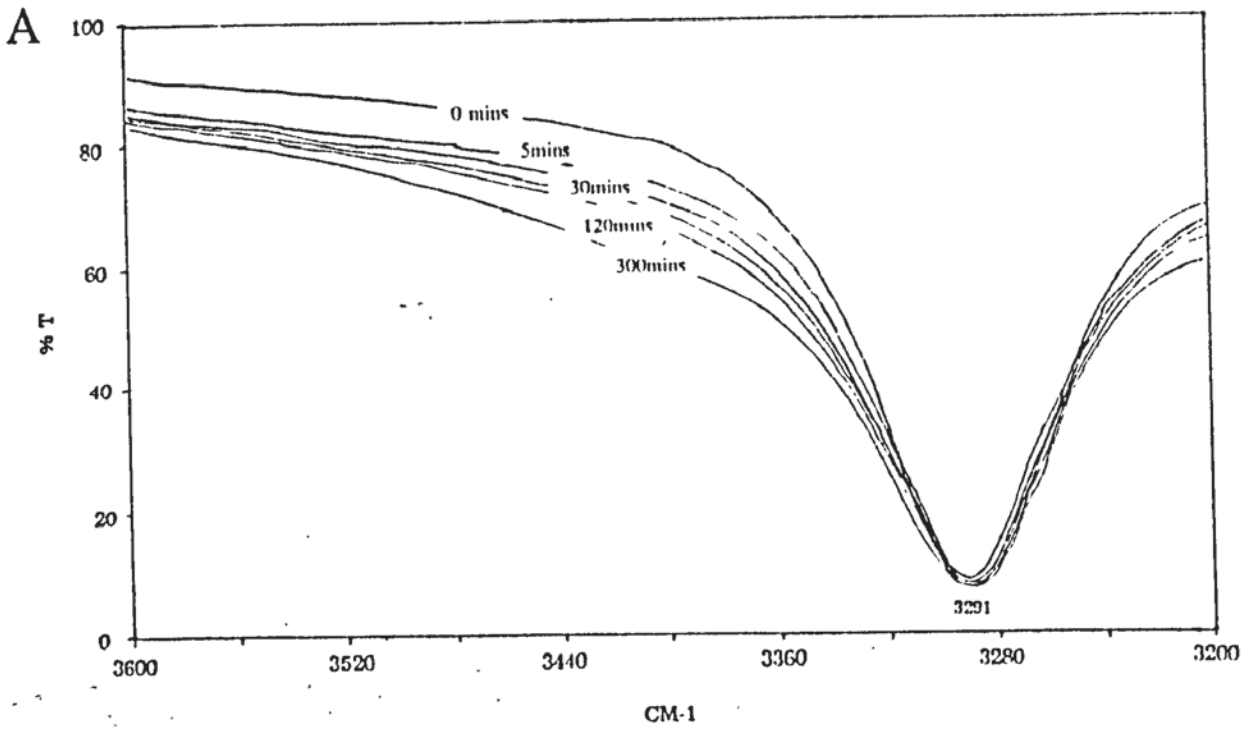
Figure 4.5 The Changing FT-IR Spectra of Model II with Increasing Oxidation Time, at 190°C, in the Regions 3600-3200cm^{-1} (A) and 1800-1550cm^{-1} (B) (samples taken out from the oxygen absorption experiments).
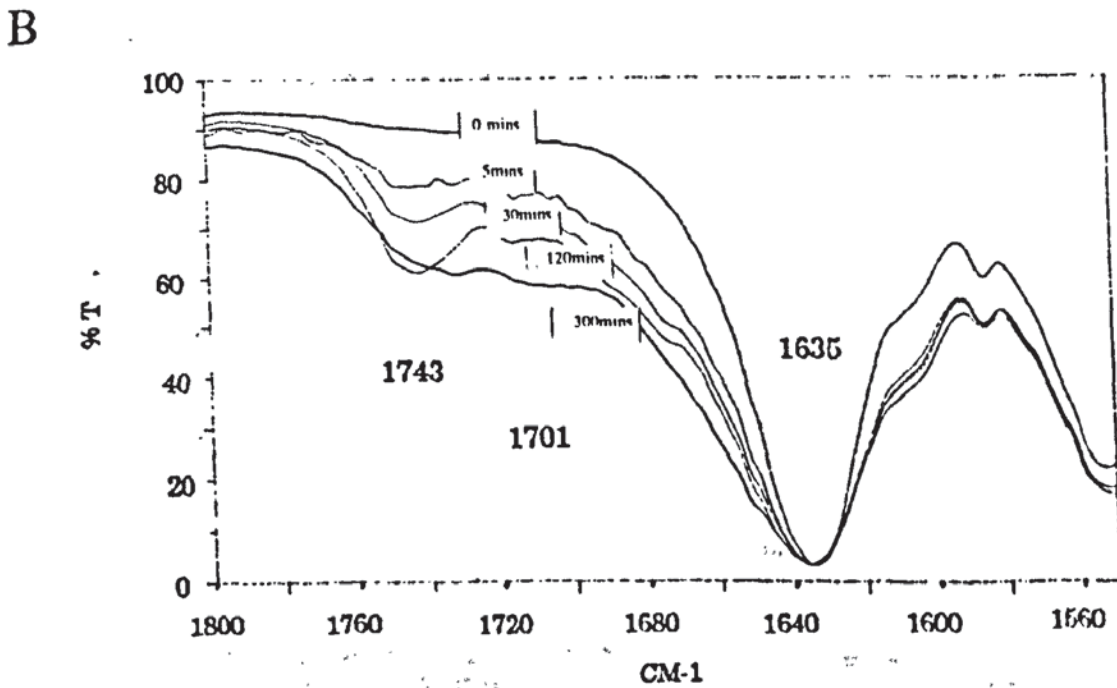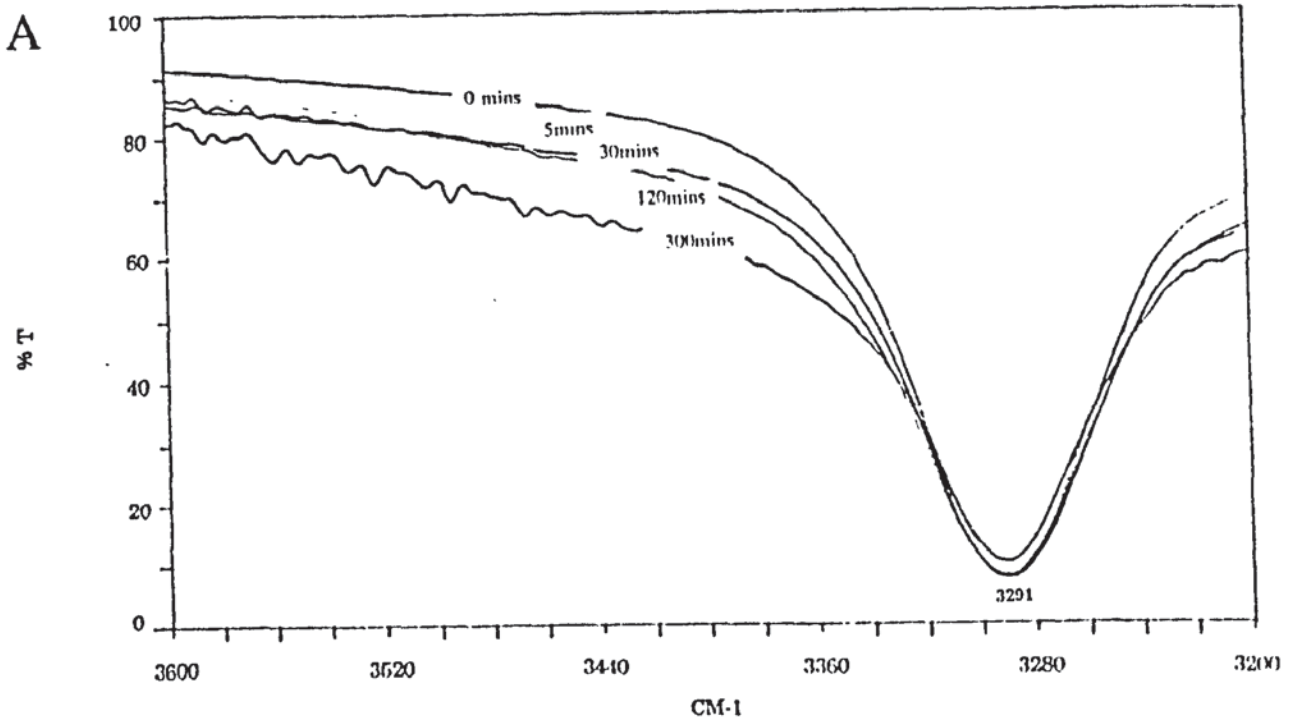
Figure 4.6 The Changing FT-IR Spectra of Model II, in the Presence of 200ppm Cobalt with Increasing Oxidation Time, at 190°C, in the Regions 3600-3200cm⁻¹ (A) and 1800-1550cm⁻¹ (B) (samples taken out from the oxygen absorption experiments).
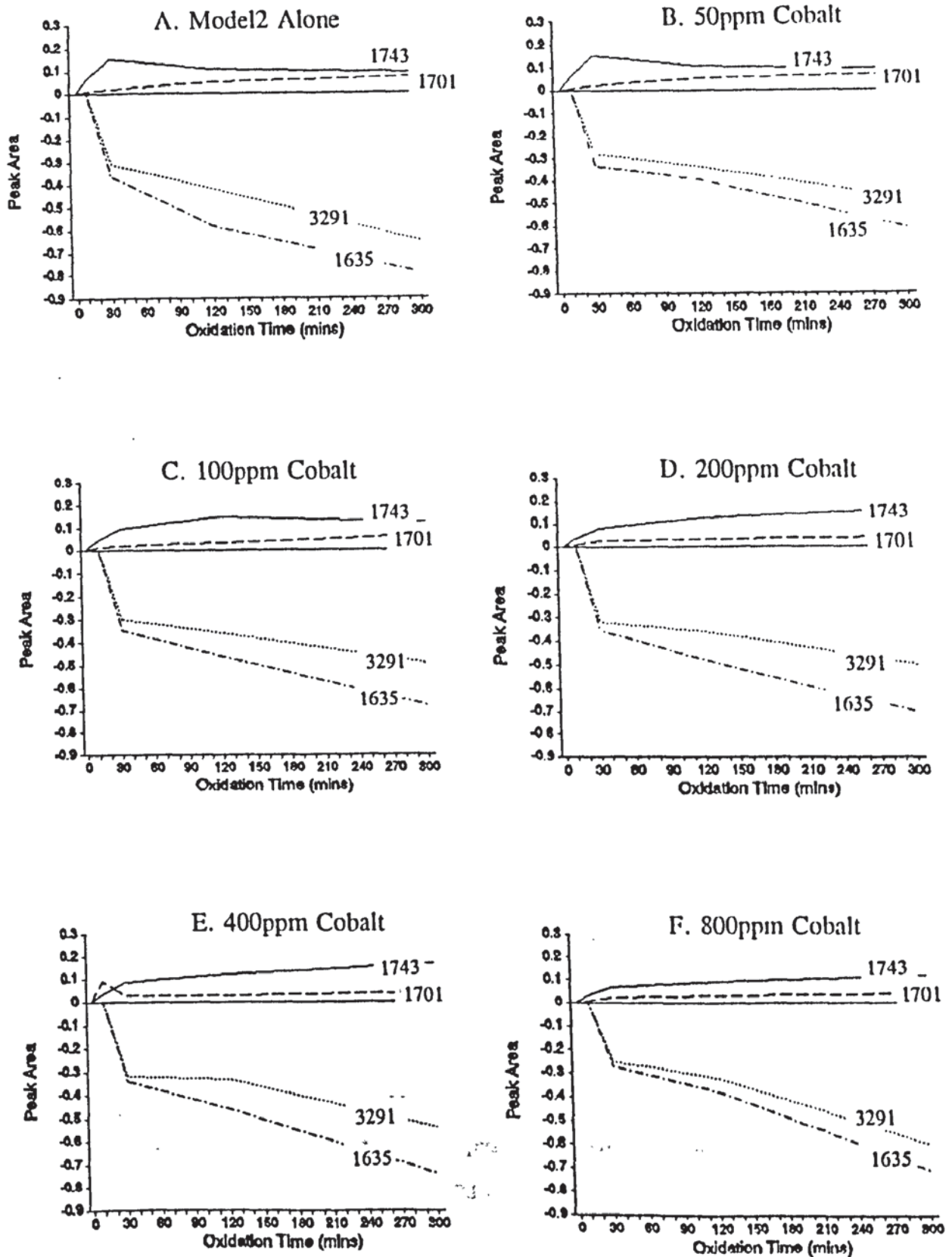
Figure 4.7 The Effect of Various Concentrations of Cobalt on the FT-IR of Model II During Oxidation at 190°C, (sampled out from the oxygen absorption experiments and analysed as KBr discs at room temperature), Showing the Growth of Various Product Peaks at 1743, 1701cm^{-1} and the Disappearance of the Peaks at 3291 and 1635cm^{-1}.
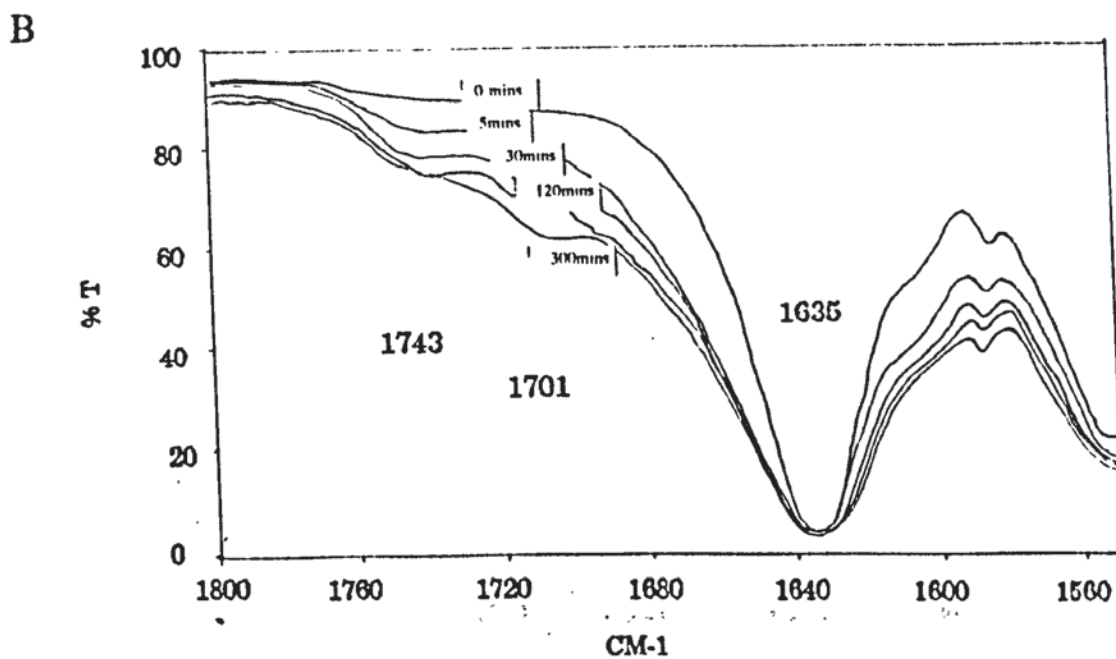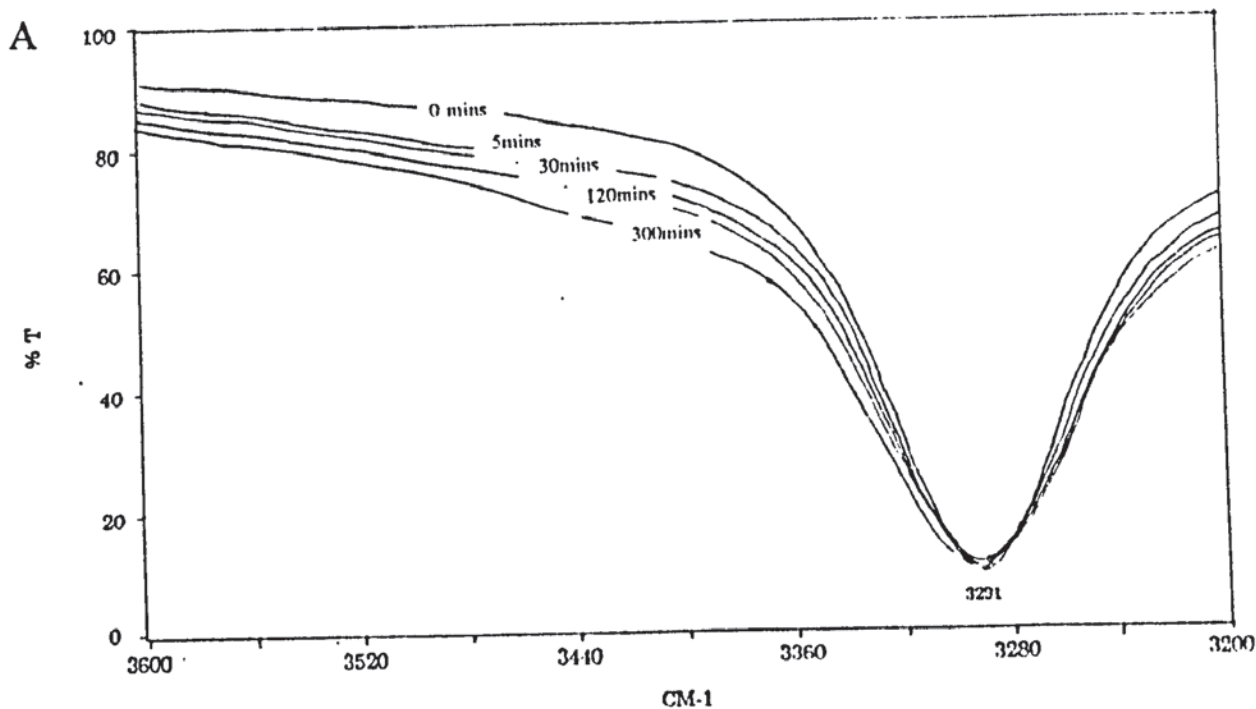
Figure 4.8 The Changing FT-IR Spectra of Model II, in the Presence of 1000ppm Sodium Phosphite with Increasing Oxidation Time, at 190°C, in the Regions 3600-3200cm⁻¹(A) and 1800-1550cm⁻¹ (B) (samples taken out from the oxygen absorption experiments).
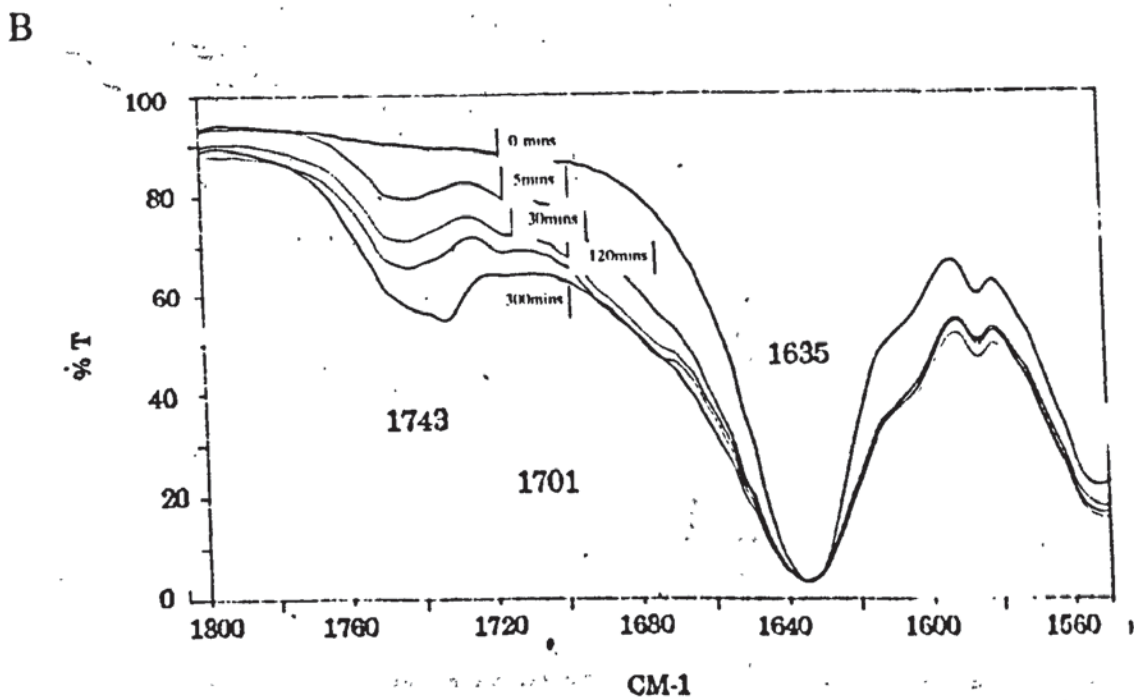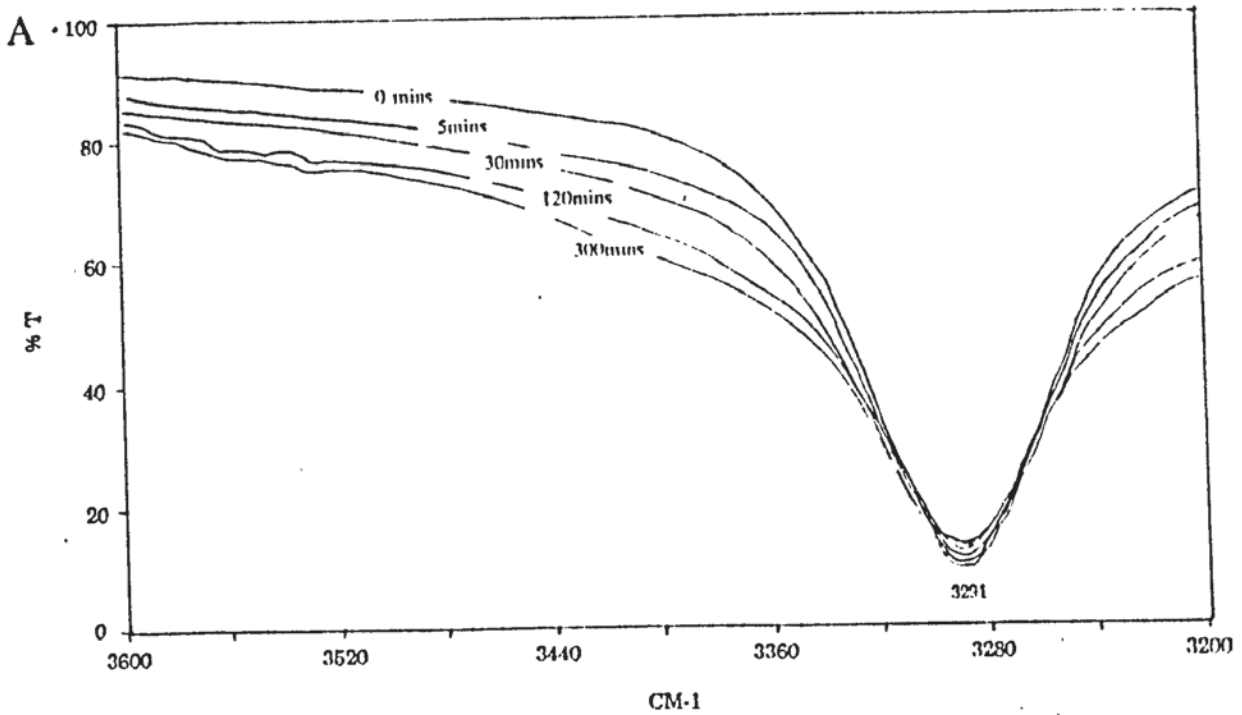
Figure 4:9 The Changing FT-IR Spectra of Model II; in the Presence of 200ppm Cobalt & 1000ppm Sodium Phosphite with Increasing Oxidation Time, at 190°C, in the Regions 3600-3200cm^{-1} (A) and 1800-1550cm^{-1} (B) (samples taken out from the oxygen absorption experiments).
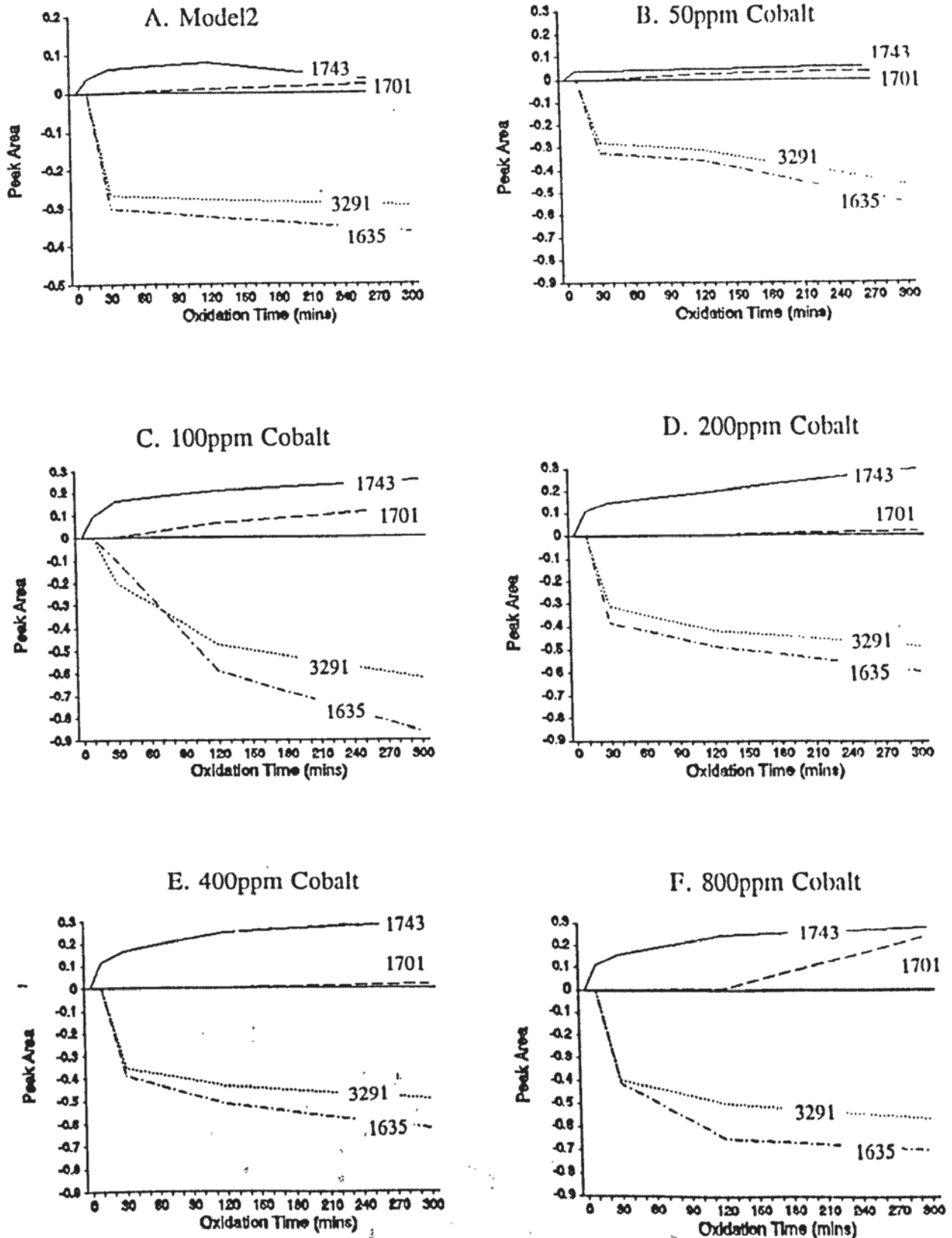
Figure 4.10 The Effect of Various Concentrations of Cobalt on the FT-IR of Model II (containing 1000ppm Sodium Phosphite) During Oxidation at 190°C, (sampled out from the oxygen absorption experiments and analysed as KBr discs at room temperature), Showing the Growth of Various Product Peaks at 1743, 1701cm^{-1} and the Disappearance of the Peaks at 3291 and 1635cm^{-1}.
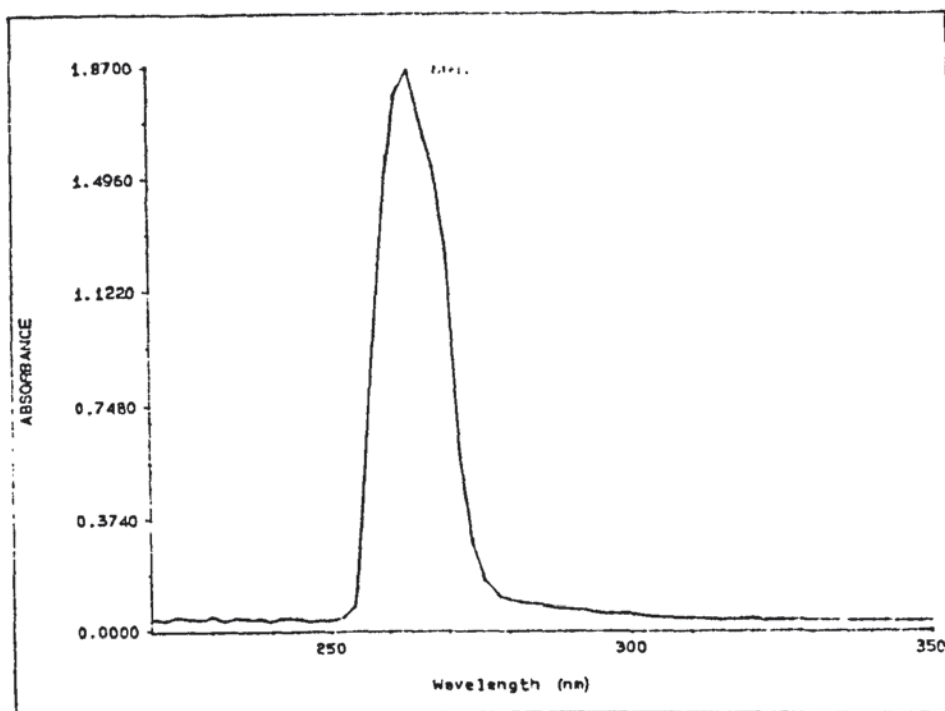
Figure 4.11 The UV-Vis Spectra of Model II, Measured in DMSO.
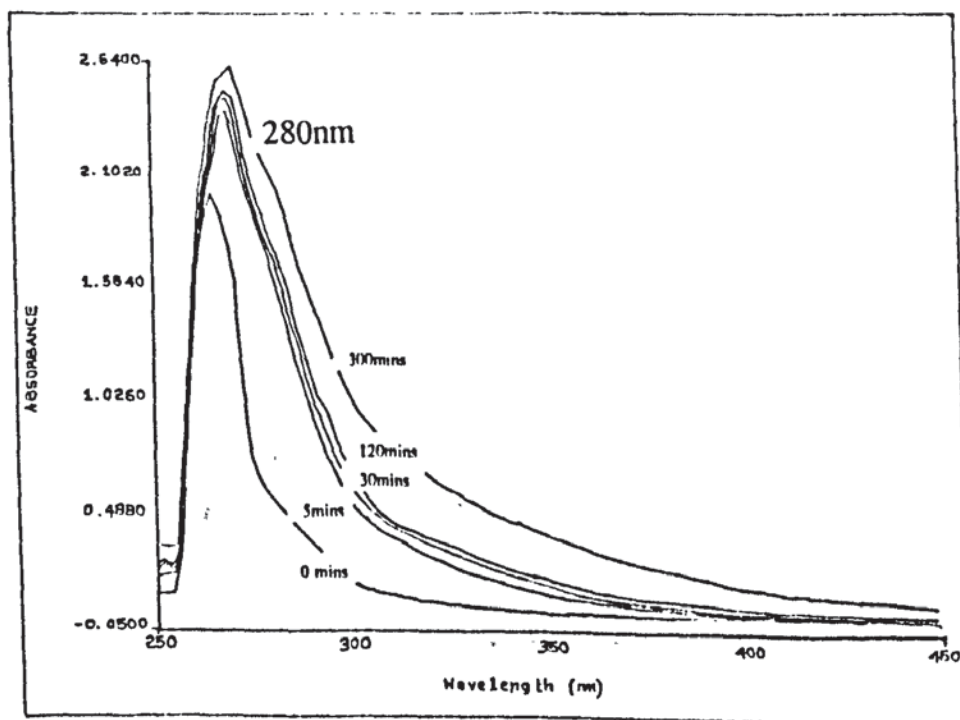
Figure 4.12 The Changing UV-Vis Spectra of Model II, after Increasing Oxidation at 190°C, in DMSO (sampled out from the oxygen absorption experiments and run at room temperature).
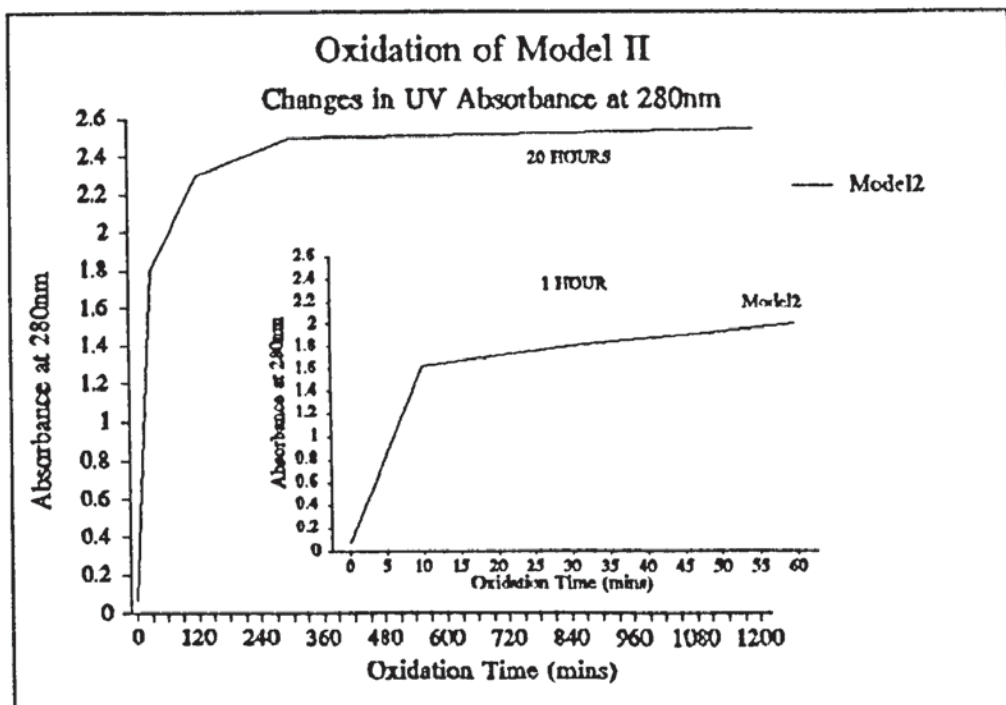
Figure 4.13 Changes in the UV-Vis, 280nm, Absorption Band During Oxidation of Model II, at 190°C, in DMSO (sampled out from the oxygen absorption experiments and run at room temperature).
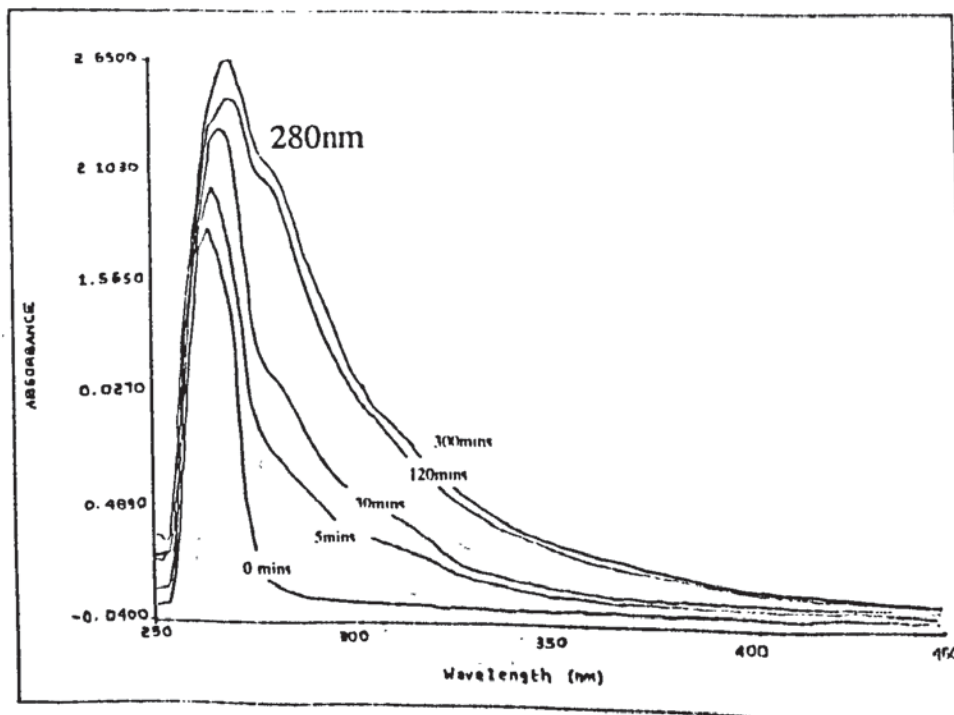
Figure 4.14 The Changing UV-Vis Spectra of Model II in the Presence of 200ppm Cobalt, after Increasing Oxidation at 190°C, in DMSO (sampled out from the oxygen absorption experiments and run at room temperature).
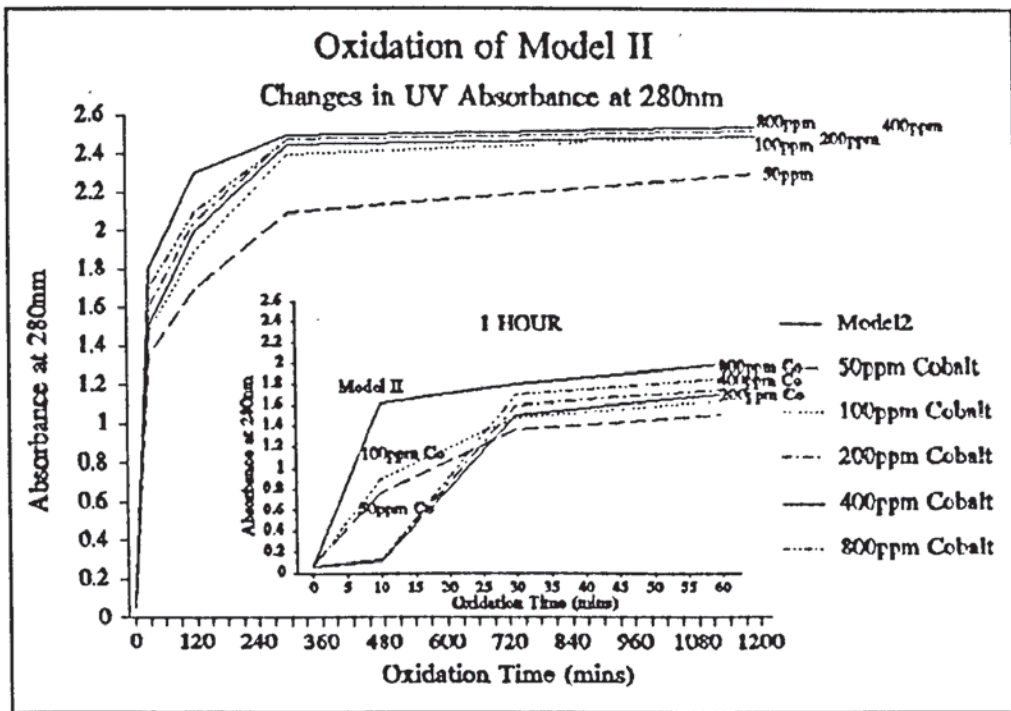
Figure 4.15 Changes in the UV-Vis, 280nm, Absorption Band During Oxidation of Model II, in the Presence of Different Concentrations of Cobalt, at 190°C, in DMSO (sampled out from the oxygen absorption experiments and run at room temp).
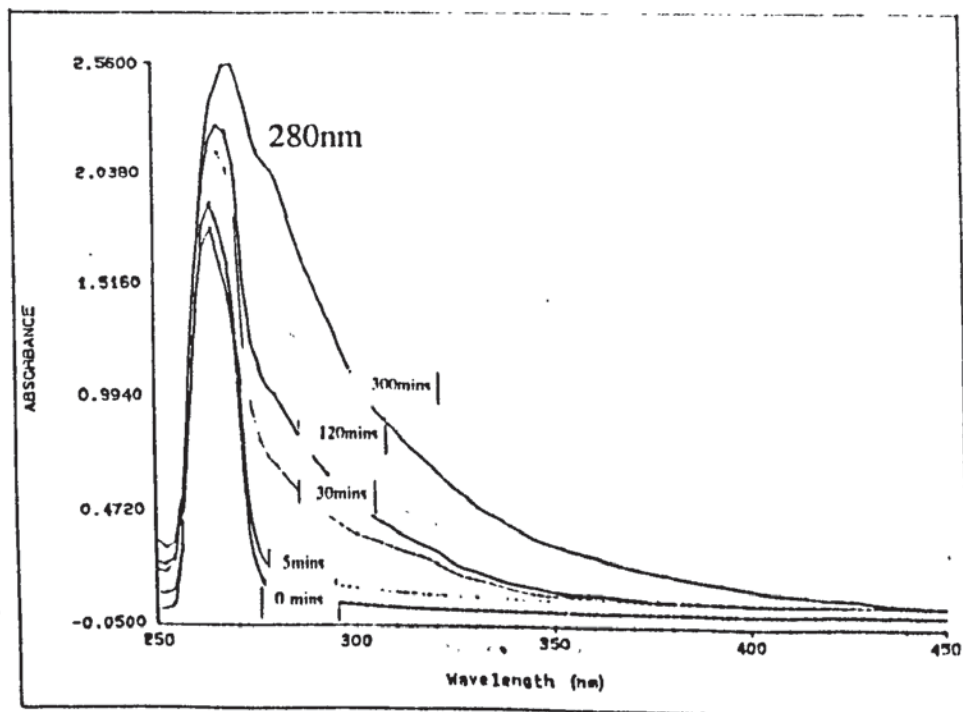
Figure 4.16 The Changing UV-Vis Spectra of Model II in the Presence of 1000ppm Sodium Phosphite, after Increasing Oxidation at 190°C, in DMSO (sampled out from the oxygen absorption experiments and run at room temperature).
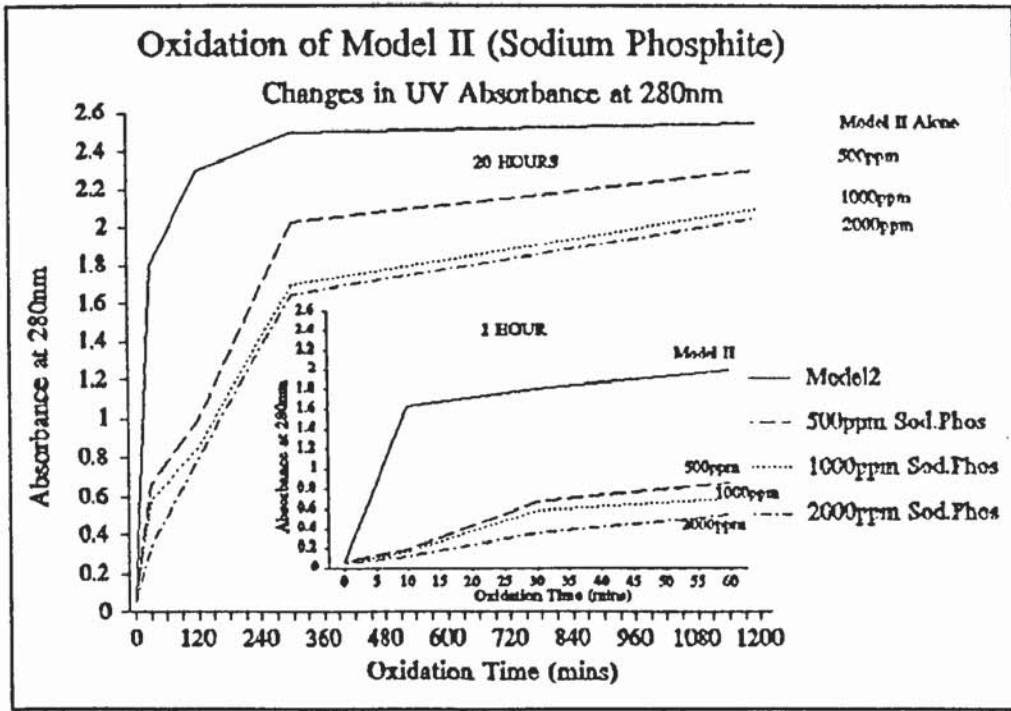
Figure 4.17 Changes in the UV-Vis, 280nm, Absorption Band During Oxidation of Model II, in the Presence of Different Concentrations of Sodium Phosphite, at 190°C, in DMSO (sampled out from the oxygen absorption experiments and run at room temperature).
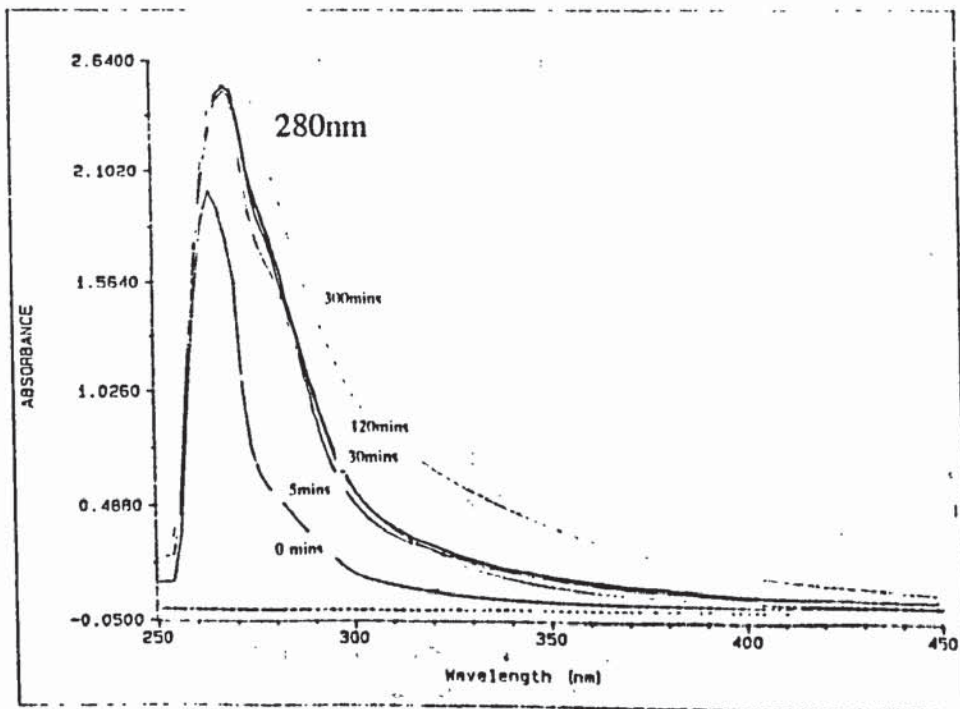
Figure 4.18 The Changing UV-Vis Spectra of Model II in the Presence of 200ppm Cobalt & 1000ppm Sodium Phosphite, after Increasing Oxidation at 190°C, in DMSO (sampled out from the oxygen absorption experiments and run at room temperature).
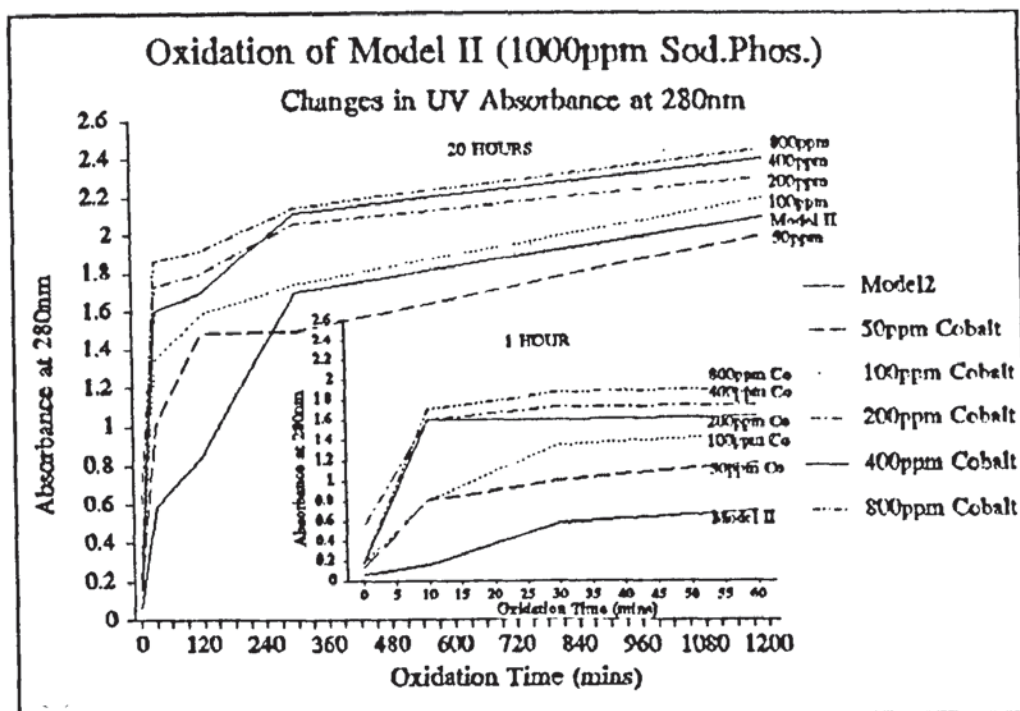
Figure 4.19 Changes in the UV-Vis, 280nm, Absorption Band During Oxidation of Model II (+ 1000ppm Sodium Phosphite) in the Presence of Different Concentrations of Cobalt, at 190°C, in DMSO (sampled out from the oxygen absorption experiments and run at room temperature).
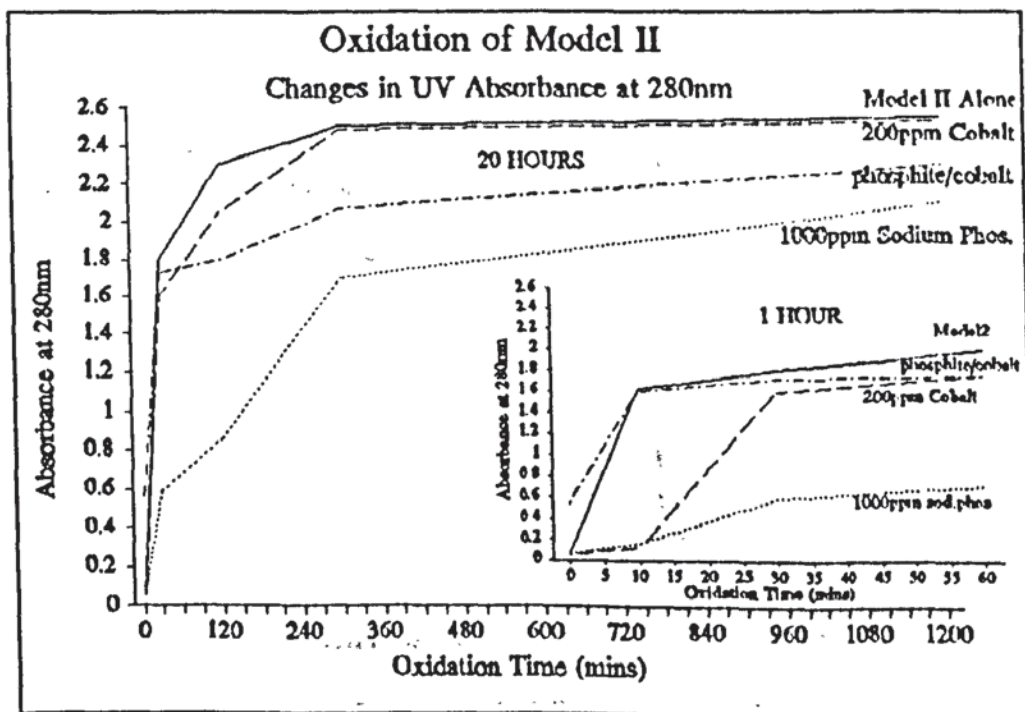
Figure 4.20 A Comparison of the Effect of Cobalt, Sodium Phosphite and a Combination of the Two Upon the Changes in the UV-Vis, 280nm, Absorption Band During the Oxidation of Model II, at 190°C, (sampled from the oxygen absorption experiment and measured at room temperature in DMSO).
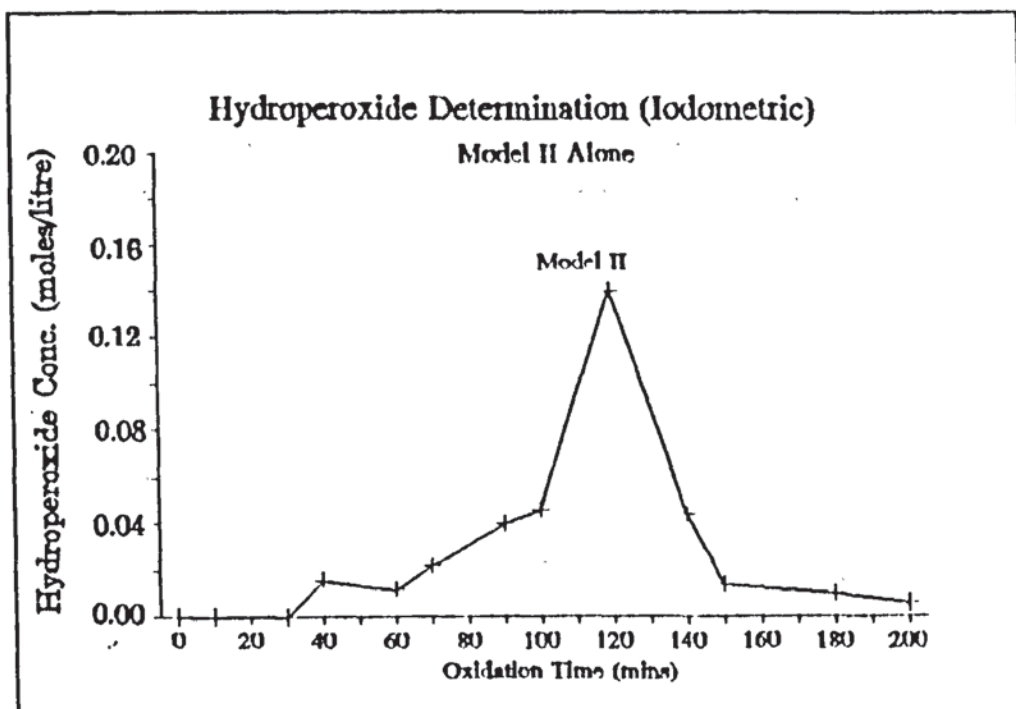
Figure 4.21 Hydroperoxide Formation During the Oxidation of Model II, in 1,2 DCB, at 150°C, Using the Iodometric Titration Technique.
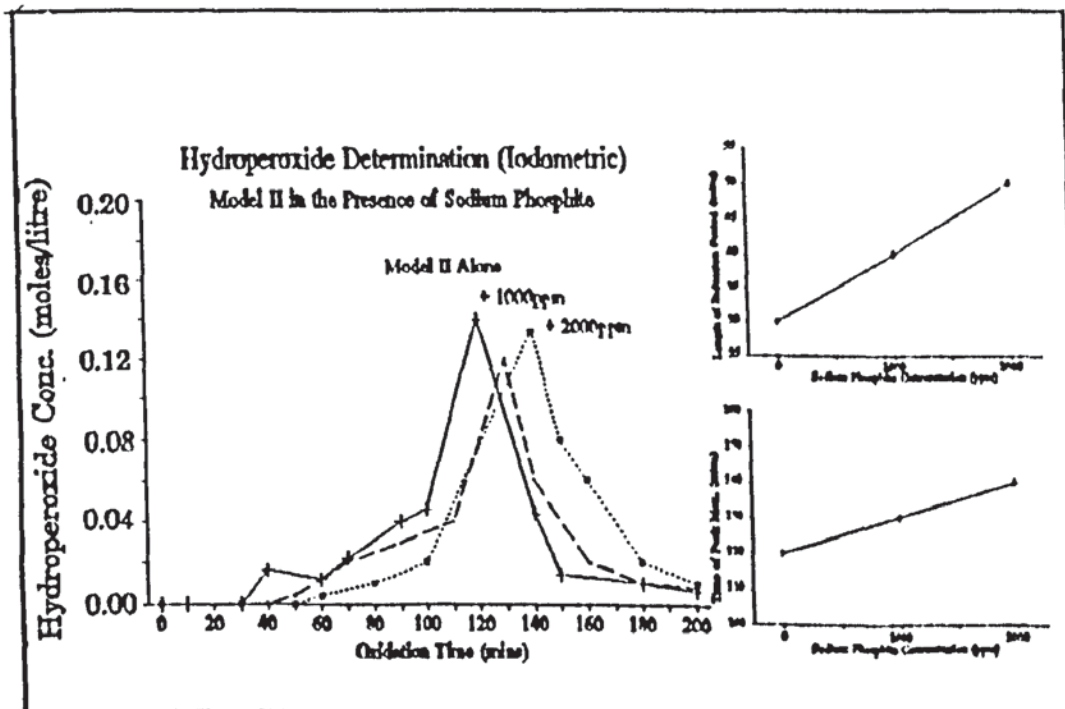
Figure 4.22 Hydroperoxide Formation During the Oxidation of Model II in the Presence of Different Concentrations of Sodium Phosphite, in 1,2 DCB, at 150°C, Using the Iodometric Titration Technique.
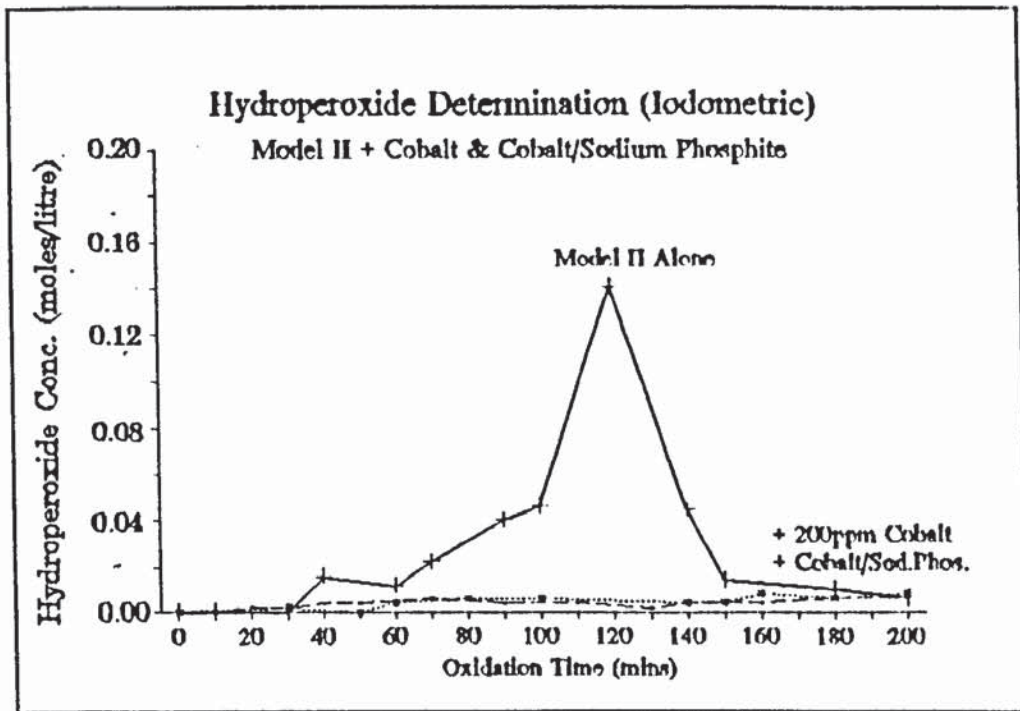
Figure 4.23 Hydroperoxide Formation During the Oxidation of Model II in the Presence of 200ppm Cobalt and a Combination of both Cobalt & Sodium Phosphite, in 1,2 DCB, at 150°C, Using the Iodometric Titration Technique.
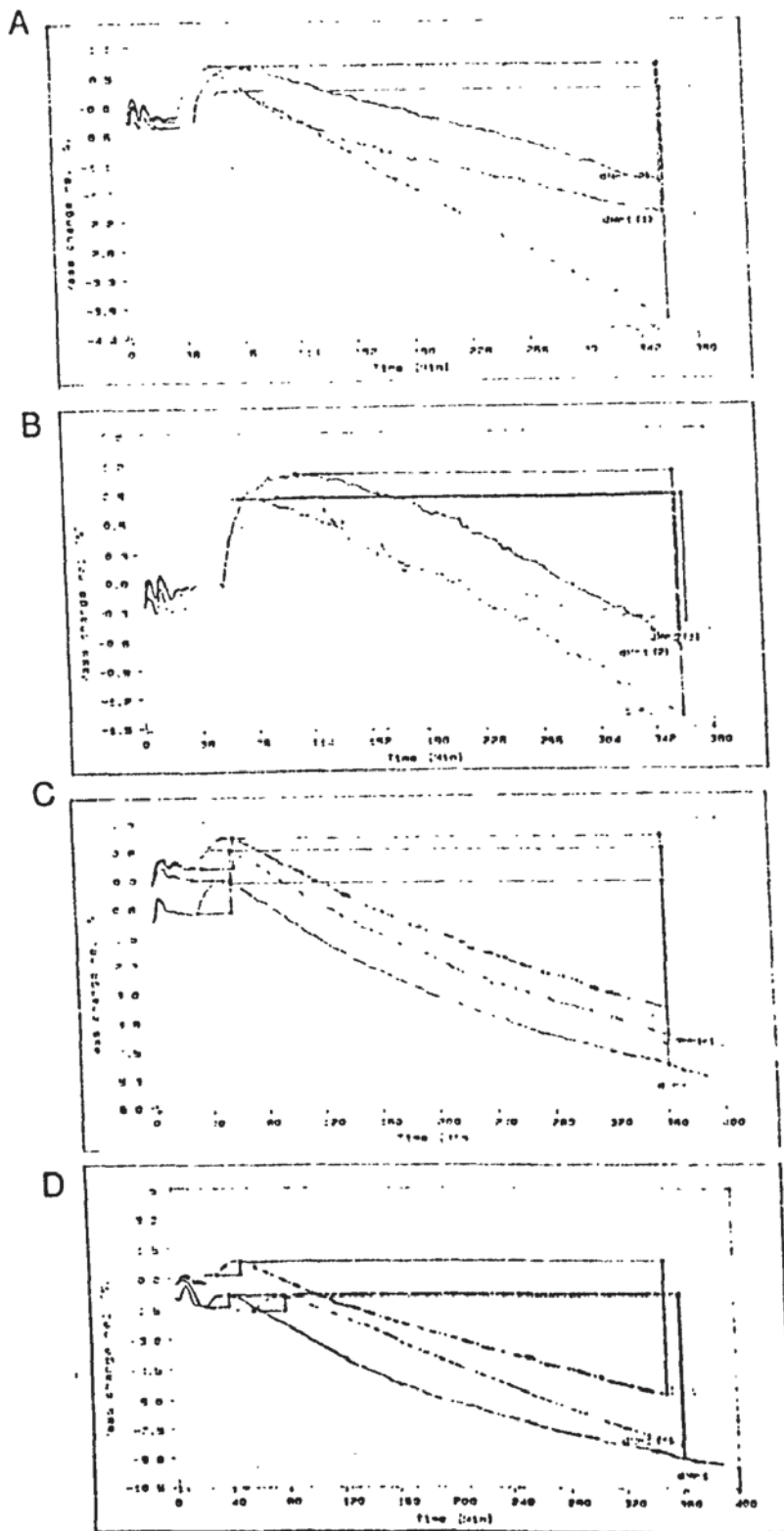
Figure 4.24 T.G.A Traces Obtained From the Isothermal Heating of Model II Alone (A) and in the Presence of 200ppm Cobalt (B), 5000ppm Cobalt (C) and 10000ppm Cobalt (D). Analysis was Carried Out at 190, 200 and 210°C in an Oxygen Atmosphere.
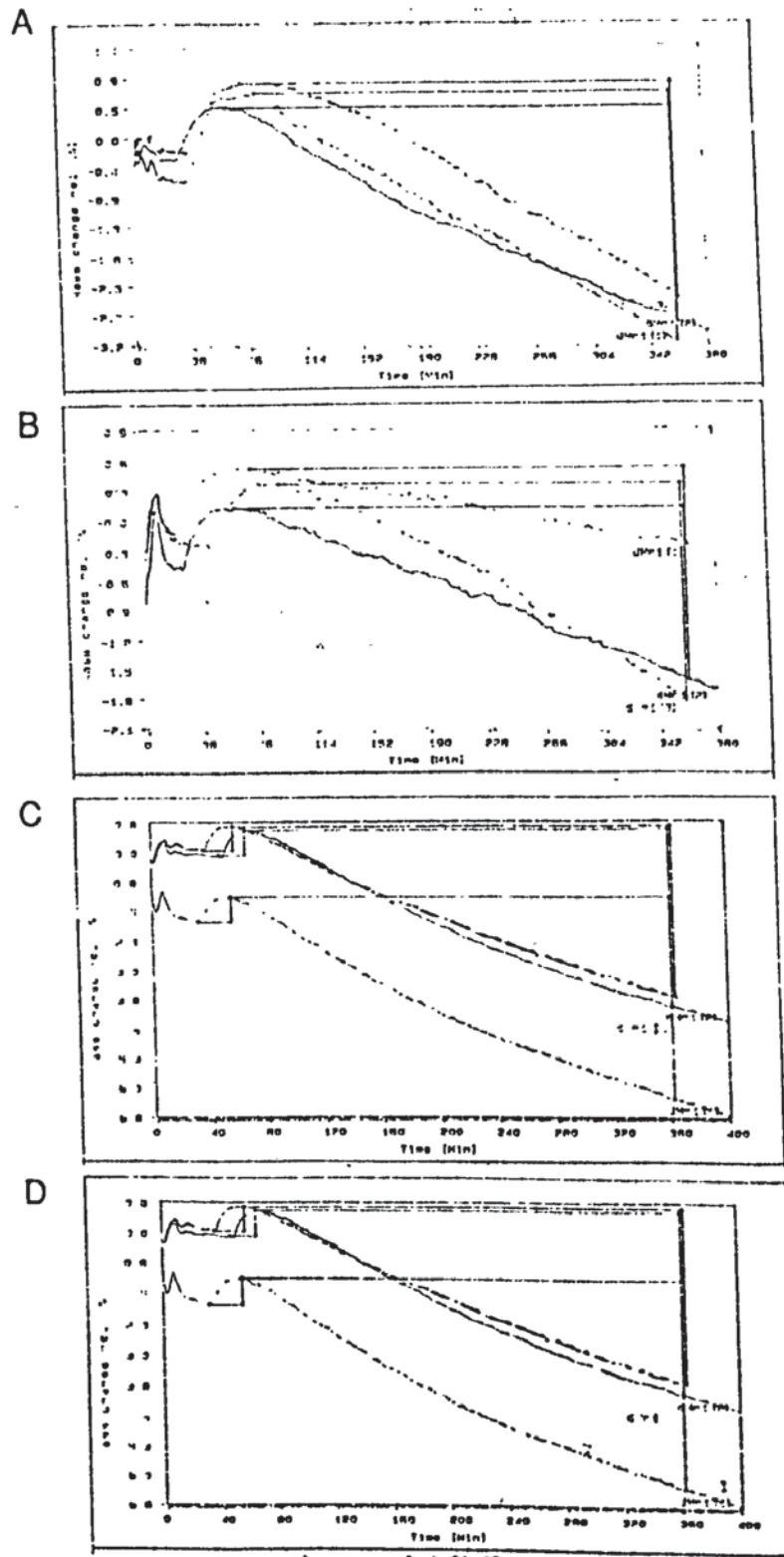
Figure 4.25 T.G.A Traces Obtained From the Isothermal Heating of Model II + 1000ppm Sodium Phosphite (A) and in the Presence of 200ppm Cobalt (B), 5000ppm Cobalt (C) and 10000ppm Cobalt (D). Analysis was Carried Out at 190, 200 and 210°C in an Oxygen Atmosphere.
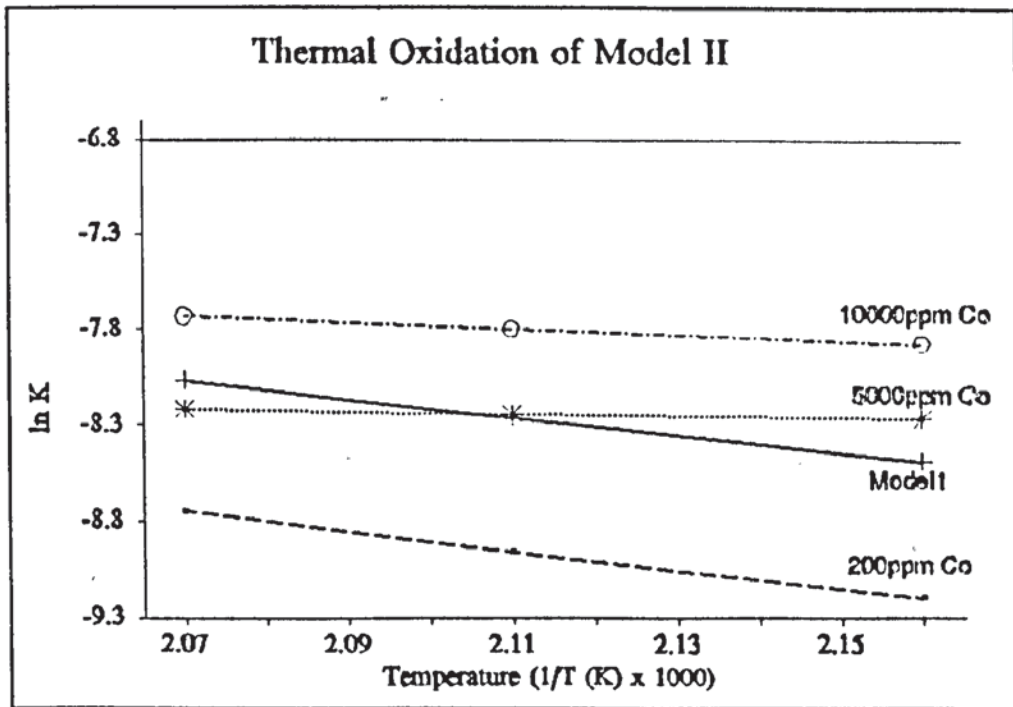
Figure 4.26 Determination of Activation Energies for the Thermal Oxidation of Model II
in the Presence of Different Concentrations of Cobalt by Isothermal
Thermogravimetric Analysis.
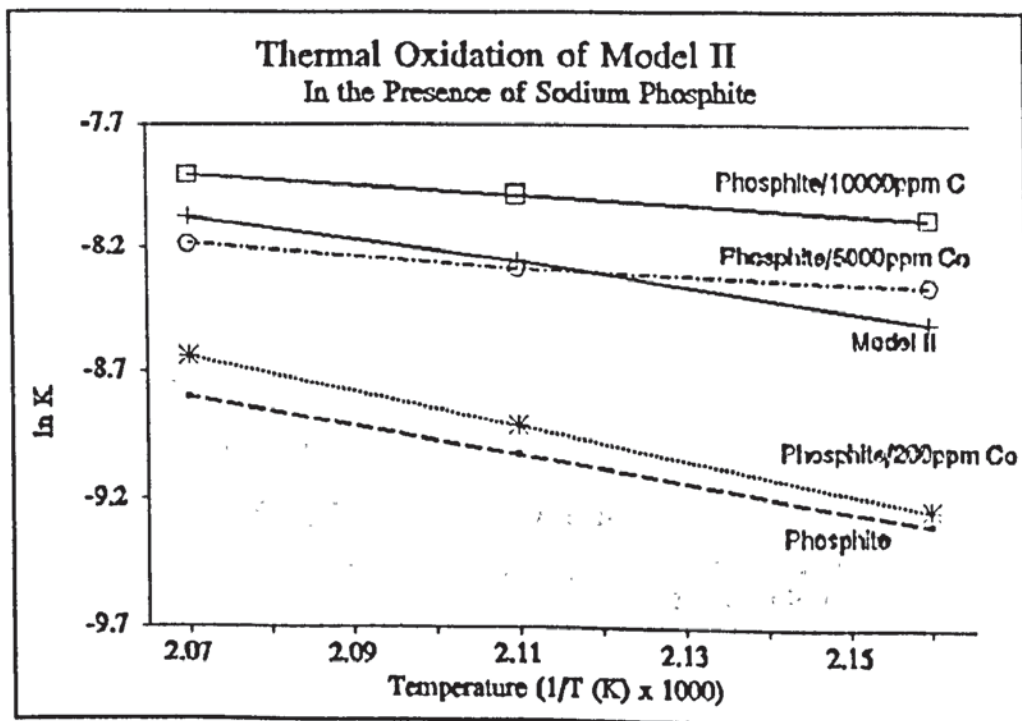
Figure 4.27 Determination of Activation Energies for the Thermal Oxidation of Model II
(+ 1000ppm Sodium Phosphite) in the Presence of Different Concentrations
of Cobalt by Isothermal Thermogravimetric Analysis.
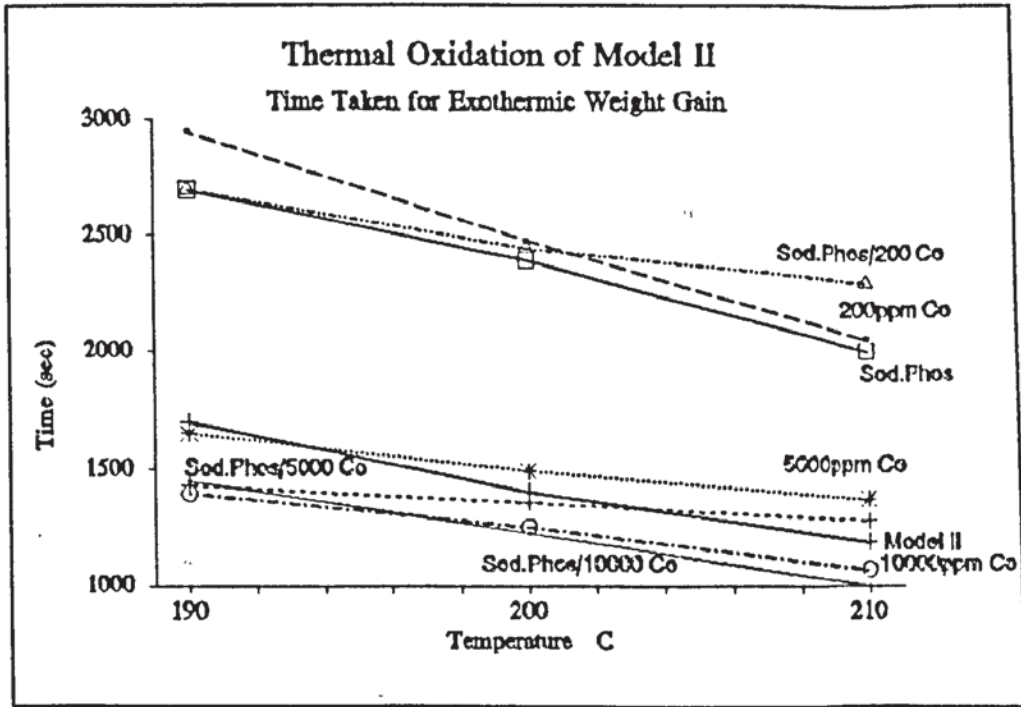
Figure 4.28 The Effect of Temperature and Cobalt Concentration on the Time Taken for the Formation of the Initial Weight Gain Produced During the Isothermal Thermogravimetric Analysis of Model II at 190, 200 & 210°C (in an oxygen atmosphere).
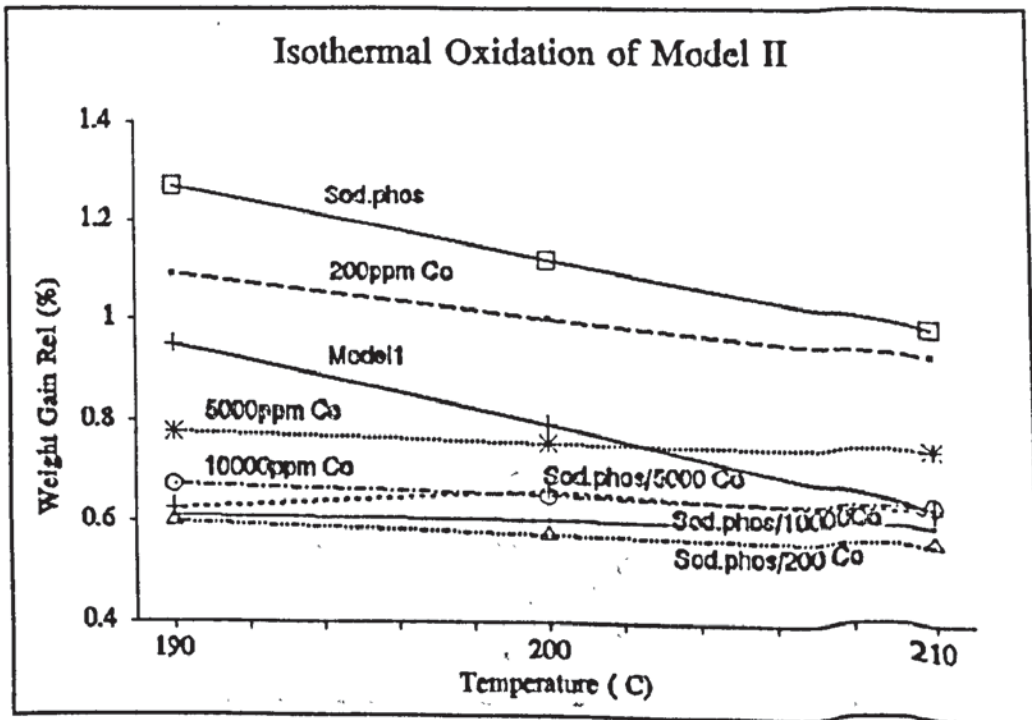
Figure 4.29 The Effect of Temperature and Cobalt Concentration on the Initial Weight Gain Produced During the Isothermal Thermogravimetric Analysis of Model II at 190, 200 and 210°C (in an oxygen atmosphere).
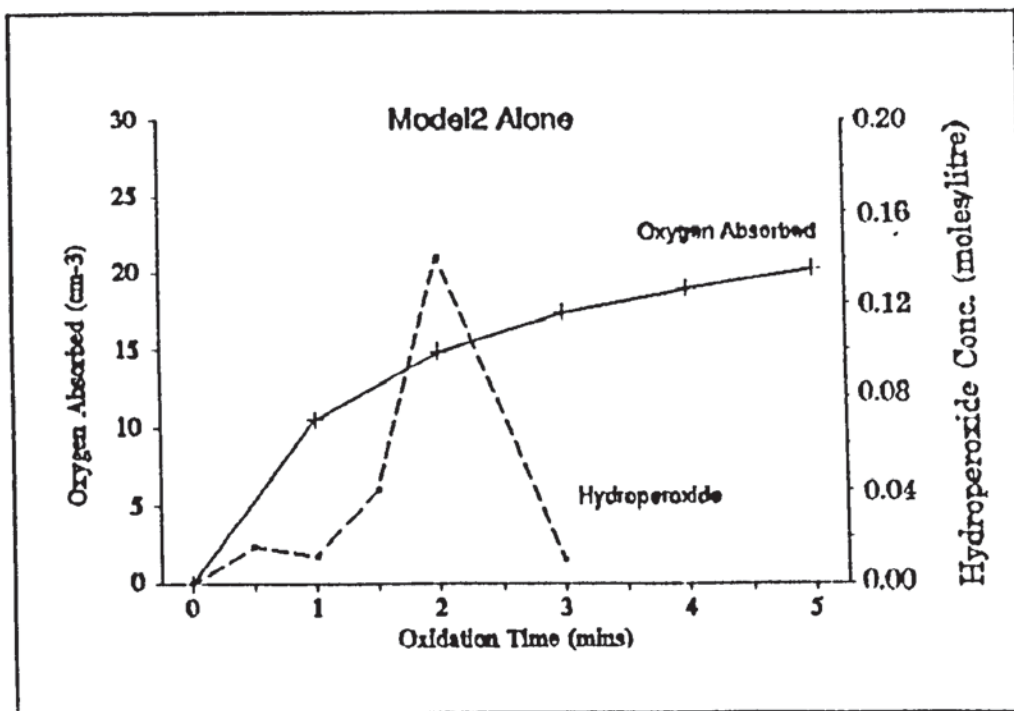
Figure 4.30 A Comparison of the Oxygen Absorbed and the Hydroperoxide Produced During the Thermal Oxidation of Model II at 190°C, in the melt phase.
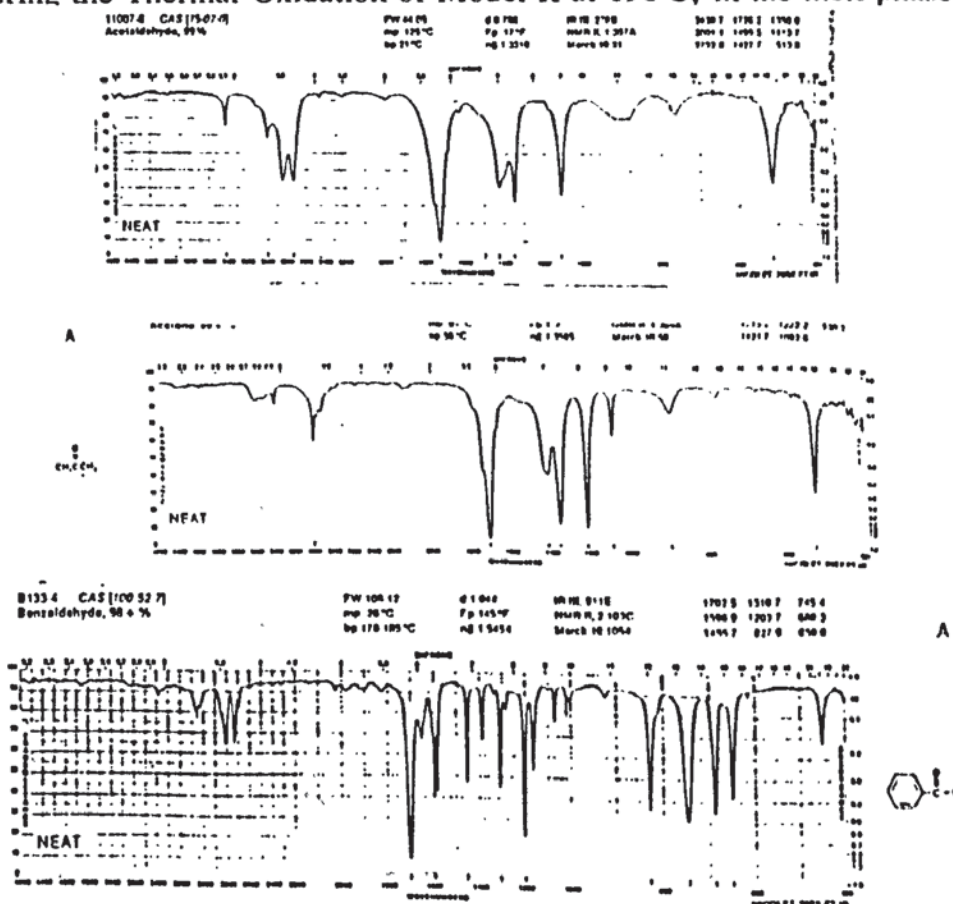
Figure 4.31 The FT-IR Spectra of Various Aldehydes and Ketones Likely to be Formed as Products of Oxidation of Model II at 190°C, Reproduced from the Aldrich Library of IR Spectra.
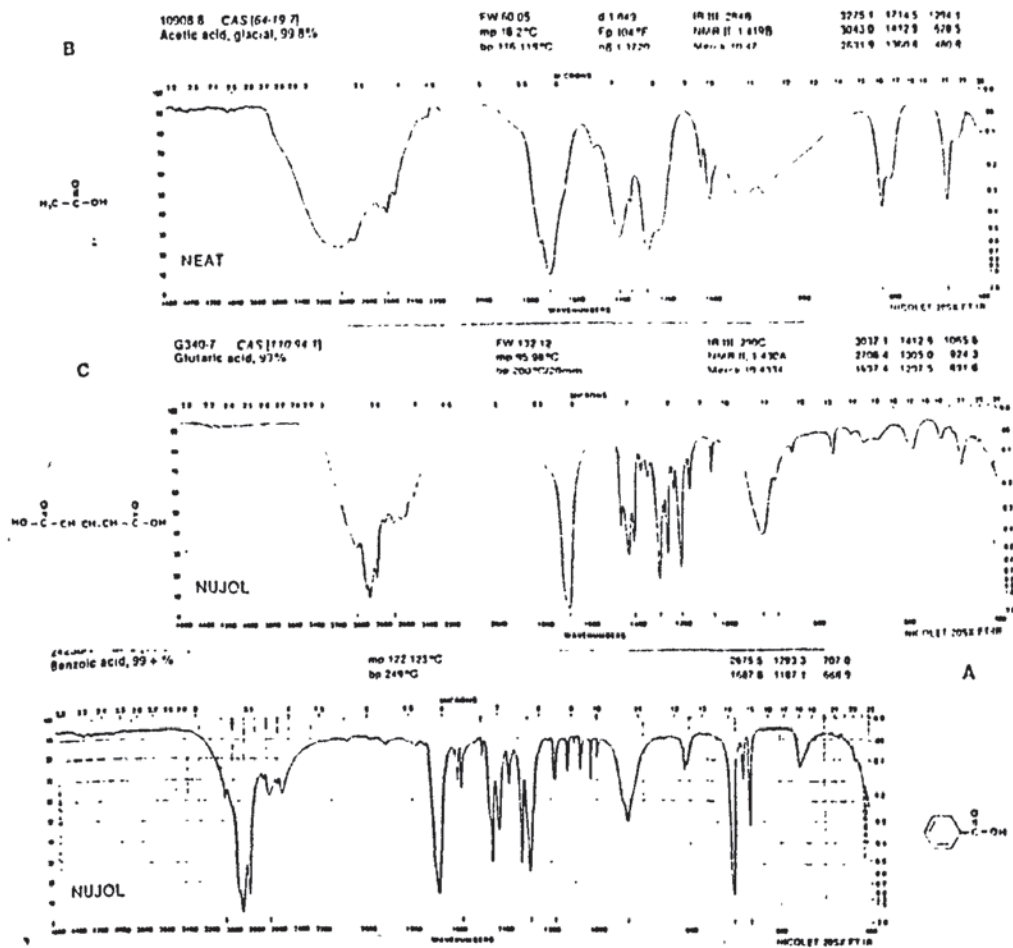
Figure 4.32 The FT-IR Spectra of Various Carboxylic Acids Likely to be Formed as Products of Oxidation of Model II at 190°C, Reproduced from the Aldrich Library of IR Spectra.
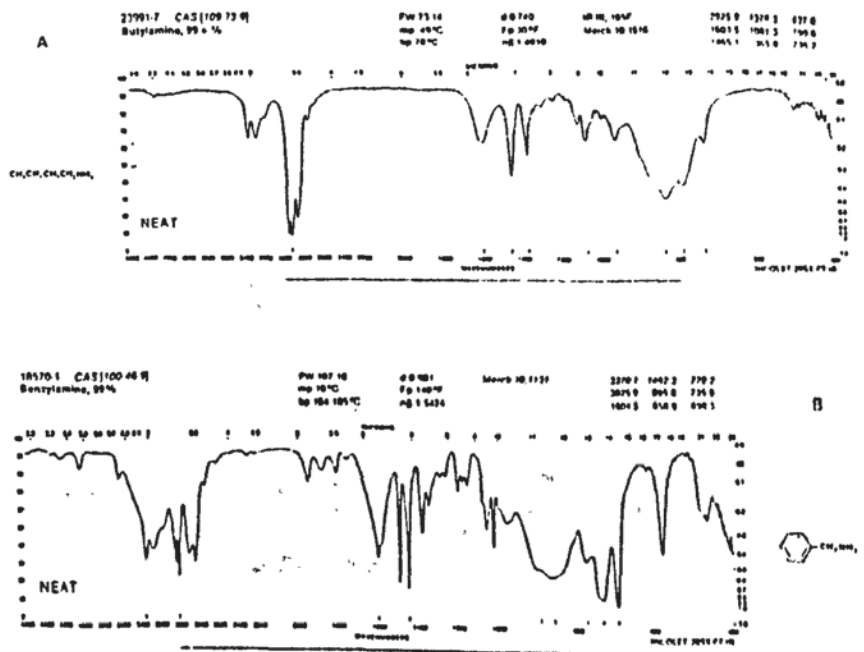
Figure 4.33 The FT-IR Spectra of Various Amines Likely to be Formed as Products of Oxidation of Model II at 190°C, Reproduced from the Aldrich Library of IR Spectra.
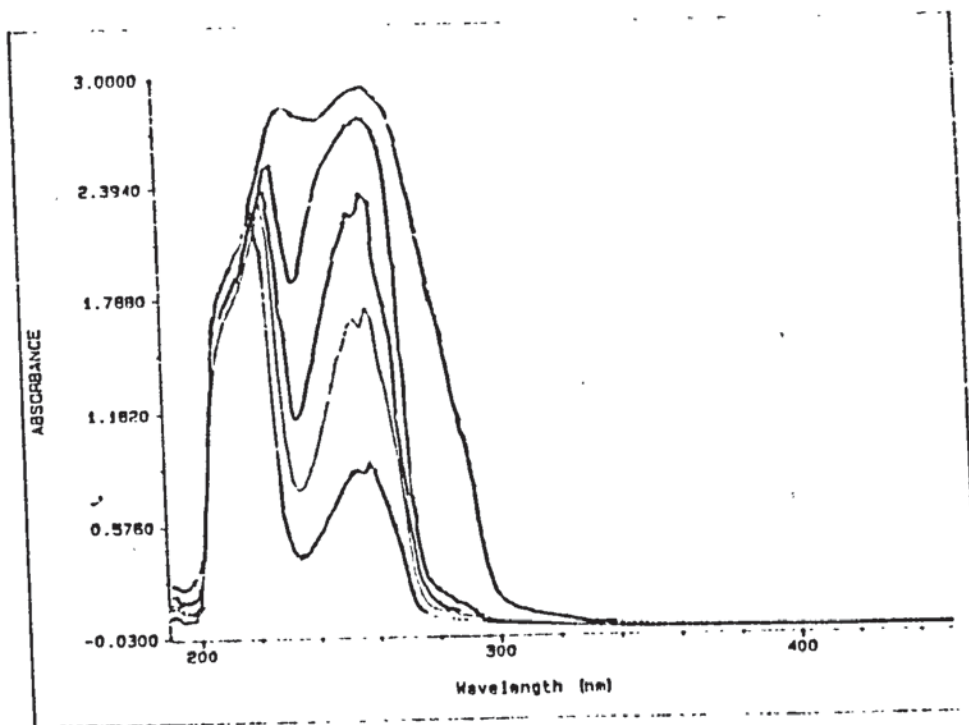
Figure 4.34 The UV-Vis Spectra of Benzylamine, in Methanol, with Increasing Concentration.
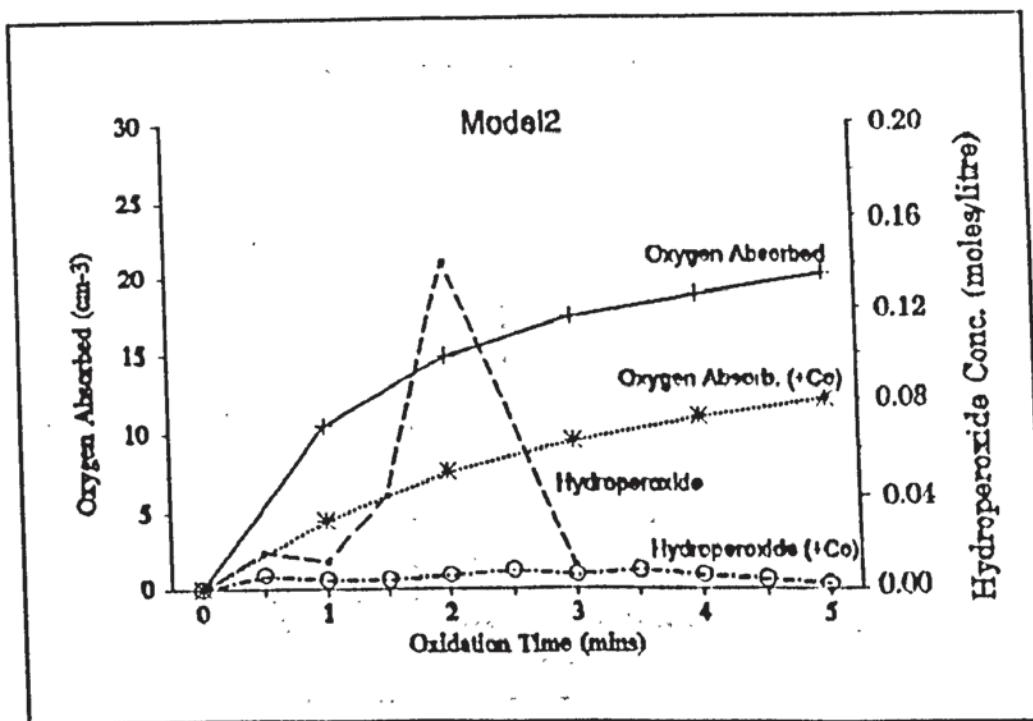
Figure 4.35 A Comparison of the Oxygen Absorbed and the Hydroperoxide Produced During the Thermal Oxidation of Model II in the Presence of 200ppm Cobalt at 190°C, in the melt phase.
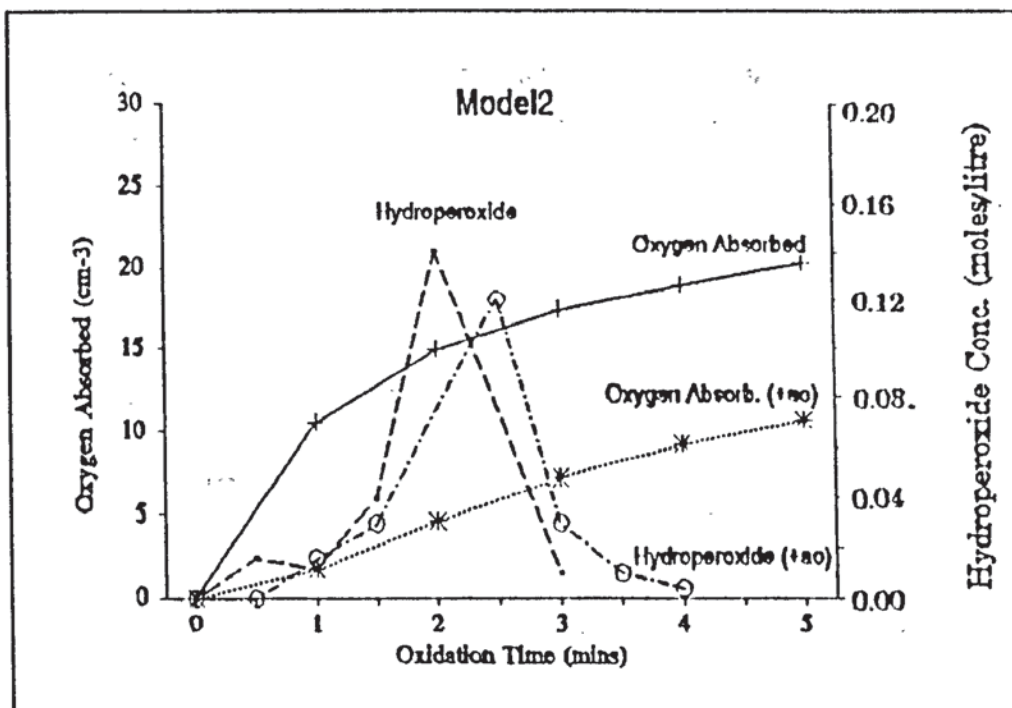
Figure 4.36 A Comparison of the Oxygen Absorbed & Hydroperoxide Produced During the Thermal Oxidation of Model II in the Presence of 1000ppm Sodium Phosphite, at 190°C, in the melt phase.
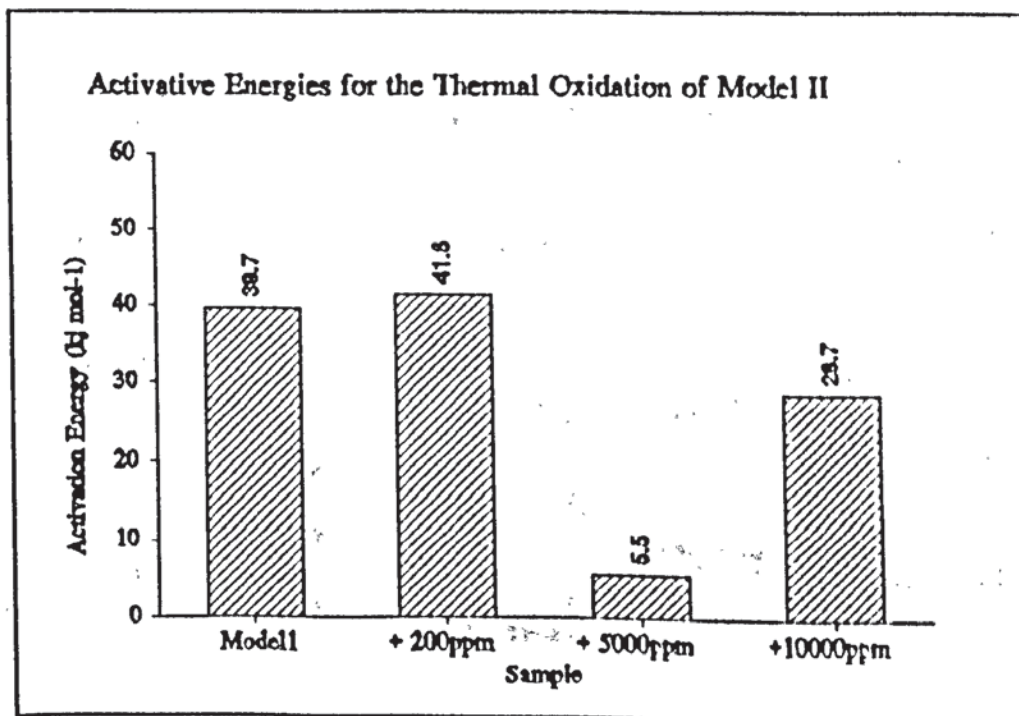
Figure 4.37 The Activation Energies Calculated for the Thermal Oxidation of Model II, with and without Cobalt.
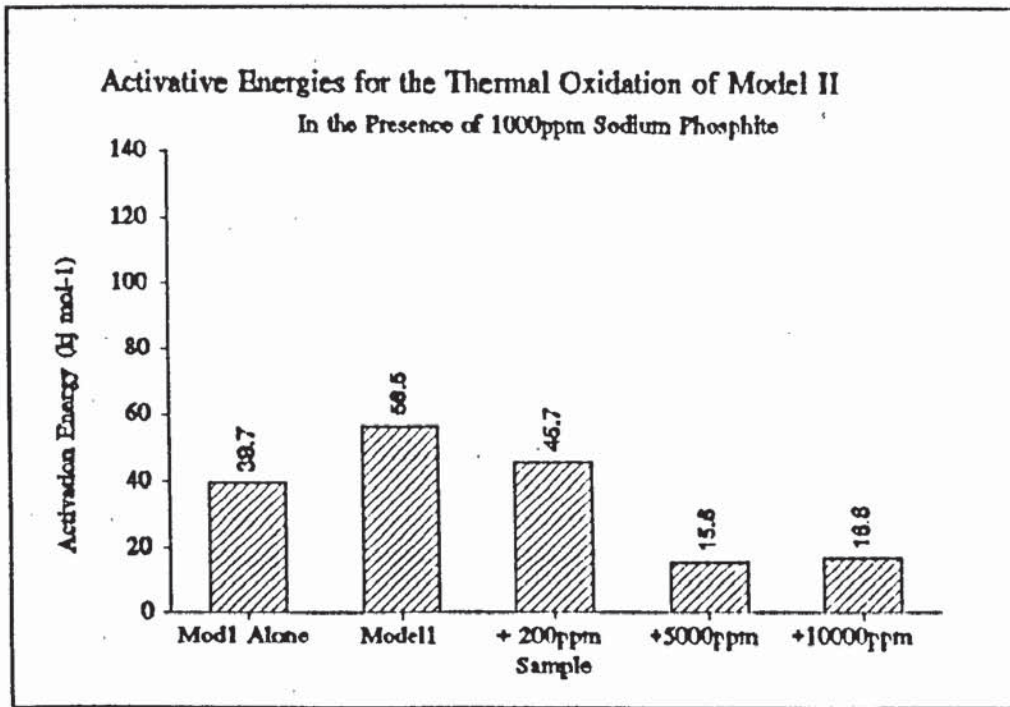
Figure 4.38 The Activation Energies Calculated for the Thermal Oxidation of Model II, in the Presence of 1000ppm Sodium Phosphite, with and without Cobalt.
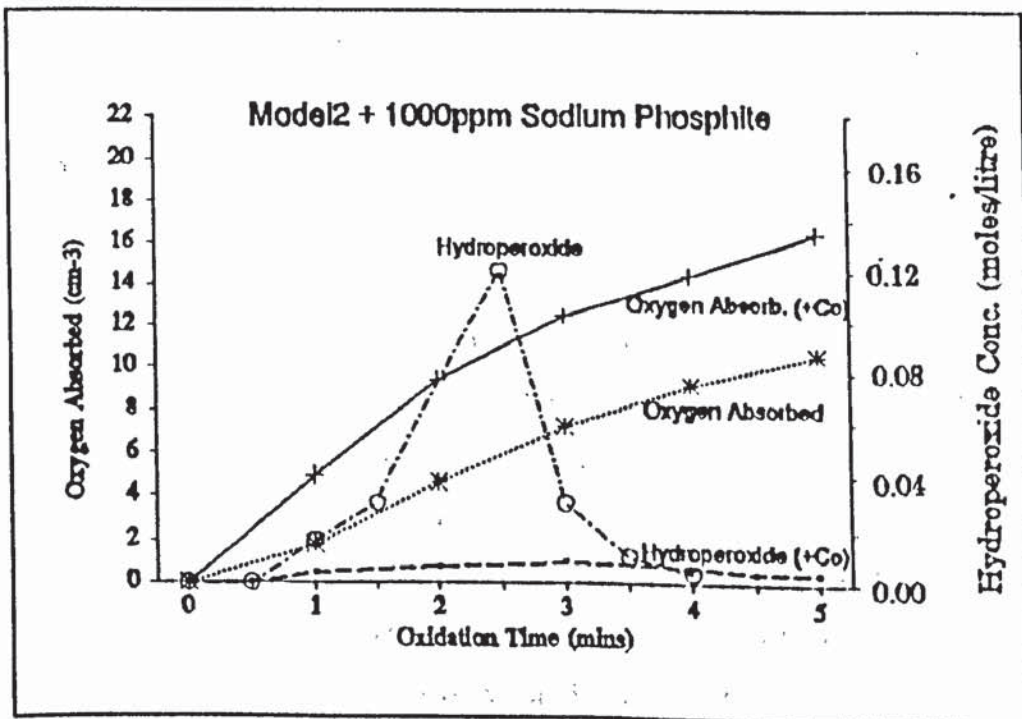
Figure 4.39 Oxygen Absorption & Hydroperoxide Formation of ModelII, in the Presence of 1000ppm Sodium Phosphite, (+ 200ppm Cobalt) at 190°C in an Oxygen Atmosphere.

Chapter 5. Possible Reactions of Cobalt Neodecanoate & Sodium Phosphite and Their Influence on the Oxidation of Model I.

5.1. Object and Methodology.

Transition metal ions have been shown to have a profound effect on the rate of autoxidation of polymer systems, this has been discussed in Chapter1. Relating general oxidative polymer chemistry to the oxidation of the nylon polymer MXD6 and respective model compounds (model1 : Benzene-1,3-dimethylhexanamide and model2 : Hexanedioate-bis-benzylamide, see table 5.1) it has been suggested by Cochran et al [67] and Patel [102] that the transition metal ion, in this case cobalt (present in the polymer as an impurity), could influence either the initiation or propagation reactions of the polymer oxidation. However, the presence of an antioxidant, (sodium phosphite at a concentration of 1000ppm) in the nylon polymer, MXD6, further complicates its mechanism of oxidation. Therefore, possible interactions between cobalt and the sodium phosphite inhibitor and their effect on the oxidation reaction mechanism have to be considered.

It was shown (chapters 3 & 4) from oxidation studies of Models I and II that sodium phosphite inhibited the oxidation of the model compound. However additions of cobalt (>50ppm) to the model, in the presence of sodium phosphite, increased the oxidation greatly, to a level similar to that of the model alone, ie. without sodium phosphite and without cobalt. The aim of the work described in this chapter is therefore to investigate whether the sodium phosphite and cobalt salt act in a combined way to increase the oxidation of the model compounds or whether the cobalt acts individually to offset the inhibiting effect of the sodium phosphite. Several attempts using different methods were initially carried out to investigate any possible effects. Particularly analysis using cyclic voltammetry was assessed, see section 5.2.2, however problems with the solubiltiy of the cobalt salt and its oxidation potential limited the usefulness of the results which could be obtained from these experiments. For these, and several other reasons DTA, in conjunction with thermogravimetry, was employed as the main investigative technique. The investigation discussed in this chapter centres around the possible reactions of sodium phosphite and cobalt neodecanoate and the work was carried out via the experimental outline shown in

scheme 5.1. Table 5.1 shows the chemical structures of Model I, the antioxidant and the cobalt compound.
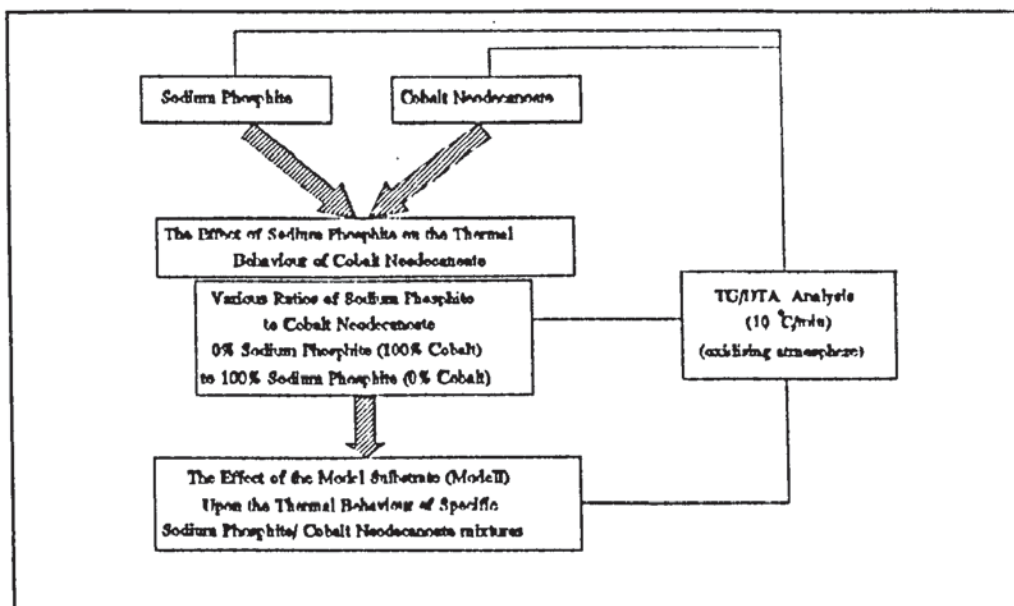
Scheme 5.1 Experimental Outline for the Study of Possible Reactions between Sodium Phosphite and Cobalt and their Influence on the Oxidation of Model I.

Molecular Weight	Chemical Structure and Name	Abbreviation
332.49	$CH_3(CH_2)_4CONHCH_2$ ⬡ $CH_2NHCO(CH_2)_4CH_3$ Benzene-1,3-Dimethylhexanamide	Model I (white solid) m.p 125°C
465.46	$Co(C_{10}H_{19}O_2)_2 \cdot 4H_2O$ Cobalt Neodecanoate	Cobalt (purple pellets) m.p, -4H₂O, 140°C
216.04	$Na_2HPO_3.5H_2O$ Sodium Phosphite	Sodium Phosphite (white crystals) m.p,-5H₂O, 150°C

Table 5.1 Various Samples used in this Study and their Corresponding Structures

5.2 Results.

5.2.1 The Interaction Between Cobalt and Sodium Phosphite : Thermogravimetric Study.

Thermal analysis was used in an attempt to examine the possibility of a mutual interactive effect between sodium phosphite and cobalt neodecanoate. Initial thermograms of the individual components, cobalt and the sodium phosphite, were examined in order to understand the thermo-oxidative characteristic of each component (the antioxidant and the cobalt). This information is crucial to the understanding of the subsequent experiments which investigated the thermal characteristics of various combinations of cobalt and sodium phosphite at different weight ratios. The conditions used for the thermal analysis are shown in table 5.2.

TG/DTA Analytical Conditions	
Atmosphere	Argon/Oxygen
Flow Rate	40/300 (cc/min)
Heating Rate	10 °C/min
Sample Reference	Empty pan

Table 5.2 Conditions used in Thermogravimetric Study.

If a DTA curve is to be interpreted correctly understanding of the characteristics of the thermogram is essential. Any physical or chemical change occurring in the test sample which involves the evolution of heat will cause its temperature to rise temporarily above that of the reference sample, thus giving rise to an exothermic peak on the DTA plot. Conversely, a process which is accompanied by an absorption of heat will cause the temperature of the test sample to lag behind that of the reference material, leading to an endothermic peak. The shape and position of these peaks can provide further information on the changes occuring in the sample. Physical transitions generally give sharp peaks with a rapid rise and return to the baseline, whereas chemical reactions tend to give broader, rounded peaks [83]. However, collapse of the sample, as a result of melting or a change in packing, or loss of volatile products, can cause irregular peak shapes [83].

However, DTA is now seldom used as the sole means of investigating a decompostion process since it is not possible to be sure which DTA peaks correspond to a chemical reaction and which are the result of physical processes, such as melting, boiling or solid-solid phase transitions [103]. For this reason, and several other reasons, DTA is employed (in this chapter) in conjunction with thermogravimetry (TG).

Figure 5.1A and 5.1B show the thermogram of cobalt neodecanoate examined under an argon and oxygen atmosphere respectively. In an atmosphere of argon (figure 5.1A) the TG curve showed a large mass loss (l) of 95% occuring between 295°C and 440°C. The DTA curve showed a number of changes but most importantly a large endotherm (c), at 383°C, was produced coinciding with the mass loss of the compound. The shape of the endotherm (c) and the associated mass loss suggests a collapse of the sample at this temperature. The two initial endotherms (a) and (b) occurring at 88°C and 147°C respectively, are probably due to loss of water in the cobalt neodecanoate, associated with a small mass loss (k).

The corresponding analysis of cobalt neodecanoate in an oxygen atmosphere (figure 5.1B) indicates the reaction is exothermic (as opposed to endothermic in an argon atmosphere). The size of the exotherm is several magnitudes higher than that of the endotherm (cf fig.5.1A) indicating a massive heat change in favour of the oxidation process and this, therefore, would be expected to predominate in any DTA trace obtained by decomposition of cobalt neodecanoate in air or oxygen atmospheres. The exotherm (a) reaches a maximum at 274°C with the onset of the 90% mass loss (l) occurring at 125°C and ending at 285°C. The onset temperature of the mass loss is therefore significantly lower in an oxidising atmosphere (see table 5.3). These characteristics and the changes occurring in the different atmospheres are summarised in table 5.3.

Characteristic	Atmosphere	
	Argon	Oxygen
Exotherm	None	274°C (large) due to decomposition
Endotherm	88°C, 147°C (loss of water), 383°C due to sample collapse	None
Mass Loss (%)	95%	90%
Onset of Mass Loss	295 - 440°C	125 - 285°C

Table 5.3 The Thermogram Characteristics of Cobalt Neodecanoate During TG/DTA Analysis in Argon and Oxygen Atmospheres at a heating rate of 10°C/min.

Figures 5.2A and 5.2B show the thermograms of sodium phosphite in argon and oxygen atmospheres, respectively. Dehydration is the most commonly encountered process with salts such as sodium phosphite [103] and is reflected on the DTA curve by clearly expressed endothermic effects. This is clearly identifiable in the thermogram of sodium phosphite in both atmospheres. Dehydration reactions can be divided into several categories, which are characterized by differences in the behaviour of substances during heating. For sodium phosphite the dehydration process occured possibly in three stages, producing endotherms, in an argon atmosphere, at 69°C (a), 128°C (b) and 150°C (c). A combination of all three produced an overall mass loss of 40.5%, with complete dehydration occuring at 165°C. This corresponds to the loss expected for the complete dehydration of the sample, as shown in figure 5.3.

In an oxygen atmosphere, figure 5.2B, the thermogram of sodium phosphite is almost identical to that measured in an argon atmosphere. The only difference is the slightly higher temperature at which the loss of water occured, complete dehydration occuring at 180°C, see table 5.4.

	Atmosphere	
Characteristic	**Argon**	**Oxygen**
Exotherm	None	440°C
Endotherm	69°C, 128°C, 150°C due to loss of water	79°C, 133°C, 160°C due to loss of water
Mass Loss (%)	40.5%	40%
Onset of Mass Loss	50 - 165°C (due to water)	50 - 180°C (due to water)

Table 5.4 The Thermogram Characteristics of Sodium Phosphite During TG/DTA Analysis in Argon and Oxygen Atmospheres at a heating rate of 10°C/min.

5.2.1.1 The Effect of Sodium Phosphite Additions on the Thermal Behaviour of Cobalt Neodecanoate in an Oxygen Atmosphere.

The analysis involved the study of the mass losses and degradation exotherms produced from various mixtures of sodium phosphite and cobalt, ranging from 0% cobalt (100% sodium phosphite) to 100% cobalt (0% sodium phosphite) examined under an oxygen atmosphere (see scheme 5.2). The relative mass change (%) and DTA curve (uV) plotted against temperature (0 to 550°C) for each mixture are shown in figure 5.4. Results for the different systems are presented in Tables 5.5 a-h.

a) **0% Sodium Phosphite (100% Cobalt)** : Cobalt alone produced only one exotherm (with a shoulder) at 274°C (p). The 90% relative mass loss (u) which occured during degradation began at 125°C and ended at 285°C, as shown in table 5.5A and figure 5.4A.

b) **15% Sodium Phosphite (85% Cobalt)** : Additions of such small amounts of sodium phosphite make it difficult to see the loss of water from the system. 85% cobalt only produced two distinct mass losses associated with a complicated broad exotherm. The initial mass loss of 18% between 135 and 250°C (u) produced no apparent exotherm. The final, major, mass loss (v) of 45% occured between 250 and 375°C and was associated with a large, broad exotherm peaking at a maximum of 309°C (p), see table 5.5B and figure 5.4B.

c) **20% Sodium Phosphite (80% Cobalt)** : 80% cobalt produced a possible 4 stage mass loss as follows, see table 5.5C and figue 5.4C.

1. 6% loss due to water from sodium phosphite (t).
2. 10.5% of the overall mass loss between 140 and 235°C (u) had no noticable exotherm.
3. The third mass loss of 19% between 235 and 335°C (v) produced a relatively small exotherm at 307°C (p).
4. The final mass loss (w) of 28% between 335 and 410°C produced a broad exotherm at 406°C (q).

d) **35% Sodium Phosphite (65% Cobalt)** : With cobalt as the main constituent the thermogram became slightly more complicated. 65% cobalt produced a possible 6 stage mass loss as follows, see table 5.5D and figure 5.4D.

1. The initial loss of 16% (t) was due to the loss of water from sodium phosphite.
2. The second mass loss of 8% (u) occured between 160 and 195°C with an exotherm at 190° C (p).
3. A mass loss of 8% between 195 and 265°C (v) produced no apparent exotherm.
4. A further mass loss of 8% between 265 and 320°C (w) produced a small exotherm at 290°C (q).
5. A 12% mass loss (x) coincided with the onset of a coupled exotherm (r). The 12% loss between 320 and 360°C was associated with an exotherm at 340°C.
6. The final mass loss of 13% between 360 and 405°C (y) produced the largest exotherm at 400°C (s).

e) **50% Sodium Phosphite (50% Cobalt)** : This particular ratio produced an initial mass loss (t) of 22% corresponding to loss of water which was present in the sodium phosphite, with three endotherms (l), (m) and (n). The loss of 38% (u) due to cobalt, produced a large exotherm (p) at 303°C, see table 5.5E and figure 5.4E.

f)   **90% Sodium Phosphite (10% Cobalt)** : The loss of mass due to water, with three corresponding endotherms (l), (m) and (n) increased slightly (t) and there was a 4% loss between 250 and 355°C (u) which produced a small exotherm at 309°C (p), see table 5.5F and figure 5.4F. An exotherm due to sodium phosphite (q), at 435°C, was apparent.

g)   **95% Sodium Phosphite (5% Cobalt)** : 5% cobalt produced a two stage mass loss, the greater of which, 36% (t), was due to loss of water, with three corresponding endotherms (l), (m) and (n). A 2% loss (u) between 260 and 350°C produced a small exotherm at 304°C due to the cobalt neodecanoate (p), see table 5.5G and figure 5.4G. Although the cobalt is only present in a small amount the intensity of the heat change of the oxidation process is so intense it appears as a small exotherm on the DTA trace. There also appears to be an exotherm (q) produced at 420°C due to sodium phosphite.

h)   **100% Sodium Phosphite** : an overall mass loss of 40% (t), with the production of three endotherms (l), (m), (n), due to the loss of water from the sodium phosphite, see table 5.5H and figure 5.4H. The exotherm at 440°C (q) is due to an oxidation reaction of sodium phosphite.

Having established the individual charateristics of sodium phosphite and cobalt neodecanoate an attempt was made to analyse any possible interactive effect of cobalt on sodium phosphite. Figure 5.5 shows that increasing the concentration of one component, eg sodium phosphite, leads to an increase in the domination of the characteristics of that component. For example, the percentage mass loss, due to loss in weight from the cobalt neodecanoate, decreased with decreasing cobalt concentration in the mixture. This was paralleled by an increase in the mass loss, due to weight loss from the sodium phosphite (associated with its dehydration), with increasing sodium phosphite in the mixture (this can also be seen in the original thermograms as an increase in weight loss (t) as the percentage of sodium phosphite is increased, figure 5.4).

Stage of Mass Loss	0% Sodium Phosphite (A)		
	% Loss	Temp.Range (°C)	Exotherm (°C)
1	90 (u)	125-285	274 (p)

Stage of Mass Loss	15% Sodium Phosphite (B)		
	% Loss	Temp.Range (°C)	Exotherm (°C)
1	18 (u)	135-250	None
2	45 (v)	250-375	309

Stage of Mass Loss	20% Sodium Phosphite (C)		
	% Loss	Temp.Range (°C)	Exotherm (°C)
1	6 (t)	0-110	None
2	10.5 (u)	140-235	None
3	19 (v)	235-335	307 (p)
4	28 (w)	335-410	406 (q)

Stage of Mass Loss	35% Sodium Phosphite (D)		
	% Loss	Temp.Range (°C)	Exotherm (°C)
1	16 (t)	0-110	None
2	8 (u)	160-195	190 (p)
3	8 (v)	195-265	None
4	8 (w)	265-320	290 (q)
5	12 (x)	320-360	340 (r)
6	13 (y)	360-405	400 (s)

Stage of Mass Loss	50% Sodium Phosphite (E)		
	% Loss	Temp.Range (°C)	Exotherm (°C)
1	22 (t)	0-110	None
2	38 (u)	200-340	303 (p)

Stage of Mass Loss	90% Sodium Phosphite (F)		
	% Loss	Temp.Range (°C)	Exotherm (°C)
1	34 (t)	0-110	None
2	4 (u)	250-355	309 (p)

Stage of Mass Loss	95% Sodium Phosphite (G)		
	% Loss	Temp.Range (°C)	Exotherm (°C)
1	36 (t)	0-110	None
2	2 (u)	260-350	304 (p)

Stage of Mass Loss	100% Sodium Phosphite (H)		
	% Loss	Temp.Range (°C)	Exotherm (°C)
1	40 (t)	0-110	None

Table 5.5 A Summary of the Thermograms Produced From Various Mixtures of Cobalt Neodecanoate and Sodium Phosphite in an Oxygen Atmosphere at a Heating Rate of 10°C/min up to a Maximum Temperature of 550°C. Tables A to G Correspond to an Increasing Percentage of Sodium Phosphite in the Mixture.

However, the changes observed from the DTA traces provides more information, concerning the efects of the two components upon each other, than the weight loss curves. Of particular interest was the effect of the increasing concentration of sodium phosphite on the decomposition exotherm of cobalt neodecanoate. The positions of thermal peaks in the presence and absence of catalysts, inhibitors etc is a technique often used in DTA analysis to give information on the relative efficiences of the various additives (ie, the more effective the inhibitor the higher the peak temprature) [83]. In figure 5.4A (100% cobalt, 0% phosphite) the cobalt produced a single decomposition exotherm at 274°C, as discussed previously (see table 5.3). However as the percentage of sodium phosphite in the mixture was increased to 15%(fig.5.4B), 20%(fig.5.4C) and 35%(fig.5.4D) the temperature of the maximum cobalt exotherm (shaded) was increased to a maxium of 400°C. This was also accompanied by a splitting of the single cobalt exotherm into a series of exotherms. When the percentage of sodium phosphite present in the mixture was further increased to 50%(fig.5.4E), 90%(fig.5.4F) and 95%(fig.5.4G) this resulted in the subsequent decrease of the cobalt exotherm (shaded),(cf 35% sodium phosphite) stabilising at approximately 304°C. This change in the temperature of the characteristic exotherm of cobalt neodecanoate is summarised in figure 5.6 which shows plots of temperature of the maximum exotherm (shaded), obtained from DTA traces (fig 5.4 A-II) and from DSC traces (fig 5.7), against cobalt/sodium phosphite composition in the mixtures. Figure 5.6 shows clearly that sodium phosphite acts to stabilise the cobalt neodecanoate, but this effect is particularly enhaced at certain concentrations of the two components, namely (20% sodium phosphite/80% cobalt) and (35% sodium phosphite/ 65% cobalt).

Having established some possible stabilising effect of sodium phosphite on cobalt neodecanoate it was imporant to investigate whether this effect would still be apparent in the presence of a model substrate. However, due to the limitations of the experimental technique, concentrations of model I, with respect to the cobalt/sodium phosphite mixture, used in the oxidation study of model I (chapter 3) ie, a cobalt range of 50 - 800ppm and sodium phosphite concentration of 1000ppm, could not be used for the thermal analysis purpose. The DTA/TG characteristics associated with the cobalt and sodium phosphite would not be observed in a mixture comprising of such small concentrations of these two
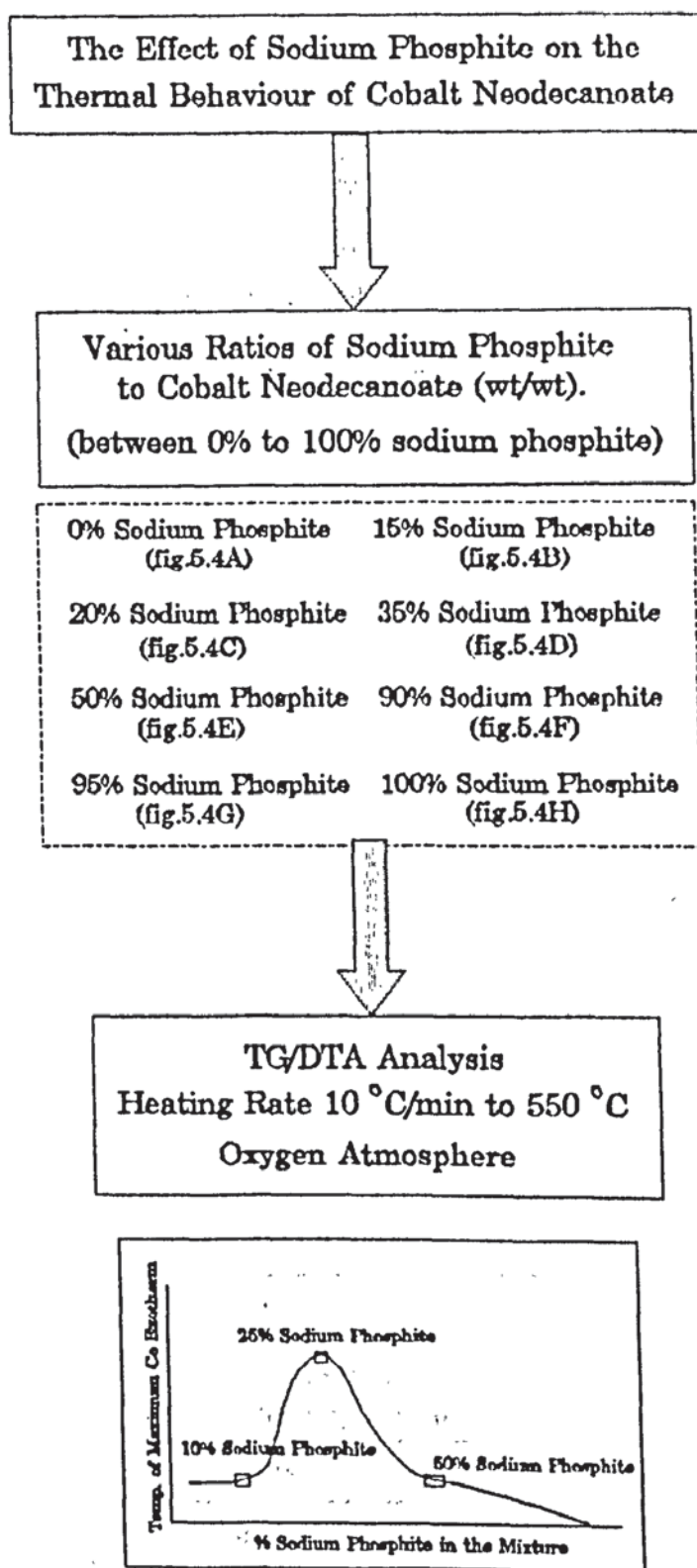
Scheme 5.2 Experimental Ouline For the Investigation of the Effect of Sodium Phosphite on the Thermal Behaviour of Cobalt Neodecanoate.

compounds. Higher concentration ratios, of the cobalt/sodium phosphite mixture to the model, than would normally be used, were therefore investigated. Prior to the investigation, of the effect of cobalt/sodium phosphite mixtures on the model, it was important to establish the effect of the individual components (i.e cobalt and sodium phosphite) on the model compound.

5.2.1.2 The Effect of Sodium Phosphite Additions to the Thermal Behaviour of Model I.

Analysis of the cobalt neodecanoate and sodium phosphite were previously carried out individually in both argon and oxygen atmospheres to determine the DTA/TG characteristics associated with each compound. Results of the thermal analysis of ModelI under argon and oxygen atmospheres are shown in figures 5.8A and 5.8B respectively. In an argon atmosphere (figure 5.8A) the first transition experienced by the model compound was due to melting. This occured at 128°C and featured a large sharp endotherm peak (I). A second endotherm (m) occured at 393°C, and this was accompanied by a 95% mass loss on the TG curve (t). This suggests an almost total breakdown of the model compound in one complete phase beginning at 298°C and ending at 430°C. In contrast to the endothermic peaks observed under argon atmosphere, examination of the models thermal behaviour under oxygen gave only one endothermic peak (l), due to melting, the decomposition reaction, in this instance, produced two exothermic peaks (m) and (n), see figure 5.8B and table 5.6.

Characteristic	Atmosphere	
	Argon	Oxygen
Exotherm	None	359°C and 520°C
Endotherm	128°C (melting) 393°C decomposition	128°C (melting)
Mass Loss (%)	95%	90% and 10%
Onset of Mass Loss	298 - 430°C	240-395°C 440-550°C

Table 5.6 The Thermogram Characteristics of ModelI During TG/DTA Analysis in Argon and Oxygen Atmospheres at a heating rate of 10°C/min.

The analysis involved the study of the mass losses and degradation exotherms produced from various mixtures of sodium phosphite and model1, ranging from 0% model (100% sodium phosphite) to 100% model (0% sodium phosphite). The relative mass change (%) and DTA (uV) curves were plotted against temperature, ranging between 0 and 550°C, for each mixture and are shown in figure 5.9 and summarised in tables 5.7 A-H.

a)   **0% Sodium Phosphite (100% Model)** : Mass loss occurred in two stages, the majority of which was lost between 225 and 395°C (u) representing 88% of the total with the production of a large exotherm at 359°C (m). The second mass loss, (v), of the remaining 12% produced a smaller exotherm at 530°C (n), see table 5.7A and figure 5.9A.

b)   **10% Sodium Phosphite (90% Model)** : The addition of 10% sodium phosphite produced a three stage mass loss. The first (t), of 5%, can be accountable to the loss of water from the sodium phosphite. The remaining two are undoubtably due to the model compound. The major loss of 75% between 205 and 390°C (u) produced an exotherm at 361°C (m). The final mass loss of 10% (v) produced an exotherm at 502°C (n), see table 5.7B and figure 5.9B.

c)   **15% Sodium Phosphite (85% Model)** : Similar to the previous trace, 15% sodium phosphite produced a three stage mass loss, 9% (t) of which was due to loss of water. The remaining losses of 71% (u) and 10% (v) again were due to the model compound. A 71% loss occurred between 215 and 390°C (u) with the maximum exotherm (m) at 363°C. The 10% mass loss (v) produced an exotherm at 493°C (n), see table 5.7C and figure 5.9C.

d)   **35% Sodium Phosphite (65% Model)** : 35% sodium phosphite resulted in the increased progressive loss of water from the mixture and the decreased loss of mass due to the model compound. The mass loss due to water was increased to 18% (t) with a 47% (u) and 7% (v) loss due to the model compound. The loss of 47% between 210 and 370°C (u) produced an exotherm at 340°C (m). The 7% mass loss (v) continued to produce an exotherm of decreasing temperature, at 446°C (n), see table 5.7D and figure 5.9D.

e) **50% Sodium Phosphite (50% Model)** : A 50:50 mixture of model and sodium phosphite again produced a three stage mass loss. 20% (t) due to water, and two separate losses of 40% (u) and 4% (v) due to the model compound. The exotherm associated with the greater mass loss was lower than the previous one at 329°C (m), with mass loss occuring between 210 and 335°C (u). The exotherm associated with the 4% mass loss (v) appeared to be stabilising at 449°C (n), see table 5.7E and figure 5.9E.

f) **65% Sodium Phosphite (35% Model)** : At this composition sodium phosphite was the greater constituent, this was indicated by the greater mass loss of 35% (t) due to loss of water from sodium phosphite. The model compound represented 27% of the total mass loss, divided between 25% and 2%. The onset of the greater mass loss, 25% (u) occurred at the slightly lower temperature, 195 to 355°C, producing an exotherm at 335°C (m). The final mass loss of 2% (v) produced an exotherm at 445°C (n), see table 5.7F and figure 5.9F.

g) **85% Sodium Phosphite (15% Model)** : A two stage mass loss occurred, 38% (t) of which is accountable to loss of water from sodium phosphite and 12% due to the model between 195 and 350°C (u) producing a small exotherm at 328°C (m), see table 5.7G and figure 5.9G.

h) **100% Sodium Phosphite** : Single mass loss of 40% due to water within the sodium phosphite. see table 5.7H and figure 5.9H (previously discussed in section 5.2.1).

5.2.1.3 The Effect of Model Additions to the Thermal Behaviour of Cobalt Neodecanoate.

The analysis involved the study of the mass losses and degradation exotherms produced from various mixtures of cobalt and model1, ranging from 0% model (100% cobalt) to 100% model (0% cobalt). The relative mass change (%) and DTA (uV) curves were plotted against temperature, ranging between 0 and 550°C, for each mixture and are shown in figure 5.10 and summarised in tables 5.8 A-H.

Stage of Mass Loss	100% Model (A)		
	% Loss	Temp.Range (°C)	Exotherm (°C)
1	88 (u)	225-395	359 (m)
2	12 (v)	465-550	530 (n)

Stage of Mass Loss	90% Model (B)		
	% Loss	Temp.Range (°C)	Exotherm (°C)
1	5 (t)	0-110	None
2	75 (u)	205-390	361 (m)
3	10 (v)	390-520	502 (n)

Stage of Mass Loss	85% Model (C)		
	% Loss	Temp.Range (°C)	Exotherm (°C)
1	9 (t)	0-110	None
2	71 (u)	215-390	363 (m)
3	10 (v)	390-520	493 (n)

Stage of Mass Loss	65% Model (D)		
	% Loss	Temp.Range (°C)	Exotherm (°C)
1	18 (t)	0-110	None
2	47 (u)	210-370	340 (m)
3	7 (v)	380-490	446 (n)

Stage of Mass Loss	50% Model (E)		
	% Loss	Temp.Range (°C)	Exotherm (°C)
1	20 (t)	0-110	None
2	40 (u)	210-335	329 (m)
3	4 (v)	390-490	449 (n)

Stage of Mass Loss	35% Model (F)		
	% Loss	Temp.Range (°C)	Exotherm (°C)
1	35 (t)	0-110	None
2	25 (u)	195-355	335 (m)
3	2 (v)	390-490	445 (n)

Stage of Mass Loss	15% Model (G)		
	% Loss	Temp.Range (°C)	Exotherm (°C)
1	38 (t)	0-110	None
2	12 (u)	195-350	328 (m)

Stage of Mass Loss	0% Model (H)		
	% Loss	Temp.Range (°C)	Exotherm (°C)
1	40 (t)	0-110	None

Table 5.7 A Summary of the Thermograms Produced From Various Mixtures of Model I and Sodium Phosphite in an Oxygen Atmosphere at a Heating Rate of 10°C/min up to a Maximum Temperature of 550°C. Tables A to G Correspond to an Increasing Percentage of Sodium Phosphite in the Mixture.

a) **0% Model (100% Cobalt)** : Cobalt alone produced a single exotherm (m) at 274°C. However the 90% relative mass loss (u), which occurred during degradation began at 125 and ended at 287°C, as shown in table 5.8A and figure 5.10A.

b) **15% Model (85% Cobalt)** : 85% cobalt produced a two stage mass loss. The initial mass loss (t), between 143 and 272°C, of 33%, produced a very small exotherm (l) at 270°C. A 47% mas loss (u) produced a large exotherm at 314°C (m) occurring between 293 and 317°C, see table 5.8B and figure 5.10B.

c) **35% Model (65% Cobalt)** : 65% cobalt produced a two stage mass loss trace. The initial loss (t) increased to 38%. A major loss (u) of 45% between 308 and 330°C produced a large exotherm (m) at 330°C, see table 5.8C and figure 5.10C.

d) **50% Model (50% Cobalt)** : The onset of the 47% mass loss (t), due to the model increased to 145°C. The mass loss of 40% (u) corresponded to the large exotherm (m) at 362°C betwen temperatures 345-365°C, see table 5.8D and figure 5.9D.

e) **65% Model (35% Cobalt)** : The initial mass loss (t), ascertained to the model compound increased to 60%, with no apparent exotherm. The onset of the mass loss increased to 165°C. A large exotherm (m) at 377°C was produced with the next mass loss (u) of 36% between 365 to 380°C, see table 5.8E and figure 5.10E.

f) **85% Model (15% Cobalt)** : A decrease in cobalt to 15% confirmed that the initial mass loss, 70% (t), is due to the model compound, occuring between 180 and 360°C (due to its increase in size with an increase in model compound). Again the mass loss (u) of 22% was associated with a large exotherm (m) at 370°C between 375 and 383°C. The final mass loss (v) of 6% between 383 and 415°C produced an exotherm at 395°C (n), see table 5.8F and figure 5.10F.

g)   **90% Model (10% Cobalt) :** The addition of 10% cobalt produced a three stage mass loss. The greatest mass loss (t) of 75% which occured between 180 and 360°C must be accountable to the model compound due to the size of loss and the temperature range during which the loss occured. However the suprising observation is the omission of any obvious exotherm associated with this mass loss. The mass loss of 13% (u) between 360 and 384°C occurred along with a sharp exotherm at 384°C (m). The final mass loss (v) of 7% occured between 403 and 448°C with an exotherm at 415°C (n), possibly due to the final decomposition stage of the model compound, see table 5.8G and figure 5.10G.

h)   **100% Model :** Mass loss occured in two stages, the majority of which was lost between 225 and 395°C (u) representing 88% of the total with the production of a large exotherm (m) at 359°C. The second mass loss (v) of the remaining 12% produced a smaller exotherm at 530°C (n), see table 5.8H and figure 5.10H.

5.2.1.4 The Effect of Varying the Concentration of Model1 in the Presence of a Fixed Concentration of Sodium Phosphite and Cobalt.

The stabilising effect of sodium phosphite on the decomposition of cobalt neodecanoate, as discussed in section 5.2.1.1, reached a maximum when the sodium phosphite was present at 25% in the cobalt/sodium phosphite mixture. The following three sub-sections therefore investigated the effect of the model substrate on this particular mixture and two further mixtures of cobalt/sodium phosphite, either side of the maxima (i. 50% and 10% sodium phsophite). The ratio of the cobalt to sodium phosphite was kept constant and the model, with respect to the cobalt/phosphite mixture as a whole was increased. The experimental details are summarised in see scheme 5.3.

Stage of Mass Loss	0% Model (A)		
	% Loss	Temp.Range (°C)	Exotherm (°C)
1	95 (u)	134-287	274 (m)

Stage of Mass Loss	15% Model (B)		
	% Loss	Temp.Range (°C)	Exotherm (°C)
1	33 (t)	134-272	270 (l)
2	47 (u)	293-317	314 (m)

Stage of Mass Loss	35% Model (C)		
	% Loss	Temp.Range (°C)	Exotherm (°C)
1	38 (t)	135-287	270 (l)
2	45 (u)	308-330	330 (m)

Stage of Mass Loss	50% Model (D)		
	% Loss	Temp.Range (°C)	Exotherm (°C)
1	47 (t)	145-325	None
2	40 (u)	345-365	362 (m)

Stage of Mass Loss	65% Model (E)		
	% Loss	Temp.Range (°C)	Exotherm (°C)
1	60 (t)	165-345	None
2	36 (u)	365-380	377 (m)

Stage of Mass Loss	85% Model (F)		
	% Loss	Temp.Range (°C)	Exotherm (°C)
1	70 (t)	180-360	None
2	22 (u)	375-383	370 (m)
3	6 (v)	383-415	395 (n)

Stage of Mass Loss	90% Model (G)		
	% Loss	Temp.Range (°C)	Exotherm (°C)
1	75 (t)	180-360	None
2	13 (u)	384-394	384 (m)
3	7 (v)	403-448	415 (n)

Stage of Mass Loss	100% Model (H)		
	% Loss	Temp.Range (°C)	Exotherm (°C)
1	88 (u)	225-395	359 (m)
2	12 (v)	465-550	530 (n)

Table 5.8 A Summary of the Thermograms Produced From Various Mixtures of Cobalt Neodecanoate and Model I in an Oxygen Atmosphere at a Heating Rate of 10°C/min up to a Maximum Temperature of 550°C. Tables A to G Correspond to an Increasing Percentage of Model I in the Mixture.

5.2.1.4.1 The Effect of Model Concentration on a 90%:10% (wt/wt) Cobalt:Sodium Phosphite Mixture.

a) **5% Model (85.5% Cobalt, 9.5% Sodium Phosphite)** : The initial mass loss (t) of 4%, produced an endotherm at 110°C, due to loss of water from sodium phosphite. This was followed by a mass loss (u) of 11% between 150 and 228°C. The proceeding mass losses occurred in conjunction with a broad complicated exotherm which produced five different exotherm maxima associated with only two obvious mass losses. The first of these was a 31% mass loss (v) between 228 and 300°C with the production of two exotherms at 230°C (m) and 295°C (n). The final mass loss (w) of 17% produced three exotherms at 320 (p), 340 (q) and 375°C (r), between 300 and 443°C, see table 5.9A and figure 5.11A.

b) **16% Model (75.5% Cobalt, 8.5% Sodium Phosphite)** : The addition of 16% model also produced a four stage mass loss and a broad complex exotherm, as follows, see table 5.9B and figure 5.11B.

1. The initial mass loss (t) of 6% was due to loss of water from sodium phosphite, although higher than expected.
2. The mass loss (u) of 32%, between 155 and 240°C, produced an exotherm at 264°C (m).
3. The third mass loss (v) of 15% was associated with a broad, jagged exotherm (n) which occured between a temperature range 295 to 355°C.
4. The final mass loss (w) of 19%, between 355 and 390°C, produced the largest exotherm (p) at 359°C.

c) **33% Model (60.5% Cobalt, 6.5% Sodium Phosphite)** : A 33% addition of model compound still produced a four stage mass loss trace as follows, see table 5.9C and figure 5.11C.

1. The initial loss (t) of 5% was probably due to the loss of water.
2. The second mass loss (u) of 26%, between 160 and 305°C, produced a small exotherm (m) at 270°C.

3. The largest mas loss (v) of 24% occurred between 305 and 395°C with the production of an exotherm (n) at 349°C.

4. The final mass loss (w) of 18%, between 395 and 410°C, produced the largest exotherm (p) at 403°C.

d) **50% Model (45% Cobalt, 5% Sodium Phosphite)** : At 50% concentration the model compound was the main constituent of the mixture, this resulted in a three stage mass loss trace, including the appearance of a broad exotherm at a high temperature range as follows, see table 5.9D and figure 5.11D.

1. The mass loss (u) of 43% was the largest, ocurring between 156 and 338°C, with the production of a small exotherm (m) at 250°C.

2. The mass loss (v) of 38% occurred between 338 and 362°C and produced the largest exotherm (p) at 349°C.

3. The appearance of the broad exotherm (q) at 380°C was associated with a 4% mass loss (w) between 377 and 432°C.

e) **67% Model (29.5% Cobalt, 3.5% Sodium Phosphite)** : 67% model compound produced a three stage mass loss as follows, see table 5.9E and figure 5.11E.

1. The greatest mass loss (u) of 53% occurred between 169 and 353°C and produced a slight exotherm (m) at 250°C.

2. The mass loss (v) of 24% between 369 and 381°C was associated with the largest exotherm (p) at 373°C.

3. The final mass loss (w) of 3% occurred between 381 and 443°C and was linked to the exotherm (q) at 443°C.

f) **75% Model (22.5% Cobalt, 2.5% Sodium Phosphite)** : Similarly to the previous trace the addition of 75% model compound produced a three stage mass loss, as follows, see table 5.9F and figure 5.11F.

1. An increasing loss (u), between 165 and 355°C, of 62%, compared to 53% previously (see 'e' above), suggested a possible link to the model compound.

2. A decreasing mass loss (v), between 371 and 390°C, of 20% was associated with the main exotherm (p) at 374°C.

3. The final, increasing, mass loss (w) between 395 and 450°C of 6% was linked to the exotherm (q) at 420°C.

g)   100% Model : Mass loss occurred in two stages, the majority of which was lost between 225 and 395°C (u) representing 88% of the total with the production of a large exotherm (m) at 359°C. The second mass loss (v) of the remaining 12% produced a smaller exotherm (n) at 530°C, see table 5.9G and figure 5.11G.

5.2.1.4.2 The Effect of Model Concentration on a 75%:25% (wt/wt) Cobalt:Sodium Phosphite Mixture.

a)   0% Model (75% Cobalt, 25% Sodium Phosphite) : This ratio produced a decomposition trace with four stages of mass loss. The first mass loss (t) of 6% was easily identified as loss of water from sodium phosphite. A second mass loss (u), which occured between 140 and 235°C, was responsible for 10.5% of the overall mass loss, with no noticable exotherm. The third mass loss (v) of 19% between 235 and 335°C produced a relatively small exotherm (m) at 307°C and the final mass loss (w) of 28% between 335 and 410°C produced a broad exotherm (n) at 406°C, see table 5.10A and figure 5.12A.

b)   10% Model (70% Cobalt, 20% Sodium Phosphite) : An addition of 10% model compound changed the mass loss trace to some degree. Mass loss occurred in possibly five stages, most of which must be associated with the decomposition of cobalt neodecanoate, see table 5.10B and figure 5.12B.

1. The most obvious loss (t) of 2% was due to water associated with sodium phosphite.

2. 9% mass loss (u) between 150 and 220°C with a small exotherm (k).

3. 17% (v) between 220 and 295°C produced a small exotherm (l) at 245°C.

Stage of Mass Loss	5% Model (A)		
	% Loss	Temp.Range (°C)	Exotherm (°C)
1	4 (t)	0-110	None
2	11 (u)	150-228	None
3	31 (v)	228-300	230(m)295(n)
4	17 (w)	300-443	320(p),340(q) 375(r)

Stage of Mass Loss	16% Model (B)		
	% Loss	Temp.Range (°C)	Exotherm (°C)
1	6 (t)	0-110	None
2	32 (u)	155-295	264 (m)
3	15 (v)	295-355	325 (n)
4	19 (w)	355-390	359 (p)

Stage of Mass Loss	33% Model (C)		
	% Loss	Temp.Range (°C)	Exotherm (°C)
1	5 (t)	0-110	None
2	26 (u)	160-305	270 (m)
3	24 (v)	305-395	349 (n)
4	18 (w)	395-410	403 (p)

Stage of Mass Loss	50% Model (D)		
	% Loss	Temp.Range (°C)	Exotherm (°C)
1	43 (u)	156-338	250 (m)
2	38 (v)	338-362	349 (p)
3	4 (w)	377-432	380 (q)

Stage of Mass Loss	67% Model (E)		
	% Loss	Temp.Range (°C)	Exotherm (°C)
1	53 (u)	169-353	250 (m) small
2	24 (v)	369-381	373 (p)
3	3 (w)	381-443	443 (q)

Stage of Mass Loss	75% Model (F)		
	% Loss	Temp.Range (°C)	Exotherm (°C)
1	62 (u)	165-355	250 (m) small
2	20 (v)	371-390	374 (p)
3	6 (w)	395-450	420 (q)

Stage of Mass Loss	100% Model (G)		
	% Loss	Temp.Range (°C)	Exotherm (°C)
1	88 (u)	225-395	359 (m)
2	12 (v)	465-550	530 (n)

Table 5.9 A Summary of the Thermograms Produced From Various Mixtures of Model I and a fixed ratio of 10% Sodium Phosphite to 90% Cobalt in an Oxygen Atmosphere at a Heating Rate of 10°C/min up to a Maximum Temperature of 550°C. Tables A to G Correspond to an Increasing Percentage of Model I in the Mixture.

4. 17 % (w) associated with the start of a broad complex exotherm. The mass loss began at 295 and ended at 380°C.

5. Finally a 16% mass loss (x), between 380 and 392°C, occurred in conjunction with the largest exotherm (n) at 391°C .

c) **18% Model (64% Cobalt, 18% Sodium Phosphite)** : 18% model produced a four stage mass loss as follows, see table 5.10C and figure 5.12C.

1. 9% (u) between 165 and 192°C with a small exotherm (k) at 170°C.

2. 13% (v) between 192 and 305°C with no exotherm.

3. The third (w) and fourth (x) mass losses were associated with a broad exotherm (m & n), the third, which occurred between 305 and 380°C produced a mass loss of 29%.

4. The fourth, and final mass loss (x), of 19% occurred between 380 and 410°C with the formation of the largest exotherm (n) at 375°C.

d) **31% Model (54% Cobalt, 15% Sodium Phosphite)** : 31% of the model compound produced a six stage mass loss as follows, see table 5.10D and figure 5.12D

1. 8% (u) between 170 and 220°C with a small exotherm at 165°C.

2. 15% (v) between 220 and 285°C with a small exotherm at 260°C.

The third, fourth and fifth mass losses were associated with a broad exotherm.

3. 11% (w) between 305 and 343°C with an exotherm at 335°C (m).

4. 8% (x) between 343 and 385°C.

5. 22% (y) corresponding to the largest exotherm (n) at 393°C between 385 and 395°C.

6. The final mass loss (z) of 6% was associated with an exotherm (p) appearing as a shoulder on the previous exotherm between 385 and 440°C peaking at 410°C.

e) **40% Model (47% Cobalt, 13% Sodium Phiosphite)** : 40% model produced a four stage mass loss as follows, see table 5.10E and figure 5.12E.

1. 6% (u) between 165 and 230 C with a small exotherm (k) at 165°C.

2. 38% (v) between 230 and 348°C with a small exotherm (l) at 255°C.

3. 24% (w) associated with the largest exotherm (n) at 355°C between 348 and 361°C.

4. 7% (x) between 355 and 445°C with a coupled exotherm (m) at 410°C.

f) **53% Model (37% Cobalt, 10% Sodium Phosphite)** : 53% model produced a two stage mass loss. The first (u) between 177 and 395°C corresponded to the production of an exotherm (m) at 354°C and a 61% mass loss. The second mass loss (v) of 14% occurred between 440 and 465°C with an exotherm (n) at 443°C, see table 5.10F and figure 5.12F.

g) **69% Model (24% Cobalt, 7% Sodium Phosphite)** : 69% model produced a three stage mass loss as follows, see table 5.10G and figure 5.12G.

1. 52% (u) between 177 and 350°C with no obvious exotherm.

2. 13% (v) between 350 and 395°C with an exotherm (m) at 388°C.

3. The final mass loss (w) of 11% produced the largest exotherm (n) at 455°C.

h) **100% Model** : Mass loss occurred in two stages, the majority of which was lost between 225 and 395°C representing 88% (u) of the total with the production of a large exotherm (m) at 395°C. The second mass loss (v) of the remaining 12% produced a smaller exotherm (n) at 530°C, see table 5.10H and figure 5.12H.

Stage of Mass Loss	0% Model (A)		
	% Loss	Temp.Range ("C)	Exotherm ("C)
1	6 (t)	0-110	None
2	10.5 (u)	140-235	None
3	19 (v)	235-335	307 (m)
4	28 (w)	335-410	406 (n)

Stage of Mass Loss	10% Model (B)		
	% Loss	Temp.Range ("C)	Exotherm ("C)
1	2 (t)	0-110	None
2	9 (u)	150-220	None
3	17 (v)	220-295	245 (l)
4	17 (w)	295-380	320 (m)
5	16 (x)	380-392	391 (n)

Stage of Mass Loss	18% Model (C)		
	% Loss	Temp.Range ("C)	Exotherm ("C)
1	9 (u)	165-192	170 (k)
2	13 (v)	192-305	None
3	29 (w)	305-380	350 (m)
4	19 (x)	380-410	375 (n)

Stage of Mass Loss	31% Model (D)		
	% Loss	Temp.Range ("C)	Exotherm ("C)
1	8 (u)	170-220	165 (k)
2	15 (v)	220-285	260 (l)
3	11 (w)	305-343	335 (m)
4	8 (x)	343-385	None
5	22 (y)	385-395	393 (n)
6	6 (z)	385-440	410 (p)

Stage of Mass Loss	40% Model (E)		
	% Loss	Temp.Range ("C)	Exotherm ("C)
1	6 (u)	165-230	165 (k)
2	38, (v)	230-348	255 (l)
3	24 (w)	348-361	355 (n)
4	7 (x)	355-445	410 (m)

Stage of Mass Loss	53% Model (F)		
	% Loss	Temp.Range ("C)	Exotherm ("C)
1	61 (u)	177-395	354 (m)
2	14 (v)	440-465	443 (n)

Stage of Mass Loss	69% Model (G)		
	% Loss	Temp.Range ("C)	Exotherm ("C)
1	52 (u)	177-350	None
2	13 (v)	350-395	388 (m)
3	11	460-490	455 (n)

Stage of Mass Loss	100% Model (H)		
	% Loss	Temp.Range ("C)	Exotherm ("C)
1	88 (u)	225-395	359 (m)
2	12 (v)	465-550	530 (n)

Table 5.10 A Summary of the Thermograms Produced From Various Mixtures of ModelI and a fixed ratio of 25% Sodium Phosphite to 75% Cobalt in an Oxygen Atmosphere at a Heating Rate of 10°C/min up to a Maximum Temperature of 550°C. Tables A to G Correspond to an Increasing Percentage of Model I in the Mixture.

5.2.1.4.3 The Effect of Model Concentration on a 50%:50% (wt/wt) Cobalt:Sodium Phosphite Mixture.

a)   **0% Model (50% Cobalt, 50% Sodium Phosphite)** : This particular ratio produced an initial mass loss (t) of 22% corresponding to loss of water which was present in the sodium phosphite. The loss of 38% (u), due to cobalt, produced a large exotherm at 303"C (p), see table 5.11A and figure 5.13A.

b)   **10% Model (45% Cobalt, 45% Sodium Phosphite)** : Mass loss occurred in two stages, 22% due to the loss of water (t) and 38% (u) corresponding to cobalt decomposition which produced an exotherm (p) at 321"C. The cobalt mass loss began at 192"C and ended at 384"C, see table 5.11B and figure 5.13B.

c)   **20% Model (40% Cobalt, 40% Sodium Phosphite)** : Again mass loss occurred in two stages. 17% mass loss (t) was ascertained to loss of water from sodium phosphite. However there was a further mass loss (u) of 40% which began at 135"C and ended at 420"C with the production a large exotherm (p) at 388"C. Some of the mass loss must have been due to the model decomposition but the mass loss only appeared as a single stage producing only one exotherm. The greater temperature range over which the mass was lost suggested some model effect, see table 5.11C and figure 5.13C.

d)   **33% Model (33% Cobalt, 33% Sodium Phosphite)** : Mass loss occurred in three stages, the first (t), of 14%, was due to loss of water. The second mass loss (u) of 52% occurred over a wide temperature range, 150-450"C, with the production of a small exotherm (m) at approximately 400"C. Finally the mass loss (v) of 5% between 450-482"C produced a sharp exotherm (p) at 453"C, see table 5.11D and figure 5.13D.

e)   **50% Model (25% Cobalt, 25% Sodium Phosphite)** : 50% model produced a three stage mass loss. An initial loss (t) of 12% was due to water from sodium phosphite. A further mass loss (u) of 61% was then produced starting at 150°C and ending at 415°C, this mass loss produced no obvious exotherm. The final mass loss (v) of 9% produced a large exotherm (p) at 443°C over a range of temperatures from 415 to 475°C, see table 5.11E and figure 5.13E.

f)   **60% Model (20% Cobalt, 20% Sodium Phosphite)** : 60% model again produced three obvious mass changes. A 6% mass loss (t) was ascertained to loss of water from sodium phosphite. This was followed by a 55% mass loss (u) beginning at 135°C to 435°C, with no obvious exotherm. The final mass loss (v) produced the only exotherm (p) at 470°C over a temperature range 435 to 500°C, see table 5.11F and figure 5.13F.

g)   **70% Model (15% Cobalt, 15% Sodium Phosphite)** : At an increased concentration of model, decomposition of the mixture still occurred in three stages. The mass loss (t), due to water, decreased to 3% but the major mass loss (u) of 76% began at 177°C and ended at 458°C with no degradation exotherm. Again the only exotherm (p), at 494°C, corresponded to the final mass loss (v) of 11% between 488 and 530°C, see table 5.11G and figure 5.13G.

h)   **100% Model** : Model alone produced a two stage mass loss. 88% was lost between 225 and 395°C (u) with the production of an exotherm (m) at 359°C. A further 12% (v) was lost producing a higher temperature exotherm (n) at 530°C, see table 5.11H and figure 5.13H.

Stage of Mass Loss	0% Model (A)		
	% Loss	Temp.Range (C)	Exotherm (°C)
1	22 (t)	0-110	None
2	38 (u)	200-340	303 (p)

Stage of Mass Loss	10% Model (B)		
	% Loss	Temp.Range (°C)	Exotherm (°C)
1	22 (t)	0-110	None
2	38 (u)	192-384	321 (p)

Stage of Mass Loss	20% Model (C)		
	% Loss	Temp.Range (°C)	Exotherm (°C)
1	17 (t)	0-110	None
2	40 (u)	135-420	388 (p)

Stage of Mass Loss	33% Model (D)		
	% Loss	Temp.Range (°C)	Exotherm (°C)
1	14 (t)	0-110	None
2	52 (u)	150-450	400 (m) small
3	5 (v)	450-482	453 (p)

Stage of Mass Loss	50% Model (E)		
	% Loss	Temp.Range (°C)	Exotherm (°C)
1	12 (t)	0-110	None
2	61 (u)	150-415	None
3	9 (v)	415-475	443 (p)

Stage of Mass Loss	60% Model (F)		
	% Loss	Temp.Range (°C)	Exotherm (°C)
1	6 (t)	0-110	None
2	55 (u)	135-435	None
3	12 (v)	435-500	470 (p)

Stage of Mass Loss	70% Model (G)		
	% Loss	Temp.Range (°C)	Exotherm (°C)
1	3 (t)	0-110	None
2	76 (u)	177-458	None
3	11 (v)	488-530	494 (p)

Stage of Mass Loss	100% Model (H)		
	% Loss	Temp.Range (°C)	Exotherm (°C)
1	88 (u)	225-395	359 (m)
2	12 (v)	465-550	530 (n)

Table 5.11 A Summary of the Thermograms Produced From Various Mixtures of Model I and a fixed ratio of 50% Sodium Phosphite to 50% Cobalt in an Oxygen Atmosphere at a Heating Rate of 10°C/min up to a Maximum Temperature of 550°C. Tables A to G Correspond to an Increasing Percentage of Model I in the Mixture.
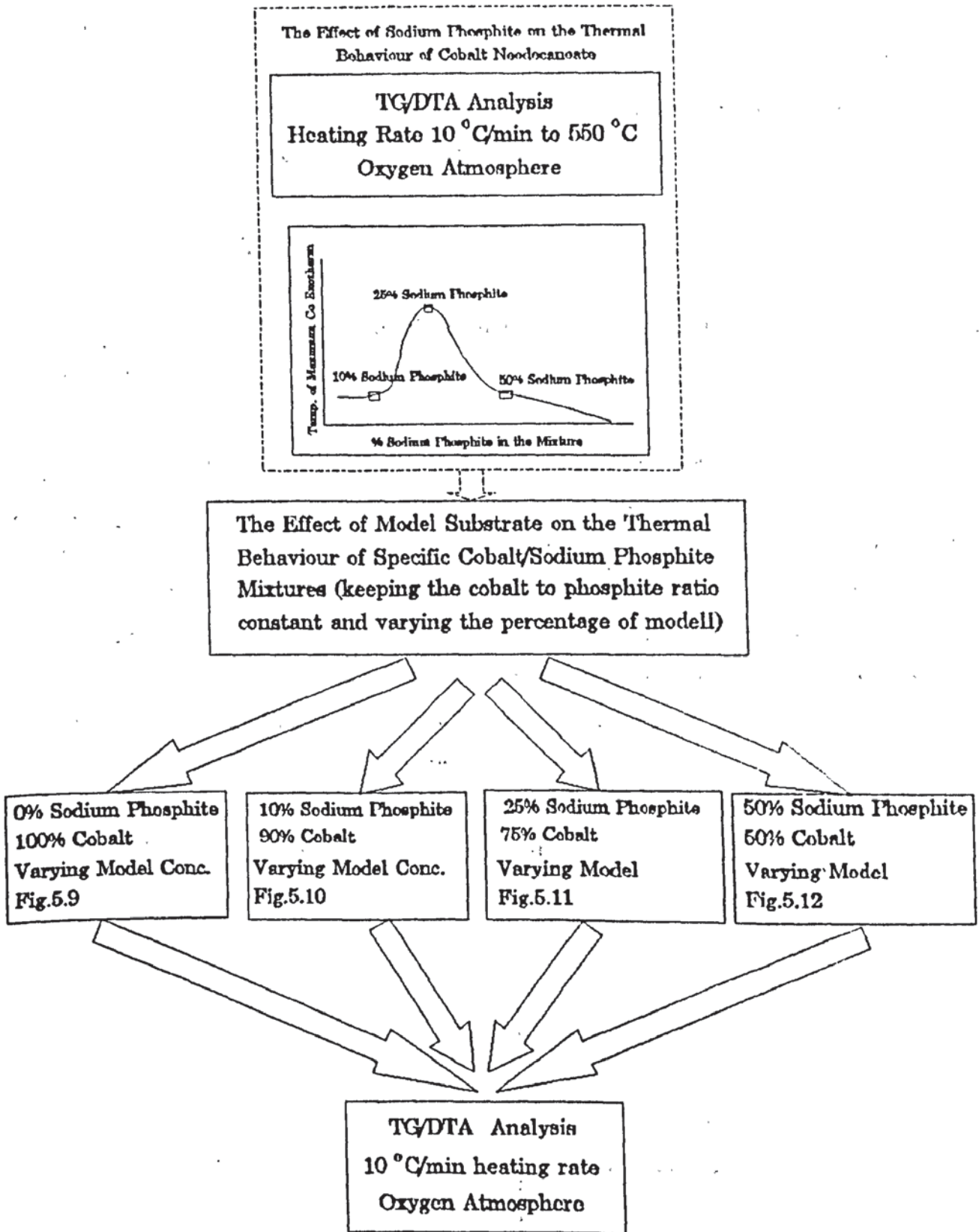
Scheme 5.3 Experimental Outline for the Investigation of the Effect of Model Substrate on the Thermal Behaviour of Specific Cobalt/Sodium Phosphite Mixtures.

5.2.2 The Interaction Between Cobalt and Sodium Phosphite : An Electrochemical Study by Cyclic Voltammetry.

5.2.2.1 The Study of Cobalt Neodecanoate (Cobalt(II) Salt).

Cyclic voltammetry was used to study the electrochemistry of the cobalt(II) salt, typically the potential of the oxidation-reduction reaction,

$$Co^{2+} \xrightleftharpoons[+e]{-e} Co^{3+}$$
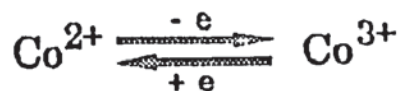
and the effect of the presence of sodium phosphite and model compound on these potentials.

Figure 5.14 shows the cyclic voltammogram of cobalt neodecanoate (cobalt(II)) in methanol using tetrabutylammonium hydrogen sulphate as the electrolyte solution with a platinum working electrode and calamel reference. From a series of experiments (figure 5.14) it became apparent that the oxidation of the cobalt(II) salt is occuring in the same potential region as the solvent breakdown. The current likely to be produced ($\sim 0.0004A$) was so small that it could not be seen over the breakdown of the solvent. Further experiments were conducted using DMSO as the solvent instead of methanol but still its breakdown occured too early masking the region of interest (use of the solvent is also limited to the solubility of the model and sodium phosphite). Failing to find any other suitable solvent, the results to be gained from cyclic voltammetry would therefore be very limited.
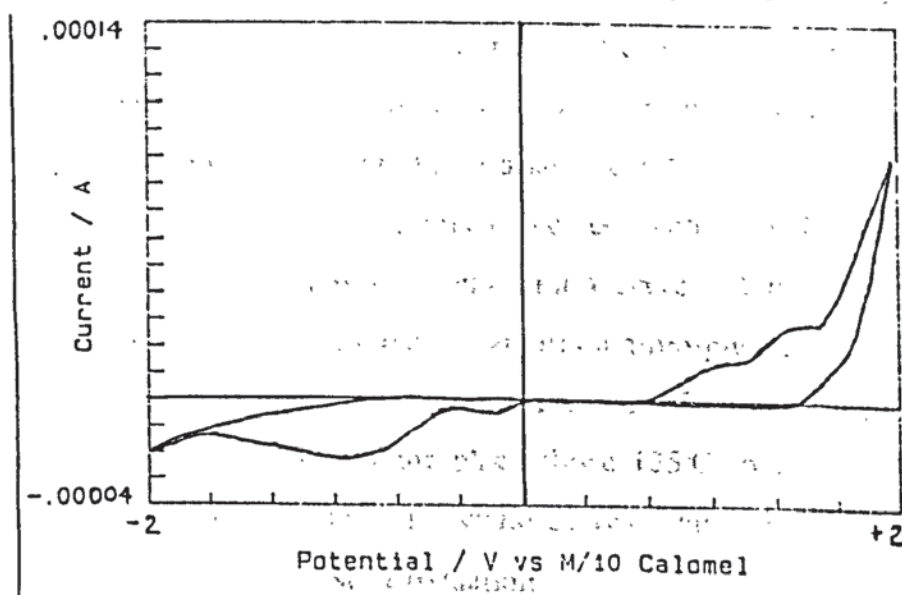
Figure 5.14 The Cyclic Voltammogram of Cobalt Neodecanoate in DMSO.

5.3 Discussion.

5.3.1 The Thermal Behaviour of Cobalt Neodecanoate and Sodium Phosphite.

The work described in this chapter was initially concerned with the oxidative thermal decomposition of cobalt neodcanoate and the effect of additions of sodium phosphite on the behaviour of cobalt. Chapters 3 and 4 discussed the possibility of the cobalt (cobalt neodecanoate) catalysing the oxidative thermal degradation of the two model compounds which represent the polyamide, MXD6. The results showed that a range of cobalt concentrations (50-800ppm) increased the oxidation of the readily oxidisable model I, at 150°C, to a small degree but failed to increase the oxidation of model II, at 190°C. However, in the presence of 1000ppm sodium phosphite (with respect to the model) additions of cobalt, particularly at concentrations above 50ppm, was found to increase the oxidation of the model compound (to a greater extent in model I). In the absence of cobalt, however, the sodium phosphite acted as an antioxidant.

Results shown in chapters 3 and 4 therefore suggested that either sodium phosphite was having some influence on the cobalt neodecanoate as well as the model compound or that the cobalt was merely overcoming the inhibiting effect of the sodium phosphite and then proceeded to catalyse the oxidation of the model. Experiments presented in this chapter were therefore designed to investigate the possible influence of sodium phosphite on cobalt neodecanoate, by TG/DTA analysis, during the oxidation of the model. Initially the decomposition of the two individual components were assessed by TG/DTA analysis in both argon and oxygen atmospheres (section 5.2.1). These results revealed that in an atmosphere of oxygen, cobalt neodecanoate produced a large exothermic heat change, as opposed to an endothermic reaction in argon, this coincided with a 90% weight loss due to its decomposition. The onset of this decomposition decreased by 170°C, compared to the decomposition of cobalt neodecanoate in an argon atmosphere, ie, decreased from 295°C in argon to 125°C in oxygen, see figures 5.1A & B. This can suggest that any reaction involving cobalt neodecanoate, taking place above 125°C, will subsequently result in the decomposition of the cobalt salt. This would decrease any possible ability, the cobalt salt may have, to behave as catalyst of oxidation.

This can therefore explain the results described in chapters 3 and 4, whereby additions of cobalt (at all concentrations) in the absence of sodium phosphite, failed to dramatically increase the oxidation of the readily oxidisable model compound, see chapters 3 and 4, figures 3.1 and 4.1 respectively. The failure to behave as a catalyst was even more obvious during the oxidation of model II (fig 4.1) which was carried out at a higher temperature (190°C) than that used for model I (150°C) which may be, in part, due to the higher cobalt decomposition in the former case.

5.3.2 The Effect of Sodium Phosphite on the Thermal Behaviour of Cobalt Neodecanoate.

The important features to be analysed, therefore, of the thermograms produced from the TG/DTA analysis of various cobalt/sodium phosphite mixtures, section 5.2.1.1., would be the onset temperatures at which the cobalt neodecanoate begins to decompose, ie, lose weight. Table 5.12 summarises the temperatures at which the maximum cobalt exotherm occurs (shaded in fig.5.4) in each mixture together with the temperature at which the mass loss associated with this exotherm also occurs. This provides an indication of the temperature at which final decomposition of the cobalt neodecanoate takes place. It appears that sodium phosphite is more effective at certain concentrations than others, i.e 20% and 35%. With sodium phosphite present at these percentages in the mixture, the maximum cobalt exotherm is increased from 274°C to 406 and 400°C respectively, with an associated mass loss onset temperature increase from 125°C to 335 and 360°C respectively, see figure 5.15. However, these two additions of sodium phosphite also increased the temperature range over which the cobalt decomposed (table 5.12, and figure 5.16). Decomposition of the cobalt became more 'drawn' out with sodium phosphite present at 20% and 35% (figure 5.16), which may explain the formation of a series of exothermic peaks as opposed to a single sharp exotherm for cobalt alone. The series of exotherms may arise from the loss of the ester groups initially before forming the cobalt oxide which will also decompose finally.

Table 5.12 also provides a summary of the temperatures at which the initial decomposition of cobalt begins to occur and the temperature range over which the total weight loss occurs.

The results suggest that not only does sodium phosphite increase the maximum cobalt exotherm, i.e final stage of decomposition (as discussed previously in section 5.2.1.1 and above) but also increases the onset temperature of the weight loss associated with this decomposition, see figure 5.15 and 5.16. In effect this confirms the stabilising effect of the sodium phosphite on cobalt neodecanoate. Sodium phosphite prolongs the temperature at which the major cobalt decomposition takes place.

% Sodium Phosphite	Temp.of Maximum Cobalt Exotherm (shaded)	Onset temp.of wt. loss associated with the maximum cobalt exotherm (u,v,w or y)	Onset temp. of initial cobalt weight loss (u)	Temperature range of total weight loss (u-[v,w or y])
0	274	125	125	125-285
15	309	250	135	135-375
20	406	335	140	140-410
35	400	360	160	160-405
50	303	295	200	200-340
90	309	250	250	250-355
95	304	260	260	260-350

Table 5.12 A Summary of the Exotherm Temperature and Onset Temperatures of Weight Loss Due to Cobalt Neodecanoate Decomposition in Various Mixtures of Cobalt Neodecanoate and Sodium Phosphite During TG/DTA Analysis at a Heating Rate of 10°C/min in an Oxygen atmosphere (data extracted from figure 5.4).

The possibility of sodium phosphite behaving as a stabiliser for cobalt neodecanoate is an important finding with regards to the results of the oxidation of model I and model II described in chapters 3 and 4. In theory, particularly in the oxidation study of model I, which was carried out at 150°C, the cobalt neodecanoate would not begin decomposing at this temperature providing sodium phosphite was present to some degree. Hence the cobalt would be stable enough to act as a catalyst for the oxidation of the model.

5.3.3. The Effect of Modell on the Thermal Behaviour Of Various Cobalt Neodecanoate, Sodium Phosphite Mixtures.

Unfortunatlely, due to experimental limitations, similar concentrations of the model, with respect to the sodium phosphite and cobalt, used in the oxidation study of model I (described in chapter 3) could not be used here, i.e 1 part model to 0.001 part cobalt and sodium phosphite. However by increasing the model concentration, with respect to fixed specific cobalt/sodium phosphite mixture, it was hoped that an increasing trend could be achieved giving a reasonable estimate to the results that could be expected using a 'real' concentration of the compound (as used in chapters 3 & 4). Again, similarly to the effect of sodium phosphite upon cobalt neodecanoate, of main interest would be the effect of increasing model on the overall onset temperature of the weight loss due to the cobalt decomposition. However, with three constituents now present in the mixture, the onset of this weight loss was hard to define ie, it became difficult to ascertain whether the mass loss taking place was due to the model or the cobalt or a combination of both. The only definite characteristic that could be indenitified from these thermograms (figs.5.10, 5.11, 5.12, 5.13) was the exotherm (shaded) due to the final decomposition stage of cobalt neodecanoate. This still, however, provided a secondary indication to the stability of the cobalt neodecanoate. The temperature of this exotherm, from the three mixtures of cobalt/sodium phosphite (11%,23% & 50% phosphite) and 0% sodium phosphite (100% cobalt), with varying model concentration was plotted and is shown in figure 5.17

Basically the results showed that an increase in the amount of model compound in all mixtures of cobalt/sodium phosphite, increased the temperature at which the final decomposition stage of cobalt took place. The higher the percentage of sodium phosphite in the mixture the greater the temperature of the final decomposition. This suggests, therefore, that the model compound, with increasing concentration, further prolongs the temperature at which final decomposition of cobalt neodecanoate takes place.

In attempt to try and translate these results to those of the oxidation of the model compounds, a 50%, 50% mixture of cobalt to sodium phosphite is taken as an example. In the presence of 50% sodium phosphite the initial decomposition of cobalt was prolonged by 75°C (table 5.12), in the model substrate results suggest that large amounts of model added to this mixture further increased the stabilisation of cobalt or prolonged the decomposition of cobalt. In relationship to the oxidation of model I, at 150°C, this 50:50 mixture of cobalt to sodium phosphite represents 1000ppm sodium phosphite and 200ppm cobalt in the model. A comparison, therefore, of the effect of 200ppm cobalt on the oxidation of model I, with and without sodium phosphite is related to the effect of sodium phosphite on cobalt neodecanoate in a 50%/50% mixture, see table 5.13.

Oxidation study of model I, at 150°C, in the presence of 200ppm cobalt, with and without sodium phosphite.	TG/DTA study of a 50%:50% mixture of cobalt:sodium phosphite
200ppm cobalt slightly increased the oxidation of model I, see figure 3.2	In the absence of sodium phosphite cobalt began decomposing at 125°C, with 90% decomposition at 285°C, see figure 5.1.
200ppm cobalt greatly increased the oxidation of model I in the presence of 1000ppm sodium phosphite, see figure 3.4	In the presence of sodium phosphite cobalt decomposition began at 200°C, with 90% decomposition at 340°C, see figure 5.4E.
Model I + 200ppm cobalt + sodium phosphite absorbed a similar amount of oxygen to Model I + 200ppm cobalt (c.f figures 3.4 and 3.2)	Increasing concentrations of model I was shown to indirectly stabilise the decomposition of cobalt neodecanoate, see figure 5.17.

Table 5.13 A Comparison of the Effect of 200ppm Cobalt on the Oxidation of Model I (with and without 1000ppm sodium phosphite) and the Effect of Sodium Phosphite on the Decomposition of Cobalt Neodecanoate, in a similar ratio.

Several conclusions can be drawn from the comparision of the oxidation sudies and the TG/DTA results :-

1) Cobalt is able to act as a catalyst for the oxidation of model I (at 150°C), due to the stabilising effect of the model on the cobalt neodecanoate, which increases the temperature at which it decomposes. In the absence of the model compound, cobalt begins to decompose at 125°C.

2) In the presence of 1000ppm sodium phosphite the cobalt is further stabilised, decomoposition occuring initially at 200°C. This increased stabilisation is however not apparent in the oxidation of model I due to temperature at which oxidation is taking place (150°C), since the oxidation is taking place at a lower temperature than that which is required for cobalt decomposition. However if oxidation was carried out at higher temperatures the stabilising effect of sodium phosphite upon the cobalt would become more apparent with increased oxidation in comparison to model+200ppm cobalt in the absence of sodium phosphite.

The analysis of the TG/DTA results were compared with the oxidation of model II in the same way as model I, above.

Oxidation study of model II, at 190°C, in the presence of 200ppm cobalt, with and without sodium phosphite.	TG/DTA study of a 50%:50% mixture of cobalt:sodium phosphite
200ppm cobalt failed to increase the oxidation of model II, see figure 4.2.	In the absence of sodium phosphite cobalt began decomposing at 125°C, with 90% decomposition at 285°C, see figure 5.1.
200ppm cobalt slightly increased the oxidation of model II in the presence of 1000ppm sodium phosphite, see figure 4.4.	In the presence of sodium phosphite cobalt decomposition began at 200°C, with 90% decomposition at 340 C, see figure 5.4E.
Model II + 200ppm Cobalt + sodium phosphite absorbed slightly more oxygen than Model I + 200ppm Cobalt, c.f figures 3.4 and 3.2.	Increasing concentrations of model I was shown to indirectly stabilise the decomposition of cobalt neodecanoate, see figure 5.17.

Table 5.14 A Comparison of the Effect of 200ppm Cobalt on the Oxidation of Model I (with and without 1000ppm sodium phosphite) and the Effect of Sodium Phosphite on the Decomposition of Cobalt Neodecanoate, in similar ratios.

Several conclusions can be drawn from the comparision of the oxidation studies of model II and the TG/DTA results :-

1) Cobalt failed to increase the oxidation of model II at 190 C, this may be due to the fact that the cobalt may have already proceeded to decompose at this temperature, even after a slight stabilisation effect by the model compound on the cobalt.

2) In the presence of sodium phosphite the cobalt increases the oxidation of the model compound. This may be due to the stabilisation effect of sodium phosphite on the cobalt which extends the temprature at which the cobalt begins to decompose. In this particular example the onset of decomposition is increased to 200°C (and probably increased further in the presence of model II). Since the oxidation of model II occurs at 190°C, the cobalt should be present in the pre-decomposition stage. It is made more apparent by carrying out the oxidation at this higher temperature of the effect of the increased stabilising effect of sodium phosphite on cobalt which was not so apparent in the oxidation study of model I (at 150°C).

In summary therefore, it is apparent from the thermograms of the various cobalt neodecanoate/sodium phosphite mixtures that sodium phosphite influences the decomposition of the cobalt in two instances :-

a)   the final onset temperature of the initial decomposition of the cobalt neodecanoate, i.e the initial temperature at which mass loss due to cobalt decomposition first occurs and,

b)   the temperature at which the final decomposition of cobalt occurs, which is reflected in the production of a large (maximum) exotherm.

Increasing the percentage of sodium phosphite in the mixture was shown to increase the onset temperature at which initial degradation of the cobalt neodecanoate took place. The effect, however, on the final decomposition of the cobalt was more complex and probably warrants further investigation to fully understand the results achieved. The revelance of the results obtained, to the oxidation of the model compounds however is not particularly important due to the fact that the sodium phosphite is affecting the cobalt, in this instance, during the later stages of decomposition i.e at temperatures > 300°C. The oxidation of models I and II is concerned with the state of the cobalt neodecanoate at 150°C and 190°C respectively. The presence of sodium phosphite increases the onset temperature for the degradation of cobalt neodecanoate beyond these temperatures, whereas in the absence of sodium phosphite the cobalt is likely to decompose during the oxidation of model II, and to a lesser extent, during the oxidation of model I.

It seems therefore that the sodium phosphite does not change the way in which cobalt affects the oxidation of the model compounds but merely stabilises the cobalt to an extent that it is present in the form as it was when added to the model ie, sodium phosphite ensures that the structure of the cobalt is not altered during the oxidation process enabling the cobalt source to act upon the oxdation of model I and model II. From the evidence obtained in chapters 3 and 4, oxidation of models I and II suggest that cobalt acts to catalyse the decomposition of the hydroperoxides ie, as a propagation catalyst.
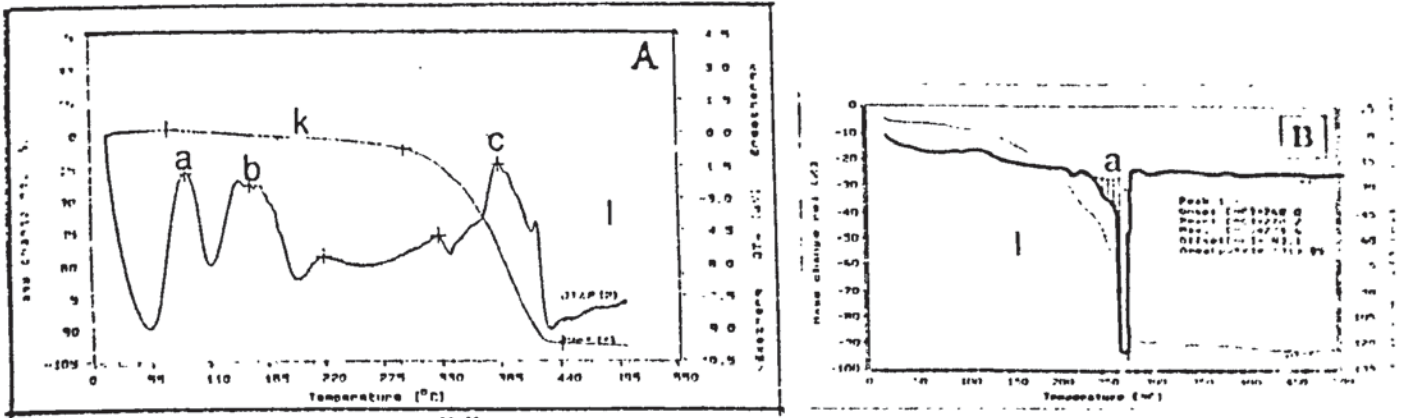
Figure 5.1 The Thermogram of Cobalt Neodecanoate in A) Argon and B) Oxygen at a Heating Rate of 10°C/min up to a Maximum Temperature of 550°C.
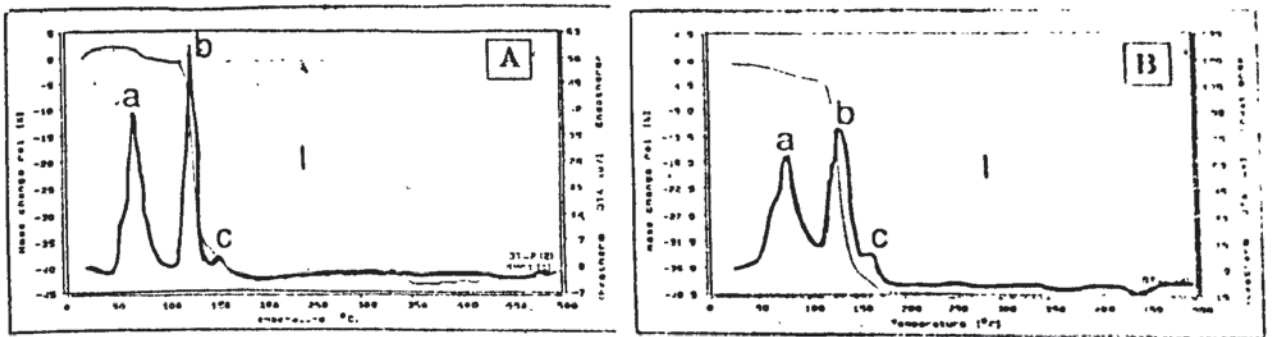
Figure 5.2 The Thermogram of Sodium Phosphite in A) Argon and B) Oxygen at a Heating Rate of 10°C/min up to a Maximum Temperature of 550°C.
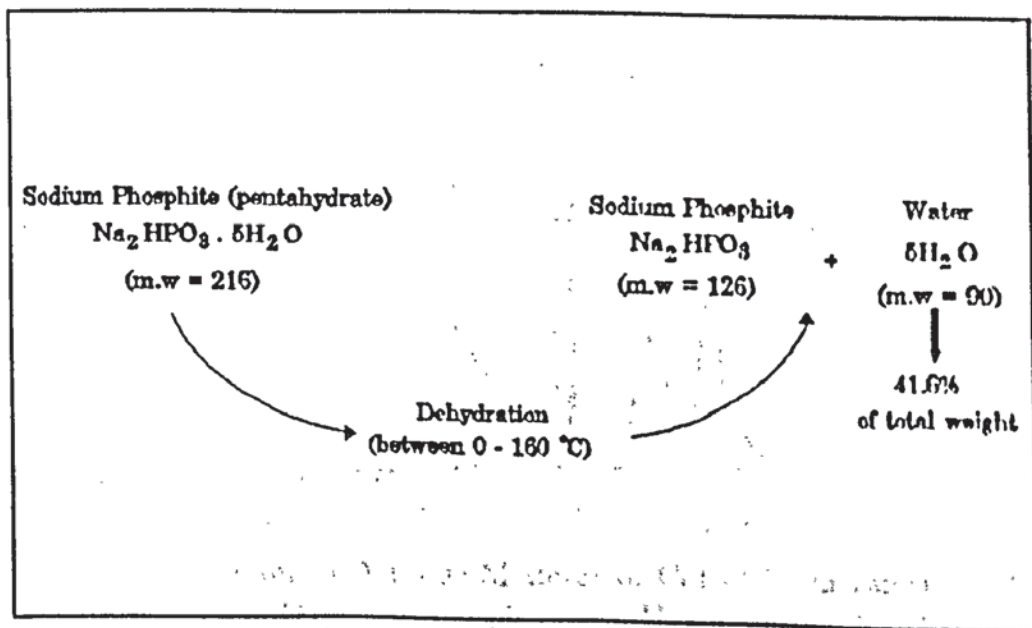
Figure 5.3 The Structure of Sodium Phosphite, Indicating the Percentage of Water Contained Within the Compound.
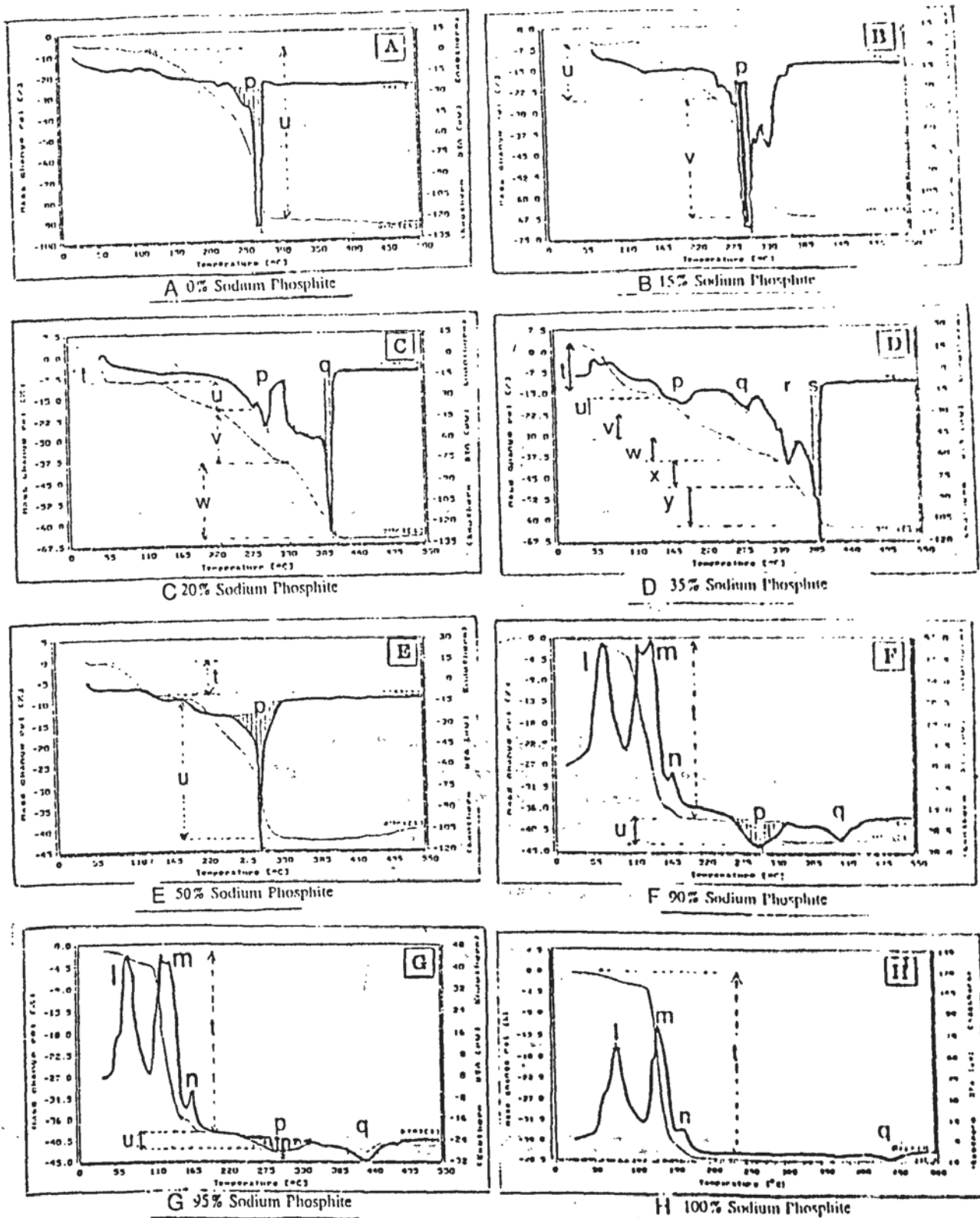
Figure 5.4 The Thermograms of Various Mixtures of Cobalt Neodecanoate and Sodium Phosphite in an Oxygen Atmosphere at a Heating Rate of 10°C/min up to a Maximum Temperature of 550°C. Figures A to G Correspond to an Increasing Percentage of Sodium Phosphite in the Mixture.
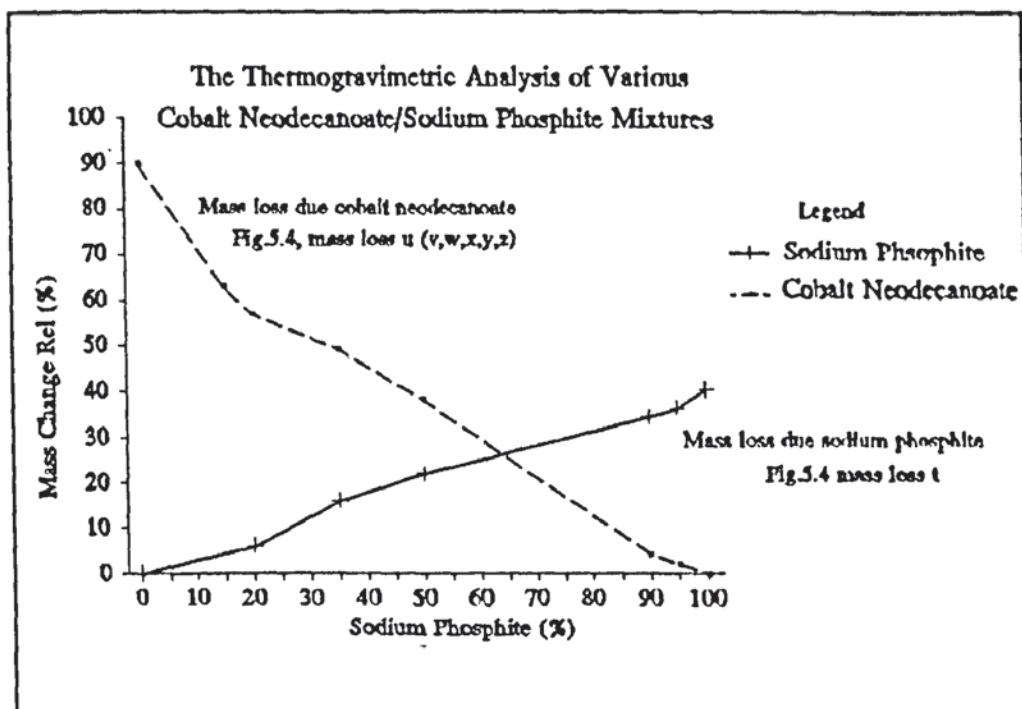
Figure 5.5 The Mass Loss Associated with the Decomposition of Sodium Phosphite and Cobalt Neodecanoate During the Thermal Analysis of a Series of Mixtures of the Two Components at a Heating Rate of 10°C/min (up to a Maximum Temperature of 550°C) in an Oxygen Atmosphere.
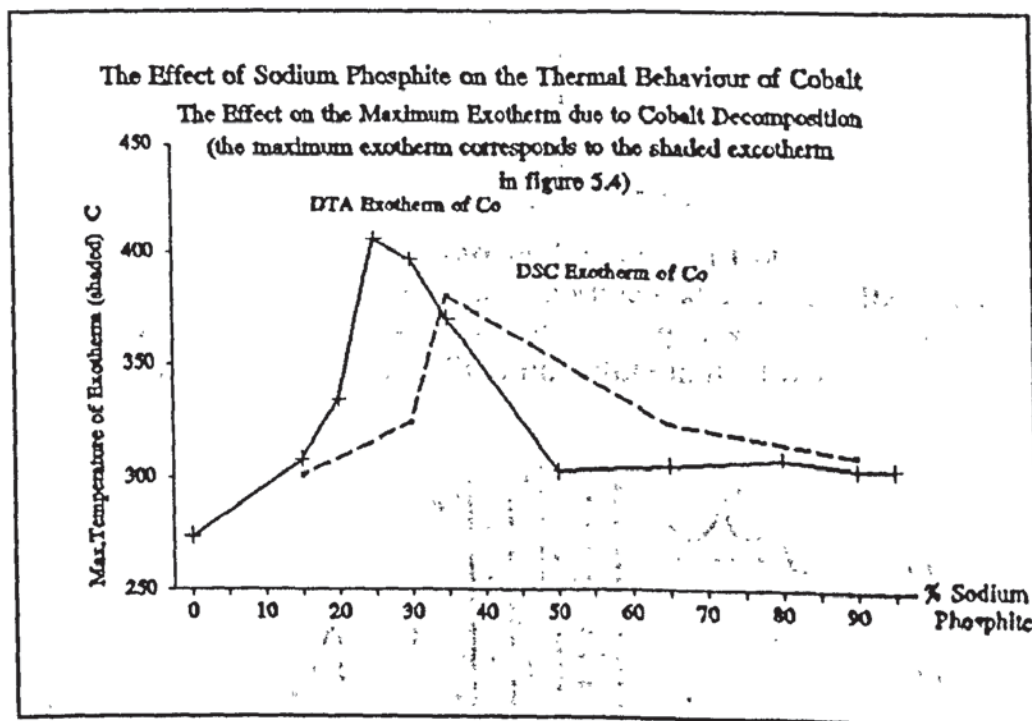
Figure 5.6 The Temperature of the Exotherm Corresponding the the Final Decomposition of Cobalt Neodecanoate During the Thermal Analysis of a Series of Mixtures Containing Cobalt Neodecanoate and an Increasing Percentage of Sodium Phosphite (analysed by both DTA and DSC).
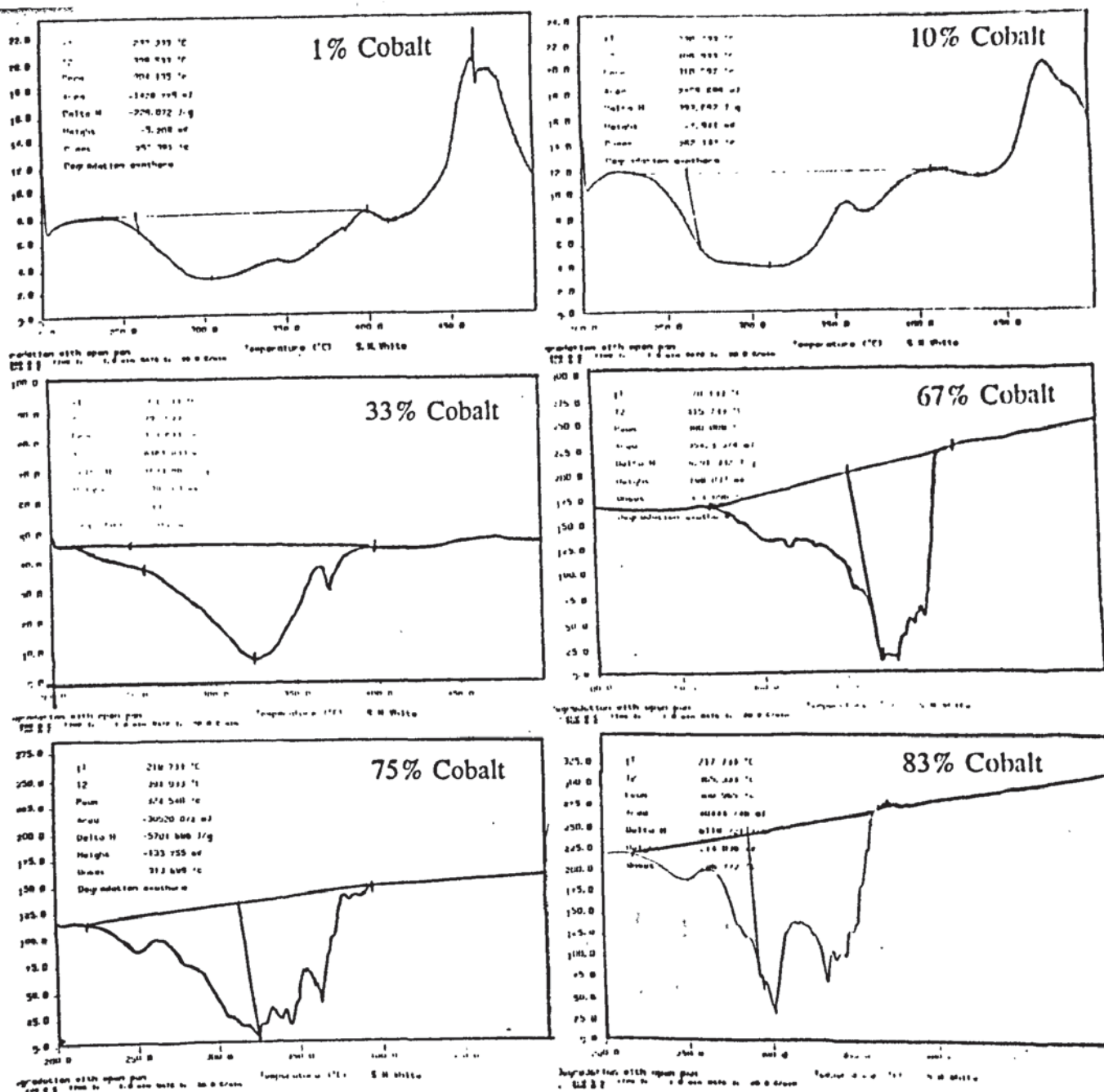
Figure 5.7 The DSC Thermograms of Various Mixtures of Cobalt Neodecanoate and
Sodium Phosphite in an Oxygen Atmosphere at a Heating Rate of 10°C/min up
to a Maximum Temperature of 550°C. Figures A to G Correspond to an
Increasing Percentage of Sodium Phosphite in the Mixture.
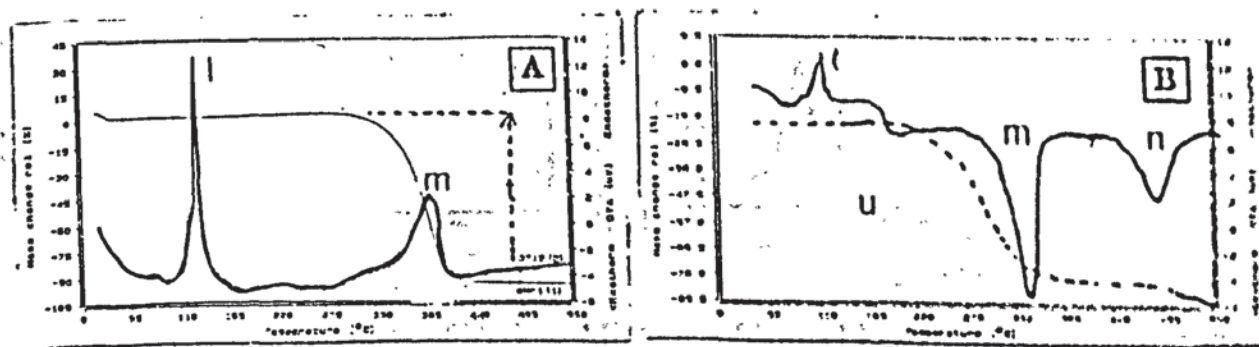
Figure 5.8 The Thermogram of Model I in A) Argon and B) Oxygen at a Heating Rate of
10°C/min up to a Maximum Temperature of 550°C.

A. 100% Model

B. 90% Model

C. 85% Model

D. 65% Model

E. 50% Model

F. 35% Model

G. 15% Model

H. 0% Model
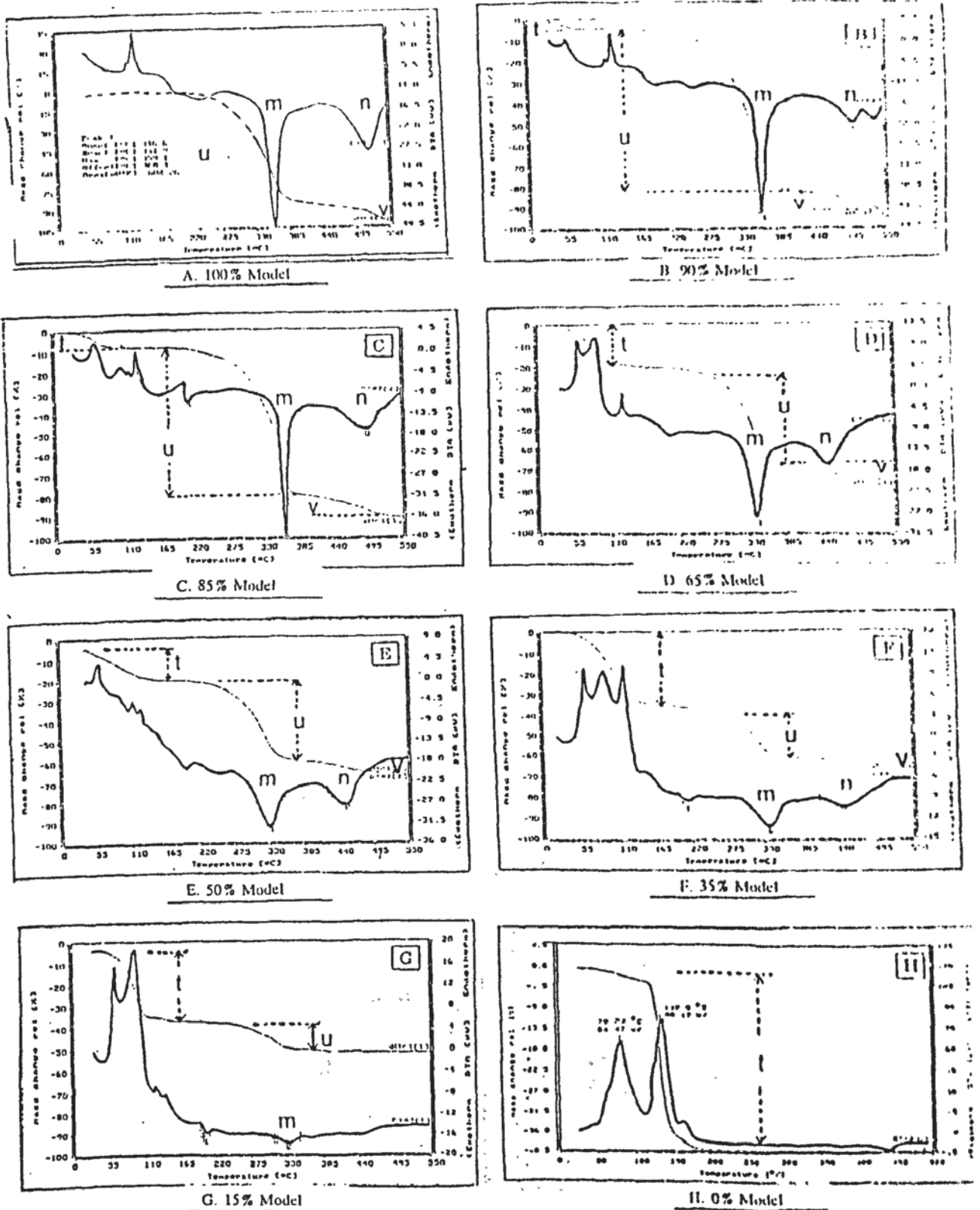
Figure 5.9 The Thermograms of Various Mixtures of Model I and Sodium Phosphite in an Oxygen Atmosphere at a Heating Rate of 10°C/min up to a Maximum Temperature of 550°C. Figures A to G Correspond to an Increasing Percentage of Sodium Phosphite in the Mixture.
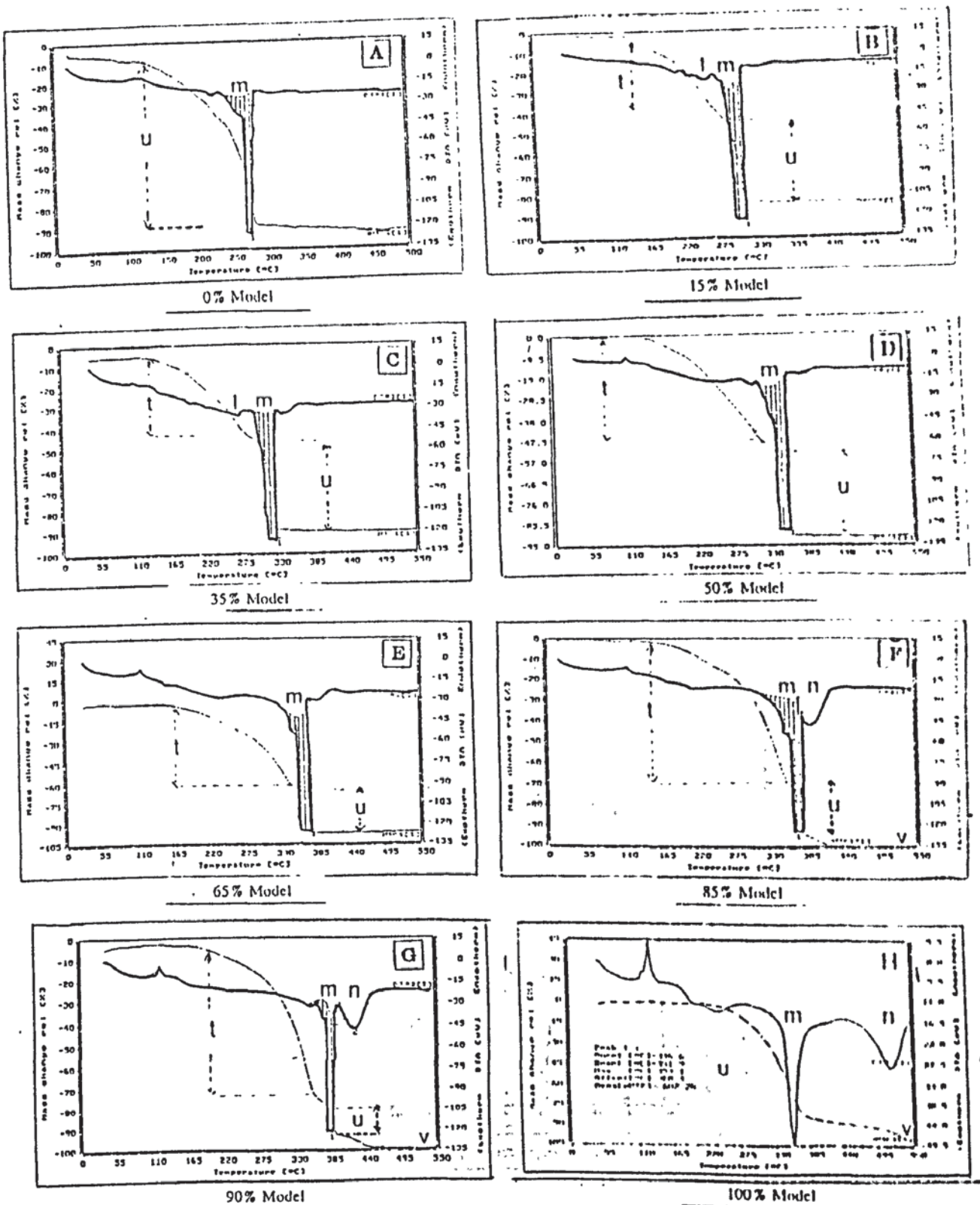
Figure 5.10 The Thermograms of Various Mixtures of Cobalt Neodecanoate and Model I in an Oxygen Atmosphere at a Heating Rate of 10°C/min up to a Maximum Temperature of 550°C. Figures A to G Correspond to an Increasing Percentage of Model I in the Mixture.

A. 5% Model

B 16% Model

C. 33% Model

D 50% Model

E. 67% Model

F. 75% Model

G. 100% Model
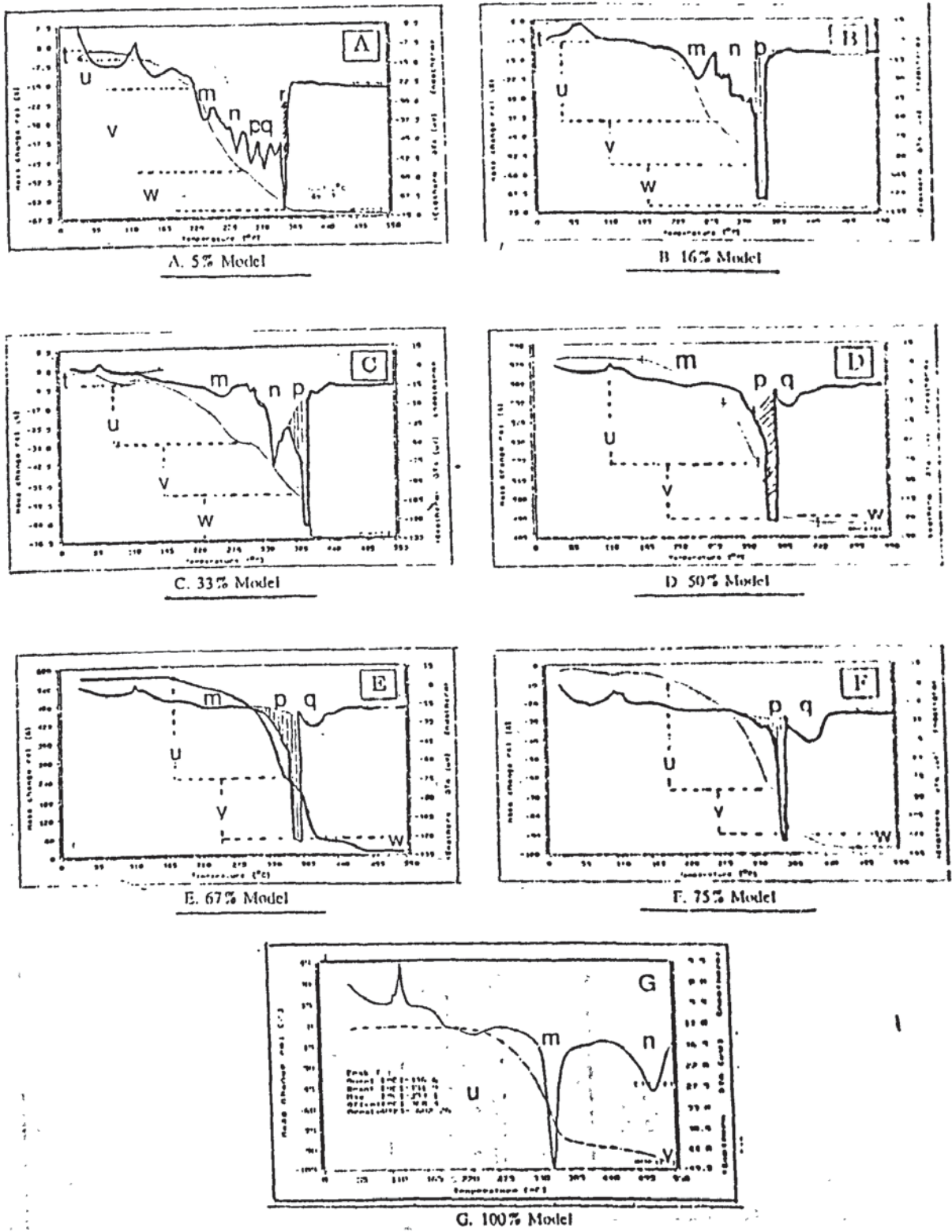
Figure 5.11 The Thermograms of Various Mixtures of Model I and a fixed ratio of 10% Sodium Phosphite to 90% Cobalt in an Oxygen Atmosphere at a Heating Rate of 10°C/min up to a Maximum Temperature of 550°C. Figures A to G Correspond to an Increasing Percentage of Model I in the Mixture.
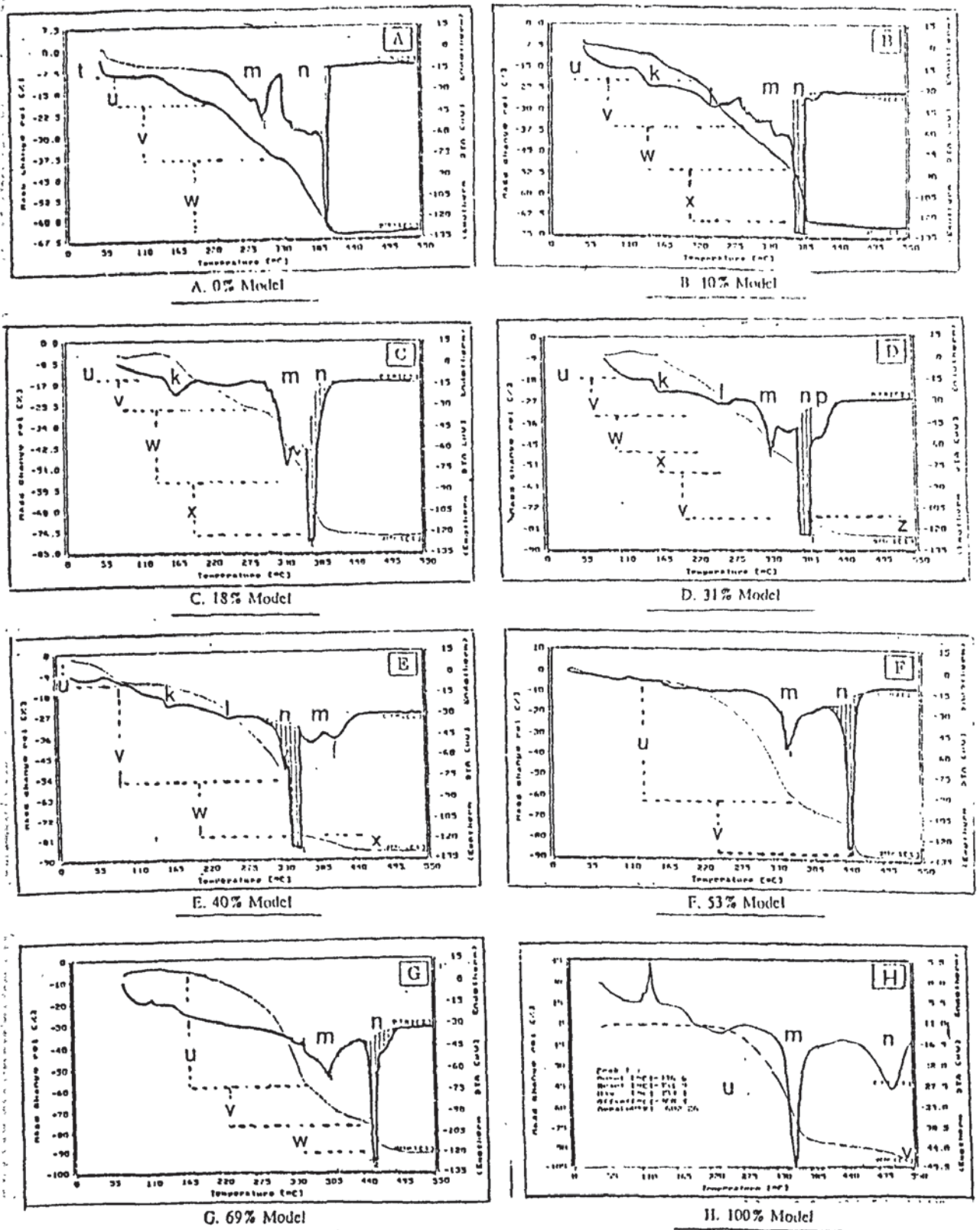
Figure 5.12 The Thermograms of Various Mixtures of Model I and a fixed ratio of 25% Sodium Phosphite to 75% Cobalt in an Oxygen Atmosphere at a Heating Rate of 10°C/min up to a Maximum Temperature of 550°C. Figures A to G Correspond to an Increasing Percentage of Model I in the Mixture.
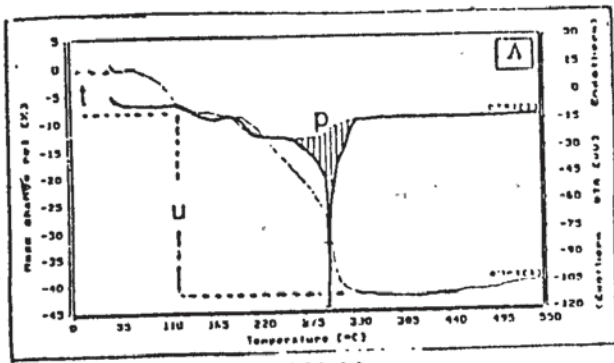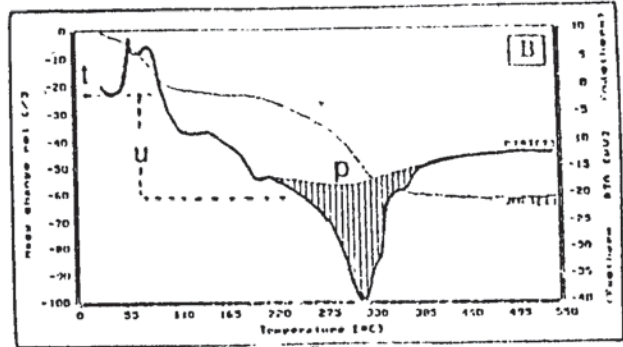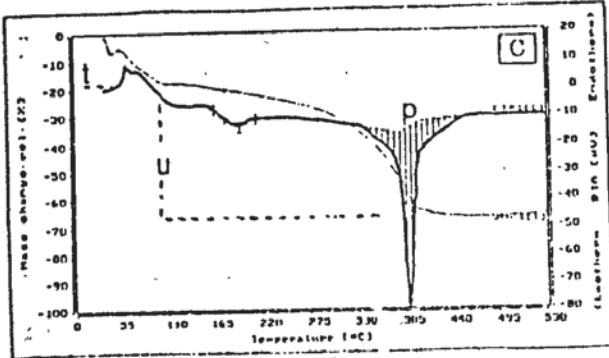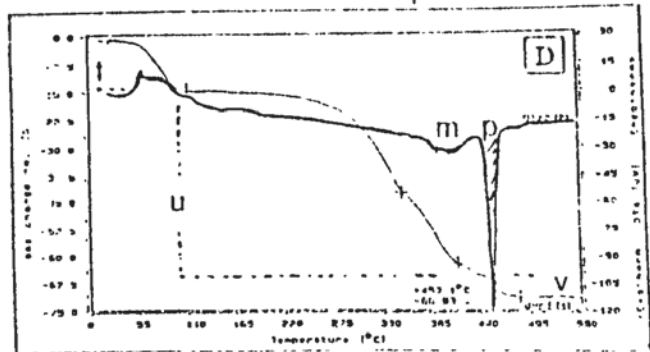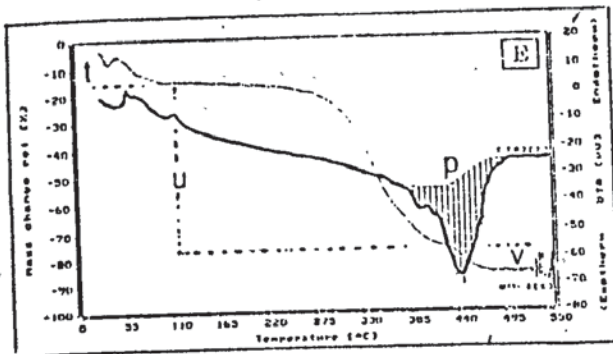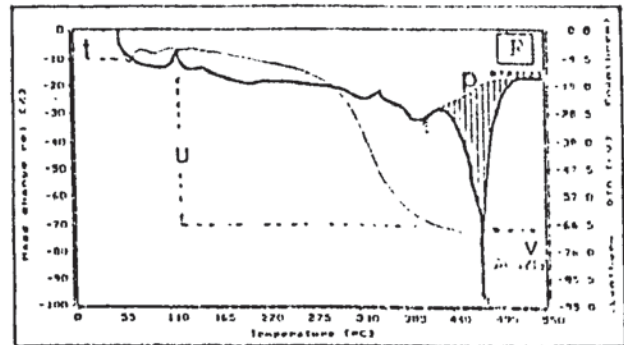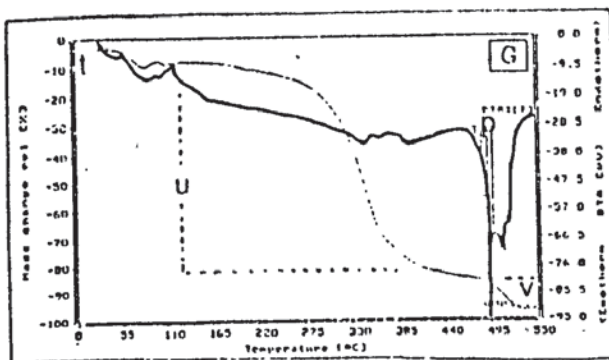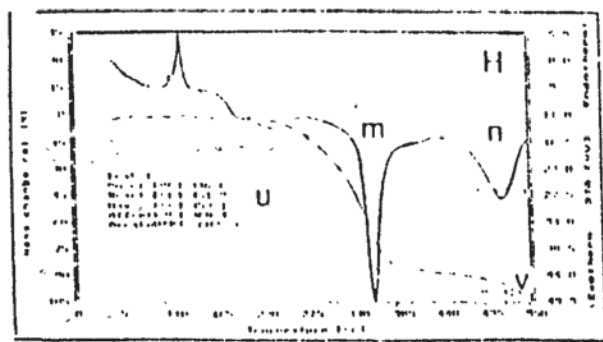
Figure 5.13 The Thermograms of Various Mixtures of Model 1 and a fixed ratio of 50% Sodium Phosphite to 50% Cobalt in an Oxygen Atmosphere at a Heating Rate of 10°C/min up to a Maximum Temperature of 550°C. Figures A to G Correspond to an Increasing Percentage of Model I in the Mixture.
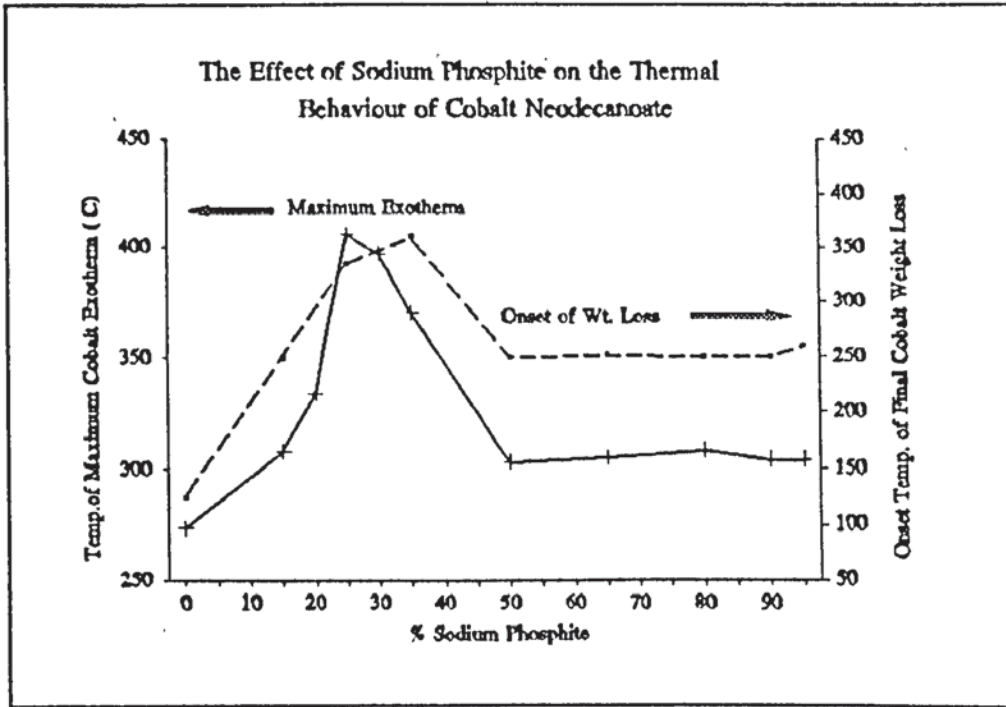
Figure 5.15 The Temperature of the Exotherm (and the Onset Temperature of the Weight Loss Associated with this Exotherm) Corresponding the the Final Decomposition of Cobalt Neodecanoate During the Thermal Analysis of a Series of Mixtures Containing Cobalt Neodecanoate and an Increasing Percentage of Sodium Phosphite (Data taken from fig.5.4 & Table 5.12).
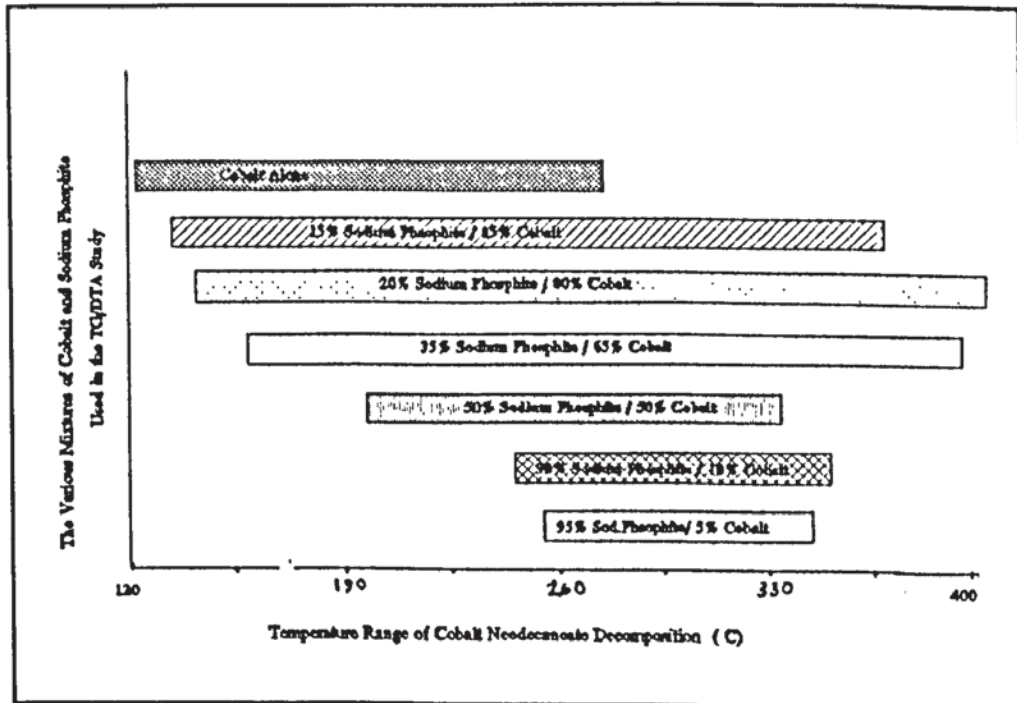
Figure 5.16 The Decomposition Range of Cobalt Neodecanoate During the Thermal Analysis of a Series of Mixtures Containing Cobalt Neodecanoate and an Increasing Percentage of Sodium Phosphite (Data taken from fig.5.4 & Table 5.12).

The Effect of ModelI on the Thermal Behaviour of Specific
Sodium Phosphite/ Cobalt Neodecanoate Mixtures.
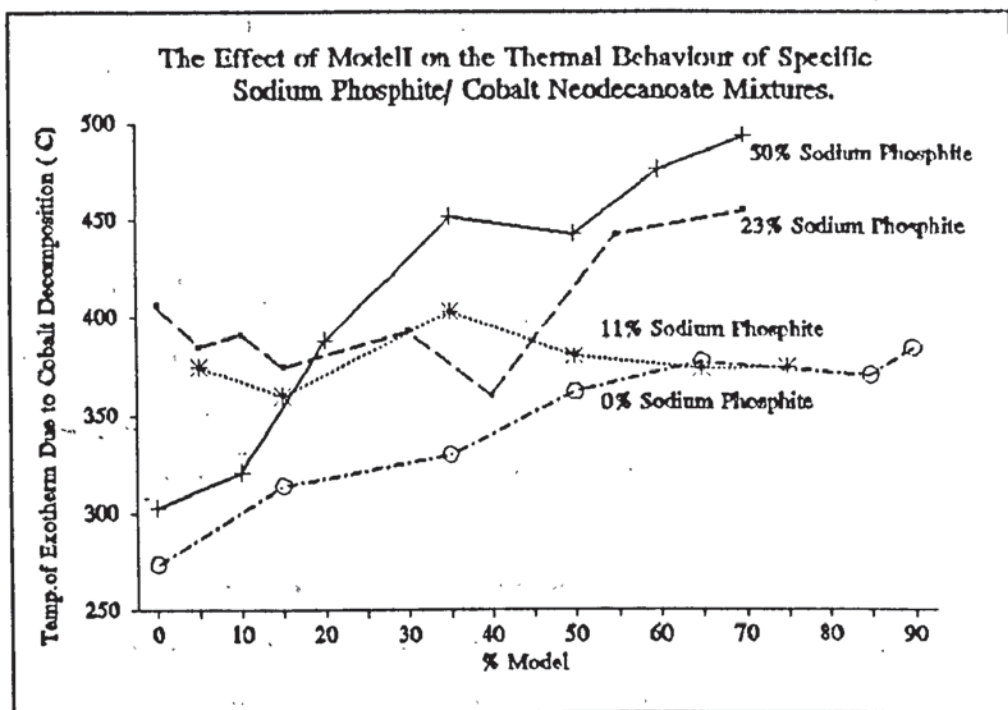
Figure 5.17 The Temperature of the Exotherm Corresponding the the Final Decomposition
of Cobalt Neodecanoate During the Thermal Analysis of a Series of Mixtures
Containing a Fixed Percentage of Cobalt Neodecanoate to Sodium Phosphite
(90%:10%, 75%:25% & 50%:50% Co:Phos) and an Increasing Percentage of
Model I,(Data taken from 5.11, 5.12 & 5.13).

Chapter 6. Separation and Identification of the Degradation Products Produced From the Thermal Oxidation of the Model Compounds.

6.1 Object and Methodology.

Most studies of the mechanism of degradation of polyamides have concentrated upon the analysis of degradation products using gas chromatography and/or mass spectrometry, particularly for volatile products. The former technique is excellent for the separation of degradation products and the latter for the determination of the structure of single compounds; they are, therefore, ideal in combination. Achhammer and co-workers [104] during their study of the degradation of nylon 6 identified simple hydrocarbons, water, carbon monoxide, carbon dioxide and ammonia as products of degradation using mass spectrometry. The technique of combined pyrolysis/gas chromatography/mass spectrometry has also been used [105]. However in a comprehensive study of the thermal oxidation of MXD6, Patel [102] encorporated the use of T.L.C and H.P.L.C, and to a lesser extent GC/MS, to separate and identify the products of degradation. In this study of the thermal oxidation of both model I and model II (see table 6.1), H.P.L.C was the main technique used. Expected products of degradation included carboxylic acids, aldehydes/ketones and amines.

Oxidative degradation of models I and II give rise to oxidation products which are both volatile and non-volatile in nature. The presence and extent of the formation of volatile oxidation products can clearly be seen in the thermogravimeric (isothermal) study of models I and II as described in sections 3.2.6 and 4.2.6, respectively. In some cases it can be seen that volatile products account for up to 17% of the overall degradation products over a 5 hour period. It is therefore important to analyse the headspace of the degrading model as well as the solid portion. The experimental procedure used for analysis described in this chapter is outlined in scheme 6.1 and incorporates both non-volatile and volatile analysis similar to the technique used successfully by S.Patel in the analysis of the degradation products of MXD6.[102].
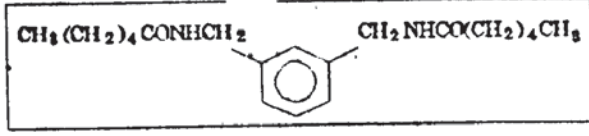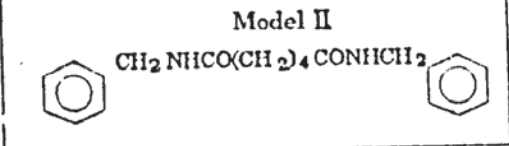
Molecular Weight	Chemical Structure and Name	Abbreviation
332.49	CH₃(CH₂)₄CONHCH₂ CH₂NHCO(CH₂)₄CH₃ Benzene 1,3 Dimethyl Hexanamide	Model I (white powder) m.p = 125°C
356.41	Model II CH₂NHCO(CH₂)₄CONHCH₂ Hexanedioate-bis-Benzylamide	Model II (white powder) m.p = 175°C

Table 6.1 The Structures and Various Characteristics of Models I and II.
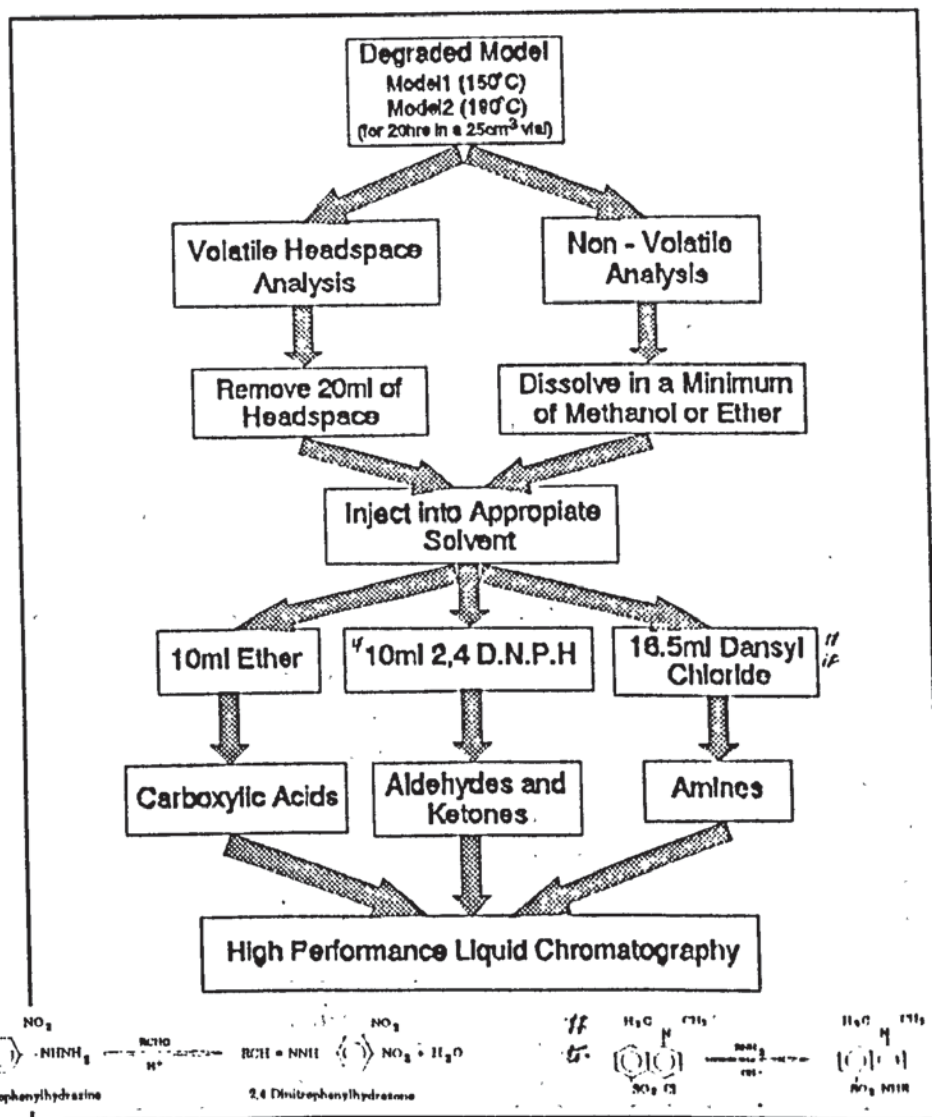
Scheme 6.1. Experimental Outline for the Analysis of Degradation Products from the Thermal Oxidation of the Model Compound by H.P.L.C

6.2 Results.

6.2.1 The Analysis of a Series of Possible Degradation Products of the Thermal Oxidative Degradation of Models I and II by HPLC.

6.2.1.1. H.P.L.C of a Series of Standard Carboxylic Acids.

6.2.1.1.1. Aliphatic Monocarboxylic Acids.

0.01% solutions of a series of monocarboxylic acids ranging from nC_1 to nC_5 were prepared in H.P.L.C grade water and 0.1ml injected onto the column. The retention time for each acid was measured and is shown in table 6.2.

Monocarboxylic Acid	Retention Time (min)
Formic	2.0
Acetic	3.6
Propionic	8.4
n-Butyric	15.0
n-Pentanoic	52.8

Table 6.2. The retention times (mins) calculated for a series of aliphatic monocarboxlic acids, HPLC analysis conducted with a spherisorb ODS-2 column, at 0.6ml/min using water (pH 2.5) as the mobile phase and a U.V Detection Source at 210nm

6.2.1.1.2. Aliphatic Dicarboxylic Acids.

0.01% solutions of a series of dicarboxylic acids ranging from nC_2 to nC_6 were prepared in H.P.L.C grade water and 0.1ml injected onto the column. The retention time for each acid was measured and is shown in table 6.3.

Dicarboxylic Acid	Retention Time (min)
Oxalic	1.6
Malonic	2.4
Succinic	5.2
Glutaric	9.6
Adipic	24

Table 6.3. The retention times (mins) calculated for a series of aliphatic dicarboxylic acids, HPLC analysis conducted with a spherisorb ODS-2 column, at 0.6ml/min using water:methanol (98:2),pH 2.5 as the mobile phase and a U.V Detection Source at 210nm

6.2.1.1.3. Aromatic Acids.

0.01% solutions of isophthalamic, m-hydroxybenzoic, isophthalic and benzoic acids were prepared in water/methanol (60:40) and 0.1ml of each was injected onto the column. The retention time for each acid was measured and is shown in table 6.4.

Aromatic Acid	Retention Time (mins)
Isophthalamic	3.2
m-Hydroxybenzoic	5.8
Isophthalic	8.8
Benzoic	15.4

Table 6.4. The retention times (mins) calculated for a series of aromatic acids, HPLC analysis conducted with a spherisorb ODS-2 column, at 0.6ml/min using water:methanol (70:30),pH 3.5 as the mobile phase and a U.V Detection Source at 254nm.

6.2.1.2. H.P.L.C of a Series of Standard Aldehydes and Ketones.

0.01% solutions of a series of DNPH aldehyde and ketone derivatives were prepared in HPLC grade methanol.The retention time for each was measured and is shown in table6.5.

Aldehyde & Ketone Derivative	Retention Time (mins)
2,4 Dinitrophenylhydrazine	2.6
Formaldehyde	4.2
Acetaldehyde	6.4
Propionaldehyde	8.3
Butyraldehyde	12.4
Valeraldehyde	17.8
Propanone	11.6
Butanone	14.5
Benzaldehyde	18.4
Isophaldehyde	16.2

Table 6.5. The retention times (mins) calculated for a series of aldehyde and ketone derivatives, HPLC analysis conducted with a spherisorb ODS-2 column, at 0.6ml/min using methanol:water (70:30),pH 3.5 as the mobile phase and a U.V Detection Source at 360nm.

<u>6.2.1.3. H.P.L.C of a series of Standard Amines.</u>

A series of aliphatic and aromatic amine derivatives were prepared, as described in section 2.4.7.3, and 0.1ml of each solution was injected onto the column. The retention time for each was measured and is shown in table 6.6.

Amine Derivative	Retention Time (min)
Dansyl Chloride	2.0
Ammonia	2.6
Methylamine	3.0
Ethylamine	3.6
Propylamine	4.6
n-Butylamine	6.2
n-Pentylamine	9.0
Benzylamine	5.7
m-Xylylenediamine	13.6

Table 6.6. The retention times (mins) calculated for a series of amine derivatives, HPLC analysis conducted with a spherisorb ODS-2 column, at 0.6ml/min using methanol:water (70:30) as the mobile phase and a U.V Detection Source at 254nm.

<u>6.2.2. Separation and Identification of the Degradation Products, by HPLC, Obtained from the Thermal Oxidation of Model 1 at 150°C.</u>

<u>6.2.2.1. Analysis of the Carboxylic Acids Formed from the Thermal Oxidation of Model1.</u>
<u>6.2.2.1.1 Aliphatic Monocarboxylic Acids.</u>

A sample of the volatile and non volatile portion of the oxidised model were prepared for H.P.L.C as described in chapter 2.6. Figures 6.1 & 6.2 show the composition of the monocarboxylic acids formed during the thermal oxidation of model 1 at 150°C. The retention time of each acid was measured and is shown in table 6.7.

Monocarboxylic Acids					
Sample	Peak Identification (RT mins)				
	1	2	3	4	5
Volatile Fig.6.1	2.0 formic	3.6 acetic	no peak	no peak	no peak
Non Volatile Fig.6.2	2.0 formic	3.6 acetic	8.4 propionic	15.0 butyric	52.8 pentanoic

Table 6.7. The retention times (mins) calculated for the monocarboxylic acids formed during the thermal oxidation of Model I at 150°C, HPLC analysis conducted with a spherisorb ODS-2 column, at 0.6ml/min using water (pH 2.5) as the mobile phase and a U.V Detection Source at 210nm.

6.2.2.1.2. Dicarboxylic Acids.

A sample of the volatile and non volatile portion of the oxidised model were prepared for H.P.L.C as described in chapter 2.6. However, no dicarboxylic acids from either the non-volatlie or volatile samples were detected.

6.2.2.1.3. Aromatic Acids.

A sample of the volatile and non volatile portion of the oxidised model were prepared for H.P.L.C as described in chapter 2.6. Figures 6.3 & 6.4 shows the composition of the aromatic carboxylic acids formed during the thermal oxidation of model I at 150°C. The retention time of each acid was measured and is shown in table 6.8.

Aromatic Acids		
Sample	Peak Identification (RT mins)	
	1	2
Volatile Fig.6.3	no peak	no peak
Non Volatile Fig.6.4	3.2 isophthalamic	8.8 isophthalic

Table 6.8. The retention times (mins) calculated for the aromatic acids formed during the thermal oxidation of ModelI at 150°C, HPLC analysis conducted with a spherisorb ODS-2 column, at 0.6ml/min using water:methanol (70:30),pH 2.5 as the mobile phase, and a U.V Dtection Source at 254nm.

6.2.2.2. HPLC of Aldehyde and Ketone Derivatives Obtained from the Thermal Oxidation of Model I.

A sample of the aldehydes and ketones produced in the volatile and non volatile portion of the oxidised model were converted to their respective 2,4-dinitrophenylhydrazine derivatives and prepared for H.P.L.C as described in chapter 2.6. Figure 6.5 & 6.6 shows the composition of the aldehydes and ketones formed during the thermal oxidation of model1 at 150°C. The retention time for each aldehyde derivative was measured and is shown in table 6.9.

Aldehyde and Ketone Derivatives				
Sample	**Peak Identification (RT mins)**			
	1	2	3	4
Volatile Fig.6.5	2.5 DNPH	4.2 formaldehyde	6.3 acetaldehyde	8.0 propionaldehyde
Non Volatile Fig.6.6	2.5 DNPH	4.2 formaldehyde	6.3 acetaldehyde	8.0 propionaldehyde
	5	6	7	8
Volatile Fig.6.5	11.6 propanone	12.5 butyraldehyde	no peak	no peak
Non Volatile Fig.6.6	11.6 propanone	12.5 butyraldehyde	16.2 isophthaldehyde	17.8 valeraldehyde

Table 6.9. The retention times (mins) calculated for the aldehyde and Ketone derivatives formed during the thermal oxidation of Model I at 150°C, HPLC analysis conducted with a spherisorb ODS-2 column, at 0.6ml/min using methanol:water (70:30), pH 3.5 as the mobile phase, and a U.V Detection Source at 360nm.

6.2.2.3. HPLC of Amine Derivatives Obtained from the Thermal Oxidation of Model I.

A sample of the amines produced in the volatile and non volatile portion of the oxidised model were converted to their respective dansyl chloride derivatives and prepared for H.P.L.C as described in chapter 2.6. Figure 6.7 & 6.8 shows the composition of the amines formed during the thermal oxidation of model I at 150°C. The retention time of each amine derivative was measured and is shown in table 6.10.

Amine Derivative				
Sample	**Peak Identification (RT mins)**			
	1	2	3	4
Volatile Fig.6.7	2.0 dansyl chloride	2.6 ammonia	3.0 methylamine	3.6 ethylamine
Non Volatile Fig.6.8	2.0 dansyl chloride	2.6 ammonia	3.0 methylamine	3.6 ethylamine
	5	6	7	8
Volatile Fig.6.7	4.6 propylamine	6.2 butylamine	9.0 pentylamine	no peak
Non Volatile Fig.6.8	4.6 propylamine	6.2 butylamine	9.0 pentylamine	13.6 xylylenediamine

Table 6.10. The retention times calculated for the amine derivatives formed during the thermal oxidation of Modell at 150°C, HPLC analysis conducted with a spherisorb ODS-2 column, at 0.6ml/min using methanol:water (70:30) as the mobile phase, and a U.V Detection Source at 254nm.

6.2.3. Separation and Identification of the Degradation Products, by HPLC, Obtained from the Thermal Oxidation of Model II at 190°C.
6.2.3.1 Analysis of the Carboxylic Acids Formed from the Thermal Oxidation of ModelII
6.2.3.1.1 Aliphatic Monocarboxylic Acids.

A sample of the volatile and non volatile portion of the oxidised model were prepared for H.P.L.C as described in chapter 2.6. Figure 6.9 & 6.10 shows the composition of the monocarboxylic acids formed during the thermal oxidation of model II at 190°C. The retention time for each acid was measured and is shown in table 6.11.

Monocarboxylic Acids					
Sample	**Peak Identification (RT mins)**				
	1	2	3	4	5
Volatile Fig.6.9	2.0 formic	3.6 acetic	8.4 propionic	15.0 butyric	52.8 pentanoic
Non Volatile Fig.6.10	2.0 formic	3.6 acetic	8.4 propionic	15.0 butyric	52.8 pentanoic

Table 6.11. The retention times (mins) calculated for the monocarboxylic acids formed during the thermal oxidation of ModelII at 190°C, HPLC analysis conducted with a spherisorb ODS-2 column, at 0.6ml/min using water (pH 2.5) as the mobile phase, and a U.V Detection Source at 210nm.

6.2.3.1.2. Dicarboxylic Acids.

A sample of the volatile and non volatile portion of the oxidised model were prepared for H.P.L.C as described in chapter 2.6. Figure 6.11 & 6.12 shows the composition of the dicarboxylic acids formed during the thermal oxidation of model II at 190°C. The retention time for each acid was measured and is shown in table 6.12.

Dicarboxylic Acids				
Sample	Peak Identification (RT mins)			
	1	2	3	4
Volatile Fig.6.11	1.6 oxalic	2.5 malonic	5.2 succinic	9.6 glutaric
Non Volatile Fig.6.12	1.6 oxalic	2.5 malonic	5.2 succinic	9.6 glutaric

Table 6.12. The retention times (mins) calculated for the dicarboxylic acids formed during the thermal oxidation of Model II at 190°C, HPLC analysis conducted with a spherisorb ODS-2 column, at 0.6ml/min using water:methanol (98:2), pH 2.5 as the mobile phase, and a U.V Detection Source at 210nm.

6.2.3.1.3. Aromatic Acids.

A sample of the volatile and non volatile portion of the oxidised model were prepared for H.P.L.C as described in chapter 2.6. Figure 6.13 shows the composition of the aromatic carboxylic acids formed during the thermal oxidation of model II at 190°C. The retention time for each acid was measured and is shown in table 6.13.

Aromatic Acids	
Sample	Peak I.D (RT mins)
	1
Volatile	no peak
Non Volatile 6.13	15.4 benzoic

Table 6.13. The retention times (mins) calculated for the aromatic acids formed during the thermal oxidation of Model II at 190°C, HPLC analysis conducted with a spherisorb ODS-2 column, at 0.6ml/min using water:methanol (70:30), pH 3.5 as the mobile phase, and a U.V Detection Source at 254nm.

6.2.3.2. H.P.L.C of Aldehyde and Ketone Derivatives Obtained from the Thermal Oxidation of Model II.

A sample of the aldehydes and ketones produced in the volatile and non volatile portion of the oxidised model were converted to their respective 2,4-dinitrophenylhydrazine derivatives and prepared for H.P.L.C as described in chapter 2.6. Figure 6.14 & 6.15 shows the composition of the aldehydes and ketones formed during the thermal oxidation of model II at 190°C. The retention time of each was measured and is shown in table 6.14.

Aldehyde and Ketone Derivatives				
Sample	**Peak Identification (RT mins)**			
	1	2	3	4
Volatile Fig.6.14	2.5 DNPH	4.2 formaldehyde	6.3 acetaldehyde	8.0 propionaldehyde
Non Volatile Fig.6.15	2.5 DNPH	4.2 formaldehyde	6.3 acetaldehyde	8.0 propionaldehyde
	5	6	7	8
Volatile Fig.6.14	11.6 propanone	12.5 butyraldehyde	no peak	no peak
Non Volatile Fig.6.15	11.6 propanone	12.5 butyraldehyde	17.8 valeraldehyde	18.4 benzaldehyde

Table 6.14. The retention times (mins) calculated for the aldehyde and Ketone derivatives formed during the thermal oxidation of ModelII at 190°C, HPLC analysis conducted with a spherisorb ODS-2 column, at 0.6ml/min using methanol: water(70:30),pH 3.5 as the mobile phase,and a UV Detection Source at 360nm

6.2.3.3. HPLC of Amine Derivatives Obtained from the Thermal Oxidation of Model II.

A sample of the amines produced in the volatile and non volatile portion of the oxidised model were converted to their respective dansyl chloride derivatives and prepared for H.P.L.C as described in chapter 2.6. Figure 6.16 & 6.17 shows the composition of the amines formed during the thermal oxidation of model II at 190°C. The retention time of each amine derivative was measured and is shown in table 6.15.

Amine Derivative				
Sample	Peak Identification (RT mins)			
	1	2	3	4
Volatile Fig.6.16	2.0 dansyl chloride	2.6 ammonia	3.0 methylamine	3.6 ethylamine
Non Volatile Fig.6.17	2.0 dansyl chloride	2.6 ammonia	3.0 methylamine	3.6 ethylamine
	5	6		7
Volatile Fig.6.16	4.6 propylamine	6.2 butylamine	no peak	no peak
Non Volatile Fig.6.17	4.6 propylamine	6.2 butylamine	no peak	9.7 benzylamine

Table 6.15. The retention times calculated for the amine derivatives formed during the thermal oxidation of ModelII at 190°C, HPLC analysis conducted with a spherisorb ODS-2 column, at 0.6ml/min using methanol:water (70:30) as the mobile phase, and a U.V Detection Source at 254nm.

6.2.4. The Use of Gas Chromatography to Study the Formation of Volatiles Produced from the Thermal Oxidation of a Models I and II Via Headspace Analysis.

High performance liquid chromatography enables the separation and identification of a wide range of compounds such as carboxylic acids, aldehydes, ketones and amines, however in an oxidising atmosphere the main volatile degradation products formed during the oxidation of models I and II are still likely to be carbon monoxide, carbon dioxide and water, as shown by various scientists in their studies of low molecular weight amides and polyamides [104,105]. Gas chromatography was therefore used for their detection via headspace analysis of the thermal oxidation of the model compounds. Two separate columns were used for the detection of permanent gases (molecular seive) and organics (poropak Q).

6.2.4.1. Volatile Analysis Using Gas Chromatography : Poropak Q Column.

1ml of headspace, of the oxidised model (model I:150°C & model II:190°C) was injected on to the column using helium as the carrier gas at a flow rate of 20ml/min. The separation of the gaseous products enabled subsequent detection by a thermal conductivity detector. The retention times of the peaks obtained were calculated and compared with a standard series (see table 6.16) to enable identification, see figures 6.18 and 6.20.

Poropak Q (75°C (TCD), Helium 20ml/min)	
Gas	Retention Time (min)
Air,Carbon Monoxide	0.5
Carbon Dioxide	0.75
Water	1.9

Table 6.16. The retention times (mins) calculated for a series of standard gases via GC.

6.2.4.2. Volatile Analysis Using Gas Chromatography : Molecular Sieve 5A.

Use of a molecular sieve column enables the separation and detection of permanent gases such as oxygen, nitrogen and carbon monoxide. In this instance it was mainly used to confirm the presence of carbon monoxide but the column's ability to separate oxygen could prove useful in providing a further technique for the measurement of oxygen absorbed. Measurement of the amount of oxygen present in the headspace with increasing oxidation time of the model compound could easily be achieved. This could be mirrored by monitoring the amount of carbon dioxide, carbon monoxide and water. As the total amount of oxygen in the headspace decreases the presence of the other three gaseous products should increase. However in this study confirmation of the gaseous products was the main concern. Similarly to the previous experiment 1ml of headspace, of the oxidising model (model I:150°C & model II:190°C) was injected on to the column using helium as the carrier gas at a flow rate of 30ml/min. The separation of the gaseous products enabled subsequent detection by a thermal conductivity detector. The retention times of the peaks obtained were calculated and compared with a standard series (table 6.17) to enable identification, see figures 6.19 and 6.21.

Molecular Sieve 5A (35°C (TCD), Helium 30ml/min)	
Gas	Retention Time (min)
Oxygen	0.8
Nitrogen	1.6
Carbon Monoxide	7.6

Table 6.17. The retention times (mins) calculated for a series of standard gases via GC.

6.3. Discusion.

The thermal oxidation of models I and II produced a variety of degradation products, including carboxylic acids (mono, di and aromatic), aldehydes, ketones, amines, carbon monoxide, carbon dioxide and water. The majority of these compounds were separated and identified using HPLC and GC, the method varying depending on the nature of the compound. Schemes 2-14 attempt to explain the formation of these various compounds, the reactions being based on standard reactions of similar amides and polyamides together with the evidence obtained from the oxidation studies of the models in chapters 3 and 4. The reaction mechanism is believed to be a free radical process involving an initiation step followed by propagation and then termination reactions. Therefore in order to initiate the reaction sufficient free radicals must be created in order to sustain the oxidation reactions.

6.3.1. Initiation.

It is possible that initiation, resulting in the formation of free radicals, could occur via a number of processes:-

a) For the oxidation of hydrocarbons, metal catalysts have been known to initiate the chain of autoxidation by forming reactive radicals. Therefore initiation may occur via a favourable complex formation betwen the cobalt and the amide chain, resulting in the abstraction of the most reactive hydrogen atom, which is the hydrogen atom in the alpha position to the NH group, which is also made more reactive by being alpha to the benzene ring, see 6.1 as an example of complexation between model I and cobalt. However, oxidation studies of model I and II (chapters 3 & 4) suggested that the role of cobalt was more likley to be as a propagation catalyst, as opposed to an initiation catalyst, although some degree of complexation cannot be ruled out.

$$H_3C\text{-}_4(H_2C)\text{-}C \qquad\qquad C\text{-}(CH_2)_4CH_3 \qquad\qquad (6.1)$$
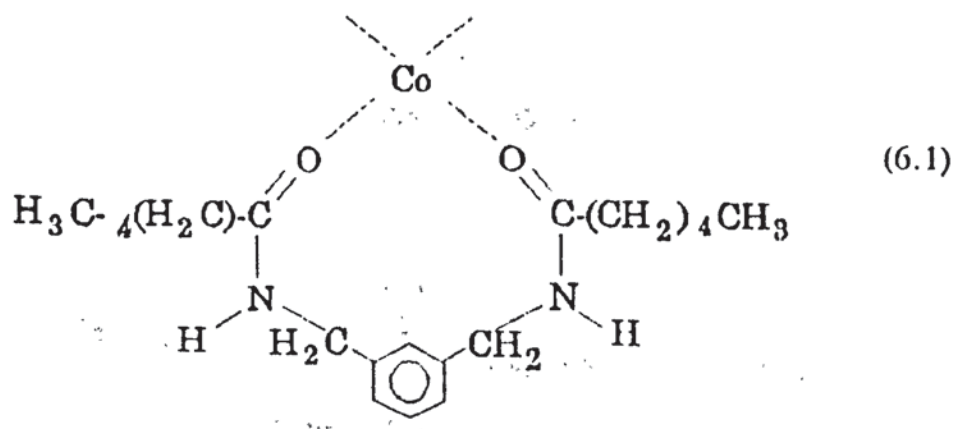
b) Loss of the same reactive hydrogen atom (alpha to the NH group) due to external forces, such as shear or heat, could also occur, reaction (6.2).

$$CH_2-NH-CO-- \xrightarrow[\text{loss of reactive hydrogen}]{\text{Heat or external forces,}} \dot{C}H-NH-CO-- \qquad (6.2)$$
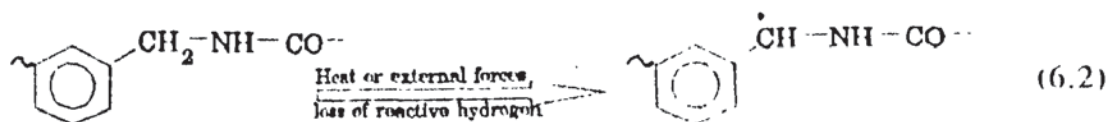
c) Radicals may also be formed from the fisssion of the CH_2-NH (6.3) and CH_2-CO bonds (6.4). Kamerbeek et al [37] and Mortimer [38] asserted that the CH_2-NH bond was responsible for initial polyamide cleavage. Their arguments were based on the assumption that the weakest bond would break more easily than the stronger bonds. For polyamides, the next theoretically weakest bond is the CH_2CO bond.

$$CH_2 \vdots NH-CO-CH_2- \xrightarrow{\text{Heat}} \dot{C}H_2 + \dot{N}H-CO-CH_2- \qquad (6.3)$$

$$CH_2-NH-CO \vdots CH_2- \xrightarrow{\text{Heat}} CH_2-NH-\dot{C}O + \dot{C}H_2- \qquad (6.4)$$
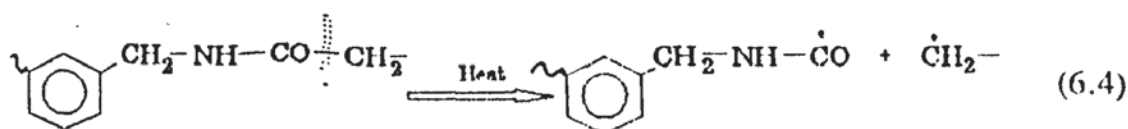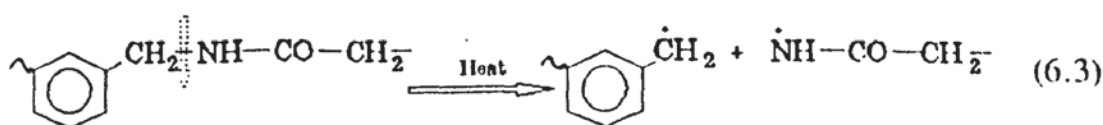
6.3.2. Propagation and Termination.

The radicals formed in the initiation processes (6.2), (6.3) and (6.4) may then react with oxygen forming peroxyl radicals (6.5) and (6.6):-

$$\dot{C}H\sim \xrightarrow{O_2} \overset{OO.}{\underset{CH\sim}{|}} \qquad (6.5)$$

Peroxy radical

$$\dot{C}H_2 \xrightarrow{O_2} \overset{OO\cdot}{\underset{CH_2}{}} \quad (\text{ or } \dot{C}H_2- \xrightarrow{O_2} \overset{OO\cdot}{\underset{CH_2-}{|}}) \qquad (6.6)$$

peroxyl radical
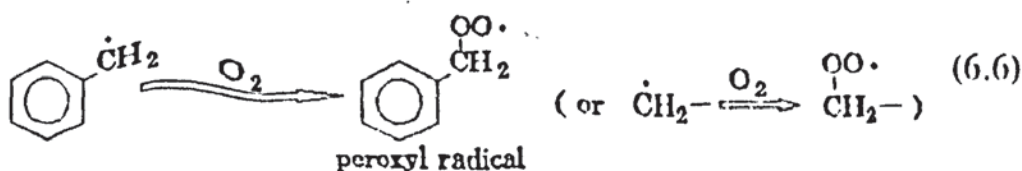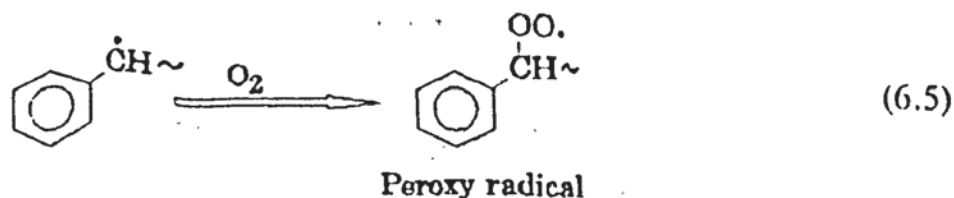
The reaction will also propagate via hydrogen abstraction and dissociation. This in turn creates further radicals capable of either an oxidation or hydrogen abstraction, reaction 6.7.

$$R-\overset{\overset{\displaystyle OO\cdot}{|}}{CH}-R' + \left[\bigcirc\right]^{CH_2} \longrightarrow R-\overset{\overset{\displaystyle OOH}{|}}{CH}-R' + \left[\bigcirc\right]^{\cdot CH} \qquad (6.7)$$

Hydroperoxide

(where R = $\left[\bigcirc\right]$ and R' = H or $-NH-CO-CH_2-$)
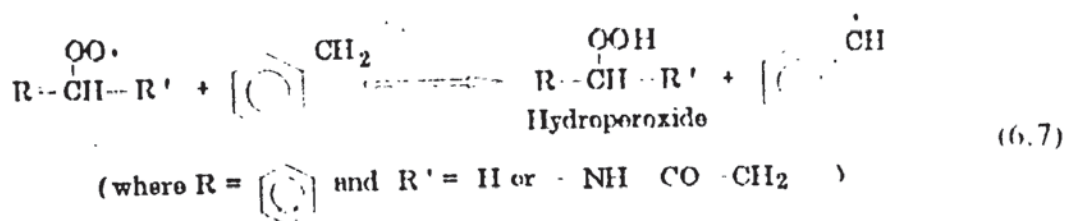
Hydroperoxide groups are however very unstable and decompose readily to give alkoxyl and hydroxyl radicals (6.8). Metal salts are known to assist in the decomposition of these hydroperoxides, this process is discussed in detail in chapter 1.

$$R-\overset{\overset{\displaystyle OOH}{|}}{CH}-R' \xrightarrow[\text{heat}]{M^{n+}} R-\overset{\overset{\displaystyle O\cdot}{|}}{CH}-R' + \cdot OH \qquad (6.8)$$

alkoxyl radical   hydroxyl radical
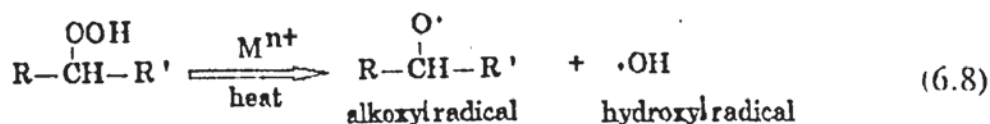
Hydroxy radicals tend to undergo hydrogen abstraction forming water (6.9), whereas alkoxyl radicals may undergo hydrogen abstraction giving rise to an alcohol (6.10) which may oxidise further, or, alternatively the alkoxyl radical may undergo β-scission, a well established mechanism [106] resulting in an aldehyde or ketone (6.11).

$$\cdot OH \xrightarrow{RH} H_2O + R\cdot \qquad (6.9)$$

$$R-\overset{\overset{\displaystyle O\cdot}{|}}{CH}-R' \xrightarrow{RH} R-\overset{\overset{\displaystyle OH}{|}}{CH}-R' + \cdot R' \qquad (6.10)$$

alcohol

$$R-\overset{\overset{\displaystyle O\cdot}{|}}{CH}-R' \xrightarrow{\beta\text{-scission}} R-\overset{\overset{\displaystyle O}{\|}}{C}\diagdown_H \quad \text{aldehyde/ketone} + \cdot R'$$

$$\Big\downarrow \text{Baeyer Villiger Oxidation} \qquad (6.11)$$

$$R-\overset{\overset{\displaystyle O}{\|}}{C}\diagdown_{OH}$$
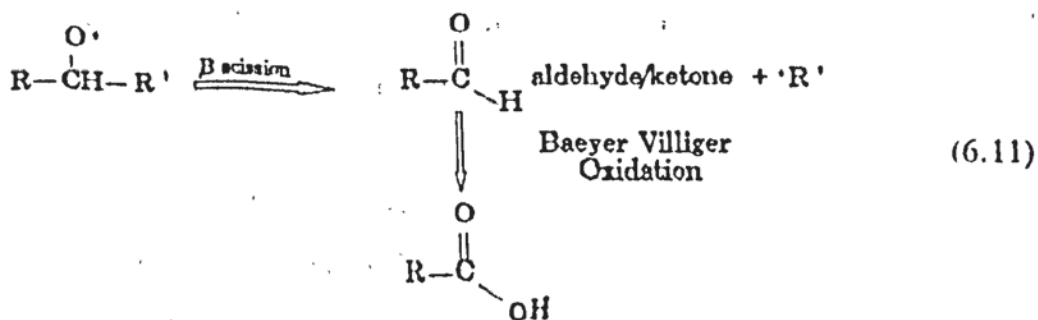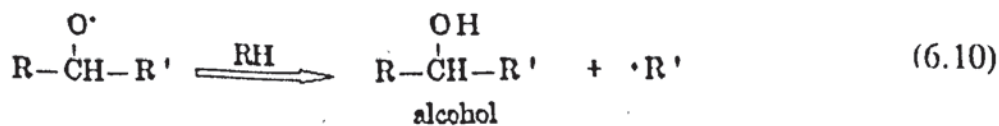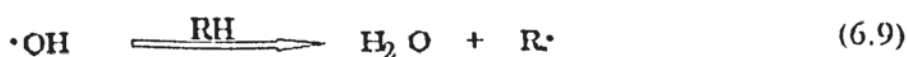
6.3.3. The Reaction Mechanism of Model I Oxidation.

Scheme 6.2 outlines the initiation mechanism for the oxidation of model I. It indicates that radical formation occurs initially via the loss of a reactive hydrogen atom in the alpha position to the NH group (and to the benzene ring). This results in the formation of a further radical (I) and aldehyde (II), via the initial formation of the peroxyl radical, subsequent hydroperoxide formation and scission of the CH-NH bond, see scheme 6.2 a-e. The radical (I) leads to the formation of a primary amine (III) from which a series of adehydes (scheme 6.3), carboxylic acids (scheme 6.4) and amines (scheme 6.5) can be formed. Evidence of which can be seen in the oxidation study of model I in chapter 3. The formation of aldehydes and carboxylic acids is thought to occur via the termination process of peroxyl radicals by a tetroxide mechanism [107], whereby the reaction involves the reversible formation of a dimer which breaks down to give an alcohol and carbonyl compound. The aldehyde (II) can result in the formation of aromatic carboxylic acids. Aromatic amines are thought to be produced by the scission of the NHCO-CH$_2$ bond and subsequent reaction of the hydroisocyanate radical with oxygen followed by decarboxylation (Scheme 6.6). Formation of the aliphatic amines occurs in a similar manner, but arises from the radical (I).

6.3.4. The Reaction Mechanism of Model II Oxidation.

Scheme 6.7 outlines the initiation mechanism for the oxidation of model II, again it is believed that radical formation occurs initially via the loss of a reactive hydrogen atom in the alpha position to the NH group (and to the benzene ring) with the susequent production of the radical (III) and the aldehyde (IV). From the aromatic aldehyde formed (IV) oxidation to the acid may proceed or, similarly to model I, scission of the CO-CH$_2$ bond in the original compound may result in aromatic amine formation (scheme 6.12).

The radical (III) undergoes hydrogen abstraction to form the amide (V). This may then react via three pathways consequently forming :-

    i) carboxylic acids (scheme 6.8 & 6.9)

    ii) aldehydes/ketones (scheme 6.10)

    iii) amines (6.11)

Monocarboxylic (scheme 6.8) and dicarboxylic (scheme 6.9) acid formation occurs via the scission of a CH_2-CO bond in (VI) forming an alkyl and hydroisocyanate radical. The alkyl radical susequently reacts with the oxygen present resulting in the sequential loss of one carbon at a time forming the series of monocarboxylic acids. Formation of the di-acid proceeds via a similar tetraoxide mechanism and subsequent oxidation of the carbonyl group. Aldehydes and ketones (scheme 6.10) result from the scission of a CO-CH_2 bond, structure (VII) and subsequent reaction of the alkyl radical formed with oxygen followed by hydrogen abstraction yields the aldehyde.

Finally amines are formed via the scission of the CO-CH_2 bond in compound (VIII). Subsequently reaction of the hydroisocyanate radical with oxygen occurs followed by decarboxylation. The resulting radical proceeds to react with the alkyl radical formed in the initial chain breaking process. Scission of a further CO-CH_2 bond and subsequent reaction the alkyl radical formed with oxygen followed by reaction with $H.$ or $NH_2.$ yields the amine or diamine.

6.3.5. The Influence of Cobalt on the Oxidation of Model I and Model II.

Many workers have investigated the influence of trace metal ions on autoxidation. As an example in Chapter 1 the work of Osawa [12-14] on the oxidative degradation of polypropylene was summarised. The rate of oxidative degradation, evaluated by measuring the oxygen uptake from a closed system, was greatest for a sample of the polymer containing cobalt ions followed by manganese, copper and iron. Furthermore, catalytic decomposition of t-butyl hydroperoxide by metal salts gave a similar trend, which led to an apparent correlation between the catalytic activity of metallic salts in the oxidation of the polymer and the decomposition of the hydroperoxide. However, the role of the metal ion may not exclusively be as a hydroperoxide decomposer but perhaps, in some cases, be more important as a reaction initiator. This was the conclusion drawn from the work of Patel on the oxidation of MXD6 [102]. Initiation was believed to occur via the formation of a favourable complex betwen the cobalt and MXD6. The possibility of such complex formation in models I and II has already been considered and the likely form of these complexes is shown in the discussion section of chapters 3 and 4.

Many factors will influence the behaviour of the catalyst, again referring to the work of Osawa [12], the initial oxidation state of the cobalt is important as well as the ligands to which it is bonded. Any changes occuring to the cobalt during oxidation of the model compounds would therefore be critical to the effect that cobalt has on the oxidation reaction. The stabilising effect of sodium phosphite, described in chapter 5, not only on the model compound itself, but also on the cobalt therefore proved to be an important factor in the thermal oxidation study of the model compounds, particularly of model II due to the higher temperature at which the oxidation reaction took place. Sodium phosphite extended the decomposition temperature of the cobalt, to enable it to behave as either an initiating or propogating catalyst for the oxidation of models I and II.

6.3.5.1 The Role of Cobalt as an Initiation Catalyst.

The formation of a complex between cobalt and models I and II has previously been dicussed in chapters 3 and 4. It was suggested that the carbonyl groups of the amide donate a lone pair of electrons to the cobalt in preference to the electron pair donation via the N-H groups. The complex is thought to activate the oxygen present thus creating a superoxide anion which is a reactive centre for which to abstract the most readily available hydrogen atom. During the course of this and further reactions, the radicals R·, ·O_2H and ·OH are formed. It is therefore postulated that these radicals are responsible for the latter stages of oxidative propagation. This therefore does not necessitate that the cobalt play any further part in the oxidation process and implies that it acts principally as a reaction initiator. However, during the oxidation studies of models I and II, cobalt was shown to decompose the hydroperoxide formed during oxidation of both model at 150°C, indicating that cobalt was functioning as a propagation catalyst.

6.3.5.2 The Role of Cobalt as a Propagation Catlyst.

In solution cobalt is known to aid in the decomposition of hydroperoxides, (6.12 & 6.13) [22,108].

$$ROOH + Co^{2+} \longrightarrow RO· + ·OH + Co^{3+} \qquad (6.12)$$

$$ROOH + Co^{3+} \longrightarrow RO_2· + ·H + Co^{2+} \qquad (6.13)$$
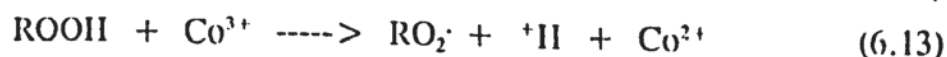
Furthermore, it is also known that the metal ion can deactivate alkoxyl radicals, (6.14) :-

$$RO· + Co^{2+} \longrightarrow RO^- + Co^{3+} \qquad (6.14)$$
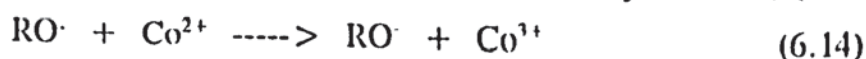
Where the concentration of the alkoxyl radicals is less than the metal ion concentration, the antioxidant effect will predominate. When the concentration of the alkoxyl radicals is greater than that of the metal ion concentration then the rate of oxidation increases.

In the solid phase, cobalt ions are believed to be essentially immobile, hence cobalt cannot fully participate in hydroperoxide decomposition or alkoxy deactivation hence the reasoning behind Patels [102] proposal that the metal ion cannot fully participate in any propogation reactions once in the solid state due to lack of mobility and therefore that the role of the cobalt is primarily that of an initiation catalyst. However in the oxidation of models I and II, in the melt, cobalt would have increased mobility, and as shown in chapters 3 and 4, the potential to catalyse the decomposition of the hydroperoxide. Therefore essentially cobalt behaves primarily as a propogation catalyst in the oxidation of models I and II and to a lesser extent as an initiating catalyst aided by the increased stability, at higher temperatures, due to the action of sodium phosphite.

Model 1 : Benzene - 1,3 - Dimethylhexanamide

$CH_3(CH_2)_4CONHCH_2$ —[ring]— $CH_2NHCO(CH_2)_4CH_3$

heat
(loss of reactive H)   a

·$CHNHCO(CH_2)_4 CH_3$ [ring]   b O_2

$O-O\cdot$ —[ring]— ·$CHNHCO(CH_2)_4 CH_3$ c RH

$O-OH$ —[ring]— $CHNHCO(CH_2)_4 CH_3$ d $-\cdot OH$

$O\cdot$ —[ring]— $CHNHCO(CH_2)_4 CH_3$ e

(II) $O=CH$ —[ring]   g

(I) + ·$NHCO(CH_2)_4 CH_3$ f RH

(III) $NHCO(CH_2)_4 CH_3$ (H)   h   i

Aromatics Products
Aldehydes/Ketones   j
Carboxylic Acids
Amines

IR spectroscopy indicates that the intensities of the amide NH and C=O absorption decrease with oxidation time, suggesting that the primary amide is not the final product of the oxidation reaction.

UV-Vis spectroscopy indicates an increase in the formation of m-xylylene diamine with increasing oxidation of Model I, at 150 C, as indicated in chapter 3, section 3.2.3 (fig.3.15)

FT-IR spectroscopy indicates the formation of aldehydes/ketones & carboxylic acids with increasing oxidation time, see chapter 3.22 (fig.3.6)

Scheme 6.2 The Reaction Mechanism for the Thermal Oxidation of Model I, Outlining in Particular the Initiation Step Via the Loss of the Most Reactive Hydrogen Atom.

H-N-CO(CH$_2$)$_4$CH$_3$ ——→ H-N-C + ·CH$_2$(CH$_2$)$_3$CH$_3$
| | ‖
H   H O

(III)

·CH$_2$(CH$_2$)$_3$CH$_3$
       2O$_2$
      →

OO·
|
-CH$_2$(CH$_2$)$_3$CH$_3$
      RH
     →

O-OH
|
-CH$_2$(CH$_2$)$_3$CH$_3$
      -·OH
     →

O·
|
-CH$_2$(CH$_2$)$_3$CH$_3$

β Scission

·CH$_2$-CH$_2$-CH$_3$ ⇌ ·CH$_2$-CH$_2$-CH$_3$
    Repeat
·CH$_2$-(CH$_2$)$_2$-CH$_3$ + CH$_2$O

formaldehyde

CH$_2$O

Tetraoxide Mechanism

NH$_2$
|
O=C-O-O-O-C(H)(H)-O-(CH$_2$)$_x$CH$_3$

H-N-C-OO·
| ‖
H O

·CH$_2$(CH$_2$)$_x$CH$_3$
|
OO·

H-N-C· + 2O$_2$
| ‖
H O

·CH$_2$(CH$_2$)$_x$CH$_3$

NH$_2$
|
O=C + O$_2$
|
OH

H
|
O=C-(CH$_2$)$_x$CH$_3$

x=3 HOC-(CH$_2$)$_3$CH$_3$ valeraldehyde

x=2 HOC-(CH$_2$)$_2$CH$_3$ butyraldehyde

x=1 HOC-(CH$_2$)CH$_3$ propionaldehyde

x=0 HOC-CH$_3$ acetaldehyde
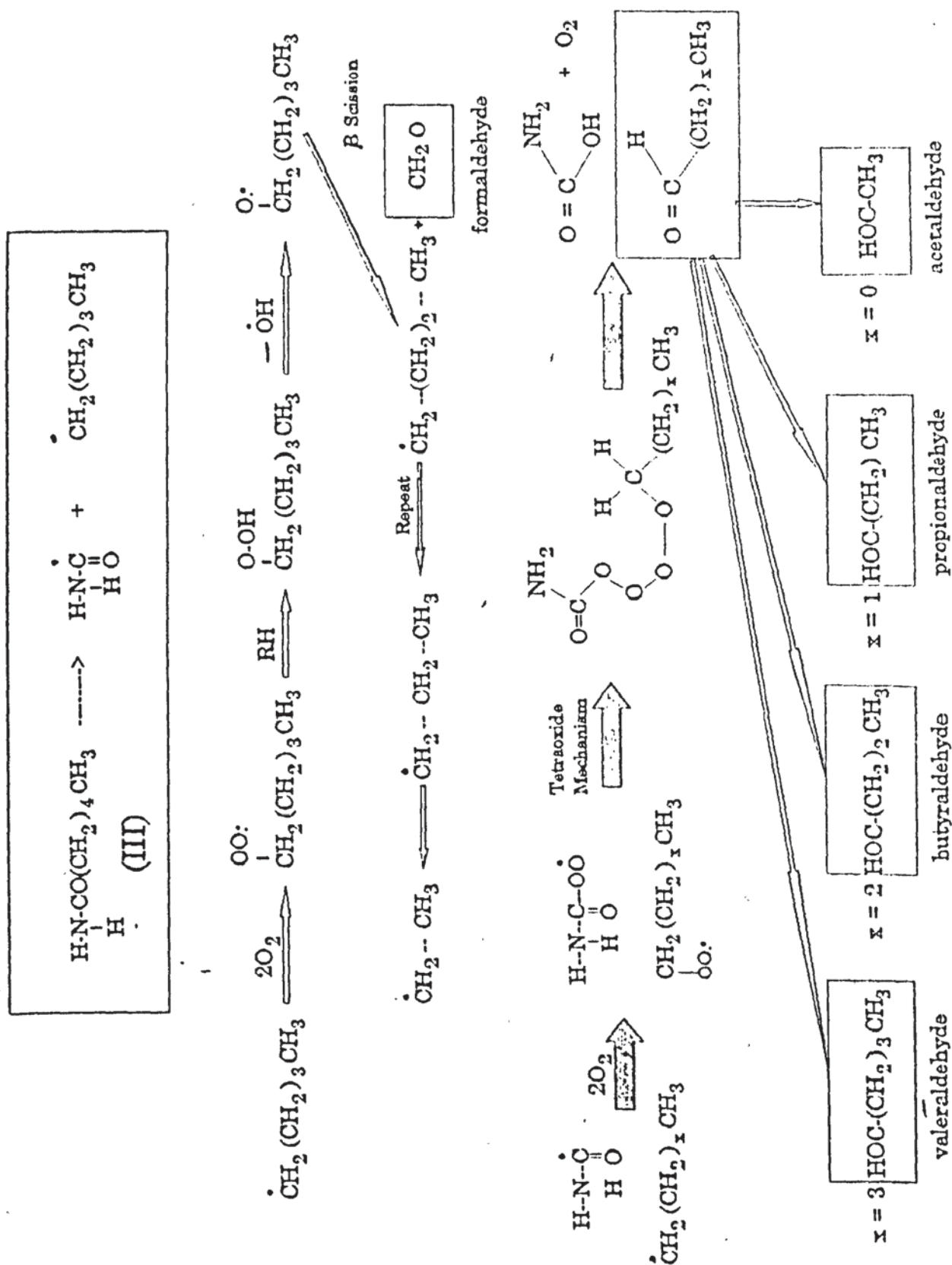
Scheme 6.3 Aldehydes and Ketones Derived From the Thermal Oxidation of Model I at 150°C.
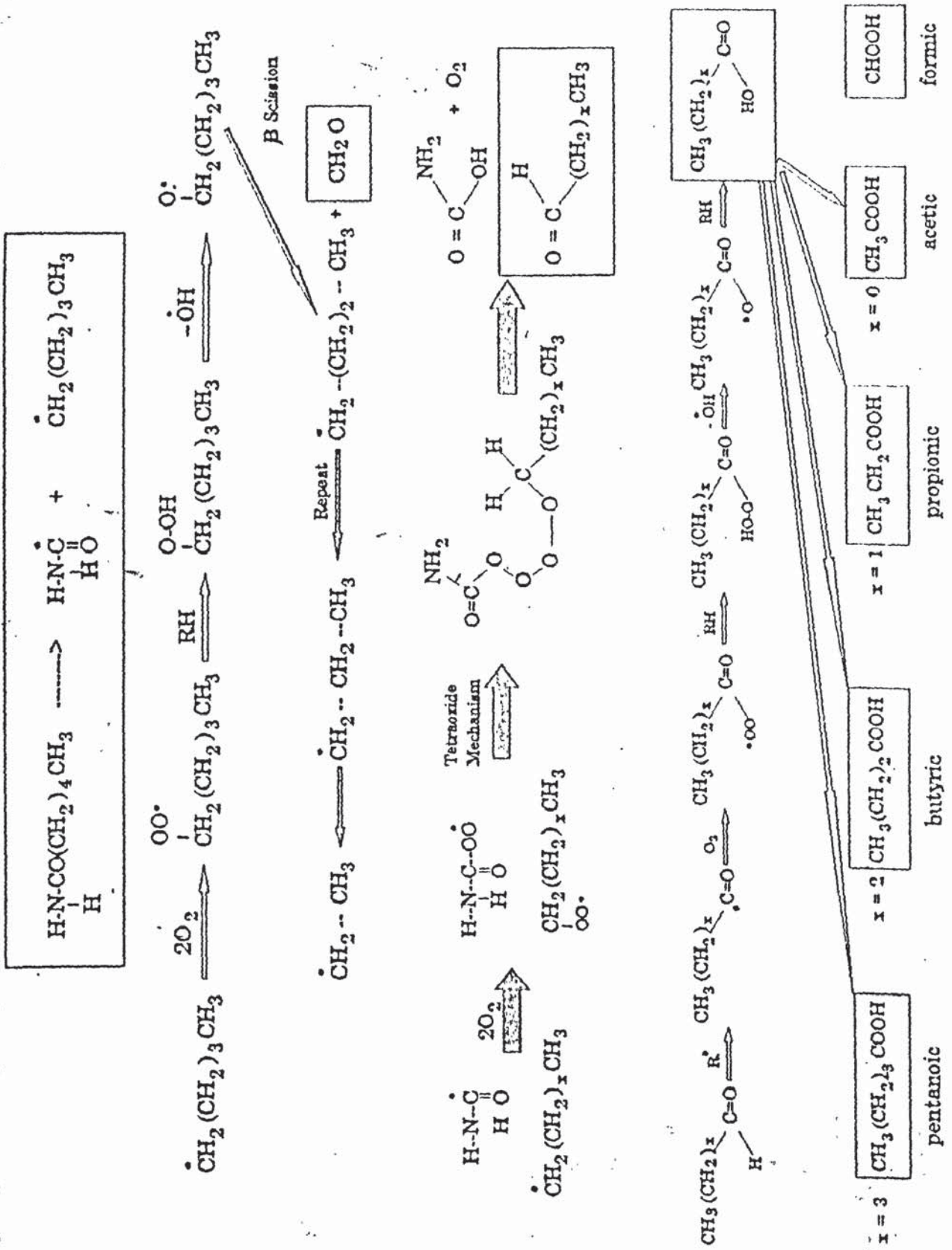
Scheme 6.4 Carboxylic Acids Derived From the Thermal Oxidation of Model I at 150°C.
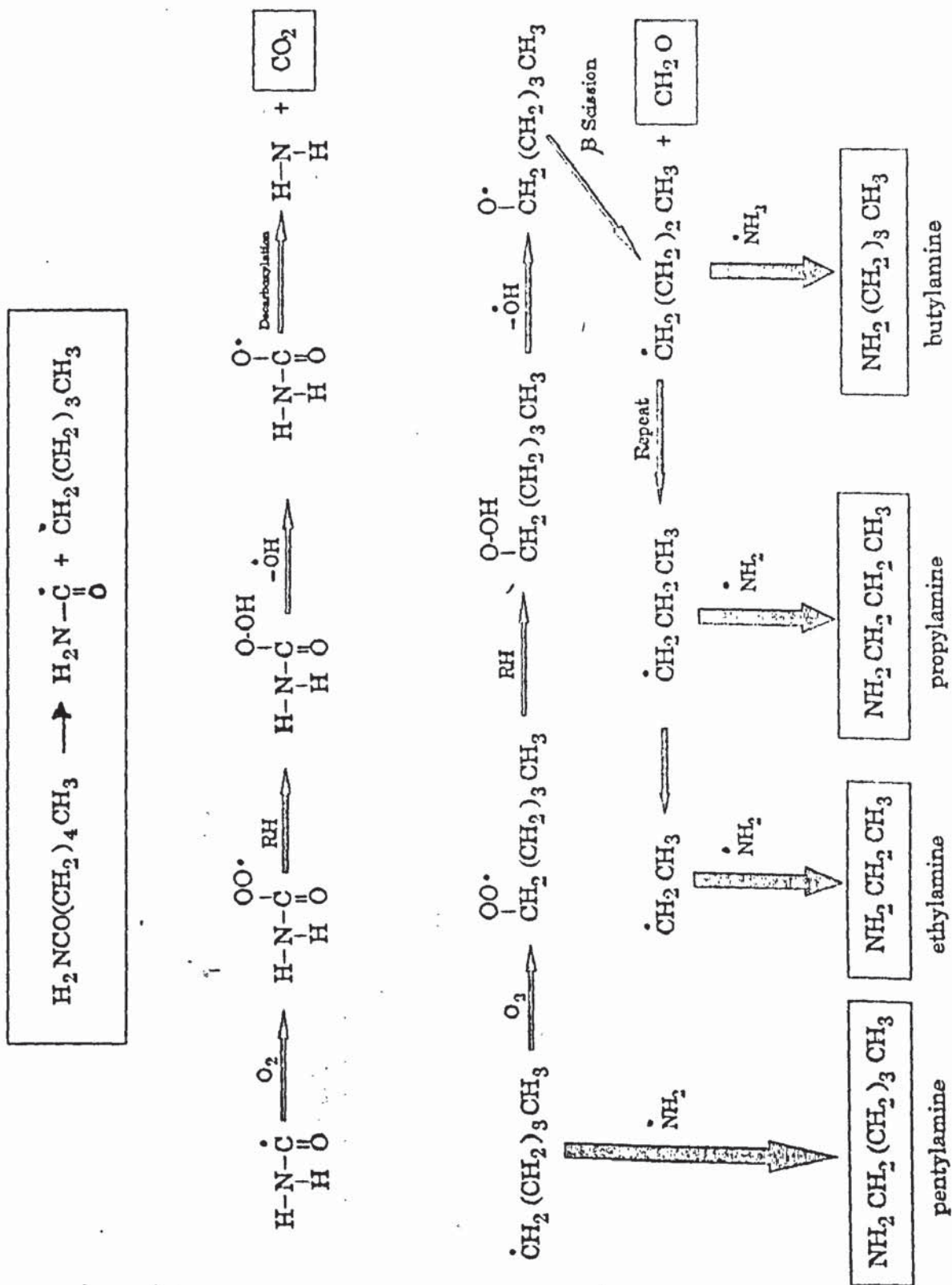
Scheme 6.5 Amines Derived From the Thermal Oxidation of Model I at 150°C.
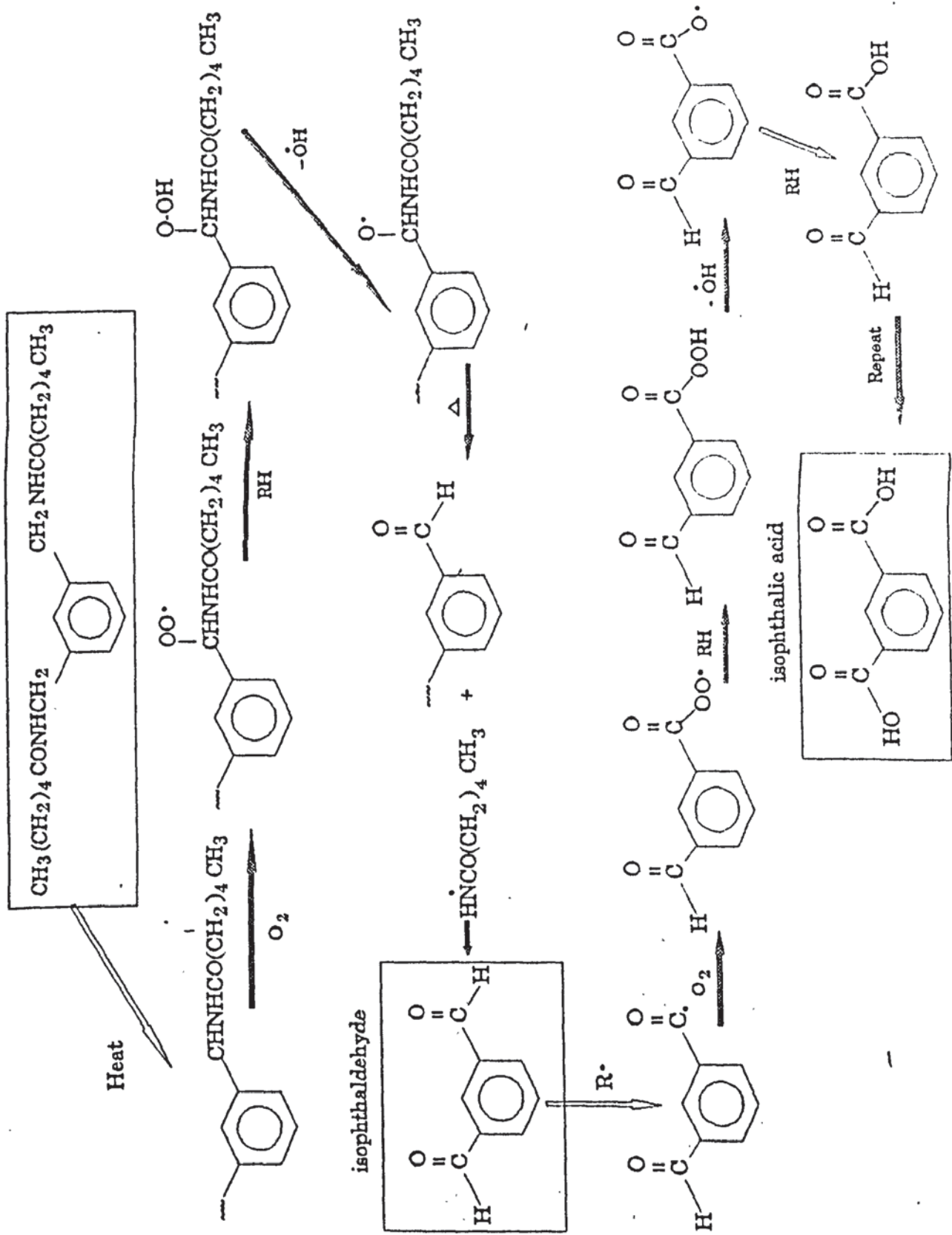
Scheme 6.6a Aromatic Products Derived From the Thermal Oxidation of Model I at 150°C.

Scheme 6.6b Aromatic Products Derived From the Thermal Oxidation of Model I at 150°C.

Scheme 6.7 The Reaction Mechanism for the Thermal Oxidation of Model II, Outlining in Particular the Initiation Step Via the Loss of the Most Reactive Hydrogen Atom.

Scheme 6.8 Monocarboxylic Acids Derived From the Thermal Oxidation of Model II at 190°C.

Scheme 6.9 Dicarboxylic Acids Derived From the Thermal Oxidation of Model II at 190°C.

Scheme 6.10 Aldehydes and Ketones Derived From the Thermal Oxidation of Model II at 190°C.
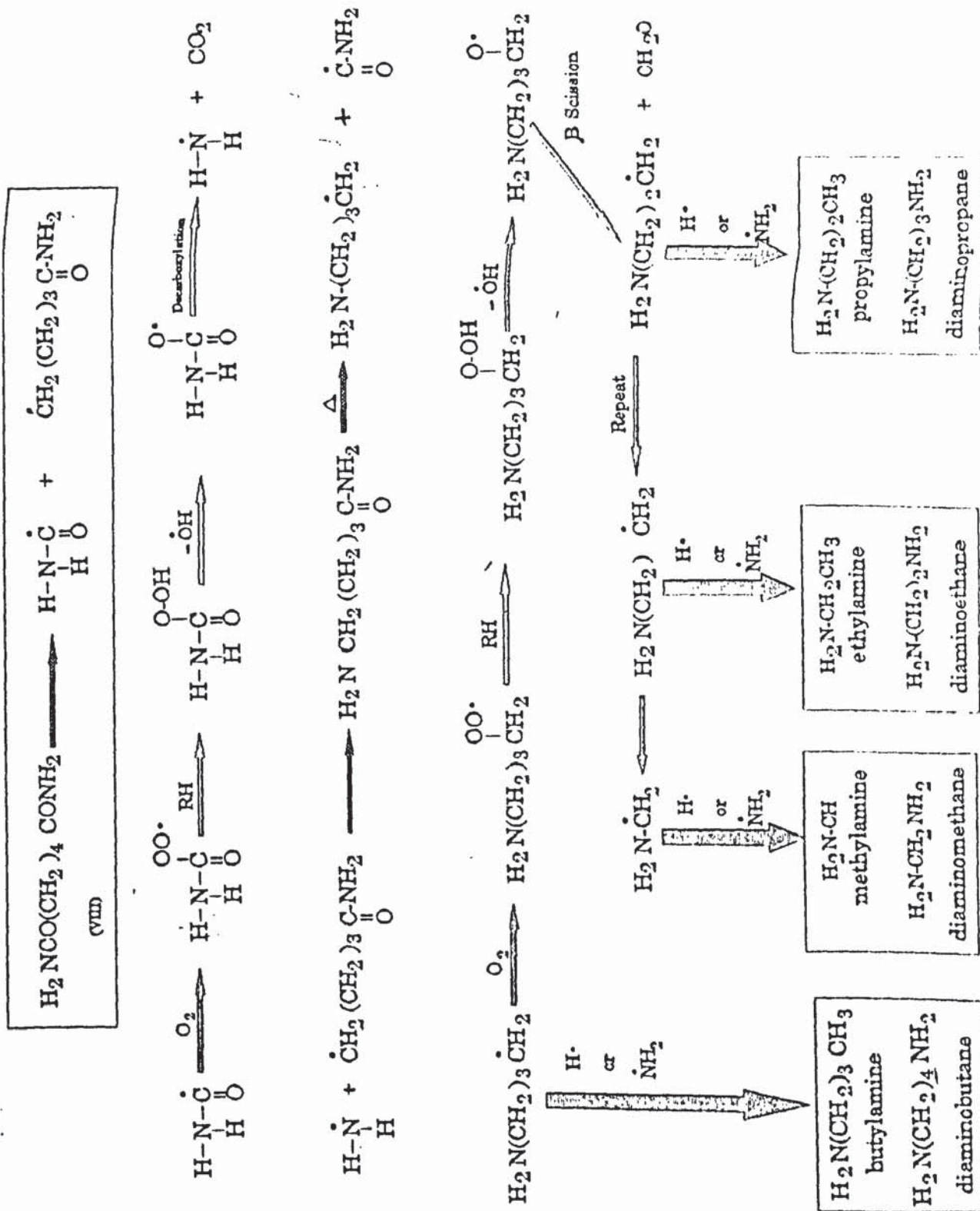
Scheme 6.11 Amines Derived From the Thermal Oxidation of Model II at 190°C.
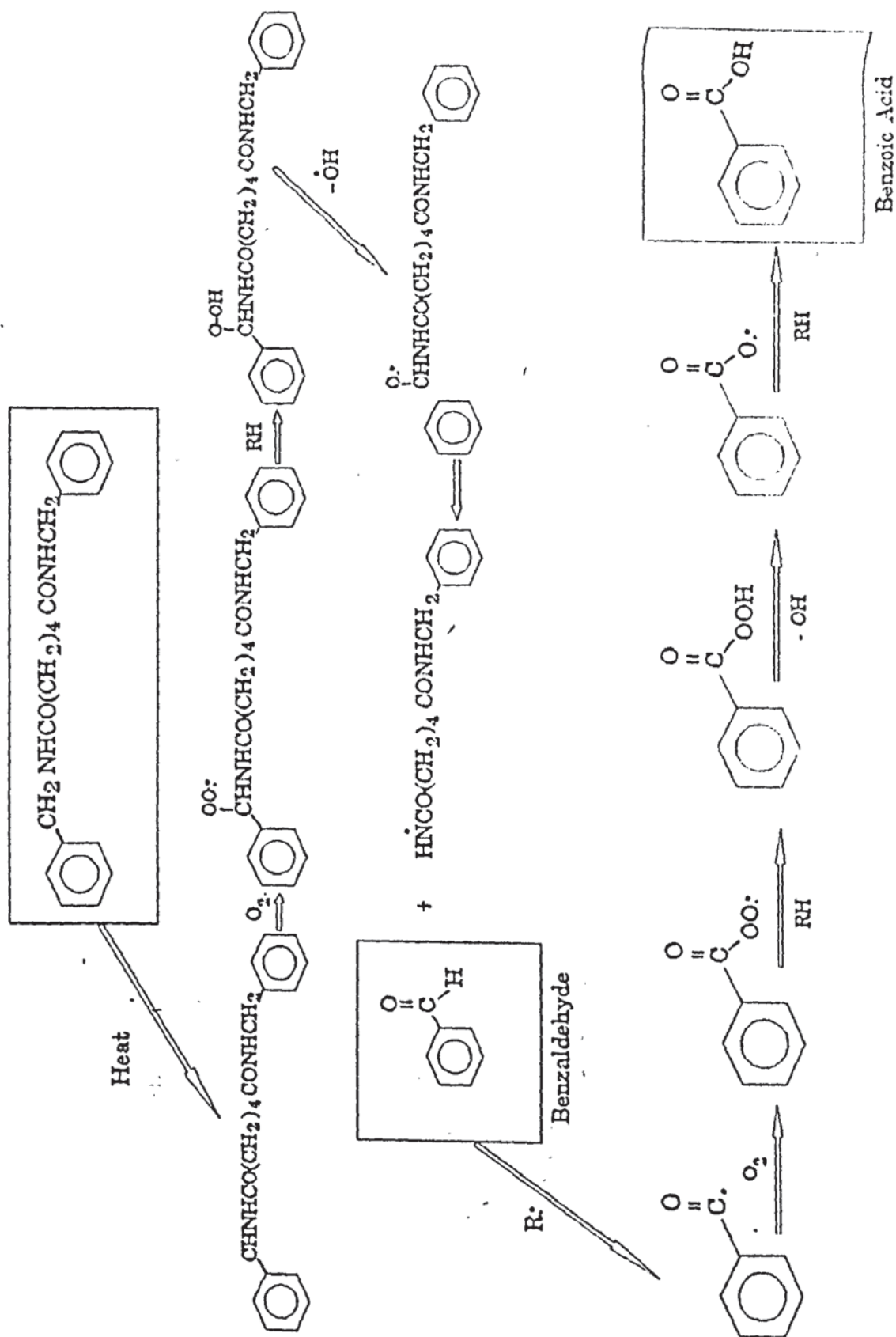
Scheme 6.12a Aromatic Products Derived From the Thermal Oxidation of Model II at 190°C.
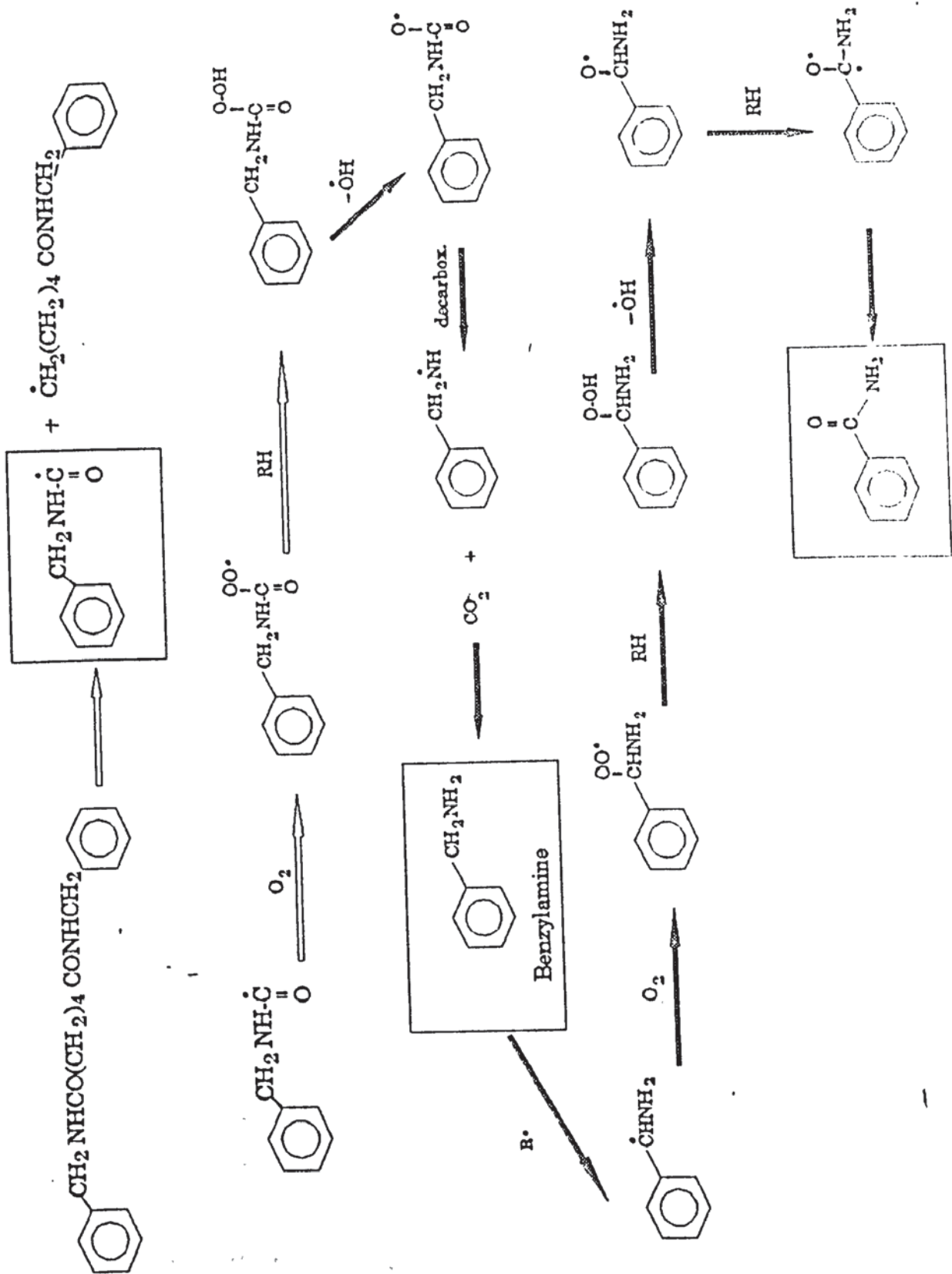
Scheme 6.12b Aromatic Products Derived From the Thermal Oxidation of Model II at 190°C.

Fig.6.1 H.P.L.C Trace of Monocarboxylic

Acids Formed During the Thermal

Oxidation of Model1 at 150°C:

a) Volatile Analysis.

Fig.6.2 H.P.L.C Trace of Monocarboxylic Acids Formed

During the Thermal Oxidation of Model1 at 150°C:

b) Non-Volatile Analysis.

Monocarboxylic Acid

1. Formic acid
2. Acetic acid
3. Propionic acid
4. n-Butyric acid
5. n-Pentanoic acid

Conditions : Water at pH 2.5
U.V. Source : 210nm
Flow Rate : 0.6ml/min
Column : Spherisorb ODS-2
         (100 x 4.6mm)
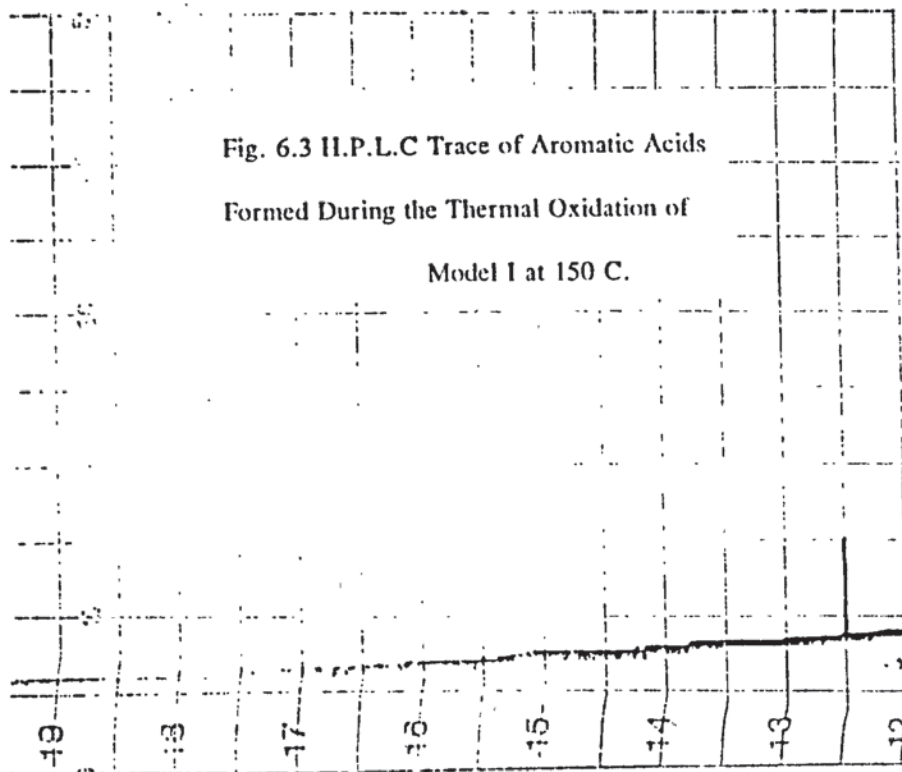
Fig. 6.3 H.P.L.C Trace of Aromatic Acids

Formed During the Thermal Oxidation of

Model 1 at 150 C.

Fig.6.4 H.P.L.C Trace of Aromatic Acids Formed

During the Thermal Oxidation of Model1 at 150°C:

b) Non-Volatile Analysis.

Aromatic Acid

1. Isophthalamic acid
2. Isophthalic acid

Conditions : Water/Methanol (70:30) at pH 3.5
U.V. Source : 254nm
Flow Rate : 0.6ml/min
Column : Spherisorb ODS-2
         (100 x 4.6mm)

Fig.6.5 H.P.L.C Trace of Aldehyde & Ketone Derivatives

Formed During the Thermal Oxidation of Model1 at 150°C:

a) Volatile Analysis.

Fig.6.6 H.P.L.C Trace of Aldehyde & Ketone Derivatives

Formed During the Thermal Oxidation of Model1 at 150°C:

b) Non-Volatile Analysis.

Aldehydes & Ketones

1. 2,4-Dinitrophenylhydrazine
2. Formaldehyde
3. Acetaldehyde
4. Propionaldehyde
5. Propanone
6. Butyraldehyde
7. Valeraldehyde
8. Isophthaldehyde

Conditions : Methanol/Water
(70:30) at pH 3.5
U.V.Source : 360nm
Flow Rate : 0.6ml/min
Column : Spherisorb ODS-2
(100 x 4.6mm)

Fig.6.7 H.P.L.C Trace of Amine Derivatives Formed During the Thermal Oxidation of Modell at 150°C: a) Volatile Analysis.

Fig.6.8 H.P.L.C Trace of Amine Derivatives Formed During the Thermal Oxidation of Modell at 150°C: b) Non-Volatile Analysis.
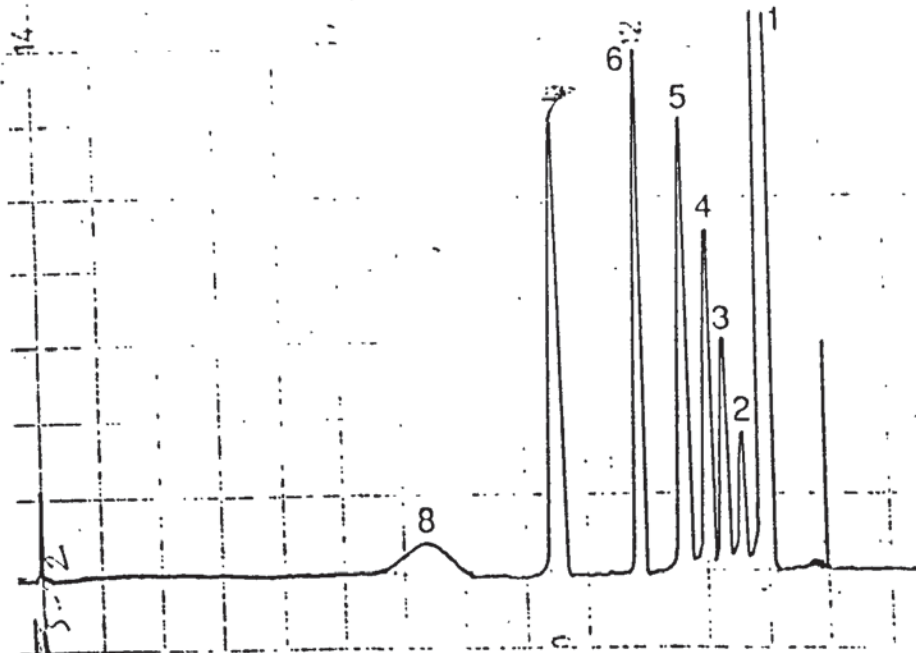
Amines

1. Dansyl Chloride
2. Ammonia
3. Methylamine
4. Ethylamine
5. Propylamine
6. n-Butylamine
7. n-Pentylamine
8. m-xylylenediamine

Conditions : Methanol/Water
(70:30)
U.V.Source : 254nm
Flow Rate : 0.6ml/min
Column : Spherisorb ODS-2
(100 x 4.6mm)

Fig.6.9 H.P.L.C Trace of Monocarboxylic Acids Formed
During the Thermal Oxidation of Model2 at 190°C:
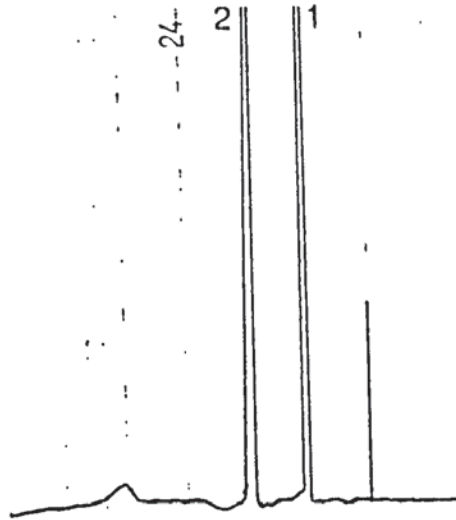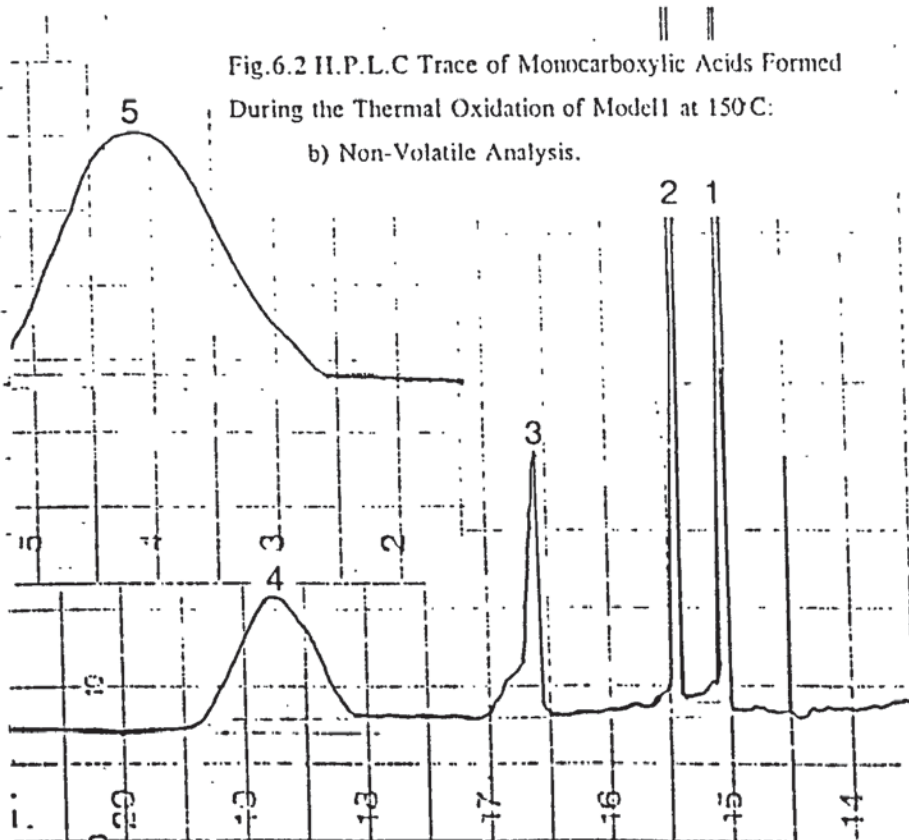
a) Volatile Analysis.

Fig.6.10 H.P.L.C Trace of Monocarboxylic Acids Formed
During the Thermal Oxidation of Model2 at 190°C:

b) Non-Volatile Analysis.

Monocarboxylic Acid

1. Formic acid
2. Acetic acid
3. Propionic acid
4. n-Butyric acid
5. n-Pentanoic acid

Conditions : Water at pH 2.5
U.V. Source : 210nm
Flow Rate : 0.6ml/min
Column : Spherisorb ODS-2
(100 x 4.6mm)

Fig.6.11 H.P.L.C Trace of Dicarboxylic Acids Formed
During the Thermal Oxidation of Model2 at 190°C:
a) Volatile Analysis.

Fig.6.12 H.P.L.C Trace of Dicarboxylic Acids Formed
During the Thermal Oxidation of Model2 at 190°C:
b) Non-Volatile Analysis.
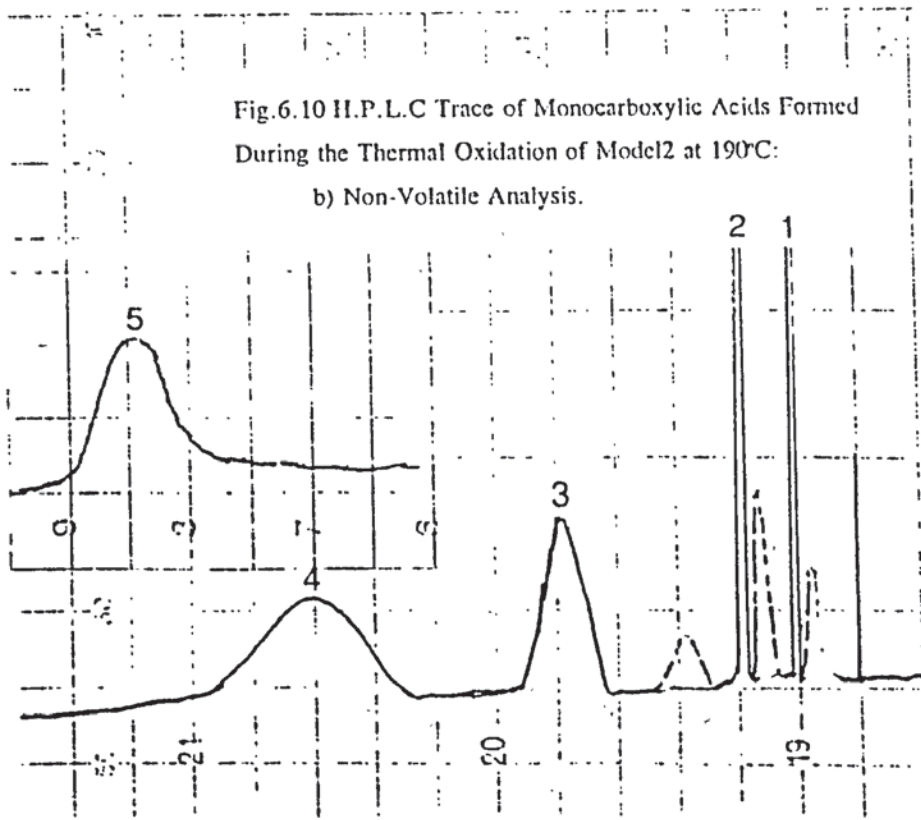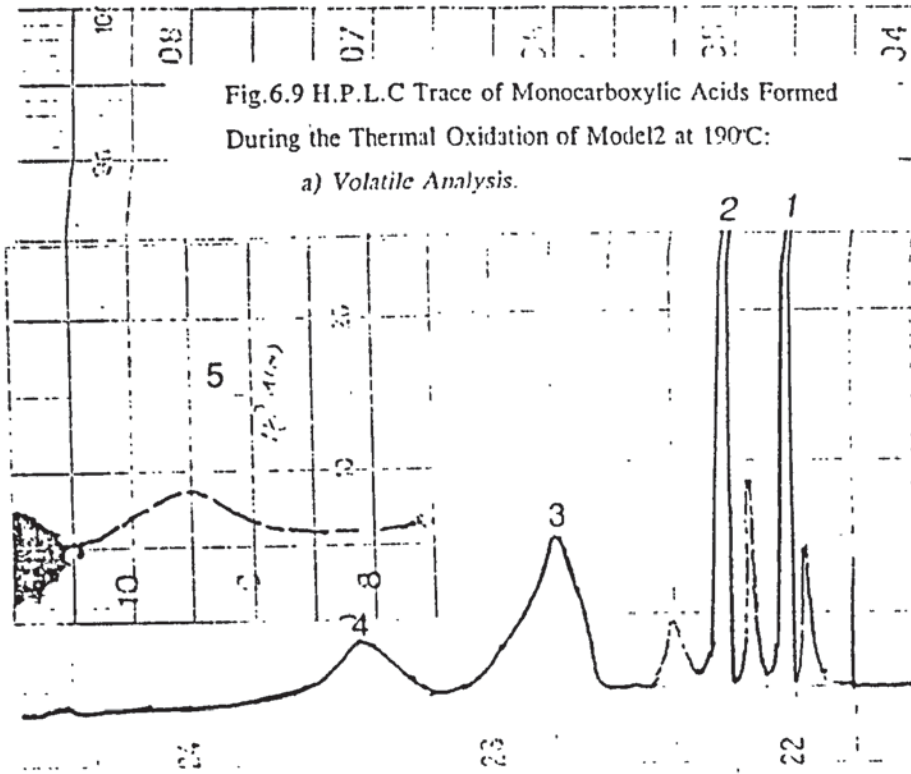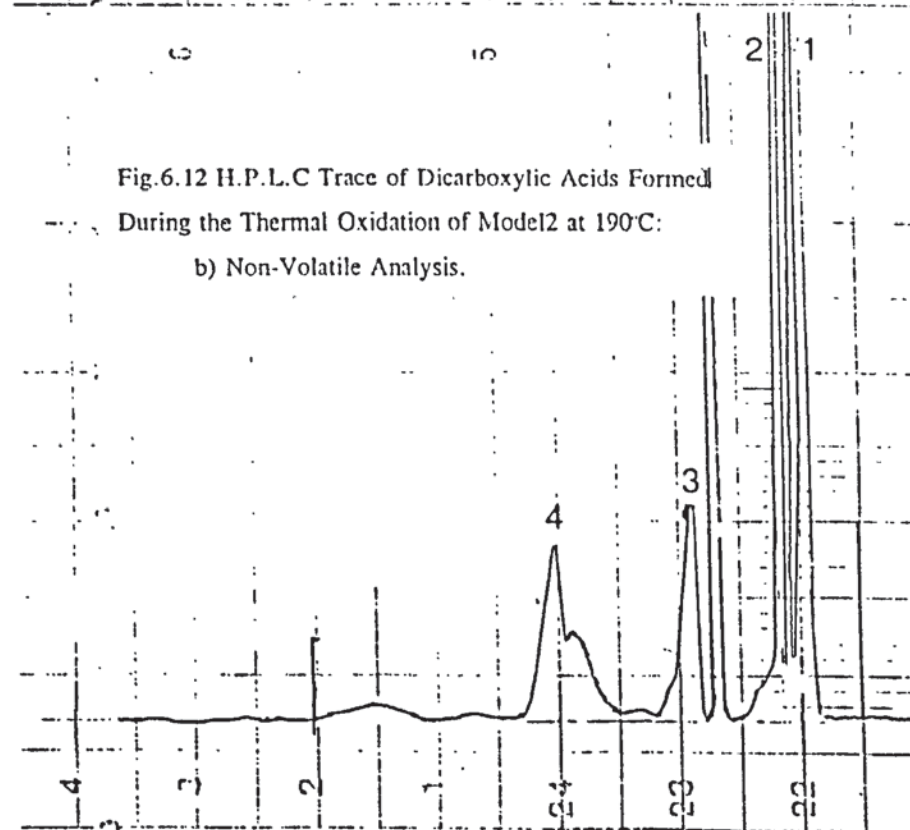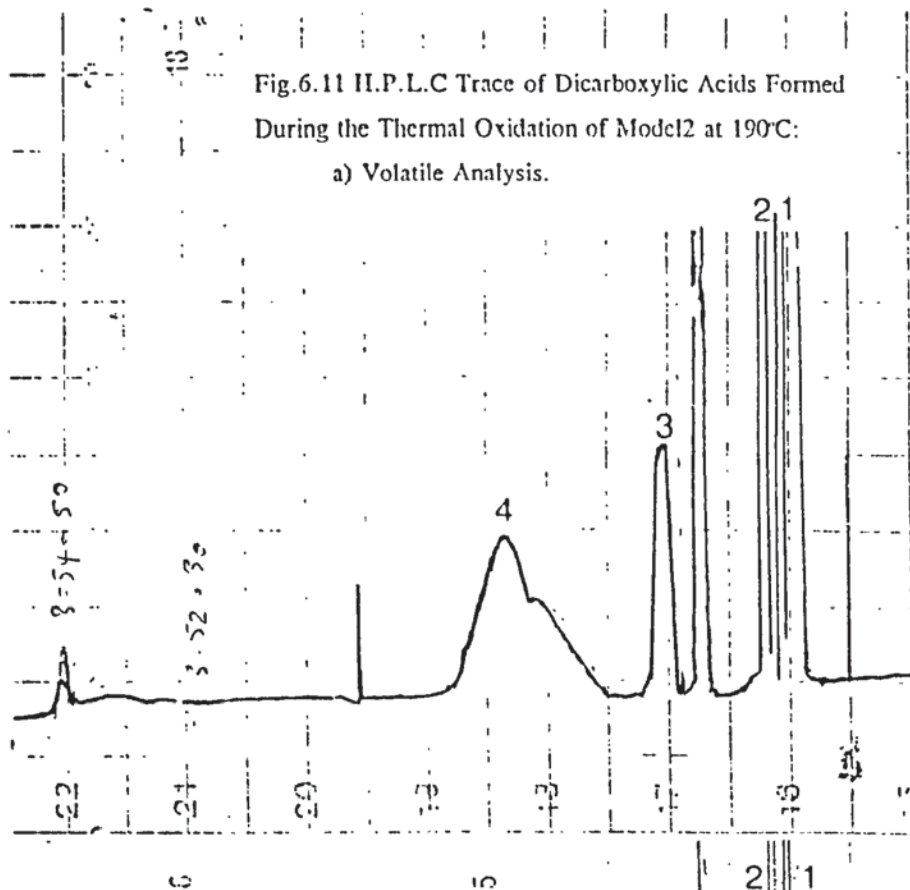
Dicarboxylic Acid

1. Oxalic acid
2. Malonic acid
3. Succinic acid
4. Glutaric acid

Conditions : Water/Methanol (98:2) at pH 2.5
U.V. Source : 210nm
Flow Rate : 0.6ml/min
Column : Spherisorb ODS-2
(100 x 4.6mm)
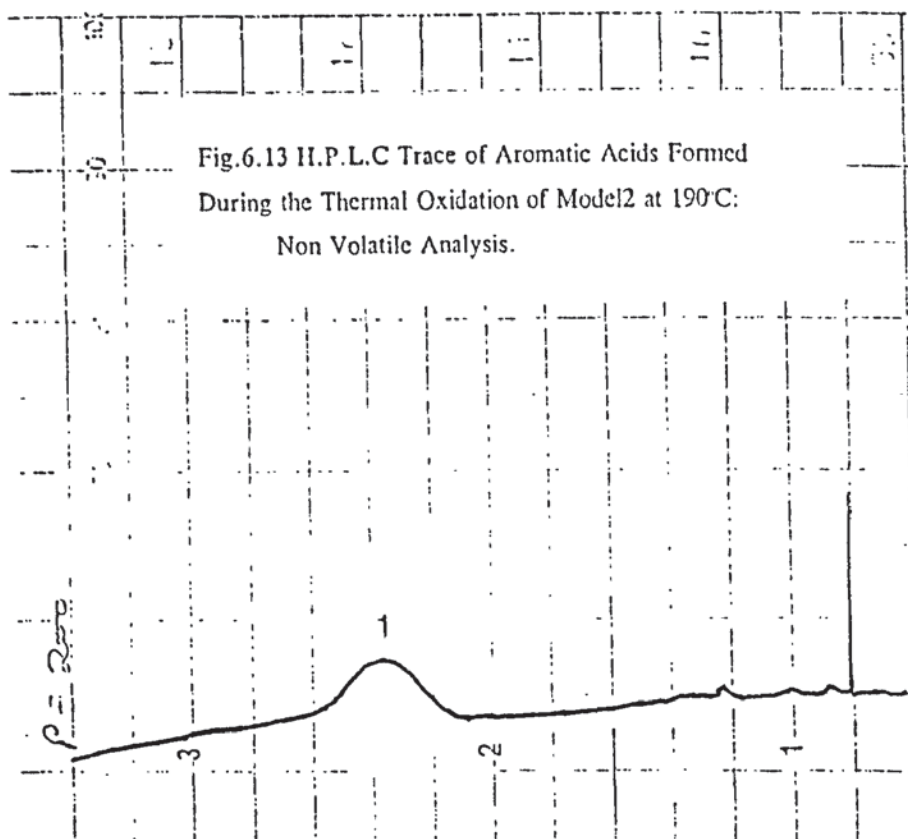
Fig.6.13 H.P.L.C Trace of Aromatic Acids Formed
During the Thermal Oxidation of Model2 at 190°C:
Non Volatile Analysis.

Aromatic Acid

1. Benzoic Acid

Conditions : Water/Methanol
(70:30) at pH 3.5
U.V. Source : 254nm
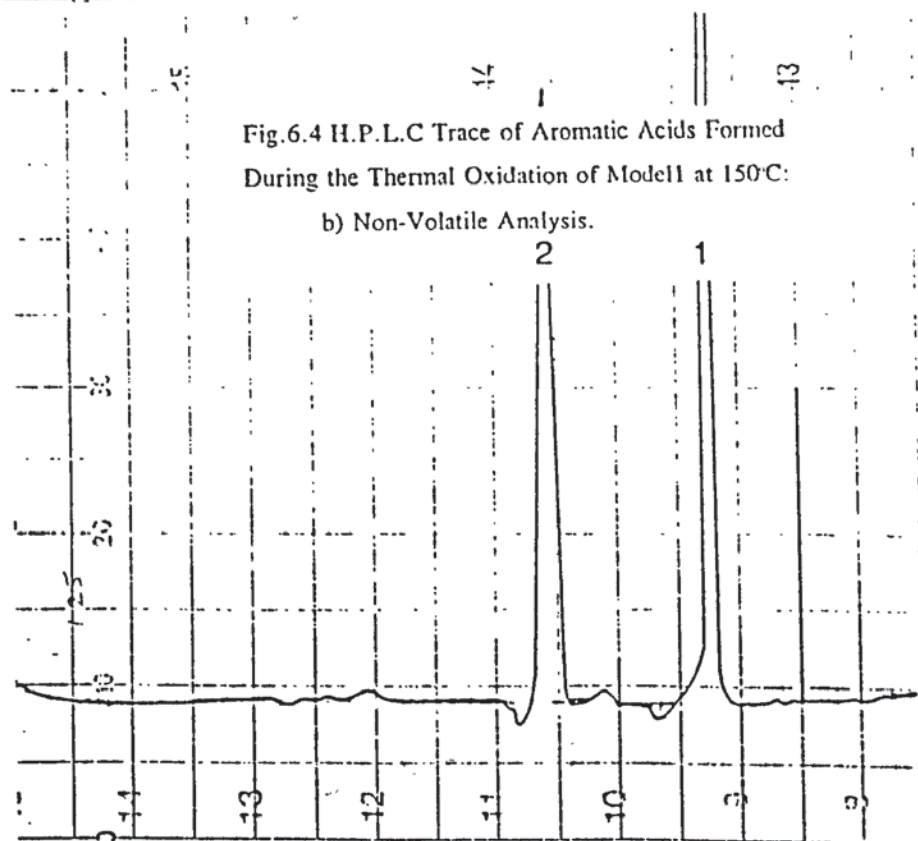Flow Rate : 0.6ml/min
Column : Spherisorb ODS-2
(100 x 4.6mm)

Fig.6.14 H.P.L.C Trace of Aldehyde & Ketone Derivatives
Formed During the Thermal Oxidation of Model2 at 190°C:

a) Volatile Analysis.
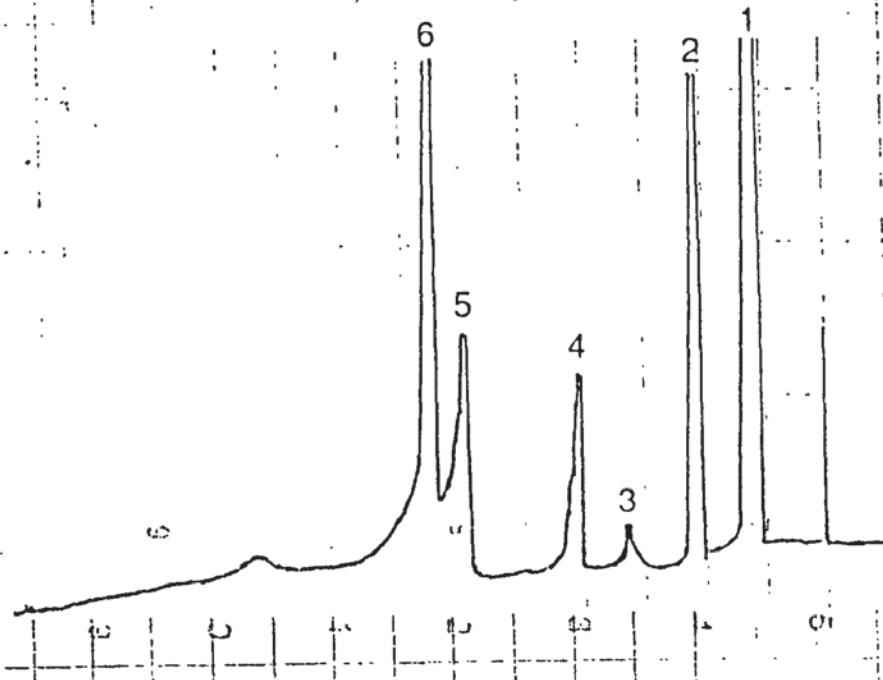
Fig 6.15 H.P.L.C Trace of Aldehyde & Ketone Derivatives
Formed During the Thermal Oxidation of Model2 at 190°C:

b) Non-Volatile Analysis.
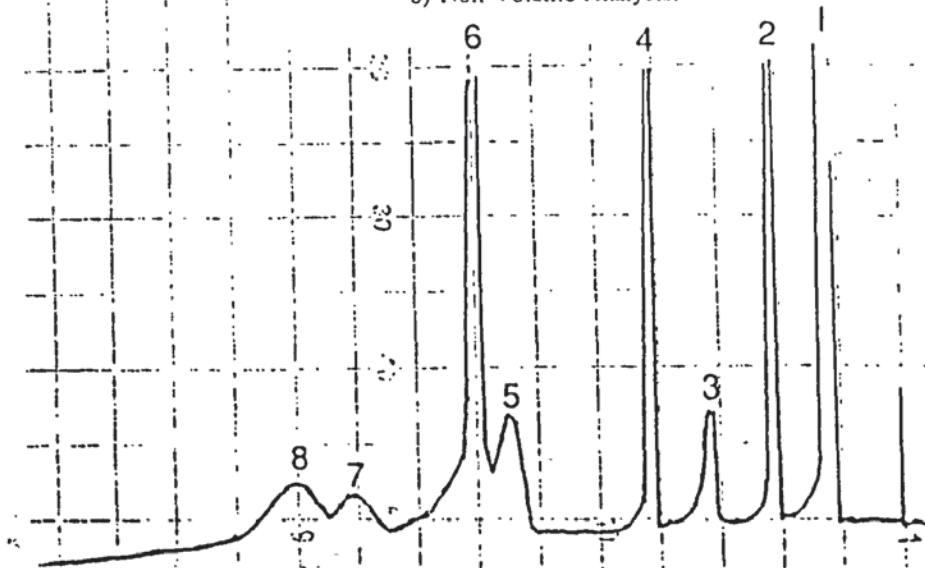
Aldehydes & Ketones

1. 2,4-Dinitrophenylhydrazine
2. Formaldehyde
3. Acetaldehyde
4. Propionaldehyde

5. Propanone
6. Butyraldehyde
7. Valeraldehyde
8. Benzaldehyde

Conditions : Methanol/Water
(70:30) at pH 3.5
U.V.Source : 360nm
Flow Rate : 0.6ml/min
Column : Spherisorb ODS-2
(100 x 4.6mm)

Fig.6.16 H.P.L.C Trace of Amine Derivatives Formed
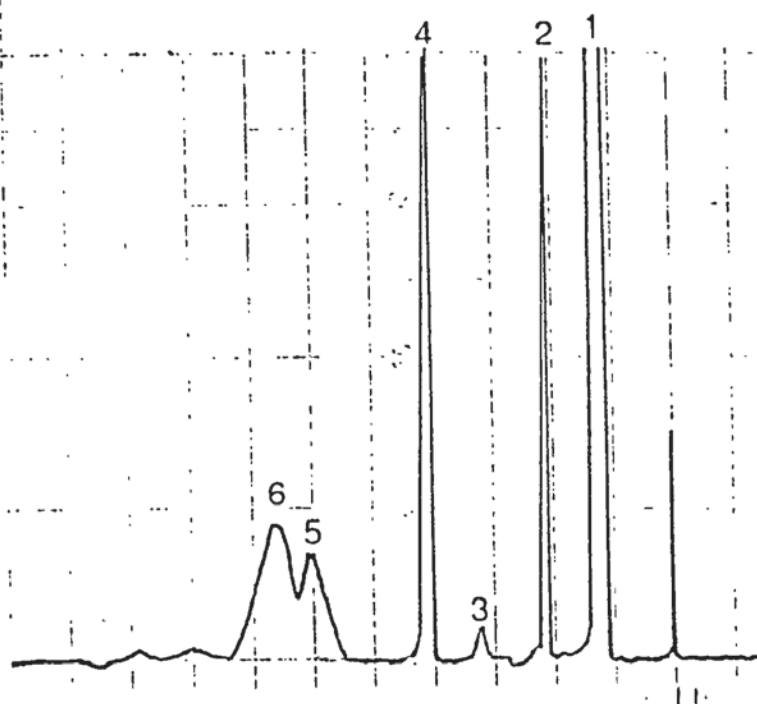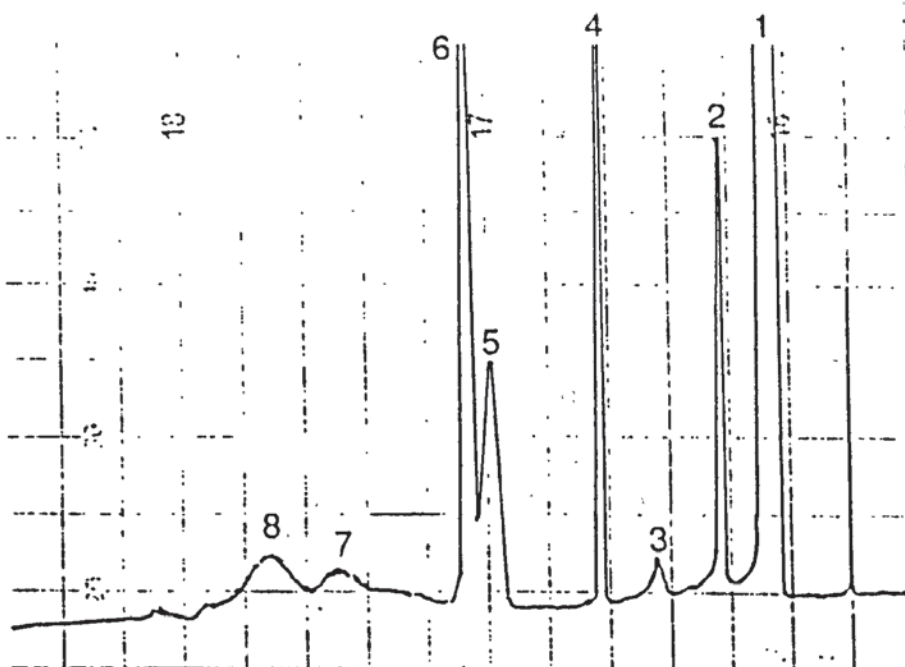During the Thermal Oxidation of Model2 at 190°C:
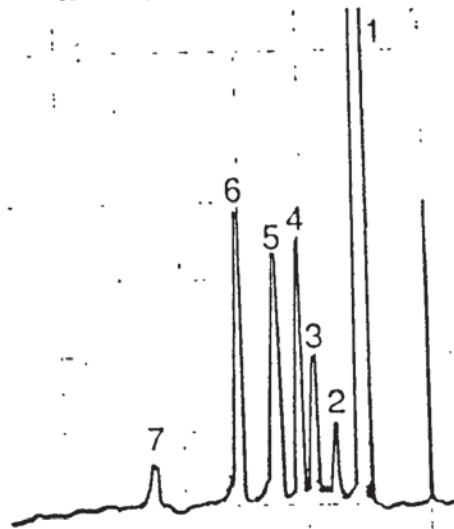
a) Volatile Analysis.
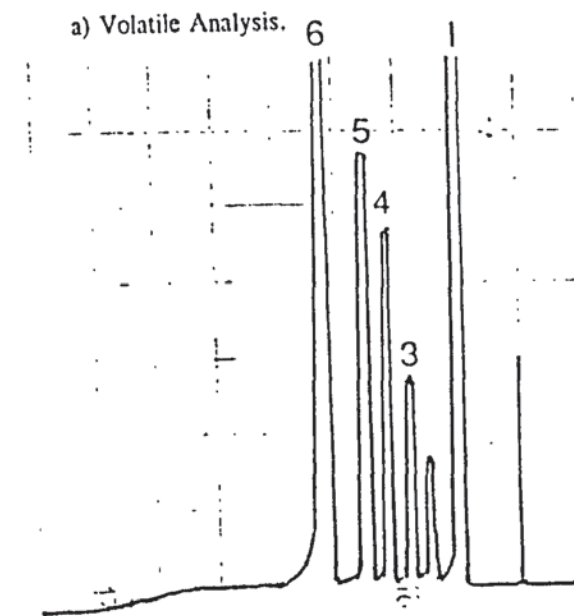
Fig.6.17 H.P.L.C Trace of Amine Derivatives Formed
During the Thermal Oxidation of Model2 at 190°C:

b) Non-Volatile Analysis.
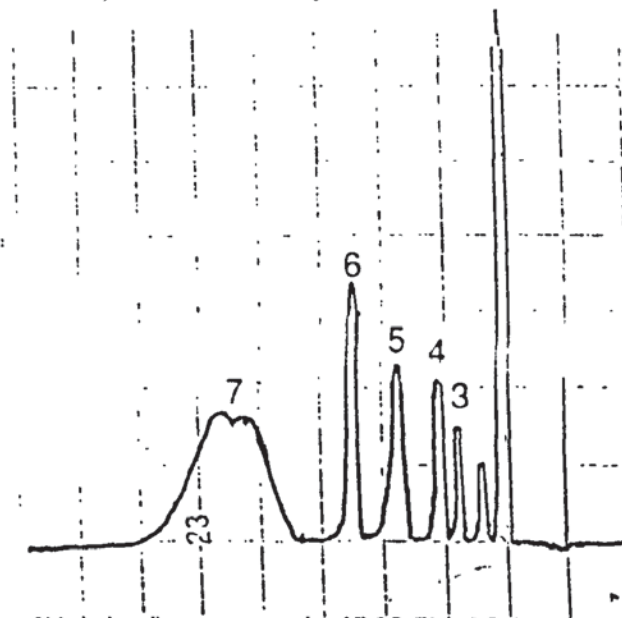
Amines

1. Dansyl Chloride
2. Ammonia
3. Methylamine
4. Ethylamine

5. Propylamine
6. n-Butylamine
7. Benzylamine

Conditions : Methanol/Water
(70:30)
U.V.Source : 254nm
Flow Rate : 0.6ml/min
Column : Spherisorb ODS-2
(100 x 4.6mm)
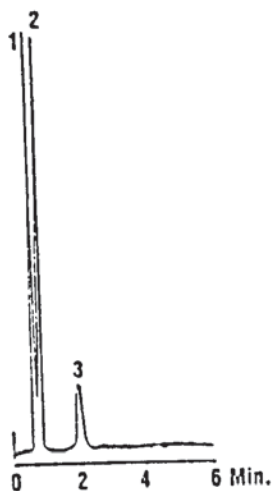
Gases

1. Air, carbon monoxide
2. Carbon dioxide
3. Water

Column : Poropak Q
Temp. : 75 C (TCD)
Flow rate : Helium, 20ml/min

Figure 6.18. The Gas Chromatogram of Gases formed during the Thermal Oxidation of Model I at 150°C, obtained via headspace.
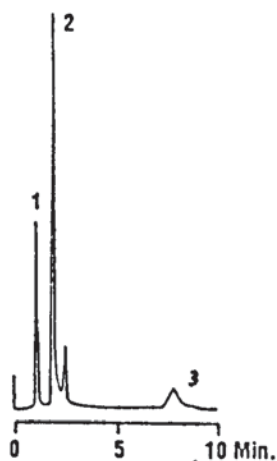
Gases

1. Oxygen
2. Nitrogen
3. Carbon Monoxide

Column : Molecular Sieve 5A
Temp : 75 C (TCD)
Flow rate : Helium, 20ml/min

Figure 6.19. The Gas Chromatogram of Permanent Gases formed during the Thermal Oxidation of Model I at 150°C, obtained via headspace.
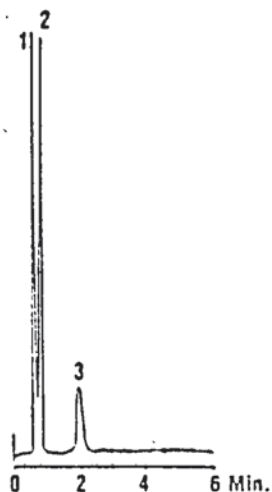
Gases

1. Air, carbon monoxide
2. Carbon dioxide
3. Water

Column : Poropak Q
Temp. : 75 C (TCD)
Flow rate : Helium, 20ml/min

Figure 6.20. The Gas Chromatogram of Gases formed during the Thermal Oxidation of Model II at 190°C, obtained via headspace.

Gases

1. Oxygen
2. Nitrogen
3. Carbon Monoxide

Column : Molecular Sieve 5A
Temp : 75 C (TCD)
Flow rate : Helium, 20ml/min

Figure 6.21. The Gas Chromatogram of Permanent Gases formed during the Thermal Oxidation of Model II at 190°C, obtained via headspace.

Chapter 7. Conclusion.

7.1 Conclusions.

1. Two model compounds I and II were prepared which represented different sections of the polyamide component (MXD6) of the polymer blend (PET/4% MXD6). Both contained two amide groups, with model I representing 1.5 units of the polymer, whereas model II represents the aliphatic portion of the chain between the two aromatic rings. Both model I and model II were shown to absorb oxygen readily, in similar amounts, at 150°C and 190°C respectively. In comparison to the oxidation of MXD6, the oxidation of models I and II seemed more extensive and immediate. The presence of an antioxidant (sodium phosphite) in a concentration of 1000ppm in MXD6 was thought to be responsible for this difference in oxidation performance. Sodium phosphite was also shown to act as an antioxidant for models I and II at all concentrations investigated. Evidence obtained from oxygen absorption studies, spectroscopic & hydroperoxide analysis and TGA degradation studies showed the inhibitive qualities of sodium phosphite on the oxidation of models I and II.

An understanding of the mechanism for the oxidation of model I and model II was achieved through an investigation of the by-products derived from the degradation of the two models at 150°C and 190°C, respectively. HPLC was the primary technique used for this purpose, however the spectroscopic analysis of the oxidising model also proved important in this respect. Table 7.1 summarises the main products of thermal oxidation of models I and II.

Mechanisms of oxidation for models I and II, based on established mechanisms of oxidation, were derived from these results. The mechanisms proposed are initiated primarily by the loss of a reactive hydrogen (alpha position to the N-H group) and to a lesser extent by the fission of the two bonds, namely the CH_2-NH bond and the CH_2-CO bond. Propogation via the formation and decomposition of hydroperoxide and a mechanism of sequential loss of a methylene group, via β scission has been proposed to account for the formation of several homologous series of products.

Series	Products	Model I	Model II
Monocarboxylic Acids	Formic	yes	yes
	Acetic	yes	yes
	Propionic	yes	yes
	n-Butyric	yes	yes
	n-Pentanoic	yes	yes
Dicarboxylic Acids	Oxalic	no	yes
	Malonic	no	yes
	Succinic	no	yes
	Glutaric	no	yes
	Adipic	no	no
Aromatic Acids	Isophthalamic	yes	no
	Isophthalic	yes	no
	Benzoic	no	yes
Aldehydes	Formaldehyde	yes	yes
	Acetaldehyde	yes	yes
	Propionaldehyde	yes	yes
	Butyraldehyde	yes	yes
	Valeraldehyde	yes	yes
Ketones	Propanone	yes	yes
Aromatic Aldehydes	Isophthalaldehyde	yes	no
	Benzaldehyde	no	yes
Amines	Ammonia	yes	yes
	Methylamine	yes	yes
	Ethylamine	yes	yes
	Propylamine	yes	yes
	Butylamine	yes	yes
	Pentylamine	yes	no
Aromatic Amines	m-xylylene diamine	yes	no
	Benzylamine	no	yes

Table 7.1 Summary of the Products From the Thermal Oxidation of Models I and II.

2. The effect of cobalt on the oxidation of model I and model II was investigated by a series of techniques, including oxygen absorption, spectroscopic & hydroperoxide analysis and isothermal thermogravimetric analysis. Using the evidence provided from this investigation a mechanism for the action of cobalt has been suggested. The techniques confirm the catalytic nature of the cobalt, when in the presence of 1000ppm sodium phosphite. In the absence of sodium phosphite the catalytic nature of the cobalt is not so clear. It has been proposed that sodium phosphite stabilises the cobalt in the oxidation experiments, preventing its decomposition at the reaction temperatures. The study concentrated on the oxidation of both models in the melt phase, hence unlike the solid state oxidation of MXD6 fibre, the mobility of the cobalt catalyst is not restricted. The action of cobalt is therefore more likely as a propagation catalyst, catalysing the decomposition of hydroperoxides formed during the oxidation process. The proposed oxidation cycle for models I and II (and other similar amides), including the role of cobalt, is summarised in scheme 7.1.

For the mechanism described in scheme 7.1, with particular relevance to the polymer (MXD6), during processing, cobalt catalysed oxidation starts and the first part of the cycle predominates. An essential part of this process is the formation of unsaturation, in this case, the imine (reaction A). This may not be very stable, (ie, readily hydrolysed to aldehyde, primary amide, acid (reactions b, c, d) and was difficult to characterise in this study. However if the reaction was carried out inside the NMR cavity (in-situ) at high temperature, then kinetics of product formation (and disappearance) could be continuously monitored, hence may be providing the opportunity of identifying the imine before it has chance to hydrolyse. Products of the second part of the cycle were identified through breakdown products of the alkoxy radical into aldehye and amide (reactions f to j). The role and importance of hydroperoxide as initiator (by redox reaction with cobalt, reactions B & C) on the scavenging ability of the polymer and its model compounds is also highlighted by the reaction scheme. The presence of hydroperoxides is essential to the second part of the cycle.

$-ArCH_2NHCO-$

$\xrightarrow[a]{\text{Shear low } O_2}$

$-Ar-\overset{\bullet}{C}HNHCO-$

$-ArCH=NCO-$

$\boxed{-ArCHO} + H_2NCO-$

$\xrightarrow[b]{\uparrow H_2O}$

$\boxed{-ArCOOH} \quad \boxed{NH_3} + \boxed{-COOH}$

$\xrightarrow[c]{\uparrow O_2} \quad \xrightarrow[d]{\uparrow H_2O}$

e

1st Cycle

LM^{3+}

LM^{2+}

A

B

High O_2

2nd Cycle

$\underset{-Ar\overset{|}{C}HNHCO-}{OOH}$

$\underset{-Ar\overset{|}{C}HNHCO-}{OO\bullet}$

C

$^-OH + LM^{3+}$

LM^{2+}

D

$\underset{-Ar\overset{|}{C}HNHCO-}{O\bullet}$

$\underset{-Ar\overset{|}{C}HNHCO-}{OOH}$

$\downarrow f$

$\boxed{-ArCHO} + \overset{\bullet}{N}HCO-$

$\xrightarrow[g]{\downarrow O_2} \quad \xrightarrow[h]{\downarrow RH}$

$\boxed{-ArCOOH} \quad NH_2CO- \xrightarrow[\text{Bond Scission}]{j} \boxed{\begin{array}{l}\text{Aldehydes/Ketones}\\\text{Carboxylic Acids}\\\text{Amines.}\end{array}}$

$\downarrow i$

$\boxed{NH_3} + \boxed{HOOC-}$
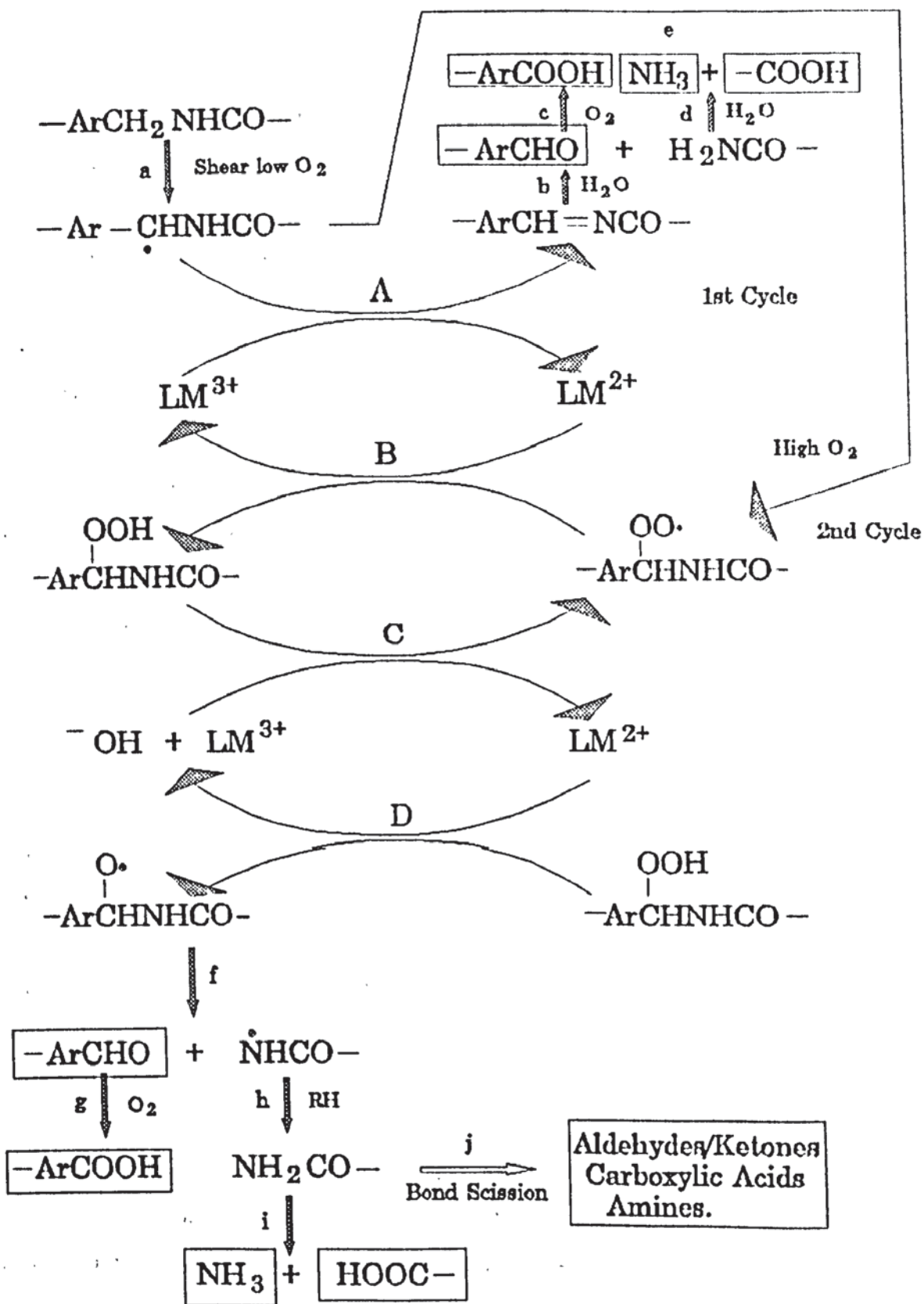
Scheme 7.1 The Proposed Oxidation Cycle for Models I and II, and Other Similar Amides.

7.2 Recommendation for Future Study.

4% MXD6 (poly m-xylylene adipamide) in a polymer blend containing PET (poly ethylene terephthalate) is known to produce a packaging container which exhibits exceptional oxygen barrier properties. This study concentrated on the thermal oxidation of two models representing the aromatic polyamide MXD6. The influence of cobalt as a catalyst for oxidation of these models was investigated and the proposed mechanism centred around the function of cobalt as a propogation catalyst, catalysing the decomposition of hydroperoxides formed during oxidation. The role of cobalt as an initiation catalyst, via complexation with the amide, seemed unlikely from the results obtained but further work on different series of models, particularly model (III) would help to prove or disprove this proposal, depending on the amount of oxygen absorbed in comparison to model I and Model II, and models based on a furhter MXD_n series, in which n is greater or less than 6 (ie, MXD4 or MXD7). A similar study conducted using other transition metals which may have an adverse effect on the reaction would be interesting and could reveal information that may aid in confirming the mechanism proposed.

The importance of sodium phosphite as both a stabiliser of the model compounds and the cobalt salt became apparent in this study. Its effect on the cobalt was not perceived prior to this study but it was proposed that sodium phosphite stabilises the cobalt, extending the temperature range at which the cobalt salt decomposes. The exact nature of this stabilisation effect is unclear and should be investigated to a greater extent particularly with respect to the use of cobalt in experiments at significantly higher reaction temperatures (ie, the processing of MXD6 which is carried out at temperatures up to 300°C).

Finally in a more general context, of particular interest for future work would be the investigation of an alternative polymer likely to produce a similar oxygen barrier property to that of MXD6 in conjunction with PET. The examination of other oxidisable polymers which do not contain nitrogen would be a good alternative bearing in mind possible future use in food packaging applications. Polyisoprene or polyester based on the the MXD6 structure are good candidates.

References.

[1] I. Labliza and J.Breene., "Active Packaging" Journal of Food Packaging, 13, 1, (1989).

[2] U.S Patent Application 4.908.151 (1989).

[3] European Application 367.835 (1989).

[4] European Application 366.254 (1990).

[5] European Application 380.830 (1990).

[6] W.L. Hawkins (ed.)., "Polymer Degradation & Stabilisation", Wiley Interscience, New York (1992).

[7] F.H Winslow, C.J Aloisio, W.L Hawkins, W. Matreyek & S. Matsuoka., "Dependence of Polyolefin Oxidation on Morphology" Chem. Ind, 533-534, (1963).

[8] G.Scott "Atmospheric Oxidation and Anti-oxidants" ch.3, p.66 (Elsevier, London 1967).

[9] L.Bateman, M.E. Cain, T. Colcough and J.I. Cunneen J., "Oxidation of Organic Sulphides" Chem. Soc, 3570-3578, (1962).

[10] J.R. Shelton and D.N. Vincent., "Retarded Autoxidation and the Chain-Stopping Action of Inhibitors" J. Amer. Chem. Soc.,85, 2433-2439, (1963).

[11] W.L. Hawkins and F.H Winslow., "Polyolefin Stabilization" Trans. Plastics Inst.(London), 29 (81), 82-86 (1961).

[12] Z. Osawa., "Developments in Polymer Stabilisation: Inhibition of Metal Catalyzed Degradation of Polymers"", 7, 193-232, Developments Series (1984).

[13] Z. Osawa and T. Saito., "Stabilisation & Degradation of Polymers", Advances in Chem. Series No. 169, P.159, (1978).

[14] Z. Osawa, T. Ishizuka., M, Sorimachi and Y. Ogiwara., "Catalytic Action of Metallic Salts in Autoxidation and Polymerization" J. Polym. Sci., B9, 497-502, (1971).

[15] A.J. Chalk and J.F. Smith., "Catalysis of Cyclohexane Autoxidation" Trans Faraday Soc., 53, 1214, 1235, (1967).

[16] A.T. Betts and N. Uri., "The Conversion of Metal Catalysts into Inhibitors of Autoxidation" Makromol.Chem., 95, 22-39, (1966).

[17] Y. Kamiya., "Autoxidation of Polypropylene Catalyzed by Cobalt Salt in the Liquid Phase" J. Polym. Sci. Part A-1, 6, 2561-2572, (1968).

[18] Y. Kamiya, S. Beaton, F. Lafortune & K.U. Ingold., "The Metal Catalyzed Autoxidation of Tetralin. The Cobalt Catalysed Autoxidation of Undiluted Tetralin and of Tetralin in Chlorobenzene" Can. J. Chem, 41, 2034-2053, (1963).

[19] Y. Kamiya, S. Beaton, F. Lafortune & K.U. Ingold., "The Metal Catalysed Autoxidation of Tetralin. The Effect of Solvent and Temperature" Can. J. Chem, 41, 2020-2033, (1963).

[20] G. Scott., "Atmospheric Oxidation & Anti-oxidants" Ch.2, P.41 (Elsevier, London 1967).

[21] M.H. Dean and G. Skirrow., "Cobalt Catalysed Decomposition of tert-Butyl Hydroperoxide" Trans Faraday Soc., 54, 849-854, (1958).

[22] G.L. Banks, A.J. Chalk, J.E. Dawson and J.F. Smith., "Catalysis of Olefin Autoxidation by Heavy Metal Ions in Non-Polar Media" Nature, 174, 274-279, (1954).

[23] C.J. Pederson., "Inhibition of Deterioration of Cracked Gasoline During Storage" Ind. Eng. Chem, 41, 924-928, (1949).

[24] L. Reich and S.S. Stivala., "Autoxidation of Hydrocarbons & Polyolefins", Marcel Dekker Inc., New York, (1969).

[25] B. Ranby and J.F. Rabek., "Photodegradation, Photoxidation & Photostabilisation of Polymers", Interscience, New York, (1975).

[26] P. George and A. Robertson., "Oxidation of Liquid Hydrocarbons" Trans Faraday Soc., 42, 21-24, (1949).

[27] R.A Sheldon and J.K Kochi., Oxid. Combust. Rev., 5, P.999, (1971).

[28] Y. Kamiya and K.Y. Ingold., "The Metal Catalyzed Autoxidation of Tetralin. The Effect of Solvent and Temperature" Can. J. Chem., 42, 2424-2433, (1964).

[29] J.D. Holdsworth, G. Scott and D.J. Williams., "Mechanisms of Antioxidant Action: Sulphur Containing Antioxidants" Chem. Soc., 4692-4699, (1964).

[30] G. Scott., "Atmospheric Oxidation & Antioxidants", P.188, Elsevier Amsterdam, (1965).

[31] A. Zweig and W.A. Anderson (Jr)., "Singlet Oxygen and Polymer Photooxidations" J. Polym. Sci. Chem. Ed., 13, 717-736, (1975).

[32] A.M. Torozzolo and F.A. Winslow., "A Mechanisms for the Oxidative Photodegradation of Polyethylene" Macromolecules, 1, 98-100, (1968).

[33] D.J. Carlsson and D.M. Wiles., J. Macromol. Sci. Rev. Chem., 14(2), 155, (1976).

[34] J.F. Black., "Metal Catalysed Autoxidation. The Unrecognized Consequences of Metal-Hydroperoxide Complex Formation" J.Amer. Chem. Soc., 100, 527-535, (1978).

[35] G. Scott., "Developments in Polymer Stabilisation: Mechanisms of Antioxidant Action", 4, 1-22, (1980).

[36] G. Scott., "Atmospheric Oxidation & Antioxidants" Ch.7, P.248 (Elsevier, London 1967).

[37] B. Kamerbeek, G.H Kroes & W. Grolle., " High Temperature Resistance and Thermal Degradation of Polymers", S.C.I Monograph No.13, London 357, (1961).

[38] B.T. Mortimer (ed).," Reaction Heats and Bond Strengths", Pergamon Press New York, 129, (1962).

[39] S.K. Kakar., " The Thermal Degradation of Nylon 6,6 " Ph.D. thesis, Department of Textile Industries, Leeds University, (1973).

[40] I. Goodman., "The Thermal Degradation of 66 Nylon: Further Studies on the Pyrolysis of Di-n-Butyl Adipamide" J. Polym. Sci, 17, 587-590, (1955).

[41] J.L. Bolland., "Kinetics of Olefin Oxidation" Quart. Revs.(London), 3, 1-21, (1949).

[42] R.F. Schwenker and L.R. Beck., "Differential Thermal Analysis of Textile and Other High Polymeric Materials" Tex. Res. J., 30, 624-629, (1960).

[43] M.B. Neiman (ed.)., "Aging and Stabilisation of Polymers", Pergamon Press, New York, (1965).

[44] E.I. Valko and C.K. Chiklis., "Effects of Thermal Exposure on the Physicochemical Properties of Polyamides" J. Appl. Polym. Sci., 9, 2855-2877, (1965).

[45] G. Valk, H. Krussmann & P. Deihl., "Degradation by Heat and Light" Makromol. Chem., 107, 158-169, (1967).

[46] G.W. Harding and B.J. Macnulty., " High Temperature Resistance and Thermal Degradation of Polymers", S.C.I. Monograph No. 13, London, 392 (1961).

[47] M.V. Lock and B.F. Sagar., "Autoxidation of N-Alkylamides. PartI. N-Acylamides as Oxidation Products" J. Chem. Soc., (B), 690-696, (1966).

[48] B.F. Sagar., "Autoxidation of N-Alkylamides. PartII. N-Alkylamide Hydroperoxides and Di-N-Alkylamide Peroxides" J. Chem. Soc., (B), 428-439, (1967).

[49] B.F. Sagar., "Autoxidation of N-Alkylamides. PartIII. Mechanism of Thermal Oxidation" J. Chem. Soc., (B), 1047-1061, (1967).

[50] W.H. Sharkey and W.E. Mochel., "Mechanism of the Photooxidation of Amides" J. Amer. Chem. Soc., 81, 3000-3005, (1959).

[51] A.G. Davies., " Organic Peroxides", Butterworths, London 1961.

[52] E. Dyer, K.R. Carle, D.E. Weimen., "Effect of Cobaltous 2-Ethylhexanoate and Other Salts on the Decomposition of Tetralin Hydroperoxide" J.Org. Chem., 23, 1464-1469, (1958).

[53] A.J Chalk and J.F. Smith., "Catalysis of Cyclohexane Autoxidation by Trace Metals in Non-Polar Media" Trans. Faraday. Soc., 53, 1214-1220, (1957).

[54] A.E. Woodward and R.B. Mesrobian., "Low Temperature Autoxidation of Hydrocarbons. The Kinetics of Tetralin Oxidation" J. Amer. Chem. Soc., 75, 6189-6195, (1953).

[55] C.E.H. Bawn, A.A. Pennington and C.F.H. Tipper., "The Catalyzed Oxidation of Trimethyl Ethylene in Solution" Faraday Soc. Discuss., 10, 282-291, (1951).

[56] N.J. Harris., Internal Report TR2039, Carnaud MetalBox Packaging Technol. (1988).

[57] N.J. Harris., Internal Report TR3410, Carnaud MetalBox Packaging Technol. (1989).

[58] N.J. Harris., Internal Report TR3191, Carnaud MetalBox Packaging Technol. (1988).

[59] H.H.G. Jellinek., "Aspects of Degradation and Stabilisation of Polymers", p.122, Elsevier (1978).

[60] S.A. Sills., Private Communication.

[61] N.J. Harris., Internal Report TR3934, Carnaud MetalBox Packaging Technol. (1989).

[62] F.A. Cotton and G. Wilkinson., " Advanced Inorganic Chemistry" 3rd Edn. P.877 and P.897, Interscience (1972).

[63] K.F. Purcell and J.C. Kotz., "Inorganic Chemistry", P.742, Saunders (1977).

[64] R.T. Morrison and R.N. Boyd., "Organic Chemistry", 4th Edn P.173-175, Allyn & Bacon.

[65] Ref. [59] P.650 - 652, Interscience, 1972.

[66] M.A. Cochran., Internal Report TR3323, Carnaud MetalBox Packaging Technol. (1988).

[67] M.A. Cochran., Internal Report TR3322, Carnaud MetalBox Packaging Technol. (1988).

[68] M.A. Cochran and N.J. Harris., Internal Report TR3510, Carnaud MetalBox Packaging Technol.(1989).

[69] J.R. Shelton and W.L Cox., "Oxidation and Antioxidant Action in Rubber Vulcanizates" Ind. Eng. Chem., 46, 816-823, (1954).

[70] S.W. Bigger, J. Scheiers and O.Delatycki " Thermal & Oxidative Studies of Polythene" 34th IUPAC Int. Sympos. on Macromol., (1992).

[71] M.U. Amin, G. Scott, L.M.K Tillekeratne., "Mechanism of the Photo-Initiation Process in Polyethylene" Eur. Polm. J., 11, 85-89, (1975).

[72] N.S. Allen and A. Parkinson., Polym. Degd. Stab., 12, 363, (1985).

[73] A. Anani, A. Mobasher, F.A Rasoul., "Use of Photoacoustic Spectroscopy in Studying the Natural Weathering of Polyethylene Films" J. Appl. Polym. Sci., 29, 1491-1497, (1984).

[74] J.P. Luongo., "Infra-red Study of Oxygenated Groups Formed in Polyethylene During Oxidation" J. Polym. Sci., 42, 139-150, (1960).

[75] F.P. La Mantia., "Natural Weatherings of Low Density Polyethylene" Eur. Polym. J;, 20 (10), 993-995, (1984).

[76] A.W. Pross and R.A. Black., "Photocatalyzed Oxidation of Polythene" J. Soc. Chem. Ind., 69, 113-116, (1950).

[77] G.A.J. Pitt and R.A. Morton., "Progress in the Chem. of Fats and other Lipids", Vol.IV, p.228, Pergammon Press (1957).

[78] P.E. Slade and L.T. Jenkins., "Techniques & Methods of Polymer Evaluation", Vol.1. Thermal Analysis, London, Edward Arnold ltd. New York Interscience (1964).

[79] D.A. Smith.,"Addition Polymers", London Butterworths, (1968).

[80] L. Reich and D.W. Levi., "Dynamic Thermogravimetric Analysis in Polymer Degradation" Macromol Rev. 1, P.173-275, (1967).

[81] J.II. Flynn and L.A. Wall., "General Treatment of the Thermogravimetry of Polymers" J. Res. Nat. Bur. Stand., A 70 (6), 487-523, (1966).

[82] A. Blazek., "Thermal Analysis"., London, Von Nostrand Reinhold (1973).

[83] T. Daniels., "Thermal Analysis", London, Kogan Page, (1973).

[84] D. Dollimore and C.J. Keattch., "An Introduction to Thermogravimetry", 2nd Edn, London, Heyden, (1975).

[85] R.C. Mackenzie., "Differential Thermal Analysis", Vols 1 and 2, London, Academic Press, (1970, 1972).

[86] T. Ozawa., "Critical Investigation of Methods for Kinetics Analysis of Thermoanalytical Data" J. Thermal Analysis, 4, 601-617, (1975).

[87] T. Ozawa., "A New Method of Analyzing Thermogravimetric Data" Chem. Soc. Jpn. Bull., 38, 1881-1886, (1964).

[88] J. March., "Advanced Organic Chemistry", 2nd Edn., p.386, McCraw-Hill, (1977).

[89] E.II. Rodd (ed.)., "Chemistry of Carbon Compounds", 1A, p.389, Elsevier (1951).

[90] I.L. Finar., "Organic Chemistry", 1, p.376, Longman London, (1973).

[91] C.F.II. Allen and W.J. Humphlett., "Organic Synthesis", Vol IV, p.80, (1963).

[92] P.J. Smith., "The Interaction Between Sulphur Antioxidants and Iron in Mineral Oils", Ph.D thesis, Aston University, (1986).

[93] M. Kharasch, A. Fono and W. Nudenburg., "The Chemistry of Hydroperoxides. VI. The Thermal Decomposition of alpha-Cumyl Hydroperoxide" J. Organic Chem., 16, 113-127, (1951).

[94] P. Bocek., "Determination of Hydroperoxides in Atactic Polypropylene" Chem. Prumsyl., 17, 439-444, (1967).

[95] K. Fung and D. Grosjean., "Determination of Nanogram Amounts of Carbonyls as 2,4-Dinitrophenylhydrazones by High Performance Liquid Chromatography" Anal. Chem., 53, 168-171, (1981).

[96] C.F. Poole and S.A. Schuette., "Contemporary Practice of Chromatography", p.516, Elsevier (1984).

[97] R.J. Fessenden and J.S. Fessenden., "Organic Chemistry", 3rd Edn, Brooks/Cole (1986).

[98] C.F.H. Allen and J.H. Richmond., "Limitations of 2,4-Dinitrophenylhydrazine as a Reagent for Carbonyl Groups" J. Org. Chem Soc., 2, 222-226, (1937).

[99] M. Gennaro, E. Mentasti, C. Sarzanini & V. Porta., "Aliphatic Monoamines, Diamines, Polyamines: An HPLC Method for their Identification and Separation by a Dansylation Reaction" Chromatographia, 25(2), 117-124, (1988).

[100] K. Blau and G.S. King (eds.)., "Handbook of Derivatives for Chromatography", Heyden, London, (1978).

[101] E.T. Denisov., "Developments in Polymer Stabilisation: Inhibitor Regeneration in Oxidation", 3, 1-20, Developments Series, (1980).

[102] S.N. Patel., "Thermal and Oxidative Degradation of an Aromatic Polyamide", Ph.D thesis, Dept. of Textile Industries, Leeds University, (1992).

[103] M.I. Pope and M.D. Judd., "Differential Thermal Analysis", Heyden, London (1977).

[104] B.G. Achhamer, F.W. Reinhart & G. Kline., "Degradation of Polyamides" J. Res. Nat. Bur. Stand., 46, 391-395, (1951).

[105] S. Straus and L.A. Wall., "Pyrolysis of Polyamides" J. Res. Nat. Bur. Stand., 60, 39-45, (1958).

[106] T. Kelen (ed.)., "Polymer Degradation", Van Nost. Rein. Co Inc., 1, (1983).

[107] D.C. Nonhebel, J.M. Tedder and J.C. Tedder., "Radicals", Cambridge Univ. Press, New York, 154, (1979).

[108] H.H.G. Jellinek (ed.)., "Aspects of Degradation and Stabilisation of Polymers", p.79, Elsevier (1978).